UNIVERSIDADE DE LISBOA

FACULDADE DE CIÊNCIAS

DEPARTAMENTO DE FISICA

U

LISBOA

UNIVERSIDADE
DE LISBOA

NON-DESTRUCTIVE CHARACTERIZATION OF ARTWORKS IN PAPER SUPPORT USING SPECTROSCOPIC TECHNIQUES

ALDA SOFIA PESSANHA DE SOUSA MORENO

DOUTORAMENTO EM FÍSICA

2013

UNIVERSIDADE DE LISBOA

FACULDADE DE CIÊNCIAS

DEPARTAMENTO DE FISICA

U

LISBOA

UNIVERSIDADE
DE LISBOA

NON-DESTRUCTIVE CHARACTERIZATION OF ARTWORKS IN PAPER SUPPORT USING SPECTROSCOPIC TECHNIQUES

ALDA SOFIA PESSANHA DE SOUSA MORENO

Tese orientada pela Prof.ª Doutora Maria Luisa de Carvalho Dias de Sousa Leonardo
especialmente elaborada para a obtenção do grau de doutor em Física

DOUTORAMENTO EM FÍSICA

2013

To my daughter, Eva.

Nothing is impossible, the word itself says *I'm possible!*

Audrey Hepburn

ACKNOWLEDGMENTS

List of publications resulting from this work

- S Pessanha, M Guerra, S Longelin, A Le Gac, M Manso, M L Carvalho, **Determination of gold leaf thickness in a Renaissance illumination using a non-destructive approach** DOI: 10.1002/xrs.2518

- S Pessanha, A LeGac, T I.Madeira, M L Carvalho **Elemental analysis by portable Ag and Rh x-ray sources of a Namban folding screen** Nucl Inst Meth Phys Research B 309 (2013) 254-259

- S Pessanha, A. Le Gac, T. I. Madeira, M. Manso, M. L. Carvalho **Characterization of a Namban folding screen from the Edo period by means of EDXRF, SEM-EDS and Raman spectroscopy** X-Ray Spectrom. 42 (2013) 128–133

- S Pessanha, M. Manso and M. L. Carvalho, **Application of spectroscopic techniques to the study of illuminated manuscripts: a survey**, Spectrochim acta B 71–72 (2012) 54–61

- S Pessanha, A LeGac, T I Madeira, J-L Bruneel, M L Carvalho, **Evaluation of the intervention of a folding screen belonging to the Momoyama period by Raman spectroscopy using different wavelengths**, J Raman spectrosc 43 (2012) 1699–1706

- A Ferreira, F Figueira, <u>S Pessanha</u>, I Nielsen and M.L. Carvalho, **Study of air induced paper discolorations by FTIR, XRF and SEM**, App Spectrosc 64 (2010) 149-153

- S Pessanha, M L Carvalho, M I Cabaço, S Valadas, J-L Bruneel, M Besnard, M I Ribeiro, **Characterization of two pairs of 16th century Nambam folding screens by Raman, EDXRF and FTIR spectroscopies**, J Raman Spectrosc, 41 (2010) 1220-1226

- M. Manso, <u>S. Pessanha</u>, F. Figueira, S. Valadas, A. Guilherme, M. Afonso, A. C. Rocha, M. J. Oliveira, I. Ribeiro, M. L. Carvalho, **Characterisation of foxing stains in eighteenth to nineteenth century drawings using non-destructive techniques**, Anal Bioanal Chem (2009) 395:2029–2036

Table of contents

RESUMO

A aplicação de técnicas analíticas, originalmente desenvolvidas para o campo das ciências de materiais, ao estudo de objectos de arte e arqueologia proporciona aos historiadores de arte e conservadores a possibilidade de obter informações acerca dos materiais de modo a responder às questões do onde, quando e por quem cada peça foi produzida. Considerações acerca do estilo, combinadas com avaliações da estética e estudo de arquivo podem, normalmente, providenciar uma resposta, no entanto, estilos podem ser copiados em épocas e lugares diferentes dos originais. Assim, a investigação da composição química dos materiais utilizados é fundamental para determinar proveniências e explorar tecnologias de produção. Por outro lado, a caracterização material de Herança Cultural é fundamental para projectos de conservação de modo a diferenciar partes originais de repintes e de modo a compreender que materias podem ser utilizados.

O trabalho aqui apresentado pretende demonstrar a eficácia da técnica de fluorescência de raios-x (do inglês XRF) com equipamentos portáteis, por vezes complementada com espectroscopia Raman, na obtenção de respostas a questões de caracterização, conservação e autenticação de obras de arte em suporte de papel e pergaminho.

O trabalho inicia com a apresentação do estado da arte no que respeita à utilização de XRF portátil e espectroscopia Raman em estudos semelhantes. Apesar da adequação desta técnicas estar já comprovada, constantes desenvolvimentos tecnológicos proporcionam novas potencialidades. Segue-se uma descrição, mais detalhada para o XRF e mais sucinta para o Raman, dos princípios que físicos que sustentam técnicas utilizadas. A primeira técnica usa radiação X para ionizar os níveis mais internos dos átomos da amostra que emitem, consequentemente, radiação caraterística desse átomo e permite uma análise elementar qualitativa e quantitativa. A espectroscopia Raman baseia-se na difusão de radiação monocromática quando irradiada sobre uma amostra. Desta interação resultam alterações nos níveis vibracionais das moleculas que podem ser detectados e as molécula identificadas.

Os resultados são apresentados sob a forma de casos de estudo que pretendem dar resposta a questões em três tópicos principais: a aplicação de μ-XRF ao estudo de descolorações em documentos e desenhos em papel; o estudo dos pigmentos utilizados em biombos de papel estilo Namban de modo a caracterizar os materiais utilizados, datar intervenções de restauro

bem como autenticar as peças; por último, o estabelecimento de metodologias para determinar/avaliar a espessura da folha de ouro aplicada em douramentos de peças de arte em suporte papel e pergaminho.

O estudo de manchas e descolorações em papel surgiu da necessidade, por parte de conservadoras e restauradoras da área de papel, de avaliar possíveis alterações na composição química de papel e manchas. Para tal escolheram-se dois dos tipos de mancha que mais infestam as bibliotecas e arquivos portugueses, as manchas de *foxing* e as manchas induzidas pelo contacto com o ar. Foi efectuada análise quantitativa e comparada a composição elementar da zona com e sem mancha e determinado um aumento de potássio na região manchada para ambas tipologias de descoloração.

O estudo dos biombos Namban também partiu da abordagem da curadora da área de mobiliário e artes orientais do Museu Nacional de Arte Antiga (MNAA), em Lisboa, que procurava informações acerca dos materiais e técnicas artísticas utilizadas nos dois pares de biombos Namban (Sécs. XVI e XVII) a propósito da exposição "Encompassing the Globe – Portugal e o Mundo nos séculos XVI e XVII". De modo a prosseguir estudos sobre este tipo de peças de arte e obter um maior *corpus* de estudo, procurámos aceder a todos os biombos Namban ou tipo Namban existentes em colecções portuguesas, públicas ou privadas. Nesse sentido surgiu a oportunidade de estudar dois biombos que se encontravam em ateliers de restauro de modo a ficarem preparados para serem enviados para uma exposição: "Giappone. Terra di incanti - Di linea e di colore" (Japão. Terra de encantos – da linha e da cor) no Museo degli Argenti no Pitti Palace em Florença (Italia). Tivemos também acesso ao par de biombos da colecção do Museu Nacional Soares dos Reis (MNSR), no Porto. Estes biombos haviam sido recentemente recuperados no National Research Institute for Cultural Properties em Tóquio e dessa intervenção havia indícios de um primeiro restauro (sobre a qual não havia registos) e cujos materiais resolvemos investigar. Como não podia deixar de ser, o Museu Oriente (MO), em Lisboa, também possui um biombo Namban em suporte papel, ao qual nos foi concedido acesso. A particularidade deste biombo, adquirido sem par, é o facto de ser mais recente do que os biombos dos outros dois museus e de se tratar de uma cópia e ampliação das cenas retratadas num dos biombos do MNAA.

Através a análise material destas peças pôde-se determinar a paleta usada pelos artistas da escola Kano durante os periodos Momoyama (1573-1603) e Edo (1603-1868): malaquite, azurite, indigo, vermelhão, vermelhor de chumbo, branco de conchas e negro de carvão. Nalguns biombos, descobriram-se materiais que só foram sintetizados na segunda metade do Séc. XIX e mesmo Séc. XX e que correspondem a restauros efectuados posteriormente. Esses materiais são. Por exemplo, amarelo e laranja de crómio, litopona ou vermelho de cádmio.

Um dos aspectos que torna estes biombos de um beleza extraordinária é o facto de possuírem um fundo coberto com folha de ouro. No entanto, e visto tratarem-se de amostras de espessura intermédia aplicadas sobre um suporte desconhecido, a análise quantitativa das folhas de ouro seria bastante incerta. A aplicação de métodos de quantificação (bem estabelecidos por XRF), quer por parâmetros fundamentais quer por comparação com padrão implicaria o conhecimento rigoroso da estrutura das camadas que compõem a amostra, bem como a existência de amostras padrão certificadas com as mesmas caraterísticas. No entanto, a caracterização da folha de ouro pode passar também pela análise qualitativa e pela determinação da espessura da folha de ouro. Nesse sentido, foi estabelecida uma metodologia, completamente não destrutiva, para determinação da espessura da folha de ouro em obras de arte em suporte papel e pergaminho, baseada nos diferentes coeficientes de atenuação das diferentes riscas dos elementos. Determinou-se deste modo uma espessura de cerca de 1.6 μm para a folha de ouro utilizada no douramento do foral Manuelino de Murça, e inferiu-se que dos biomos estudados o que teria a folha de ouro menos espessa seria o biombo pertencente ao Museu Oriente.

O aspecto mais importante deste trabalho é o facto de todas as análises de fluorescência de raios-X terem sido efectuadas *in situ*, nos museus ou ateliers de restauro e apenas quando necessário terem sido recolhidas amostras para análise complementar por espectroscopia Raman. Deste modo, os dois critérios mais importantes a cumprir em análises em Herança Cultural foram mantidos: as peças não foram danificadas nem retiradas do seu ambiente especificamente controlado.

Palavras-chave: XRF portátil; Raman confocal; pigmentos; autenticação; espessura de camadas

ABSTRACT

The work here presented aims at demonstrating the efficacy of X-ray fluorescence (XRF) with portable setups, sometimes complemented by Raman spectroscopy in providing answers for characterization, conservation and authentication issues related with artworks in paper and parchment support.

The work begins with a short section regarding the state of the art on the use of portable XRF and Raman spectroscopy in the study of artworks in paper and parchment support. The suitability of the techniques has already been greatly established, however constant improvements from the technological point of view, grant different capabilities.

The work is presented as a group of case studies with the intention of providing answers in three major topics: the application of µ-XRF to the study of discolorations in paper documents and drawings, the study of the pigments used in Namban paper folding screens to accomplish their characterization, dating and authentication and the establishment of methodologies for determining/evaluating the thickness of gold leaf used for gilding.

In some of these case studies we were approached by conservators who had specific demands and then we pursued similar artworks to improve the corpus of study.

The most remarkable aspect of these studies is that all XRF analyses were performed *in situ* and when there was need for complementary information micro-samples were collected for Raman analysis. This way, the main goals in Cultural Heritage studies were obtained: the artworks were not damaged nor removed from their original location.

Keywords: portable XRF; confocal Raman; pigments; authentication; layer thickness.

CHAPTER I – STATE OF THE ART

1. State of the art

The application of analytical techniques, originally developed in the field of materials science, to objects of art and archaeology gives the art historians and archaeologists the possibility to gain information about the material composition of such objects and prepares answers to the questions of where, when or by whom such an artifact was made [1]. Stylistic considerations combined with aesthetic evaluations and comprehensive archive studies can commonly provide an answer. However, styles were sometimes copied at locations and times completely different from those of their origin. Hence, investigations of the physical properties and chemical composition of the pieces are useful and increasingly applied to allocate an object to a particular historic or prehistoric context, to determine the correctness of the provenance or to explore the technology used for the manufacturing [2-4]. Furthermore, scientific investigations are also valuable and in some cases indispensable for conservation projects in order to differentiate the original parts of an object from later additions, former restoration works, and to understand what materials can and cannot be used.

Material analysis for Cultural Heritage is almost as old as the scientific documentation of objects of art and archaeology. It was Martin H. Klaproth (1743-1817) who reported in 1795 the chemical composition of Roman coins, ancient alloys and glass based upon gravimetric analyses and newly developed chemical recipes for the separation of Cu, Pb and Sn and their quantitative determination. For his studies large amounts of sample material had to be dissolve in nitric acid, a procedure unacceptable nowadays! At the beginning of the 20th century, microchemical techniques and spot tests were developed which reduced the amount of sample [2]. The thriving development of electronics in recent decades has brought new analytical instruments which, opened new horizons with respect to the material characterization of artworks, namely artworks on paper and parchment support: (XRF) X-Ray Fluorescence in different configurations [5, 6], (SEM-EDS) Scanning Electron Microscopy coupled with Energy Dispersive Spectrometry [7], (PIXE) Particle Induced X-ray Emission [8], (XANES) X-Ray Absorption Near Edge spectroscopy [9], Raman spectroscopy [10], (FTIR) Fourier Transform Infrared Spectroscopy [11],

(NMR) nuclear magnetic resonance spectroscopy [10] , (GFAAS) Graphite Furnace Atomic Absorption Spectroscopy [12], etc.

Depending on the information required, one might use a combination of truly non-invasive techniques (i.e. those which do not require a sample to be removed from the object, and which leave the object in essentially the same state before and after analysis), non-destructive techniques (i.e. a sample or complete object can be re-analyzed with the same or other technique, for further examination) and micro-destructive techniques (i.e. those which consume or damage a few picoliters of material). The distinction between these techniques and types of analyses is of particular importance in the Cultural Heritage field. Nevertheless research scientists generally use the term ''non-destructive'' for any of the above-mentioned analysis methods. In all cases, however, the goal is the maximization of information and the minimization of the consumed volume [13].

Amongst the previously mentioned techniques XRF and Raman spectroscopy, particularly combined together, are the most suitable techniques for, non-destructive, material characterization in Cultural Heritage studies, particularly for artworks in paper and parchment support.

1.1. X-ray fluorescence

In the field of Cultural Heritage, numerous objects cannot be moved from their original location due to physical constraints or because they are simply too valuable. Regarding artworks in paper or parchment support the need of portability is even greater because of the delicate state of conservation of some of the pieces that cannot leave the dedicated environment of the museums/archives. In order to study such pieces, portable energy dispersive X-ray fluorescence spectrometers, that allow *in situ* analysis, were developed and rapidly became a widely used piece of equipment. Piorek [14], Cesareo et al [15] and more recently Bosco [16] reported the history of the development of portable XRF spectrometer: The first-generation instruments appeared in the 60s, which used radioisotopes and targeted at single element detection such as sulfur in oil. An instrument with several filters was also developed in order to detect several elements one after another. The second-generation portable analyzer, which was an energy dispersive instrument, was

developed for geological prospecting in the mid-70s. This instrument used a proportional detector and had to be calibrated using paper and pencil. In the 80s, the third-generation portable energy dispersive spectrometers with a semiconductor detector were developed, in which microprocessors originated the first use of fundamental parameter method. In the 90s, miniaturization of the instrument has been accelerated due to the development of personal computers, detectors, and batteries. Thus the fourth-generation portable spectrometers appeared. On the other hand, the miniaturization of the X-ray tube has been achieved by insulating the tube with resin or ceramic instead of insulating oil. The development of digital signal processor (DSP) also contributed to miniaturization of portable XRF spectrometers. The development of low-power x-ray tubes allowed the instrument to be used safely without any shielding. The main characteristics of these tubes are air cooling, low weight and stability. On the other hand, several types of non-cryogenic, miniaturized detectors are in constant improvement [17]. However, many light elements require advanced instrumentation which often limits practical work to atomic numbers above 13 (Al). Furthermore, only L-lines rather than the K-lines of high atomic number elements (~above 50- Sn) can be measured. That is the cost of portability! There are of course, several degrees of portability, ranging from one of the equipments used by Čechác et al [18] with an annular radionuclide source and a Si(Li) detector cooled with liquid nitrogen, to the ultra-compact, handheld equipment, used by Chaplin et al [19]. There are also equipments that combine different techniques, like the PRAXIS™ (trans)portable equipment used by Van der Snickt [20], where a Raman probe is combined with the EDXRF system using a polycapillary X-ray lens to collimate the beam and a SDD detector cooled by Peltier effect; and the portable equipment combining XRD/XRF that Duran et al. [3, 21] used for the characterization of illuminated manuscripts. This equipment is composed by an air-cooled iMOXS-MFR™ x-ray tube with Cu anode and maximum power of 30 W [22] and a Si-drift detector (Röntec GmbH). A polycapillary half-lens at x-ray tube's end provides a 4 mm diameter parallel x-ray beam. Most of these equipments are laboratory made, and there are several research groups that dedicate to the implementation and improvement of such systems. An example is the equipment used by Ferrero et al [6] to study the inks on 17th century paper engravings by means of portable EDXRF. The spectrometer combines an x-ray tube from Scientific Instruments, model P/N XRG35 with

W anode (max. 0.3 mA and 35 kV) and an Al collimator provides X-ray spots of 5 mm diameter on the sample. The detector is an Amptek™ Si-PIN. The evaluation was made by comparing the peak areas of elements in the ink and in the paper. The same group performed a study on the inks of another paper engraving, now from the 16th century, this time using a EDXRF system with two detectors [23]. This equipment is composed by an X-ray tube (EIS S.r.l.) with Pd anode (max 35 kV, 1 mA) and provides a collimated beam of 2 mm of diameter. The first detector is a Si-PIN detector (Röntec Inc.) and the second one is a high efficiency CdTe detector (Amptek Inc.) The combination of these two detectors makes it possible to detect low and high energy photons, with the high resolution Si-PIN and the high efficiency CdTe detector. Manso et al [24] used a portable equipment to study illuminated manuscripts from the 16th century, stored in the Portuguese National Archive. The portable EDXRF spectrometer was used *in situ* for inks, pigments and parchment characterization. The spectrometer consists on an Eclipse II Amptek X-Ray tube with an Ag anode. The radiation is collimated by a Ta collimator allowing a 5 mm diameter beam on the sample. The detector is an Amptek XR-100CR™ Si PIN with energy resolution is 190 eV at 5.9 keV and the acquisition system is Amptek PMCA. The angle between the incident and emitted beam is 90° and the sample was positioned at the focal point of two laser beams. An equipment made with the same components but with 30º geometry and a polycapillary collimator on the detector window was used by Cesareo and Brunetti [25] to study 19th century stamps. They considered that in stamp only a negligible amount of radiation interacts with the sample, so a linear relationship is established between the quantity of element ($\mu g/cm^2$) and the XRF counts. This way, they evaluated the elemental composition of the paper and the pigments used in the collection of stamps.

Artworks in paper or parchment support constitute the simplest stratigraphies, sometimes only one or two layers over the support, however it is important to distinguish information coming from different layers. Čechác et al. [18] studied the Kα/Kβ and Lα/Lβ ratios of characteristic X-rays of the pigment layers in model samples created to simulate illuminated manuscripts. The principle of this technique lays in the different absorption coefficients for the Kα and Kβ lines (and also for the Mα, Lα and Lβ lines). If an element is deposited on a surface, the emitted X-rays are only slightly affected by absorption in the specimen. On the other hand if an element is present at some depth in a bottom layer of the

specimen, its characteristic radiation has to penetrate through an upper layer and the characteristic X-ray fluxes are significantly changed. The Kα/Kβ ratio is usually reduced, because the attenuation coefficient for a Kα line is higher than for Kβ. The ratio can be increased only if another element with an absorption edge between the two lines is present in the specimen. This technique was applied to a set of Bohemian books dating back to the 14th and the 15th centuries.

The studies mentioned so far were performed using laboratory made equipments, however there are commercial portable and handheld equipments available for similar applications. For instance, Trentelman et al [26] used the Bruker Tracer III-V™ handheld spectrometer [27] (Re anode, operated at 40 kV, 2 μA, Ti/Al filter) to analyze of 15th century illuminated manuscripts by Jean Bourdichon, and the ARTAX800™ XRF spectrometer also by Bruker to perform line and area scans on other artworks from the same author [28]. Also an ARTAX spectrometer was used by Miguel et al [29] to study the pigments in an 12th century illuminated manuscript, and by Burgio et al to study 16th-18th century Islamic manuscripts [30] and of modern pigments on purportedly medieval miniatures by the 'Spanish Forger' [31] both *in situ* at the Victoria and Albert museum in London. Aceto et al [32] used the Assing Lithos3000™ [33] to study the pigment-caused degradation in a 9th century Italian manuscript. This commercial system utilizes a small-focus Mo x-ray tube and a Si-drift detector. Quantitative analyses were also performed using Lithos3000 3.2 dedicated software with matrix correction and light elements evaluation. A few years later Aceto [34] used both Thermo Scientific® NITON spectrometer XL3T-900 GOLDD™ model [35], equipped with Ag tube (max. 50 kV, 100 μA, 2W) and large area SDD detector, and the ARTAX200 equipped with Mo tube (max. 50 kV, 0.7 mA, 30 W), SDD detector, to study two 6th century Byzantine manuscripts. Bruni et al [36] also used the Lithos 3000 as part of the multianalytical study of a painted and drawn parchment of the late 15th century, or the beginning of the 16th, partly attributed to Andrea Mantegna. In this work authors made use of a Zr filter to monochromatize the radiation coming from the x-ray tube.

The main advantage of this technique, especially when using portable equipment and performing analysis *in situ*, is the complete non-invasiveness of the method. However, the harmful power of x-rays is known so it is often asked by the conservators and curators the

degree of non-destructiveness of the technique. It is a fact that absorption of radiation by an atom bound to other atoms may alter its chemical state permanently, that when dealing with sensitive materials like paper, the object can become darker, brittle and even decompose mechanically [37]. In the case of x-rays , the probability that the primary interaction of a photon causes permanent destruction is very low, however the large number of secondary (fluorescent) photons and electrons emitted during the relaxation process has altogether a considerable destructive potential. In order to evaluate this effect, Mantler and Schreiner [38] irradiated paper samples for up to 4 hours with a XRF spectrometer using maximum power (30 kV and 100 mA). A faint yellow became visible after 15 minutes, after 1 hour cracks were clearly visible and after 4 hours the specimen broke apart at the attempt to remove it from the sample holder. These results show that precautions must be made, namely the use of a much lower intensity and shorter exposition times, when analyzing delicate specimens such as paper or parchment artworks.

1.2.   Raman spectroscopy

It is argued that Raman spectroscopy is the most excellent technique for, single-handedly, studying and identifying inorganic solids, especially when they are in heterogeneous mixtures at a micrometer scale [39-41]. Raman spectroscopy probes molecular and crystal lattice vibrations and therefore is sensitive to the composition, bonding, chemical environment, phase and crystalline structure of the sample material. It is a fingerprinting technique and materials are identified by comparing their characteristic vibrational spectra with those in databases [42-44].

Robin J H Clark and his co-workers have been great promoters of the application of Raman Spectroscopy to the study of Cultural Heritage, in particular illuminated manuscripts with over 15 publications. These publications comprise review articles on the application and developments of Raman spectroscopy [41, 45-49] and case studies where Raman microscopy alone [39, (50-53] or in combination with other techniques [19), 30, 54, 55] could characterize an artist's palette or even detect forgeries [31, 56]. These case studies focused mainly in pigment characterization and included the inedited analysis of the King

George III copy of the Gutenberg bible, the study of several European Medieval manuscripts, as well as of Persian, and of Islamic origin.

The characteristics of the Raman technique that make it so well qualified for the analysis of these materials include its molecular specificity, non-destructiveness, applicability to samples of large or non-uniform shape and relative immunity to interference. If we couple a standard optical microscope to a Raman spectrometer, we obtain high magnification visualization of a sample and Raman analysis with a microscopic spot. In a typical set-up, a microscope is coupled to a spectrometer with an intensified diode array or Charge-Coupled device (CCD) detector. Laser radiation is brought to a focus on each grain via the microscope objective (up to x100). The Raman scattering by the sample retraces the path of the incident beam, being collected by the same objective and directed to the monochromator and then to the detector [39]. Raman microscopy has been used to investigate pigments in artworks on paper support either by collecting micro-samples [5], [57-60] or by placing the manuscript directly under the microscope [29, 30, 52, 59, 60].

Eremin et al. [11] collected samples from Tosa Mitsunobu's "The tale of Genji" to study the used pigments with a Keiser Hololab 5000R [63] spectrometer (lasers 514 nm and 785 nm). More recently [64] they used the Senterra [65] Raman microscope from Bruker® (532, 633 and 785 nm) to study samples removed from 18th to 20th century Thai manuscripts, and found the first evidences of the use of copper citrate as pigment.

Chaplin [56] used a Renishaw System 1000 Raman spectrometer (632.8 nm and 515 nm laser sources) to make the distinction between original 1847 and 1858–1862, forged and reproduction postage stamps of Mauritius. Bicchieri et al [66] used the Renishaw in-Via reflex Raman microscope [67] (785 nm laser) to study the inks in an 18th century Italian manuscript without sampling.

Spatial resolution can be further improved by use of confocal geometries. Traditional Confocal Raman microscopes make use of a pinhole aperture placed in front of the spectrograph entrance slit. The Raman light is focused onto the pinhole and the diverging beam after the pinhole is then refocused onto the entrance slit of the spectrograph. Different pinhole apertures can be used to control the degree of confocality, while the entrance slit is used to control the spectral resolution of the spectrometer. Raman microscopes with confocal geometry have been applied to the study of pigments in illuminated manuscripts

by Magistro et al [68], Bicchieri et al [69] and Deneckere et al [70]. Aceto et al [57] used a Confocal Raman microscope to characterize the inks that had undergone severe degradation process in a 9th century Italian manuscript. Manso et al [24] used XploRA Raman microscope [71] from Horiba® (532, 638 and 785 nm) to study the samples of pigments and inks used in the Manueline foral charter of the town of Sintra. More recently Shi et al [72] used same equipment to study the pigments used in three paper currencies issued under the reign of the Chinese Ming and Qing Emperors between 15th and 19th centuries.

In the past years, the appearance of compact, portable Raman equipments with probe heads that are connected to the excitation laser source and base Raman analyzer by fiber optic cables, made possible the *in situ* use of Raman spectroscopy in the study of Cultural Heritage. P. Vandenabeele et al compared different spectroscopic aspects of such existing instruments, as spectral resolution, wavelength calibration, laser cut-off and general spectral quality to evaluate their suitability for this purpose [73]. These equipments have been also employed in the study of pigments in illuminated manuscripts especially when the value of the codices does not allow the moving from museums or libraries, or that when sampling, even gentle micro-sampling cannot be performed [36, 52, 70, 74, 75]. Bersani et al [40] used two portable equipments, the micro-Raman apparatus of Horiba Jobin-Yvon, model HE (632.8 nm) and the Renishaw RP10 compact spectrometer (514.5 nm) to study five medieval illuminated manuscripts *in situ* at the Biblioteca Palatina in Parma. In spain, Castro et al used the Renishaw RA100 System [76] coupled to a micro-probe (785 nm laser) to study the paper and the pigments used in two colored maps [7], [10] and modern wallpapers [77, 78].

CHAPTER II – X-RAY FLUORESCENCE

2. X-RAY FLUORESCENCE

2.1. BASIC PRINCIPLES OF X-RAY FLUORESCENCE

The principle of XRF technique is the use of excitation radiation to produce ionization in the inner shells of the atoms present in a sample due to photoelectric absorption.

If a photon with energy larger than the binding energy of an inner electron interacts with this bound electron, part of its energy can be absorbed and the electron is ejected. A vacancy is then created in one of the fully occupied inner shells and an electron from an outer shell will fill the vacancy and might cause the emission of an X-ray photon [79, 80] (Fig. 2.1). The newly created vacancy in the outer shell can be filled in turn by an electron still farther out, and another X-ray photon can be emitted. This process repeat and series of photons will be emitted until a free electron ultimately replaces an outermost valence electron so that the atom has finally returned to the ground state.
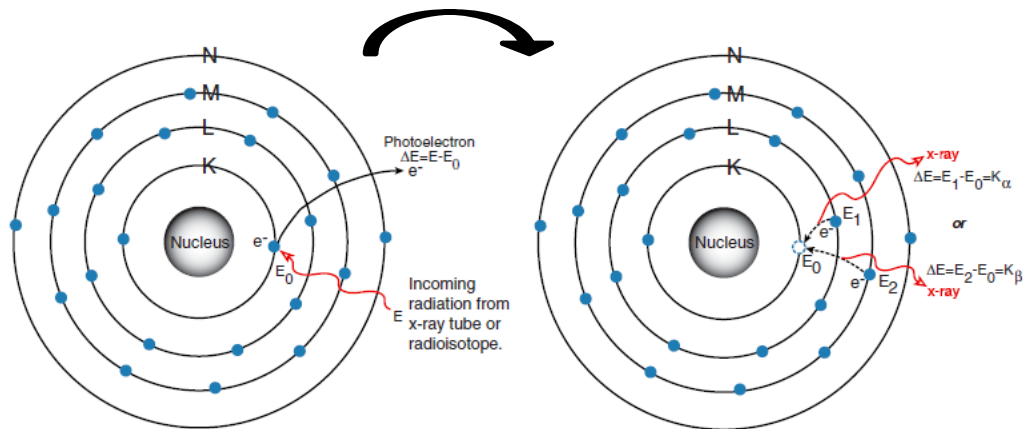
Fig. 2.1. – Schematics of X-ray fluorescence phenomenon. [81]

Alternatively, an excited atom may return to a state of lower energy by ejecting one electron from a less tightly bound state. The nonradiative transition is called **Auger effect**. The probability of the Auger effect increases with a decrease in the difference of the corresponding energy states, and it is the highest for low Z elements [79]. If the vacancy is filled by an electron from a higher sub-shell from the same shell, the transition is called **Coster-Kronig**.

An important consequence of the Auger effect is that the actual number of X-ray photons produced from an atom is less than expected. The probability that a vacancy in an atomic shell or subshell is filled through a radiative transition is called **fluorescence yield** (ω), and could be defined as the ratio of the useful X-ray photons arising from a certain shell to the total number of ionized atoms. Figure 2.2 represents the fluorescence and auger electron yields as function of the atomic number of the emitter. The fluorescence yield is very low for low Z elements and this one of the reasons why X-ray spectrometric techniques are less sensitive for lighter elements. Conversely the Auger yield can be defined as the ratio of non radiative transition and the total number of ionized atoms
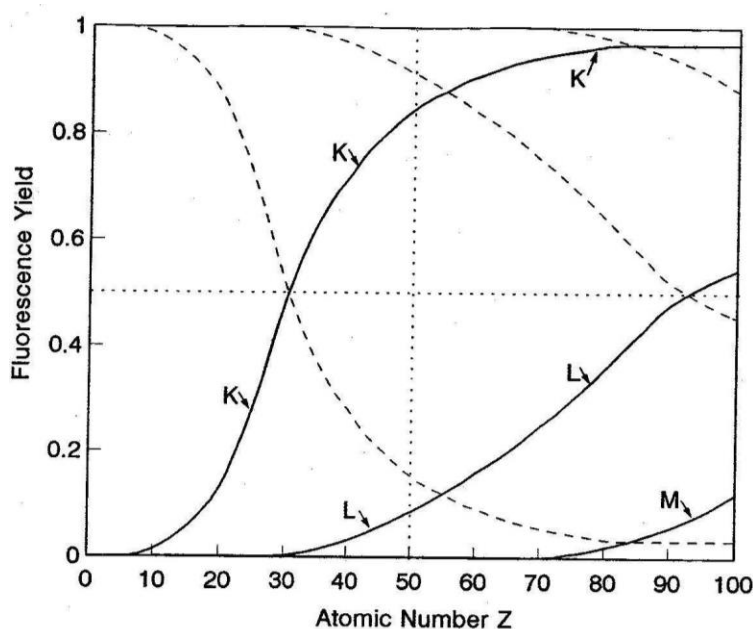
Fig. 2.2. – Fluorescence (___) and Auger electron (- - - -) yields as function of the atomic number (Z) [80].

Although not every electron is permitted to fill an inner vacancy, there are a lot of allowed transitions according to the selection rules of quantum theory:

$$\Delta l = \pm 1; \qquad \Delta j = 0, \pm 1 \qquad\qquad [79]$$

Where l is the azimuthal quantum number and j the total angular momentum.

The most important allowed transitions yielding X-ray characteristic emission are shown in Figure 2.3. The two most used notations the two most used notations for representing the characteristic X-rays are also exemplified, the "Siegbahn notation", developed by Manne Siegbahn, and the IUPAC (International Union of Pure and Applied Chemistry) notation.

16
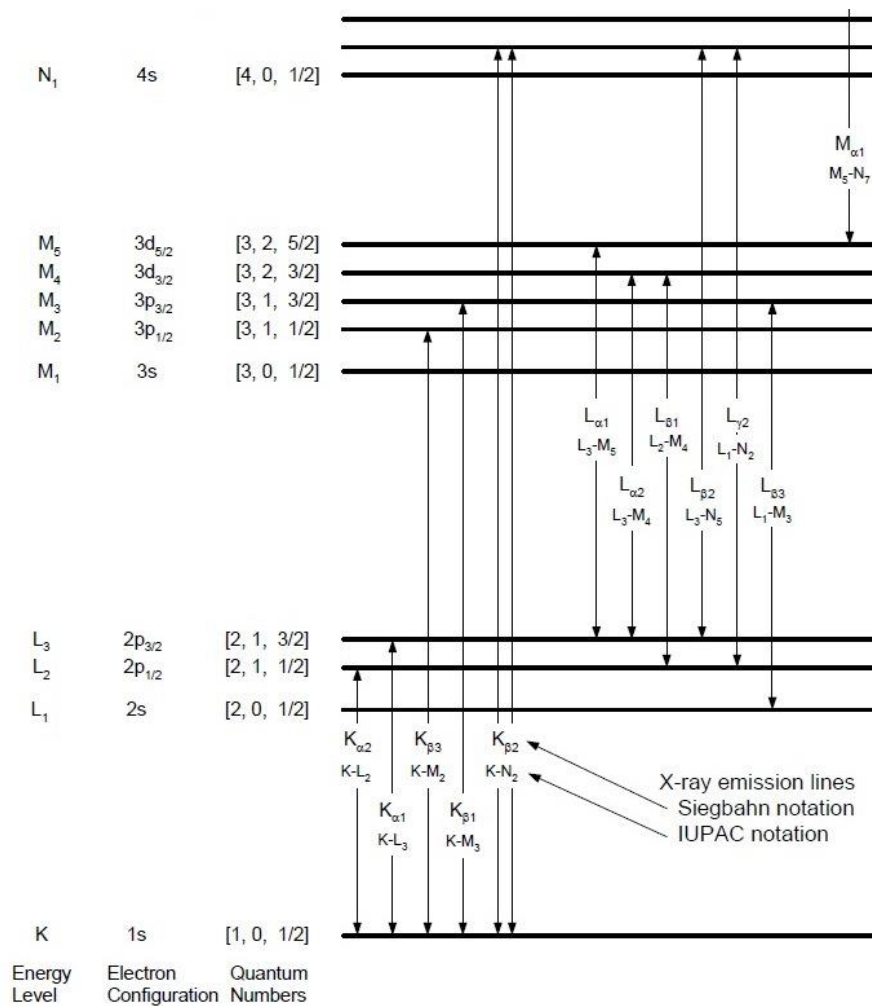
Fig. 2.3. – Commonly used terminology and energy levels of X-ray lines. [81]

Moseley´s law can be used to determine energy of an **X-ray characteristic line**, E:

$$E = k(Z - \sigma)^2 \qquad \text{(2.1) [80]}$$

Where Z is the atomic number of the corresponding element, k is a constant for a particular spectral series and σ is a screening constant for the repulsion correction due to other electrons in the atom.

2.2. INTERACTION OF X-RAYS WITH MATTER

2.2.1. Attenuation of X-rays

If an X-ray beam of intensity I_0 hits layer of material of thickness x:
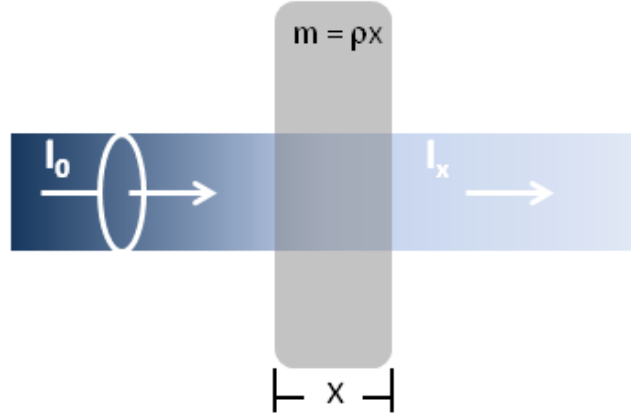
Fig. 2.4. Schematic representation of the attenuation of X-rays through a material.

The attenuation of the intensity of the beam is described by the Lambert-Beer law,

$$I_x = I_0 e^{\left[-\left(\frac{\mu}{\rho}\right)\rho x\right]} \quad \text{(eq. 2.2)}$$

Where μ (cm^{-1}) is the linear attenuation coefficient and μ/ρ (cm^2/g) is the mass-attenuation coefficient for material of density ρ (g/cm^3). The intensity exponentially depends on the thickness of the layer. The mass attenuation coefficient (μ/ρ) is a quantity that depends on the composition of the material and the energy of the X-ray photons.

The attenuation of X-rays is caused by the interaction of the photons with the electrons, inner or outer, or even with the nuclei. It results from three effects: photoelectric absorption, X-ray scatter and pair production. As indicated in Fig. 2.5, pair production does not occur for E < 1 MeV so this phenomenon is not relevant for X-ray spectroscopy [80].
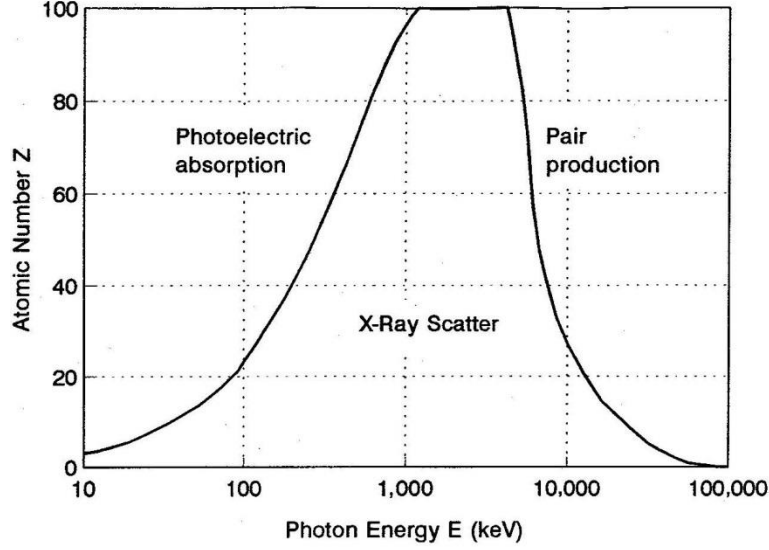
Fig. 2.5 –Predominant effects for the attenuation of X-rays [80].

For the used energies in X-ray Fluorescence the most important effect for X-ray attenuation is **photoelectric effect**. Photoelectric effect occurs when an electron of an inner shell is expelled by an incoming photon of sufficient energy. The primary photon is completely annihilated while a secondary photon is emitted after the electronic rearrangement and the X-ray fluorescence phenomenon occurs (as described in section 2.1). The kinetic energy of the characteristic photon (E_{ph}) can be obtained as the difference of the binding energies of the initial, E_i, and final, E_f, shells. For example, the energy of the Kα shell would correspond to the difference of the binding energies for the K and L_3 shells:

$$E_{ph} = E_i - E_f \quad (\text{eq. 2.3}) \rightarrow \quad E_{K_{\alpha 1}} = E_{L_3} - E_K$$

Photoelectric absorption is evaluated numerically by a specific mass absorption coefficient (τ/ρ), the sum of all possible expulsions of electrons from the various atomic shells K, L, M, etc..

$$\left(\frac{\tau}{\rho}\right) = \left(\frac{\tau}{\rho}\right)_K + \left(\frac{\tau}{\rho}\right)_L + \left(\frac{\tau}{\rho}\right)_M + \cdots \quad (\text{eq. 2.4}) \qquad (80)$$

The different additive parts can be further split up according to the corresponding subshells. Figure 2.6 shows the plot of mass absorption coefficient (τ/ρ) versus the photon energy and corresponding absorption edges energies.

19
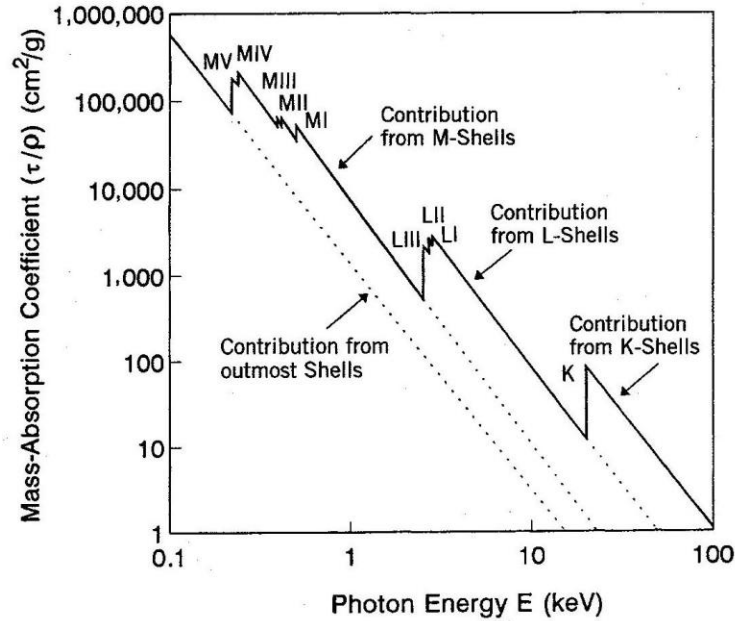
Fig. 2.6. Photoelectric mass absorption coefficient $\left(\frac{\tau}{\rho}\right)$ for Mo as function of energy. [80]

The second component of X-ray attenuation is caused by the scattering of X-ray photons though two possible processes:

- **Rayleigh scattering** (coherent scattering) - a process by which photons are scattered by bound atomic electrons and in which the atom is neither ionized nor excited. The incident photons are scattered with unchanged frequency and with a definite phase relation between the incoming and scattered waves. Rayleigh scattering occurs mostly at the low energies and for high-Z materials. [79]

- **Compton scattering** (incoherent scattering) – is the interaction of a photon with a loosely bound outer electron, leading to a change of direction and loss of energy of the incident photon. The electron is also ejected in a different direction: (Fig. 2.7).
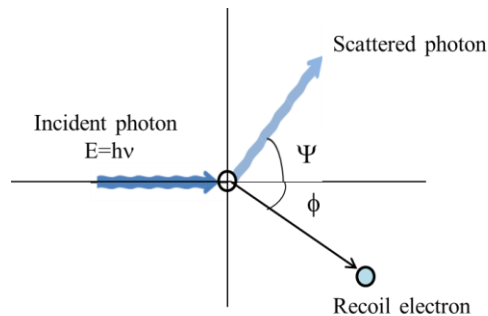
Fig. 2.7.Representation of the Compton scattering effect.

The loss of energy a photon experiments in Compton scattering results from the conservation of total energy and total momentum at the collision. A photon with the energy, E, is deflected into another direction with energy, E', when deflected by an angle, Ψ, while the electron takes off the residual part of energy $\Delta E=E-E'$. The fraction E'/E can be calculated according to:

$$\frac{E'}{E} = \frac{1}{1+(1-cos\,\Psi)\frac{E}{Ee}} \quad \text{(eq. 2.5)}$$

Where, E_e, is the rest energy of an electron (511 keV).

The intensity of the scattered radiation shows a dependence on the initial energy, E, and the deflection angle, Ψ, as shown in Figure 2.8.
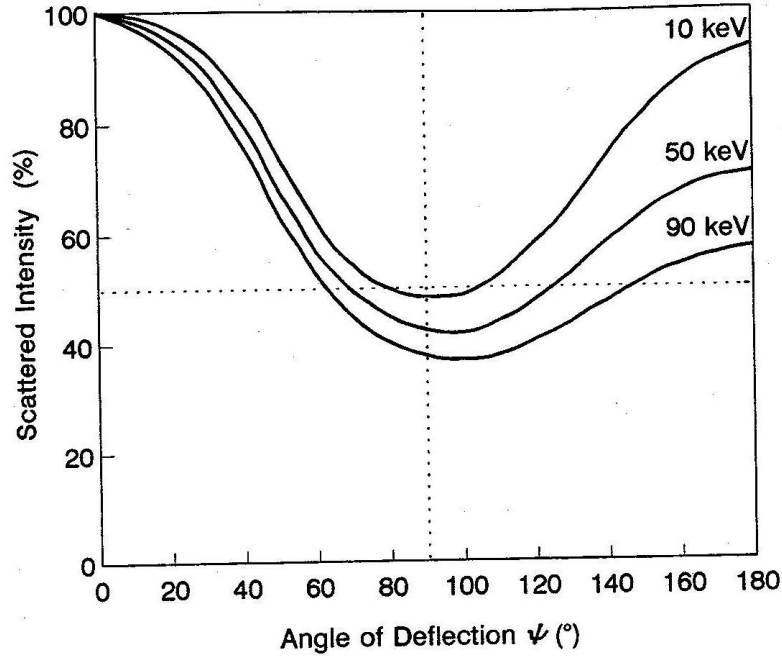
Fig. 2.7.Normalized fraction of scattered intensity (Compton scatter) as a function of the angle of deflection, Ψ [80].

The minimum for the scattered intensity is achieved for a deflection around 90°-100°. For that reason a 90° geometric arrangement of the X-ray tube, sample and detector is generally chosen to minimize inelastic scatter into the detector. Similar results were recently obtained by Guerra et al. [82] by comparing the Compton and Rayleigh scattering of the tube

radiation for different materials and different geometries for symmetrical in-plane spectrometers in the 1-30 keV range.

Even under the best geometrical conditions, and from a practical perspective, the sample matrix is the main responsible for the diffusion effects, and for the total amount of scattered radiation by Compton and Rayleigh effects. Pessanha et al. [83] compared these effects for different mean Z samples and obtained that for light matrices, the predominant effect is Compton scattering, while for heavy matrices the Rayleigh effect takes the lead.

These effects have to be added to photoelectric mass absorption (τ/ρ) leading to the total **mass attenuation coefficient** (eq. 2.2):

$$\left(\frac{\mu}{\rho}\right) = \left(\frac{\tau}{\rho}\right) + \left(\frac{\sigma_{sct}}{\rho}\right) \text{(eq. 2.6) [80]}$$

Where $\left(\frac{\sigma_{sct}}{\rho}\right)$ is the mass-scatter coefficient, which takes into account both scattering effects.

The mass attenuation coefficient (μ/ρ) is proportional to the total photon interactions cross-section per atom according to:

$$\frac{\mu}{\rho} = \frac{\sigma N_A}{A} \qquad \text{(eq. 2.7) [84]}$$

Where σ is the sum of the cross-sections for all the elementary scattering and absorption processes (barns/atom= 10^{-24} cm^2/atom), A is the atomic weight (g mol^{-1}) and N$_A$ the Avogadro number (6.022×10^{23} atom mol^{-1}).

If the absorber is a chemical compound or mixture, its mass attenuation coefficient follows an additive law so that values can readily be calculated from values of the individual elements if the elemental composition is known:

$$\left(\frac{\mu}{\rho}\right) = \sum_i w_i \left(\frac{\mu_i}{\rho_i}\right) \quad \text{(eq. 2.8) [84]}$$

Where the values of w$_i$ are the mass fractions of the different elements present in the compound/mixture.

2.2.2. Reflection of X-rays

When radiation passes from a medium to another of different physical density, i.e. different refractive indices it will be deflected from its original direction, as can be seen in Fig. 2.8:
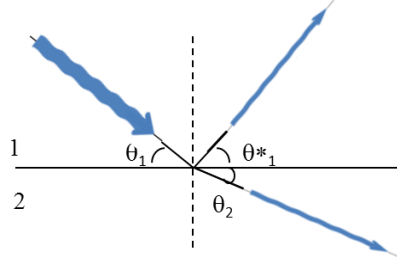
Fig. 2.8. Incident, reflected and refracted beams at the interface of two media.

The glancing angles of the incident beam and the reflected beam are equal ($\theta_1=\theta^*_1$) and the glancing angles of the incident beam and the refracted beam follow Snell´s law:

$$n_1 \cos \theta_1 = n_2 \cos \theta_2 \qquad \text{(eq. 2.9)}$$

Where n_1, n_2 are the refractive indices of medium 1 and 2, respectively.

For X-rays, any medium is optically less dense than vacuum ($n'<n_{vac}=1$) so the refractive index for all materials is smaller than unity by only a small decrement, and can be written as a complex quantity:

$$n=1-\delta-i\beta \qquad \text{(eq. 2.10) [80]}$$

Where, $1-\delta$, represents the real part of the refractive index, and the imaginary, β, is a measure of the attenuation. The variation of the decrement, δ, with the X-ray energy, for energies above the absorption edge of the material, is given by:

$$\delta = \frac{N_A}{2\pi} r_e \rho \frac{Z}{A} \lambda^2 \qquad \text{(eq. 2.11)}$$

Where N_A is the Avogadro's number, r_e is the classical electron radius (2.818×10^{-13} cm), ρ is the density (g cm^{-3}), Z and A (g mol^{-1}) are, respectively, the atomic and the mass number of the element and, λ, the wavelength of the primary beam.

The imaginary component can be expressed by:

$$\beta = \frac{\lambda}{4\pi} \left(\frac{\mu}{\rho} \right) \rho \qquad \text{(eq. 2.12)}$$

Where (μ/ρ) is the mass attenuation coefficient.

Values of δ remain very small throughout the X-rays region, being generally in the order of 10^{-6}, with the consequence that radiation is weakly refracted by any material. Taking into account that for X-rays, any medium is optically less dense than vacuum the refracted beam is deflected towards the boundary plane (see Fig. 2.8). If the angle of refraction, θ_2, becomes 0º, the refracted beam will emerge tangentially to the boundary surface. The angle of incidence is then called critical, θ_{crit}, and, according to equation 2.9 is given by:

$$\cos \theta_{crit} = n_2 \qquad \text{(eq. 2.13) [80]}$$

For angles lower than the critical angle, θ_{crit}, no beam enters into the second medium, the incident beam is completely reflected back into the first medium and **total reflection** occurs. Since θ_{crit} is very small its cosine can be approximated by:

$$\cos \theta_{crit} \approx 1 - \frac{\theta_{crit}^2}{2} \qquad \text{(eq. 2.14)}$$

Equation 2.15 together with equation 2.12 gives the approximation:

$$\theta_{crit} = \frac{1.65}{E} \sqrt{\frac{Z}{A} \rho} \qquad \text{(eq. 2.15)}$$

For low-medium atomic number elements, A≈2Z so we can write

$$\theta_{crit} \approx \frac{1.17}{E} \sqrt{\rho} \qquad \text{(eq. 2.16)}$$

Where the energy, E, is given in KeV and the density, ρ, in g.cm^{-3} in order to get the critical angle in degrees. Again, this equation is only valid for photon energies above the absorption edges of the material. The angles are typically in the range of 0.1º-1º, for example, for glass the critical angle for an incident energy of 17.44 keV (Mo Kα) is 0.098º [80]. The reflectivity of a material is the intensity ratio of the reflected and incident beam and depends on the energy of the beam. The reflectivity is below 0.1% for glancing angles of 1º and more and rises up to 100% around the critical angle. For glass, at an incident energy of 17.44 keV and at the critical angle, the reflectivity is 93.4%.

2.3. Portable spectrometers

X-ray Fluorescence (XRF) portable spectrometers are becoming very popular for the *in situ* analysis of elements. This is mainly because XRF is a nondestructive, multielemental technique that is extremely well suited for the analysis of any material, mainly in the field of Cultural Heritage [2, 85]. An XRF spectrometer consists of an X-ray excitation source, an x-ray detector with electronics and a pulse-height analyzer. Recent technological developments have resulted in small, low-power, dedicated X-ray tubes, thermoelectrically cooled x-ray detectors and small pulse-height analyzers. Therefore, completely portable XRF spectrometers are available that can be taken outside the laboratory and brought to the artwork.

2.4. Production of x-rays

The method used in this work to produce X-rays is to use an X-ray tube.

In an X-ray tube, a beam of electrons emitted by the filament are accelerated by a strong electric field and directed to a target (anode). Electrons impinging on the target material interact with the electrons of the atoms, and if they have kinetic energy greater than the binding energy of an orbital electron, the bound electron may be ejected from the atom. By returning to the ground state, characteristic radiation of the element of the target is emitted. Furthermore, electrons are decelerated due to the Coulomb field of the nucleus. Deceleration implies that kinetic energy is lost, one of the ways in which the electron losses energy is by emitting a photon with the same energy as the lost kinetic energy. This process is called Bremsstrahlung and if a large number of electrons interact with a target material, the resulting Bremsstrahlung radiation consists of photons with a continuum of energies from zero to a maximum value equal to the initial electron kinetic energy [84].

If an X-ray tube is operated at a voltage, $V_{0máx}$, all electrons get the final maximum energy, $E_{máx}$, according to:

$$E_{máx} = eV_{máx} \qquad \text{(eq. 2.17)}$$

The intensity distribution of the continuum bremsstrahlung can be described by

$$N(E)dE = kiZ\left(\frac{E_{máx}}{E} - 1\right)dE \qquad \text{(eq. 2.18) [80]}$$

Where N(E)dE is the number of photon with energies between E and E+dE; k is a constant; i is the tube current; and Z is the atomic number of the target material.

This formula, illustrated by Fig. 2.9, shows that the number of photons is inversely related to the energy E of these photons, decreasing to zero when E approximates $E_{máx}$ given by the anode voltage.
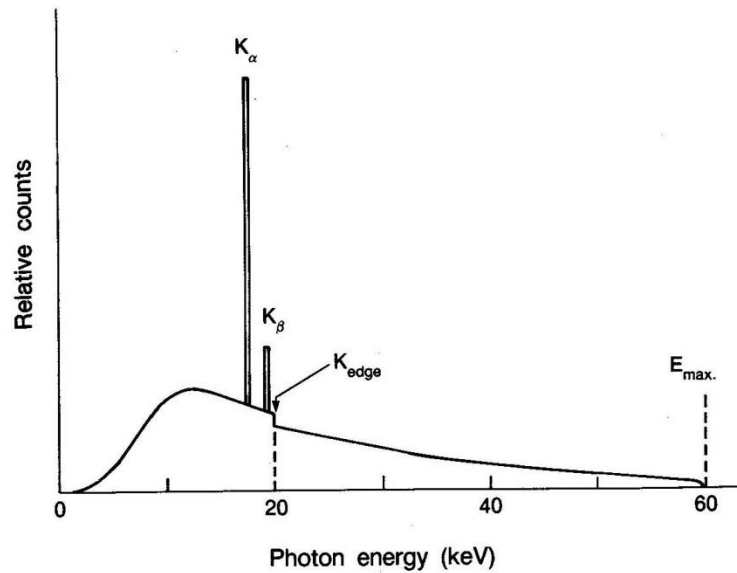
Fig. 2.9. Spectrum emitted from a Mo anode X-ray tube operated at 60 kV.

2.4.1. X-ray tubes

There are different types of X-ray tubes according to the specific application. The most important physical parameters to characterize an X-ray tube are the maximum high voltage and current, and the anode material. From equation 2.18 we can see that the strongest continuous radiation can be obtained from anode materials of high atomic number, however the conversion of the high voltage electrons into X-rays is a very inefficient process and the majority of the energy appears as heat. Under these conditions it is vital that the anode is a good heat conductor. X-ray tube windows are normally made of Beryllium (Be) because of their high transmission for low energy X-rays, but Be is a poor conductor so if a window is too thin it can lead to fracture. Because the amount of electron backscatter increases with

the atomic number of the anode, window heating problems are more critical for higher atomic number anodes. This way, a compromise has to be considered when choosing the thickness of the Be window for a specific anode [86].

In the last few years, small-sized X-ray tubes have been produced expressly for EDXRF analysis. Manufacturers include Oxford Instruments® [87], Amptek® [81], Varian® [88] and Moxtek® [89]. They are characterized by various anode materials (W [90], Mo [91], Rh [92], Ag [60], Cu [93], etc.), high voltage up to 50 kV and current up 2 mA so that just regular air cooling or cooling with a simple fan is needed [15].

According to the position of the anode and consequently the Be window we can differentiate reflection and transmission target and side-window or end-window X-ray tubes respectively (Fig. 2.10). In a side-window tube the angle between the target surface and the normal to the window (anode angle) can amount to 15–25º. As for end-window tubes usually have transmission targets thin enough (about 2 µm) to allow X-rays to pass through the target and X-rays are emitted in the same direction as the electrons are moving.
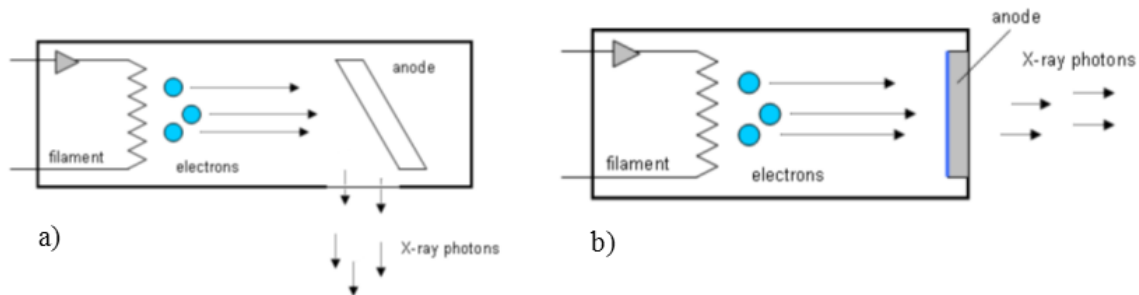
Fig. 2.10. – a) Side-window and b) end-window X-ray tubes [94]

2.4.2. Collimation and focusing

Normally the X-rays exit the tube with a conical angular distribution of 100º-150º so a collimation is needed to reduce the beam size to a desired value and position. The simplest way to do this is to intercept the X-ray beam with a collimator, i.e., a shield absorbing the incident photons, except those crossing a hole of proper diameter in the shield itself [84].

The drawback of this method is the loss of beam intensity, the smaller the size of the hole, the higher the loss of intensity. To overcome this limitation, capillary and polycapillary lenses can be used to focus the beam. X rays striking the interior of hollow channels at grazing incidence are guided along the channel by total reflection (Fig. 2.11a) (section

2.2.2.). Focusing or collecting effects come from the overlap of the beams from thousands of capillary channels, rather than from the action within a single tube (Fig. 2.11b). As for single capillaries, x rays can be transmitted down a curved hollow tube as long as the tube is small enough and bent gently enough to keep the angles of incidence less than the critical angle for total reflection (Fig 2.11b). One side of each capillary of the bundle is pointing to the X-ray source and the other side is pointing to the focus area (Fig. 2.11c).
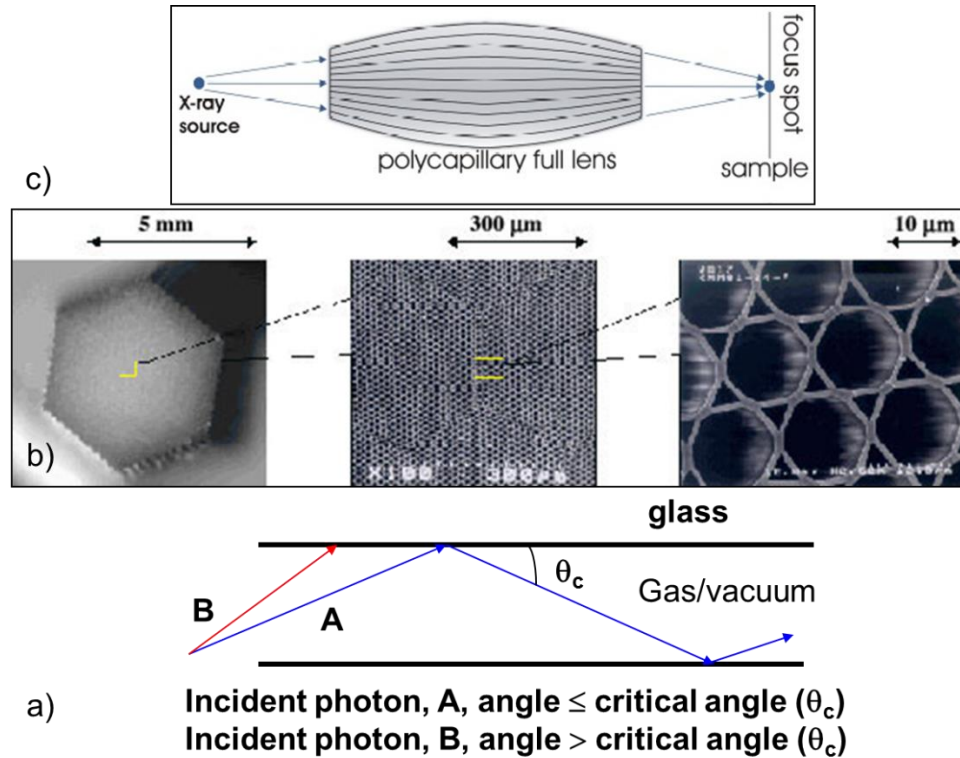
Fig. 2.11. –a) X-rays traveling in a bent capillary tube. The ray entering close to the center of curvature strikes at a larger angle b) Cross-sectional scanning electron micrograph of a polycapillary optic.
c) Sketch of the interior channels of polycapillary optic.

The reflection of x rays, which are reflected down the length of the capillary, is governed by the critical angle, which is approximately 1.5 mrad or 0.1° at 20 keV and is inversely proportional to photon energy (eq. 2.16). Together with the increased absorption of X-rays in the lower energy region, these two phenomena make up a band pass feature. By selecting the capillary dimension properly we are able to design capillaries for different requested beam sizes and anode material.

2.5. Detection of X-rays

A detector is an instrument that yields information about the radiation crossing it, characterized by the types of radiation that it is able to detect, by its structural characteristics such as area, thickness, composition, entrance window, and by several working parameters such as energy resolution, sensitivity, efficiency and time resolution [95]. The most common X-ray detectors used for portable spectrometers are semiconductor detectors, namely Si-PIN and Si-drift detectors (SDD), available from different manufacturers, Amptek [81], Vortex [96], Ketek [97], etc.

In a Si-PIN photodiode there are two planar contacts, the anode and the cathode, with a uniform electric field between them. An X-ray interacts at some location, ionizing the Si atoms and producing electron-hole pairs. The electric field sweeps the carriers to their respective contacts, causing a transient current pulse to flow through the diode (Fig. 2.12a). On the other hand, in the drift diode the planar cathode is maintained but the anode is very small and surrounded by a series of electrodes. The SDD is cylindrically symmetric, so the anode is a small circle and the drift electrodes are annular. These electrodes are biased so as to create an electric field which guides the electrons through the detector, where they are collected at the anode (Fig.2.12b). In both cases the pulses are amplified and classified with a pulse-height analyzer that produces a spectrum [84].
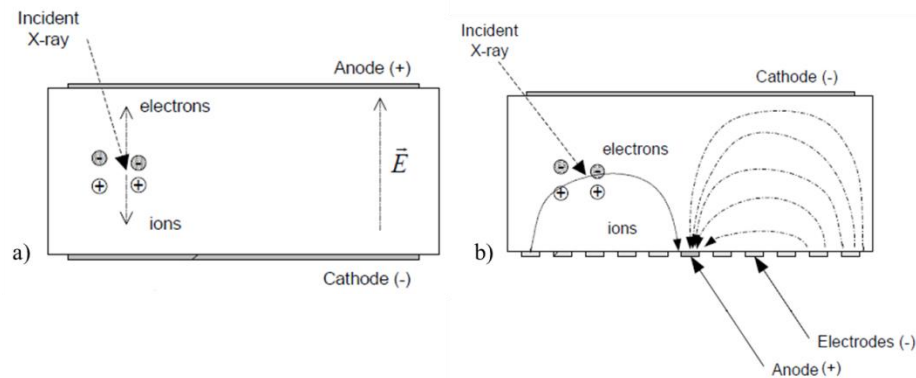
Fig. 2.12. – Sketch illustrating the operation of a) conventional photodiode b) drift diode detector. [81]

Since the average energy to create an electron-hole pair is well defined ($\varepsilon=3.76$ eV at 77K for Si) the total number of charges is directly proportional to the energy of the incident photon, and the frequency of such events is proportional to the photon´s intensity.

One of the most important parameters of a detection system (detector plus amplifier and multichannel analyzer) is the **energy resolution**, which measures the capacity of the system to distinguish between photons very close in energy. The energy resolution of the detector alone is also called intrinsic and depends on the statistical spread in the number of events, i. e., the number of pairs produced in a semiconductor detector by a photon with a given energy.

The energy resolution is normally expressed as the full width of the peak at half maximum height (FWHM) of the measured distribution. The larger the FWHM, the more difficult will be to identify of peaks corresponding to photons of close energies. The measured distribution can be described by means of a Gaussian function, whose expression is given by:

$$G(E) = \frac{N_0}{\sigma\sqrt{2\pi}} e^{\left[-\frac{1}{2}\left(\frac{E-E_0}{\sigma}\right)^2\right]} \qquad\qquad \text{(eq. 2.19) [95]}$$

Where σ is the standard deviation, N_0 is the peak area and E_0 is the peak centroid. The FWHM is related to the σ as:

$$\text{FWHM} = 2{,}35\sigma \qquad\qquad \text{(eq. 2.20)}$$

The contribution of statistical fluctuations in the conversion process of the photon energy into charge carriers is unavoidable. This statistical resolution is generally characterized by a variance ($\sigma_E{}^2$) proportional to the number of carriers generated in the detector. For a given conversion factor, ε, from energy to number of carriers, the standard deviation of carriers is $\sigma_n = \sqrt{\frac{E}{\varepsilon}}$, the resolution:

$$\text{FWHM}=2.35\sigma_E=2.35\varepsilon\sigma_n = 2.35\sqrt{E\varepsilon} \qquad \text{(eq. 2.21)}$$

In semiconductor detectors the variance of the generated charge is smaller than the predicted by Poisson statistics. This deviation is taken into account by introducing the **Fano factor** as follows:

$$\sigma = \sqrt{F\bar{n}}. \qquad\qquad \text{(eq. 22)}$$

Where F is the Fano factor and $\bar{n}$ is the average number of carriers.

This results in a resolution of:

$$FWHM = 2.35\sqrt{FE\varepsilon} \qquad\qquad \text{(eq. 2.23) [95]}$$

In the early 90's the average resolution of a portable, thermoelectrically cooled detector was 850 eV. The 200 eV FWHM barrier was broke in 1996 by the Amptek Si-PIN detector further selected to the Mars Pathfinder mission [17], and nowadays, manufacturers promise a resolution of 145 eV for Si-PIN and 125 eV for Si-drift detectors [81].

In order to characterize a detection system, it is also important to determine the fraction of the total number of photons emitted by the source, which actually interact in the detector volume and are completely absorbed, the **detection efficiency**. A first limitation to the detection efficiency arises from the limited active area of the detector and from the distance with respect to the source (*geometrical efficiency*). Moreover, the specific absorption coefficient of the detector material at a given photon energy and its thickness limit the number of photons which are actually absorbed (*intrinsic efficiency*). Finally, events that deposit only part of their energy in the detector do not contribute to the full energy peak in the spectrum (*photopeak efficiency*). [95] Fig. 2.13 shows the efficiency/transmission curves for the Amptek super SDD detector with Si thickness of 500 µm. We can see that the efficiency is over 90% between 3 and 5 keV and nearly 100% between 5 and 10 keV, then decreasing to 40% for 20 keV.
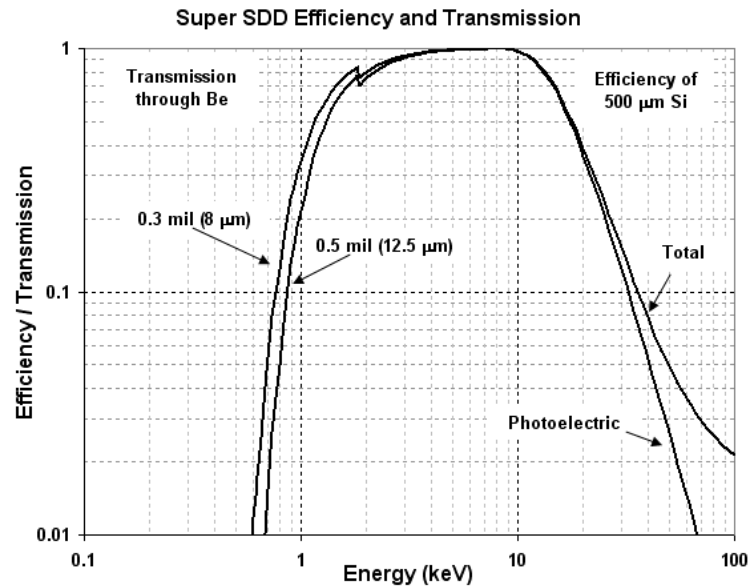
Fig. 2.13. Efficiency/transmission curves for the Amptek super SDD detector. [81]

Another important parameter characterizing a detector is its **sensitivity**, corresponding to the capability to produce a usable pulse for a given type of radiation and energy. This parameter depends on the following factors: the detector cross-section and the detector volume which determine the probability that the incident radiation will convert its energy into the detector; the detector window, that will absorb part of the incident radiation setting the lower limit of the energy that can be detected; the intrinsic detector noise that will determine the minimum amount of pulse producing an usable signal. [84]

2.6. Spectrum evaluation

To evaluate an X-ray spectrum it is necessary to understand all the phenomena that contribute to the final appearance of the spectrum. This includes not only the two main features, characteristic lines and background, but also a number of spectral artifacts.

The natural width of characteristic radiation of a particular X-ray line has a Lorentz distribution. Peak profiles observed with a semiconductor detector are the convolution of this Lorentz distribution with the nearly Gaussian detector response function, giving rise to what is known as a Voigt profile. Since the Lorentz width of K and L shell lines, is of the order of only 10 eV for elements with Z<50, whereas the width of the detector response function is of the order of 160 eV, a Gaussian function is an adequate first-order approximation of the line profile [98].

When the photoelectric events occur deep inside the detector, the characteristic detector material X-rays are reabsorbed and contribute to the full energy peak. However, for events which occur near the surface, there is a significant probability that the characteristic X-ray escapes and the corresponding amount of energy is lost from the signal. In the case of Si detectors, the **escape peak** will have the energy of the original peak minus 1.74 keV. **Incomplete charge collection** occurs when some of the electron-hole pairs are not swept to the electrical contacts, resulting in a charge signal measured lower than expected and, consequently, in an energy measurement lower than the energy of the incident X-ray and a tailing in the low energy side of the peak in the spectrum. These artifacts could be reduced by preventing the incident radiation from interacting in the periphery of the detector by means of collimation [79].

Other common spectral artifacts are **sum peaks**. These peaks arise from a specific form of peak pileup where two events from high-intensity peaks arrive in the pulse processing electronics so close together in time that the pileup inspector cannot recognize them as two events. The effect of this is for the signals to be seen as one and for them to be registered at the energy that is the sum of the two [79].

Typically, processing software packages such as WinAXIL® (windows version of **A**nalysis of **X**-ray spectra by **I**terative **L**east Squares) [99] and PyMCA® [100, 101] will take sum and escape peaks into account but they do not reinstate the lost intensity to the parent peak. In order to describe the low energy tailing due to incomplete charge collection, these packages can include a tail function to be incorporated to the Gaussian peak shape model [102].

The **background** is mainly due to coherent and incoherent scattering of the excitation radiation by the sample (2.2.1). The shape can be, therefore, very complex and depends both on the initial shape of the excitation spectrum and on the sample composition. Incomplete charge collection of intense fluorescence lines in the spectrum also complicates the background, the cumulative effect of the incomplete charge collection of all lines causes the apparent background at low energies to be significantly higher than expected on the basis of the primary background processes.

2.7. Quantification procedure

Quantitative analysis is used to obtain information about the relative amount of elements present in the sample in terms of their concentration. The most common method for quantitative determinations in XRF is the Fundamental Parameter method. This method is based on the following assumptions: i) all elements are equally distributed in the sample; ii) the intensity of the fluorescence X-ray radiation is proportional to the concentration of the measured element iii) the effects of other elements present in the sample can be calculated using known physical parameters and iv) measured intensity is dependent on the experimental configuration and measurement conditions [79, 103].

The intensity I_{P_i} of a characteristic peak of an element, i, is the result of primary fluorescence and inter-elemental effects. Primary fluorescence results from the direct effect of the incident beam or primary radiation on the element considered. Inter-elemental effects are related with secondary radiation produced by other elements in the sample. As characteristic radiation is emitted from the specimen, it is absorbed by all matrix elements by amounts relative to their mass attenuation coefficients. Depending on the energy of the primary beam and on the elements in the sample, this radiation can produce additional fluorescence in the element, which gives an enhanced signal from the sample [103]. The relationship between intensity and concentrations can be given by:

$$I_{P_i} = I_0 K_i m \, c_i A_i \qquad \text{(eq. 2.24)}$$

Where, I_0 is the primary intensity (incident beam), K_i is the calibration factor, c_i, is the concentration of the element, i, m is sample's mass per unit area (g cm^{-2}) and A_i the attenuation factor [104]. This last parameter is given by:

$$A_i = \frac{1 - e^{-\Sigma_j \, c_j \left[\frac{\frac{\mu}{\rho}(E_{1,j})}{sin\varphi_1} + \frac{\frac{\mu}{\rho}(E_{i,j})}{sin\varphi_2} \right] m}}{\Sigma_j \, c_j \left[\frac{\frac{\mu}{\rho}(E_{1,j})}{sin\varphi_1} + \frac{\frac{\mu}{\rho}(E_{i,j})}{sin\varphi_2} \right] m} \quad \text{and} \quad \Sigma_j \, c_j = 1 \text{ (eq. 2.25) [103]}$$

Where $\frac{\mu}{\rho}(E_{1,j})$ corresponds to the mass attenuation coefficient of the element, j, at the incident energy and $\frac{\mu}{\rho}(E_{i,j})$ stand for the mass attenuation coefficient for element, j, at characteristic energy for element, i. φ_1 nd φ_2 are the angles for incoming and emitted radiation from the sample.

The calibration factor, K_i, is given by:

$$K_i = \Omega \varepsilon_i C_i' \omega_i \sigma_{X_i} P_{L \to M} \quad \text{(eq. 2.26)}$$

Where σ_{X_i} is the cross section for producing characteristic radiation of an element, i, ω_i is the fluorescent yield for element i, $P_{L \to M}$ is the transition probability from level L to M in

element, i, C_i' is the absorption in air and detector window of the characteristic photons of element, i, ε_i the efficiency of the detector for element, i, and Ω the detector solid angle.

A simpler quantitative determination can be made using calibration lines with standard reference materials and ignoring the matrix effects. From eq. 2.23 a linear relationship can be seen between characteristic X-ray line intensity and elemental concentration, provided that there is no significant change in the attenuation factor. This means that, by matching the matrix of the calibration standards with the unknown specimen a direct correlation can be made between measured X-ray intensity and elemental composition [105]. This is the basis of the compare mode method of quantification of the WinAXIL© software package, which determines the sensitivity for each element by comparison with standard reference materials.

The major drawback of this method lies in the selection of the calibration standards, since they need to reflect the matrix and elemental composition of the unknown sample. Furthermore, we must also consider heterogeneity problems, insufficient precision in the collection of data, insufficient accuracy in the provided analyses of the standards and absorption or enhancement problems in the sample matrices [105].

2.8. Portable XRF equipments used in this work

Three portable XRF equipments were used in this work:

The **CFAUL-micro** XRF equipment consists Oxford XTF 5011 X-ray tube (87) with Mo anode (50 kV, 1 mA). The detector used was a Vortex-EX® SDD thermoelectrically cooled with a nominal area of 50 mm^2 and a Be window 12.5 µm thick (FWHM of 160 eV at Fe–Kα). The X-ray generator and detector were coupled to a vacuum chamber (10 mBar) in 45° geometry. The beam is focused by means of a poly-capillary lens by XOS [106] allowing a focal spot of 90 µm for the Fe-Kα (6.39 keV). The chamber also possesses a camera allowing the visualization of the analyzed area and thus the capture of the image and the spot of analysis, which was highlighted by the two lasers. The camera is sealed with removable Kapton® polymide film [107].
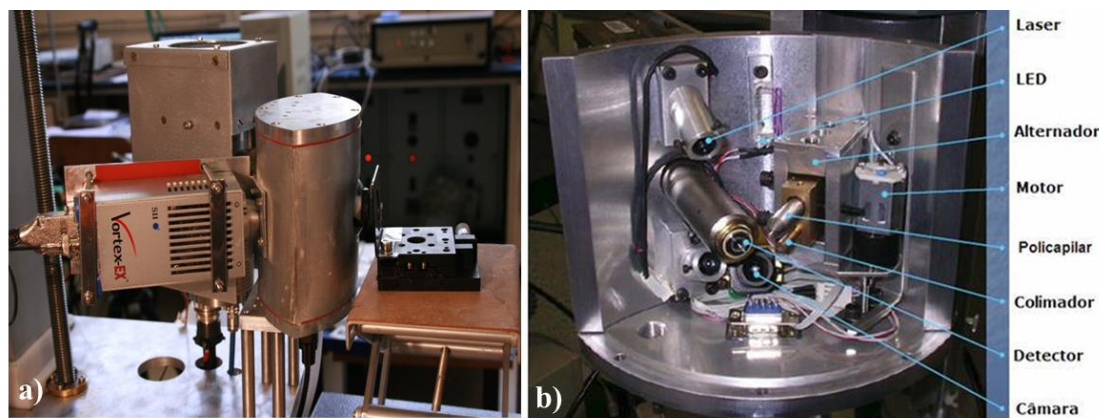
Fig. 2.14- a) Photography of CFAUL-micro setup; b) internal view of the vacuum chamber.

The **CFAUL-Eclipse II** equipment consists on a X-ray generator ECLIPSE II from Amptek (30 kV and 100 µA) with a Ag anode and an Amptek XR-100CR of Si-PIN thermoelectrically cooled detector with a 7 mm^2 detection area and 300 µm thick, and a 25 µm Be window. The energy resolution is 190 eV at 5.9 keV and the acquisition system is Amptek PMCA. For collimating the beam an acrylic support with a 2 mm pinhole in Ta was used and a spot size of 0.5 cm on the sample is obtained. The components are placed in an aluminum structure in 90 ° geometry and mounted on a tripod with 1.5 m vertical amplitude.

Fig. 2.15- a) Photography of CFAUL-eclipse II setup

The **CFAUL-eclipse IV** consists on a Amptek Eclipse IV X-ray generator with Rh anode (45 kV and 50 µA) and Amptek XR-100SDD with a 25 mm^2 detection area collimated down to 17.12 mm^2, 500 µm thickness (fully depleted) and a 12.5 µm Be window. The energy resolution is 140 eV at 5.9 keV. For collimating the beam a brass support with a 2 mm pinhole in Ta was used and a spot size of 0.5 cm on the sample is obtained. The components are placed in an aluminum structure in 90 °.
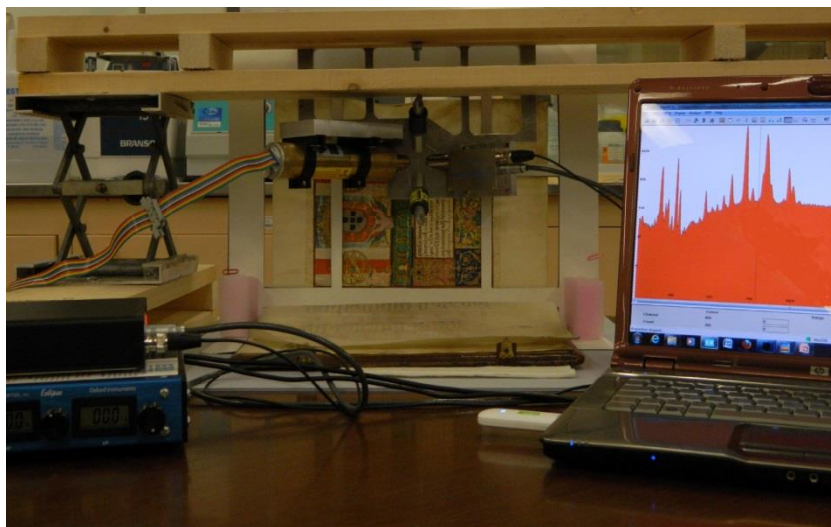
Fig. 2.16- a) Photography of CFAUL-eclipse IV setup

CHAPTER III – RAMAN SPECTROSCOPY

3. Raman spectroscopy

Raman spectroscopy has become an important analytical and research tool in material characterization in the field of Cultural Heritage. Raman spectroscopy is a light scattering technique, and can be thought of in its simplest form as a process where a photon of light interacts with a sample to produce scattered radiation of different wavelengths. In 1928, when Sir ChandrasekhraVenkata Raman discovered the Raman phenomenon, only crude instrumentation was available. Gradually, improvements in the various components took place and in the mid 1990's, a next generation of smaller, compact instruments started to evolve until portable, fiber optic assisted ones were available [108].

3.1. Basic principles of Raman spectroscopy

As discussed in the previous chapter, when monochromatic radiation is incident upon a sample it will interact with the sample by means of reflection, absorption and/or scattering. Raman spectroscopy is based on the scattering of monochromatic radiation when irradiated upon a sample. Light scattering phenomena may be described in terms of electromagnetic radiation produced by oscillating dipoles induced in the molecule by the electromagnetic fields of the incident radiation [109]. The induced dipole moment occurs as a result of the molecular **polarizability**, i.e., the ability of the electron cloud of a molecule to be distorted from its normal shape by an external field.

In a typical Raman experiment, a laser is used to irradiate the sample with monochromatic radiation. The incident photon is momentarily absorbed and a transition occurs to a virtual state, a short-lived distortion of the electron distribution by the electric field of the incident light, and a new photon is created and scattered [110]. If the transition occurs back to the ground state the process is called **Rayleigh scattering** and no energy is lost. **Raman scattering** is far less probable than Rayleigh scattering and results from a transition from the virtual state into an exited state of molecular vibration. Two types of Raman scattering exist: **Stokes** and **anti-Stokes** (Fig. 3.1). Molecules initially in the ground vibrational state give rise to Stokes Raman scattering, while molecules initially in vibrational excited states give rise to anti-Stokes Raman scattering. Since, at ambient temperature, most molecules are found in the ground state, the Stokes Raman lines are much more intense.
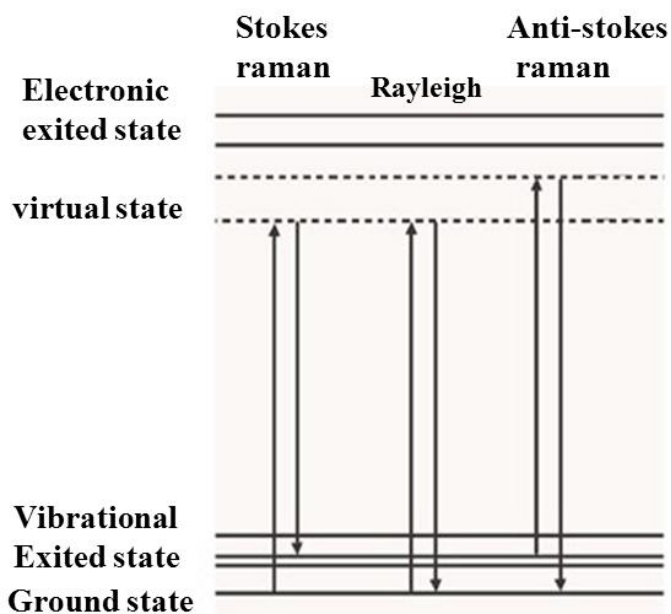
Fig. 3.1. Energy level diagram showing the states involved in Raman signal.

The incident photons will thus interact with the present molecule, and the amount of energy change (either lost or gained) by a photon is characteristic of the nature of each bond (vibration) present. Not all vibrations will be observable with Raman spectroscopy, only the ones which cause a change in polarizability are Raman active, but sufficient information is usually present to enable a very precise characterization of the molecular structure [109]. The symmetry of a molecule will define what vibrations are Raman active. In general, in-phase vibrations and non-polar groups are most easily studied.

A Raman spectrum consists of scattered intensity plotted vs. energy, as shown in Figure 3.2. Each peak corresponds to a given Raman shift from the incident light energy.
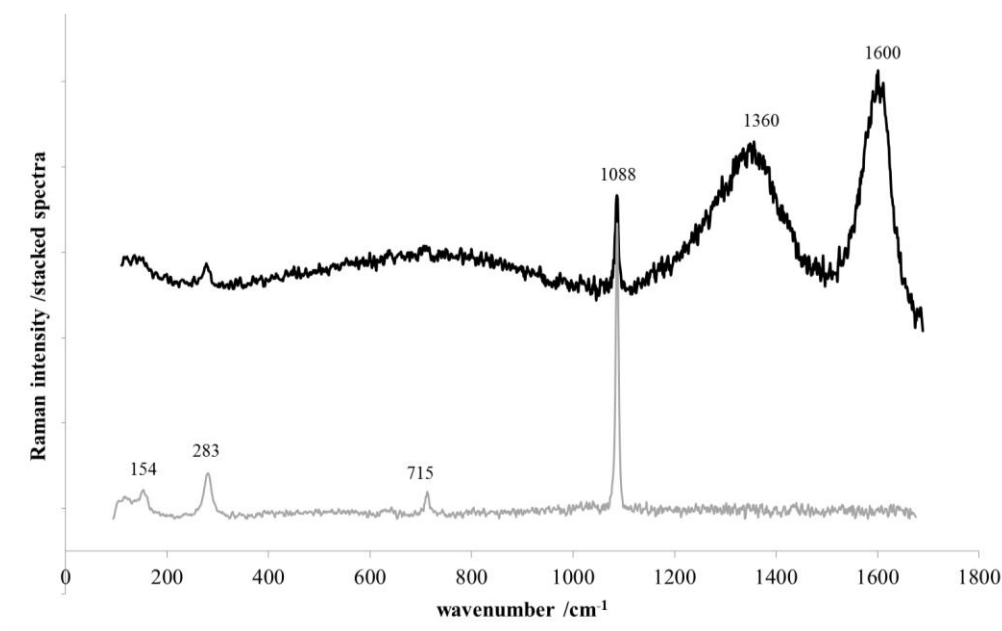
Fig. 3.2.- Raman spectra of pigments obtained with a 514 nm laser.

3.2. Raman Instrumentation

The most important feature of a Raman instrumentation is the capability of eliminating the overwhelmingly strong Rayleigh scattered radiation while analyzing the weak Raman scattered radiation. A Raman instrument typically consists of a laser excitation source (UV, visible, near-IR), collection optics, a monochromator and a detector. The choice of the optics material and the detector type will depend upon the laser excitation wavelength employed.

The most popular excitation sources in Raman spectrometry are continuous-wave (CW) lasers and diode lasers. **Diode lasers** can be obtained at specific wavelengths from the blue to the near-IR region, and their major advantage regarding other sources is their high efficiency with minimum power and cooling and their small size [108]. The correct selection of the laser wavelength is of great importance in Raman spectroscopy. The Raman scattering intensity is proportional to ν^4, where ν is the frequency of the exciting laser radiation, so excitation at 400 nm therefore leads to a 16 times higher Raman signal than excitation at 800 nm [111]. However, many samples, especially those of an organic nature such as paper or parchment, will be quite fluorescent species. Exciting these samples with a green laser (532 nm) may promote this fluorescence, and may swamp any underlying Raman spectrum to such an extent that it is no longer detectable. This way, the use of a red

laser (633 nm) or near-IR (785 nm) may provide a solution, because with the lower photon energy the electronic transition may not be promoted, hence the fluorescence, and so the Raman scatter may be far easier to detect. Conversely, as we increase the wavelength, from green to red to near-IR, the scattering efficiency will decrease, so longer integration times or higher power lasers may be required. Thus, it is often most practical to have a number of laser wavelengths available to match the various sample properties one may encounter.

Since the Raman scattering is inherently weak, the laser beam must be focused properly onto the sample and the scattered radiation collected efficiently. The most efficient way to do so is by coupling a standard optical microscope to a Raman spectrometer. Then we obtain high magnification visualization of the sample and Raman analysis with a microscopic spot. In a typical setup, laser radiation is focused on each grain via the microscope objective (up to 100x). The Raman scattering by the sample retraces the path of the incident beam, which is collected by the sample objective and directed to the monochromator and then to the detector [47]. The major drawback of using a microscope is the greater risk of heating the sample and thermally destroying it with an overly intense laser beam of at as one focuses the light to a microscopic spot.

A **monochromator** consists of an entrance slit, followed by a mirror to insure the light is parallel, a diffraction grating, a focusing mirror, which directs the dispersed radiation to the exit slit, and onto a detector. Polychromatic radiation is sorted spatially into monochromatic components using a diffraction grating to bend the radiation by an angle that varies with wavelength. The diffraction grating contains many parallel lines (or grooves) on a reflective planar or on a concave support that are spaced a distance similar to the wavelength of light to be analyzed. Incident radiation approaching the adjacent grooves in-phase is reflected with a path length difference and the path length difference depends upon the groove spacing, the angle of incidence (α), and the angle of reflectance of the radiation (β_1, β_2) (Fig.3.3) [109]
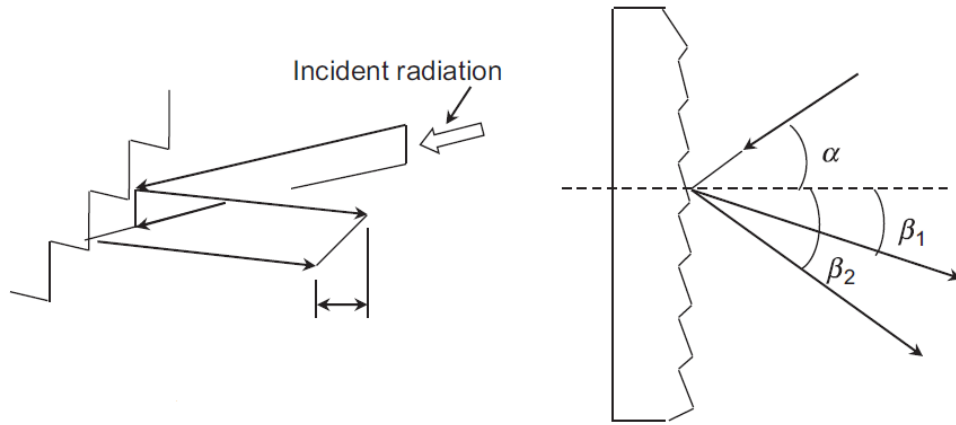
Fig. 3.3. Schematic of a diffraction grating.(110)

In the recent years, the most used detectors in Raman spectroscopy are **charge coupled devices** (CCDs) [36, 40, 72, 73]. A CCD detector consists of an array of light-sensitive Si-photodiodes, each connected to a capacitor. In the photodiode, every detected photon creates an electron-hole pair which is separated by the internal electric field and the electrons are stored in the capacitor. At the end of the measurement read out electronics pull the charge from the elements, at which point each individual charge reading is measured. CCD detectors are typically one dimensional (linear) or two dimensional (area) arrays of thousands or millions of individual detector elements (also known as pixels). The first element of the array will detect light from the low wavenumber edge of the spectrum, the second element will detect light from the next spectral position, and so on until the last element that detects light from the high wavenumber edge of the spectrum. The first important characteristic of the detector is its quantum efficiency (QE), which is the percentage of detected photons to total incoming photons. As the light sensitive area of a CCD is partially blocked by electrical interconnection lines, the QE of a typical (front-illuminated) detector is about 45% at 500 nm [108].

Spontaneous Raman scattering is very weak, so the main difficulty of Raman spectroscopy is separating it from the intense Rayleigh scattering. More precisely, the major problem here is not the Rayleigh scattering itself, but the fact that the intensity of stray light from the Rayleigh scattering may greatly exceed the intensity of the useful Raman signal in the close proximity to the laser wavelength. In many cases the problem is resolved by simply cutting off the spectral range close to the laser line using interference (notch) filters which cut-off

spectral range of ± 80-120 cm^{-1} from the laser line. This method is efficient in stray light elimination but it does not allow detection of low-frequency Raman modes in the range below 100 cm^{-1}.

3.2.1. The Raman confocal microscope

Spatial resolution can be improved by making use of confocal geometries. Confocal microscopy offers several advantages over conventional wide-field optical microscopy, including the ability to control depth of field, elimination or reduction of background information away from the focal plane, and the capability to collect serial **optical sections** from thick specimens.

Traditional confocal Raman microscopes use a pinhole aperture placed before the input slit of the monochromator. The Raman scattering is focused onto the pinhole, and the diverging beam after the pinhole is then refocused onto the input slit of the monochromator. Different pinhole apertures can be used to control the degree of confocality, whereas the input slit is used to control the spectral resolution (Fig.3.3) [111].
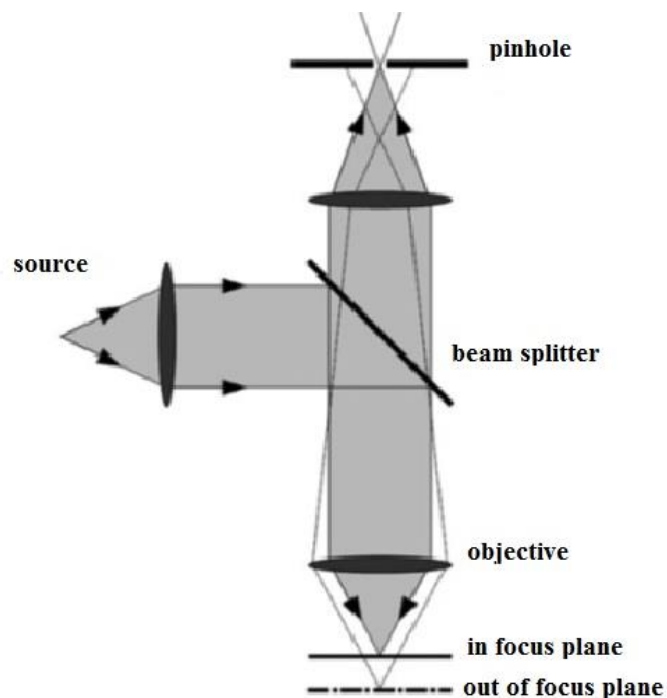
Fig. 3.4. Confocal raman representation [111].

Advances in instrumentation for generating, sorting, and detecting Raman scattered light have overcome many of the limitations. These obstacles included the intrinsic weakness of the Raman scattering phenomenon, the scale and cost of the requisite instrumentation, and the tendency of the weak Raman signal to be overwhelmed by broadband fluorescence from some samples. The introduction of high throughput optical configurations, efficient Rayleigh rejection filters and high quantum yield CCD detectors have improved tremendously the sensitivity of modern Raman instruments while simultaneously reduced reducing their cost.

3.3. Raman confocal microscopes used in this work

At CFAUL facilities, measurements were made using a Horiba-Jobin Yvon Xplora® confocal spectrometer [71], equipped with three laser diode sources operating at 532 nm, 638 nm and 785 nm the power on the samples was reduced with neutral density filters up to 1 mW. The scattered light collected by the objective was dispersed onto an air cooled CCD array by 1200 or 1800 grooves/mm grating, a pinhole of 300 µm and an entrance slit of 100 µm were used. Spectra were collected using both 50× and 100× objectives. The average spectral resolution was of 7 cm^{-1}.
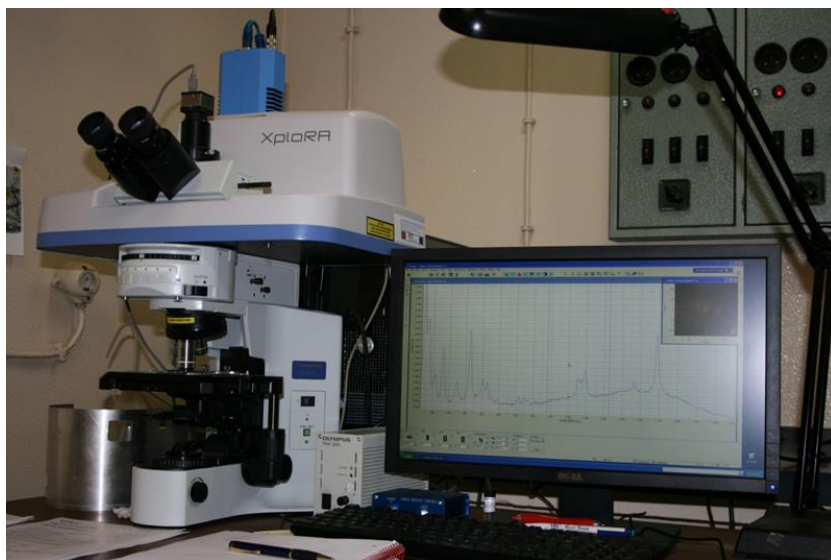
Fig. 3.5. XploRA Confocal raman microscope at CFAUL.

At ISM-CRNS a Dilor-Jobin Yvon LabRam 1B spectrometer equipped with an Olympus BH2 microscope system in a confocal geometry was used. A Spectra Physics argon–krypton model 2018 laser (514.5 nm) was used and the power on the samples was reduced with neutral density filters up to 2.5 mW. The scattered light collected by the objective was dispersed onto an air-cooled CCD array by a 1800 grooves/mm grating giving an spectral resolution of 4 cm^{-1}. Depending on the experiment, a 50× or a 100× objective was used and the confocal aperture was adjusted to 420 or 700 μm.

Fig. 3.6. Dilor-Jobin Yvon LabRam [112].

CHAPTER IV – μ-XRF IN THE STUDY OF PAPER DISCOLORATIONS

4. μ-XRF IN THE STUDY OF PAPER DISCOLORATIONS

4.1. Experimental

4.1.1. . μ-XRF equipmentt

The equipment used in the following case studies was described in section II as CFAUL-micro and has the major advantage of allowing the focusing of the x-ray beam in a spot size of 90 µm by means of a polycapillary focusing lens (Fig. 4.1). Furthermore, taking advantage of the vacuum chamber, there are only 5 mm of air path to the sample, which decreases substantially the detection limits for lighter Z elements.

Fig. 4.1 – Photography of the CFAUL-micro setup, *in situ*, at the laboratory adjacent to Museu Nacional de Arte Antiga.

4.1.2. Detection limits

The detection limits (DL) by EDXRF, were calculated according to the widely used expression:

$$DL = \frac{3C_i\sqrt{n_B}}{n_P} \qquad \text{(eq. 4.1) [113]}$$

Where, C_i is the concentration of the element i;

n_B is the counting rate for the background;

n_P is the counting rate for the corresponding peak.

The results for orchard leaves (NBS standard reference material 1571) are presented in Table 4.1.1:

Table 4.1.1. Detection limits ($\mu g.g^{-1}$) obtained by EDXRF in orchard leaves, NBS standard reference material 1571.

	P	S	Cl	K	Ca	Mn	Fe	Cu	Zn
DL	63	23	31	71	88	2	5	2	2

4.1.3. Quantification procedure

The spectra deconvolution and fitting were performed using WinAXIL® software package and quantification was performed through compare mode method (section 2.7).

Four Standard Reference Materials with identical matrix and elemental composition were analyzed under the same experimental conditions, hence the calibration and attenuation factors in equation 2.24 can be disregarded. The software determines the sensitivity for each element and provides quantification.

Three Standard Reference materials (Poplar leaves GBW 07604; Bush branches GBW 07603; Tea leaves GBW 07605) were used to configure the method and the accuracy was checked by analyzing a fourth Standard Reference Material orchard leaves NBS1571. Results are presented in table 4.1.2.

Table 4.1.2. Mean elemental concentration and standard deviation ($\mu g.g^{-1}$) obtained in this work for orchard leaves NBS1571 and certified values.

	P	S	Cl	K	Ca	Mn	Fe	Zn	Cu
Present work	2300± 400	3000± 1000	760± 90	16000± 2000	18000± 3000	80±10	260±60	19±7	8±2
Certified value	2100± 100	2300± 100	700± 10	14700± 300	20900± 300	91±4	300±20	25±3	12±1

4.2. Characterization of foxing stains in 18th-19th century drawings

4.2.1. Introduction

Foxing on paper has been actively researched since the 1930's by scientists and conservators to elucidate its causes and to establish protocols for recognition, prevention
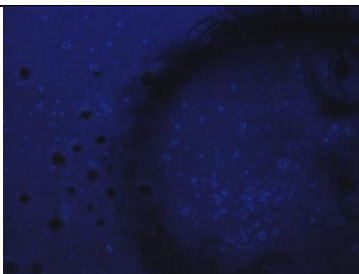
and treatment. Foxing is a term used to describe a large range of damage and discoloration in paper, and generally refers to small, roundish spot stains of reddish brown color, with sharp or irregular edges. Although the causes of foxing are not yet completely understood, they are usually ascribed to mold growth and/or heavy-metal-induced degradation of cellulose and sizing. Metal has been considered one of the major causes of foxing. It may arise either from the papermaking process or from airborne dust [114]. Metals found in foxing spots include Fe, Sn, Cu, Cu-Hg or Cu-Zn, and were typically identified using scanning electron microscopy coupled to energy dispersive spectrometry (SEM-EDS), X-ray fluorescence (XRF) and atomic absorption spectroscopy analysis (AAS) [114-116]. Fungal infection of foxing had been reported as early as 1917. Published research making use of light microscopy and SEM for examining foxing, visually proved the presence of fungi in the affected areas [117, 118], however it is still difficult to determine whether mold is the causal agent of degradation or if the mold growth is opportunistic in nature, taking advantage of the weakening of paper due to chemical factors. In an early stage of formation, the foxing stain can be recognized by the detection of UV fluorescence (Table 4.2.1). As foxing formation progresses, UV fluorescence decreases and the visible rust color increases instead [114, 119]. In order to study the influence of the presence of metals in foxing stains several paper documents from the 18th and 19th centuries were analyzed using μ-EDXRF. The microanalysis is crucial in this application because the diameter of the stains is in the 1mm order of magnitude. The documents were analyzed in the laboratory for conservation adjacent to Museu Nacional de Arte Antiga (MNAA), this way they were always stored in the appropriate conditions.

4.2.2. Specimen description

Foxing stains were studied in fourteen drawings, eleven belong to the artist Domingos Sequeira (1768-1823) while the remaining three belong to the artist Cirilo Wolkmar Machado (1748-1823). The fourteen drawings had been subdivided into four groups according to paper texture and tone (Table 4.2.1): groups A and B are respectively composed of four tinted brownish-green and five tinted brown-reddish medium thick wove papers from Domingos Sequeira. These nine drawings depict the 1810 royal court representatives. Group C, also belonging to Domingos Sequeira, is composed of two cream

white wove papers that present a strong discoloration in some of its areas suggesting having been in contact with extremely high temperatures through the contact of a glazing glass and dating from 1796. Cirilo's drawings date from 1798 (group D) and were executed on thin white laid paper.

Table 4.2.1. Batches of the studied papers grouped according to tone and texture. Image details from drawings in bold are shown under normal and UV light.

Groups of drawings	Tone	Image detail in under normal light showing the paper and foxing tones	Image detail under UV light
Group A Inv. 1613 Inv. 1617 Inv. 1624 **Inv. 1625**	Brown-green paper		
Group B Inv. 1603 Inv. 1604 Inv. 1605 **Inv. 1615** Inv. 1620	Brown-red paper		
Group C Inv. 1924 **Inv. 1925**	Cream paper		
Group D **Inv. 2945** Inv. 2946 Inv. 2947	White paper		

4.2.3. Results

Quantitative elemental analysis of the paper areas distributed the drawings in batches, according to the similarities of their elemental composition, as can be seen on the dendrogram in Fig. 4.2.1. The hierarchical cluster analysis was obtained using *Statistica 8* and single linkage method and Euclidian distances were used. According to this analysis, the 14 papers were grouped into five clusters (A1, A2, B, C and D) meaning that group A was divided in two groups, being the elemental composition of group A2 more similar to group B.
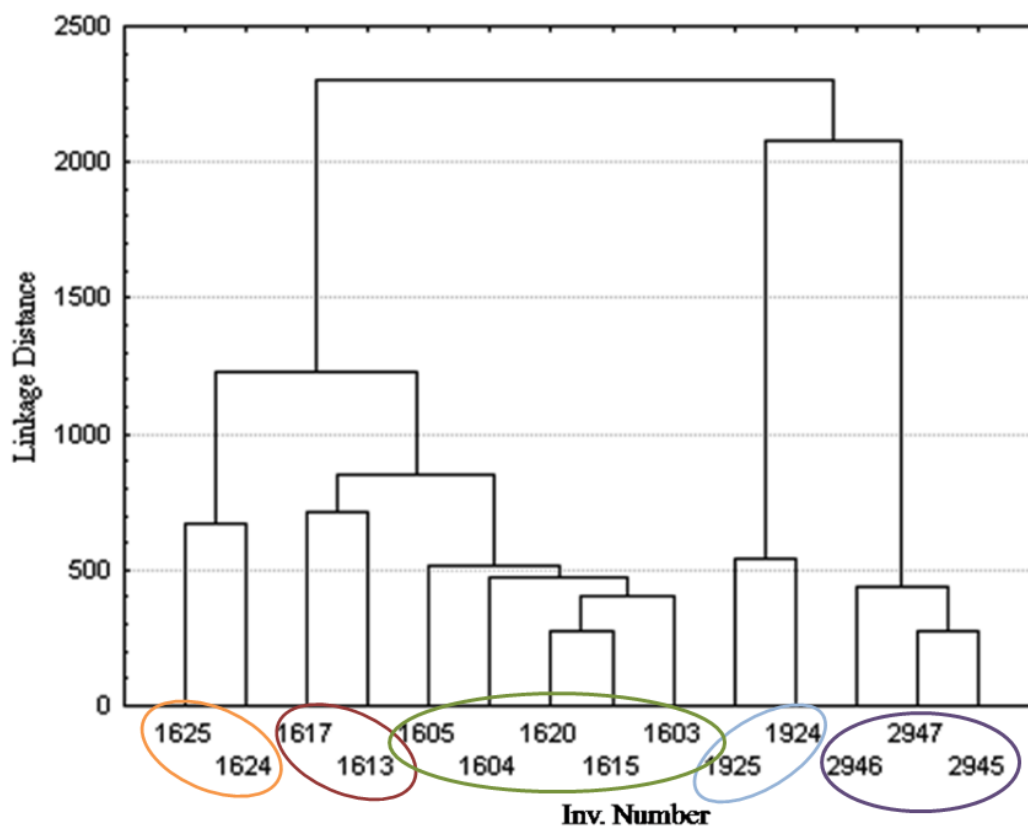
Fig. 4.2.1. Batches of paper according to their elemental composition.

Table 4.2.1 presents the results obtained when comparing the elemental composition of foxing stains and unstained paper (in an adjacent area). The levels of Al, Si, P, S, Mn and Fe between stain and unstained area in paper are similar. This result was interesting, as an

increase of Fe was expected by the paper conservators that collaborated in the work. High Ca levels were already expected in paper and not directly related to foxing stains.

Table 4.2.1. Mean elemental concentration ($\mu g.g^{-1}$) and standard deviation for unstained paper and foxing stain present in the studied drawings.

Sample	Group A1		Group A2		Group B	
Description	Paper	Foxing	Paper	Foxing	Paper	Foxing
Al	2000±400	2500±400	1400±280	1500±300	1400±280	1600±300
Si	2500±500	2400±450	1900±350	2200±400	2800±500	3000±600
P	600±100	600±100	700±100	900±100	700±100	600±100
S	2100±400	2200±450	2300±400	2100±400	2000±400	2100±400
Cl	BDL	BDL	BDL	BDL	BDL	BDL
K	800±100	1800±200	1100±100	1700±200	810±100	1000±100
Ca	1300±200	1500±200	1100±200	900±100	1000±200	900±100
Mn	30±5	30±5	20±3	25±4	40±5	50±8
Fe	2800±500	2700±500	1900±380	2000±400	1000±200	1300±200
Cu	40±5	40±5	25±5	25±5	20±4	30±6

Table 4.2.1 (cont.). Mean elemental concentration ($\mu g.g^{-1}$) and standard deviation for unstained paper and foxing stain present in the studied drawings.

Sample	Group C		Group D	
Description	Paper	Foxing	Paper	Foxing
Al	1000±200	1100±200	600±100	600±100
Si	1200±200	1000±200	1800±300	2000±400
P	340±60	330±50	600±90	600±100
S	1900±380	1900±380	1900±350	1900±350
Cl	720±80	BDL	1000±100	BDL
K	260±30	190±20	80±10	580±70
Ca	4000±600	4100±600	2100±300	3100±500
Mn	14±2	11±2	BDL	BDL
Fe	50±10	40±8	40±8	50±10
Cu	BDL	BDL	BDL	BDL

More interestingly, results showed that whenever Cl was present in paper (group C and D) it tended to disappear in the stains (Fig. 4.2.2). Potassium revealed a different behavior between groups of drawings. While in group B and C its concentration in paper and stain remained fairly constant, in groups A1, A2 and D it has shown a remarkable growth in the stain. A similar behavior was already witnessed by Manso et al. [120] when studying artificial aged model papers by cellulosomes, *Clostridium cellulolyticum* were the increase of K levels was accompanied by an intense decrease of Cl levels. Bicchieri et al. [115] also reported an increase of K values in foxing stains when compared to paper unstained areas in 17th century documents.
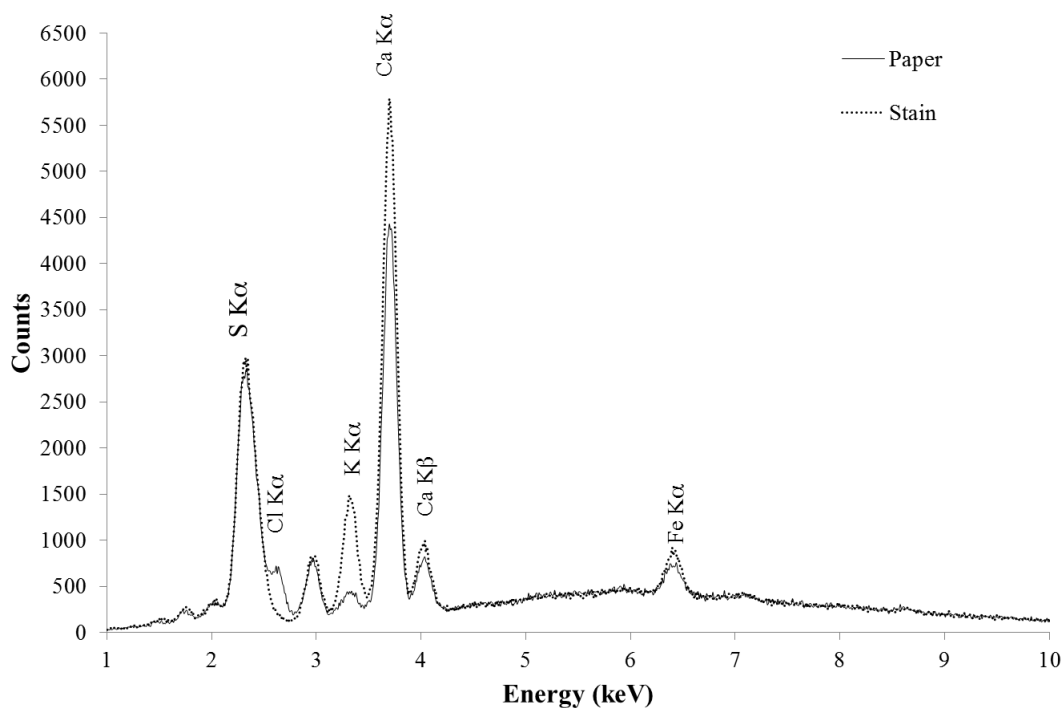
Fig. 4.2.2. Comparison of the μ-EDXRF spectra obtained from foxed and unstained spots of drawing Inv. 2945. Spectra were acquired at 40 kV and 0.5 mA during 300s.

4.3. Study of air induced paper discolorations by μ-EDXRF

4.3.1. Introduction

Air-induced paper discoloration is described as being different from other discoloration morphologies. It seems to be the result of prolonged exposure to air in a humid and polluted environment without appropriate protecting coverage. In this work, three folios from the same 18th century book presenting three degrees of discoloration and opacity and subjected to different environmental conditions were examined and its elemental composition was compared.

4.3.2. Specimen description

The paper samples in this case study are three folios belonging to an unbounded and incomplete *Glossarium* printed in 1766, donated in 1983 by the Portuguese National Library for experimental conservation treatments. The folios designated as A, B and C are rag, gelatin sized handmade papers (Figs. 4.3.1). From 1983 to 1997, the folios were stored in different environments and were not submitted to any type of treatment. Folio A which exhibits a light tone was protected by a folder of tracing paper inside a metal archive drawer. Folio C which corresponds to the brown paper, was shown in 1986 during a six month exhibition, as an example of a document extremely attacked by insects. It was secured with metal pins onto white painted low density fiberboard. No glass was present. It is interesting to note that the exhibition room was located next to a heavy traffic street with no trees and a narrow sidewalk. After the exhibition, folio C remained in the same position, in the same room, in total darkness, for at least another year and remained in the same exhibition board, unprotected from the direct contact with air, for another 10 years in a dim corridor of the building. Folio B was exhibited inside a showcase in the same exhibition room as folio C and followed the same time path except for the last 10 years, when it was returned to its folder in a metal drawer cabinet.

Comparing the three folios by means of optical properties, it is possible to see that folio A after remaining inside a drawer is non-oxidized and retains its original cream color while folio C, which had been in direct contact with air, in the conditions stated above, not only

became very brown but also acquired a gain in opacity. Folio B also seems oxidized although its tone is mildly intense when compared with the tone presented by C.

Fig. 4.3.1. Photography of folios A, B e C under normal light.

4.3.3. Results

The mean elemental concentrations of Al, Si, K, S, Ca, Mn and Fe for the three folios are presented in table 4.3.1.

Table 4.3.1. Mean elemental concentration ($\mu g.g^{-1}$) and standard deviation for the three studied folios.

	A	B	C
Element	Mean ± SD	Mean ± SD	Mean ± SD
Al	2480± 420	2250± 150	2600± 100
Si	4500± 600	4400± 700	5500± 500
P	1200± 100	1400± 100	1300± 100
S	3000± 100	3000± 100	3000± 100
K	250± 50	400± 50	400± 80
Ca	1250± 250	1100± 100	1100± 1000
Mn	60± 10	50± 10	60± 10
Fe	70± 10	80± 10	70± 10

A slight increase of the K content was again observed for the stained folios (B and C) when compared with folio A (Fig. 4.3.2). This behavior is similar to the one described in the previous case study, although the staining agent was different.

No other elemental variation was found, namely for Ca, leading us to believe that the formation of gypsum was due to a rearrangement of the elements that constituted the paper.
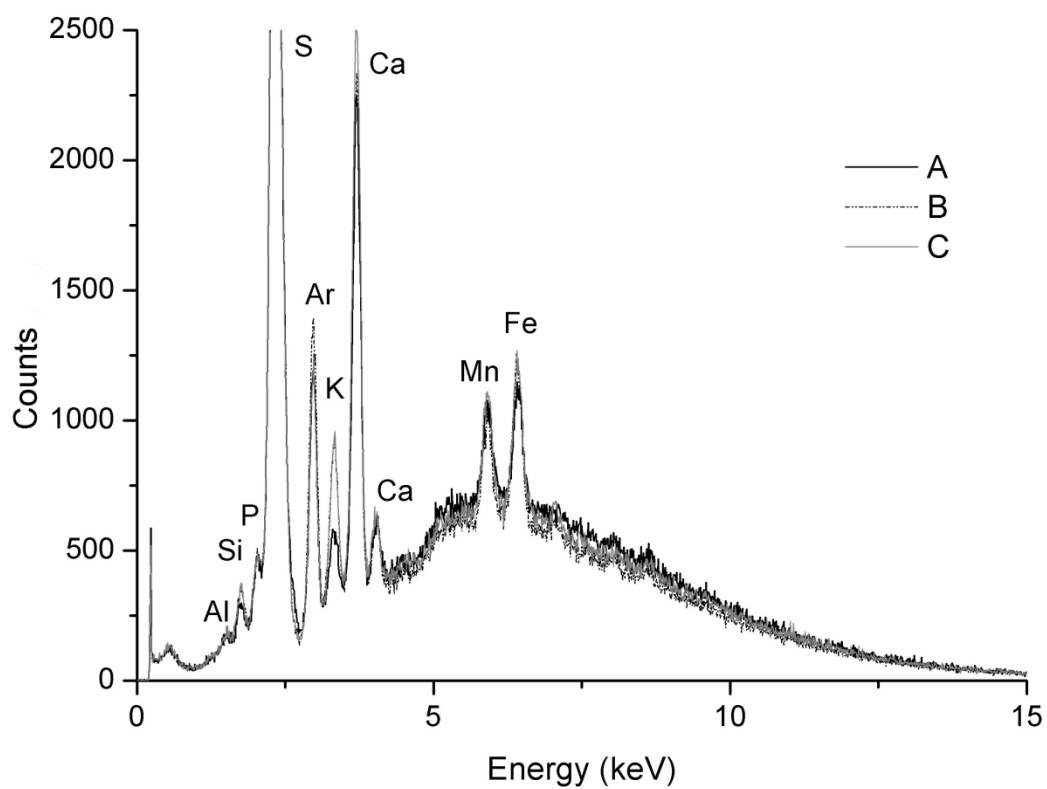
Fig. 4.3.2. Comparion of the EDXRF spectra obtained for the three folios. Spectra were acquired at 40 kV and 1 mA during 300s.

CHAPTER V. MATERIAL CHARACTERIZATION OF NAMBAN FOLDING SCREENS

5. MATERIAL CHARACTERIZATION OF NAMBAN FOLDING SCREENS USING PORTABLE XRF AND RAMAN SPECTROSCOPY

5.1. Experimental

5.1.1. X-Ray Fluorescence

The XRF equipment used in the following case studies was described in section II as CFAUL-eclipse II (Fig. 5.1.1) and has the major advantage of being very light and very easy to assemble. The spot size of 0.5 cm is perfectly suitable and no micro analysis was necessary because the characters and features are in the centimeter scale. Furthermore, we took advantage of the 90º geometry to reduce bremsstrahlung and Compton scattering. Measurements were performed in all extension of the screens adding up to more than 550 measurements in 9 screens.

Fig. 5.1.1 – Photography of the CFAUL-portable setup, *in situ*, at Museu Nacional de Arte Antiga

5.1.2. Raman spectroscopy

The Raman confocal microscopes used in these case studies were described in section III as CFAUL-XploRA and ISM-CRNS-LabRam.

After a thorough scan of the screens using XRF, an educated and aware choice of sampling areas was made in order to ensure the representativeness of the Raman measurements. The number of samples collected varied from screen, but an average of 15 samples were collected from each screen/pair and Raman analyses were performed directly on each sample.

Fig. 5.1.2 – Photography of the micro-sampling process, using a surgical scalpel, carried out by an expert.

5.2. Introduction

Namban is the art style inspired by the arrival of the Portuguese sailors to Japan and the commercial trade then initiated. The contacts established between Portugal and Japan from 1543 onwards, were characterized by a climate of cordiality and the development of common interests between the two cultures [121]. It was in such a context that these screens were commissioned, recording the special atmosphere of festivity and novelty that was represented by the arrival of the black boat of the namban jin (the barbarians from the south, as the Portuguese were known), at the port of Nagasaki. The great care and attention to detail with which all the different people are represented, the depiction of the ship and its

precious cargo, and above all the decisive presence of the Jesuit missionaries, elevated these screens to a level of meaning far beyond that of a simple visual record, making these pieces a unique document in the context of Portuguese-Japanese relations [122]. A recent survey by a team of scholars based at the National Museum of Japanese History has catalogued 92 surviving examples distributed among collections in Japan, Europe and the United States [122]. According to Japanese specialist Tadao Takamizawa, there are three types of compositions for the Namban screens: the first and most widespread one, referred as type A, portrays, in the left screen, a portuguese *nao*, anchored and unloading in an Japanese port (probably Nagasaki), paired in the right screen with a procession of the ship's captain and his entourage through the port town and their encounter with Jesuit priests. Type B, the second template for Namban screens, essencially combines the two scenes of the type A formula in the right screen, compressing into six panels the arrival of a portuguese ship in a Japanese port and an ensuing encounter between its traders and missionaries on land. It matches this with a left screen that portrays the same ship leaving a foreign port. Type C screens follows this same arc, but while it combines depictions of the Portuguese ship and procession in the right screen, it pairs this combination in the left screen with the imagined activities of southern barbarians in their homeland, ranging from formal gatherings to some leisure activities [123]:

Folding screens, called *byobu*, have been used by the Japanese for hundreds of years to create intimate spaces, as room dividers, as well as add beauty to any room. Traditional *byobu* are usually two to six panel screens made of paper with a lacquered wood edge [124, 125]. A wooden lattice core is covered on both sides with layers of baste fiber paper from the paper mulberry varying in weight, sheet size and configuration in a prescribed order using wheat starch paste. With the multiple layers mounted under tension, the surface is sufficiently rigid to support the paint layers [126]. Before painting is executed, the paper support may be prepared in a number of ways, which include sizing, beating, dyeing, application of grounds and application of metal leafs. Usually Japanese screens have large areas of gold leaf as part of the design "field", and this might also be regarded as a further method of decorating the support [127].

5.3. The Namban folding screens at Museu Nacional de Arte Antiga (see ANNEX)

5.3.1. Specimen description

There are two pairs of Namban screens at Museu Nacional de Art Antiga (MNAA) (Figs. 5.3.1). The first pair of screens, a type B screen (Fig. 5.3.1a), is marked with the seal of the painter Kano Naizen (1570-1616). The story is narrated from left to right, showing the preparations for the departure of the ship from a port that is supposed to be Goa, an intention that is underlined by the representation of elephants and another type of architecture. In the second screen, a representation of the ship's arrival at the port of Nagasaki, and the disembarkation of its precious goods, depicted in great detail can be seen. The Chinese silks can be perfectly identified, as well as the exotic animals and all the other products traded by the Portuguese at various points around the Far East, transported in a procession that is headed by the ship's "capitão-mor". Further to the right, members of various missionary orders have gathered in front of a church to await the arrival of this committee [128]. The second pair of screens, belonging to type A (Fig. 5.3.1b) and attributed to the painter Kano Domi (1568-1600), again the black ship is seen docking to Nagasaki port in the left-hand screen, while trading negotiations are being conducted aboard, whilst on land the unloading of the precious cargo is being carefully supervised. In the right-hand screen, the procession led by the ships' commander can be seen walking in the direction of the house of the Jesuits. This is followed by a group of people dressed in rich costumes, and the parade also contains representations of the Chinese litter, exotic animals and the famous glazed pots used for transporting spices. The exhibition "Encompassing the Globe- Portugal and the world in the 16th and 17th centuries" produced by the Smithsonian Institution, in Washington DC, was held between June and September 2007. This exhibition, of about 200 pieces proceeding from several of the most prestige collections, travelled the world and was held at MNAA in Lisbon in 2009. This prompted the interest of performing, for the first time, the material characterization of these two pairs of Namban folding screens that were the central pieces of the exhibition. Furthermore, the museum curator in charge of the exhibition had concerns regarding the manufacture of the screens, namely if they were completely covered with gold leaf prior to the application of the paint layers.

Fig. 5.3.1- Photographies of the screens belonging to MNAA collection a) signed by Kano Naizen b) attributed to Kano Domi. Sampling areas for Raman spectroscopy are also marked.

5.3.2. Results

The pigments found in both pairs of screens were very similar. The presence of Cu in the XRF spectra (Fig. 5.3.2 a) of both green and blue areas indicated the use of copper carbonate pigments, such as malachite ($CuCO_3Cu(OH)_2$) and azurite ($Cu(OH)_2.2CuCO_3$), respectively. The confirmation on the use of Malachite was obtained through Raman analysis, by means of the characteristic bands at 153, 179, 220, 271, 350, 432, 509, 1063, 1098 and 1492 cm^{-1} [42]. Furthermore, the characteristic bands of indigo dye ($C_{16}H_{10}N_2O_2$) at 252, 545, 598, 759, 1250, 1310, 1361, 1454, 1584 and 1698 cm^{-1} [129] were found in the Raman spectrum obtained from a blue micro-sample (Fig. 6.3.2 b).
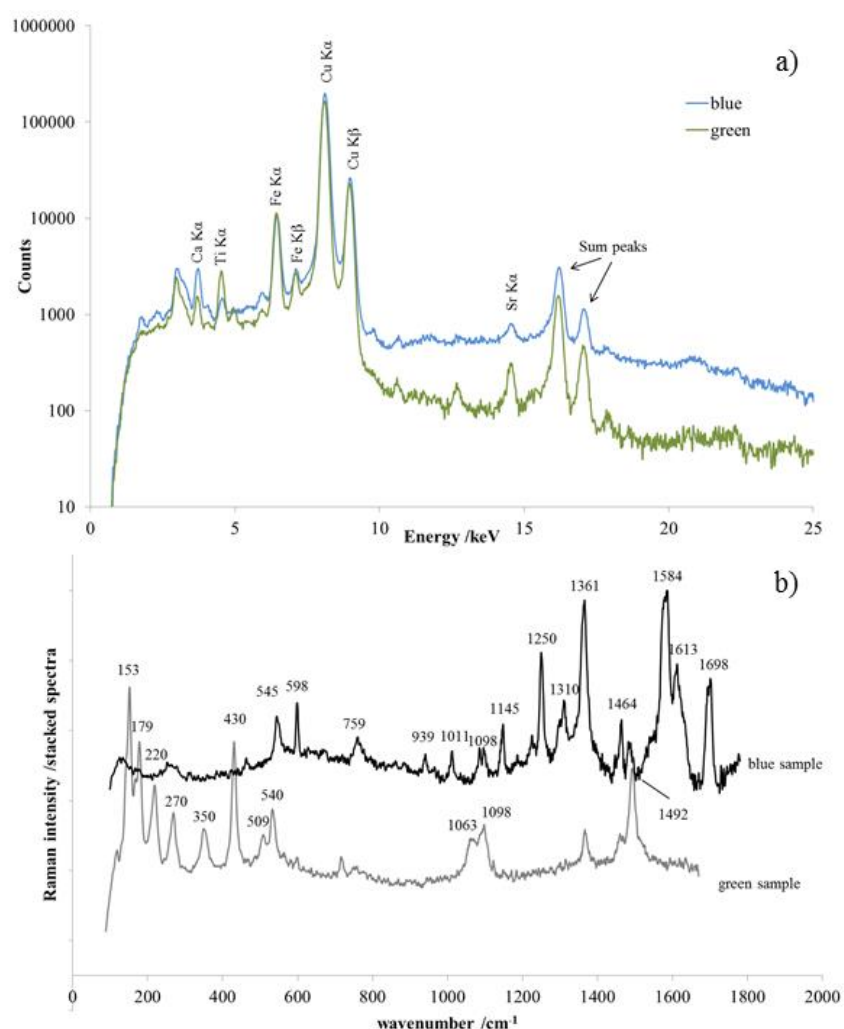
Fig. 5.3.2 – a) Comparison of XRF spectra obtained for blue (Kano Naizen) and green (Kano Domi) areas of the screens. Spectra acquired at 30 kV, 100μA during 300s. b) Raman spectra obtained for blue and green samples collected from Kano Naizen's screens. Spectra obtained with the 514 nm laser, 420 μm, hole, 100 μm slit, 50x objective during 30s.

There XRF spectra obtained for the red areas presented two different elemental compositions: the most common presented the high amounts of Hg indicative of the use of vermillion (HgS), while a lighter shade presented Pb instead of Hg (Fig. 6.3.3. a). The existence of red lead (Pb_3O_4) in the second shade of red was confirmed be the presence of a strong band at 550 cm^{-1} followed by bands at 478, 391, 315, 228 and 120 cm^{-1}, [42] characteristic of red lead found in the Raman spectrum of the sample (Fig. 5.3.3.b). No good spectrum of vermillion was obtained.
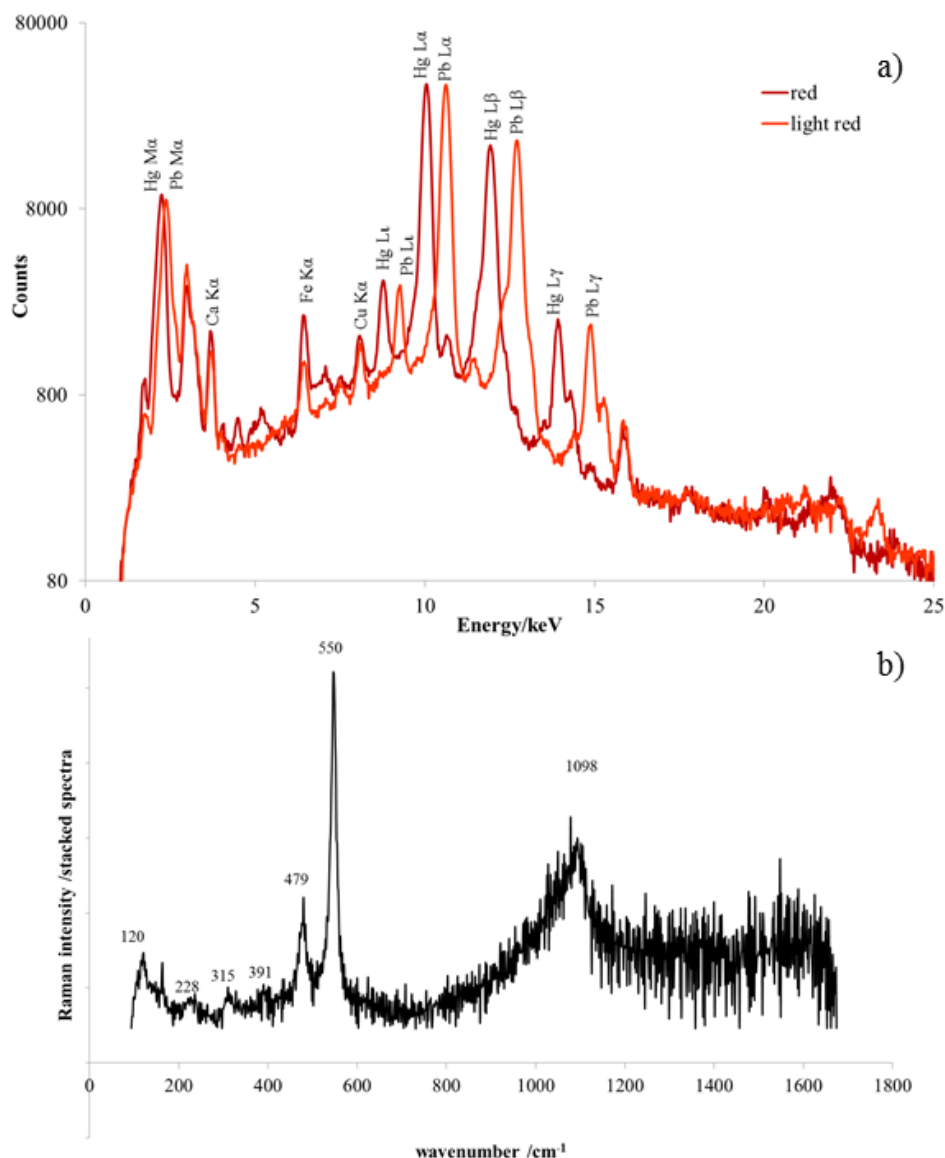
Fig. 5.3.3 Comparison of the XRF spectra obtained for different shades of red. Spectra acquired at 30 kV, 100µA during 300s. b) Raman spectrum obtained for a bright red (Kano Domi) micro-sample. Spectra obtained with the 514 nm laser, 420 µm, hole, 100 µm slit, 10x objective during 50s.

The XRF spectra obtained for all the white areas in both screens revealed essentially the presence of Ca (Fig. 5.3.4a). Calcium carbonate ($CaCO_3$) was unequivocally detected by a very strong peak at 1088 cm^{-1} [42] in the Raman spectrum of the micro-sample (Fig. 5.3.4.b). Until the 15th century, clay was always used as the white pigment for paintings, but between the 15th and 16th centuries, powdered oyster shell took the place of clay and continued to be used throughout the Edo period until today. In fact, Japan seems to be the only country that has used oyster shell as a white pigment, leading us to believe this was the case of the white pigment in the screens [130]. Regarding the black areas, the Raman spectrum obtained for a black micro-sample revealed two broad bands at approximately 1360 and 1600 cm^{-1}, that are characteristic of black pigments made up of disordered carbon, such as charcoal or bone black (Fig. 5.3.4 b). The spectrum also presents a strong band at 1086 cm^{-1} together with bands at 153 and 277 cm^{-1} attributed to $CaCO_3$, which may occur as an impurity of carbon black [131], and explain the high amount of Ca encountered in the black areas in the XRF analysis.
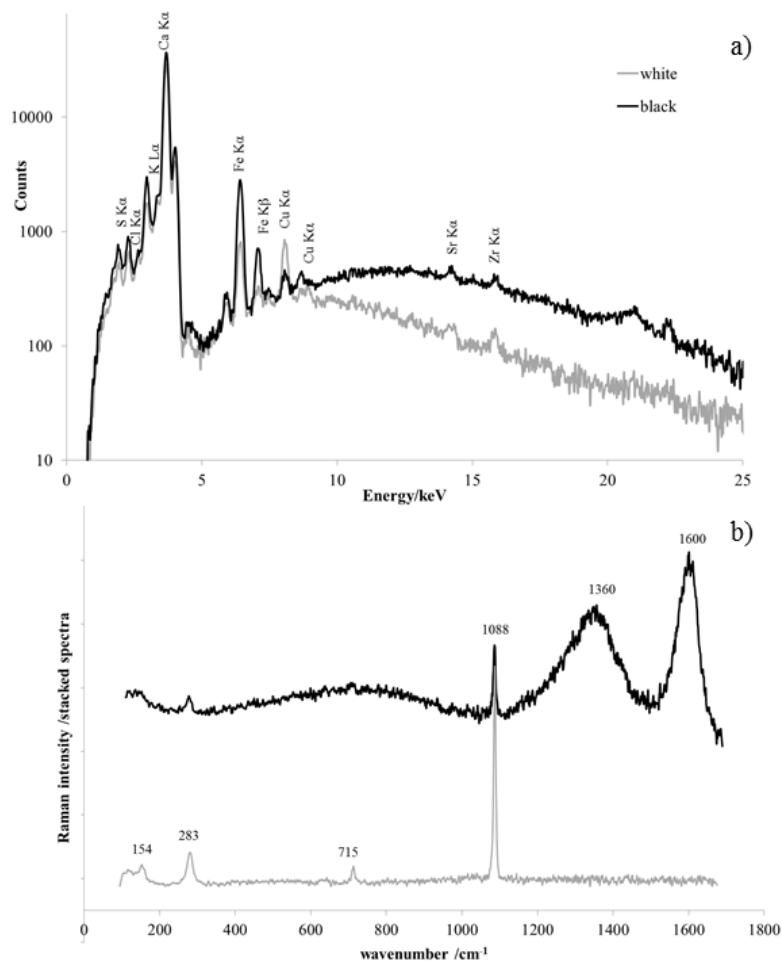
Fig. 5.3.4. a) XRF spectra obtained for black (Kano Domi) and white (Kano Naizen) areas of the screens. Spectra acquired at 30 kV and 100 µA during 300s. b) Raman spectra obtained for black (Kano Naizen) and white (Kano Naizen) micro-samples. Spectra obtained with the 514 nm laser, 420 µm, hole, 100 µm slit, 50x objective during 60 and 25s, respectively.

As expected, precious materials such as gold and silver were found in the screens (Fig. 5.3.5 a). Silver was found in several XRF measurements in the brownish sea and sky of Kano Domi screens. On the other hand, high amounts of Au were found through XRF analysis of golden areas: gold leaf and golden painted with brush.
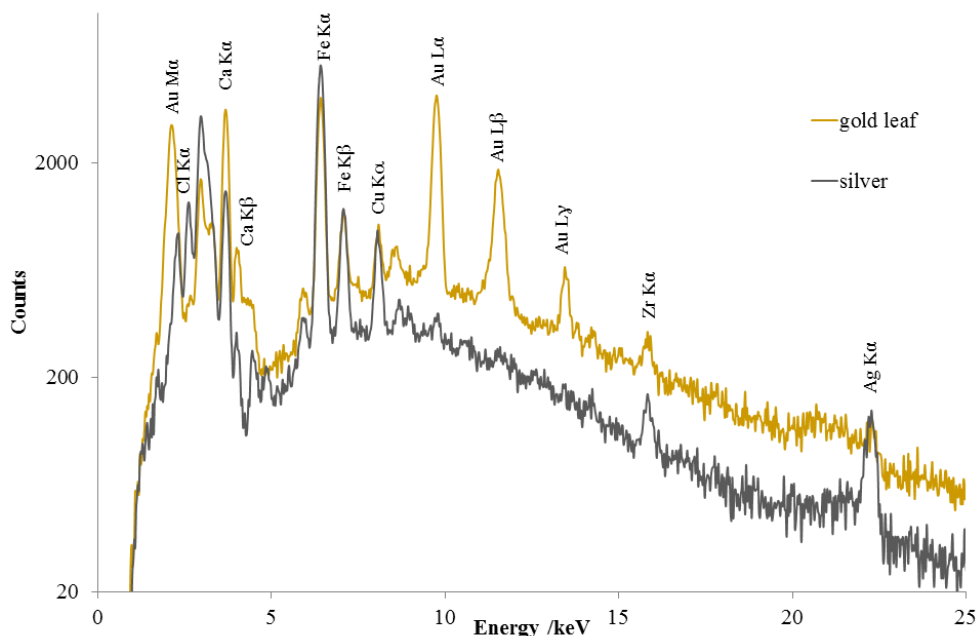
Fig. 5.3.7. XRF spectra obtained for gold (Kano Naizen) and silver (Kano Domi) areas of the screens. Spectra acquired at 30 kV and 100 µA during 300s.

Conversely to the expectations of the museum curator, that the whole screens were covered with gold leaf and the paint applied afterwards, the experimental results obtained by XRF did not show Au in the majority of the analyzed spots. Since gold was hardly ever detected in black or white areas (lighter materials) or in small details, e.g. figures, animals or plants, we believe that the gold leaf did not cover the whole surface of the screens:

We considered a simple model of the stratigraphy of the screens as shown in Fig. 5.3.8, were we have a 100 µm thick layer of $CaCO_3$ over a layer of Au and a layer of paper. The average layer thickness was obtained through observing the collected samples at the optical microscope as cross-sections (see Annex).
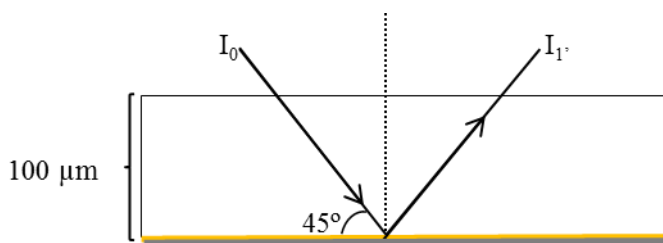
Fig. 5.3.8. Schematic representation of a simple model of the stratigraphy.

69

If we considered an incident monochromatic beam of 20 keV (in fact we used the bremsstrahlung from the tube working at 30 keV) crossing the layer of $CaCO_3$, according to eq. 2.2, the intensity of the transmitted radiation would be:

$$I_1 = I_0 e^{-\frac{\mu}{\rho}\rho x} \ll=\gg I_1 = I_0 e^{-8.3 \cdot 0.0141} \ll=\gg I_1 = 0.9 I_0$$

with:

$\sum (\chi_i (\mu/\rho)_i \cdot \rho_i)$ for $CaCO_3$ at 20 keV is 8.3 cm^{-1} and mass attenuation coefficients obtained at (132).

This means that only 10% of the incident radiation is attenuated in the $CaCO_3$ layer. Regarding the Au Lα characteristic radiation (~10 keV):

$$I_{1'} = I_{0'} e^{-\frac{\mu}{\rho}\rho x} \ll=\gg I_{1'} = I_{0'} e^{-59.4 \cdot 0.141} \ll=\gg I_{1'} = 0.44 I_{0'}$$

Considering $I_1=I_{0'}$, this means that 40% of the Au Lα fluorescence signal is transmitted through the $CaCO_3$ layer. This reasoning disregards the fluorescence yield and detectors efficiency for Au-L lines, meaning that the real intensity would be a bit smaller. Also not taken into account is the binding medium which decreases the density of the layer and therefore increase the intensity of the transmitted radiation. However, this simple model of the stratigraphy of the white areas, i.e., the sails, shows that if there were gold beneath the white pigment it would be detected. Since this was not the case, in most of the white and black areas (Fig. 5.3.4) we can conclude that, in contrast to what the curator assumed, the screens were not completely covered in gold leaf and then painted on. Most likely, the artist first drew the elements to decorate the screens prior to applying the gilding.

5.4. The Namban folding screens at Museu Nacional Soares dos Reis (see ANNEX)

5.4.1. Specimen description

The set of folding screens at Museu Nacional Soares dos Reis (MNSR) also belong to the type A screens, with the representation of the Portuguese Nao at a port in the left hand screen, along with a panorama of the shire, while the right hand screen depicts a perspective of the city of Nagasaki, a group of Portuguese sailors and a Christian church (Fig. 5.4.1). As these screens are works of an unusual historical and artistic value, they were often requested in various national and international exhibitions for artistic, historical and commemorative purposes [122]. At the end of the 1980s, an exhibition entitled Art Namban, les Portugais au Japon was part of the Európália89 festival held in Brussels [133]. The screens were then studied by specialists and attributed to the Kano School and were tentatively dated to between 1600 and 1610, a classification that still stands as of today.

As the pieces had been revealing some structural conservation problems for several years, they were subjected to a thorough restoration intervention at the National Research Institute for Cultural Properties in Tokio (NRICPT) between 2000 and 2002. According to the restoration report, a restoration procedure, "performed in the western countries", had been carried out previously, in which a glossy coating had been applied along with some color retouching. Very little is known about these treatments. Conservators at NRICPT dismounted the screens and substituted the frame, removed the glossy coating and consolidated the paint layers to prevent further detaching. With case study, we intended to characterize the restoration procedure "performed in the western countries", and understand why the new colors appear more degraded than the original ones.

Fig. 5.4.1- Photographies of the screens belonging to MNSR collection.

5.4.2. Results

The XRF spectra obtained for blue areas rendered different elemental composition (Fig. 5.4.2a). While some features appear to be painted using a copper based pigment, further identified as azurite $(2CuCO_3.Cu(OH)_2)$ by Raman spectroscopy, some clothes of characters presented Ti, Cr, Co, Ni and Zn in their composition. Figure 5.4.2b shows the Raman spectra obtained from a sample collected in spot 495. The pigment Phtalocyanine blue $(CuC_{32}H_{16}N_8)$ [42] was put in evidence with characteristic bands at as well as calcite

(CaCO₃) with all lasers. Cobalt blue (CoO.Al₂O₃) was identified with the 514 nm laser [42]. Furthermore, titanium dioxide in the anatase mineral form (TiO₂) [42] and two broad bands centered at 1330 and 1500 cm^{-1} corresponding to carbon black were found with the 532 nm laser.

Fig. 5.4.2 a) Comparison of the XRF spectra obtained for different shades of blue. Spectra acquired at 30 kV, 90µA during 200s. b) Raman spectra obtained for a blue sample collected from spot 495. Spectra acquired with 638 and 532 nm lasers, 300 µm hole, 100 µm slit, 50x obj., during 5x20s, 5x5s, 5x3s and 5x10s, respectively. Bottom spectrum acquired with 514 nm laser, 700 µm hole, 100 µm slit, 50x obj., during 20s.

The XRF spectra obtained from the green areas presented high amounts of Cu (Fig. 5.4.3a), indicating the presence of a copper-based green pigment. Malachite ($CuCO_3.Cu(OH)_2$) was identified by Raman spectroscopy using all the laser sources (Fig. 5.4.3b), sometimes mixed with calcite ($CaCO_3$) to produce a lighter shade, sometimes mixed with hematite (Fe_2O_3) to produce a darker shade.

Fig. 5.4.3 -a) XRF spectra obtained for a green area. Spectrum acquired at 30 kV, 90µA during 200s. b) Raman spectrum obtained for a green sample. Spectrum acquired with 638 nm laser, 300 µm hole, 100 µm slit, 50x obj., during 5x15s.

Regarding the red areas, Hg was found in great amount in the XRF spectra (5.4.4a), being confirmed the presence of Vermillion (HgS) by Raman spectroscopy (Fig. 5.4.4b). This pigment was also found mixed with white calcite to obtain the pink color.
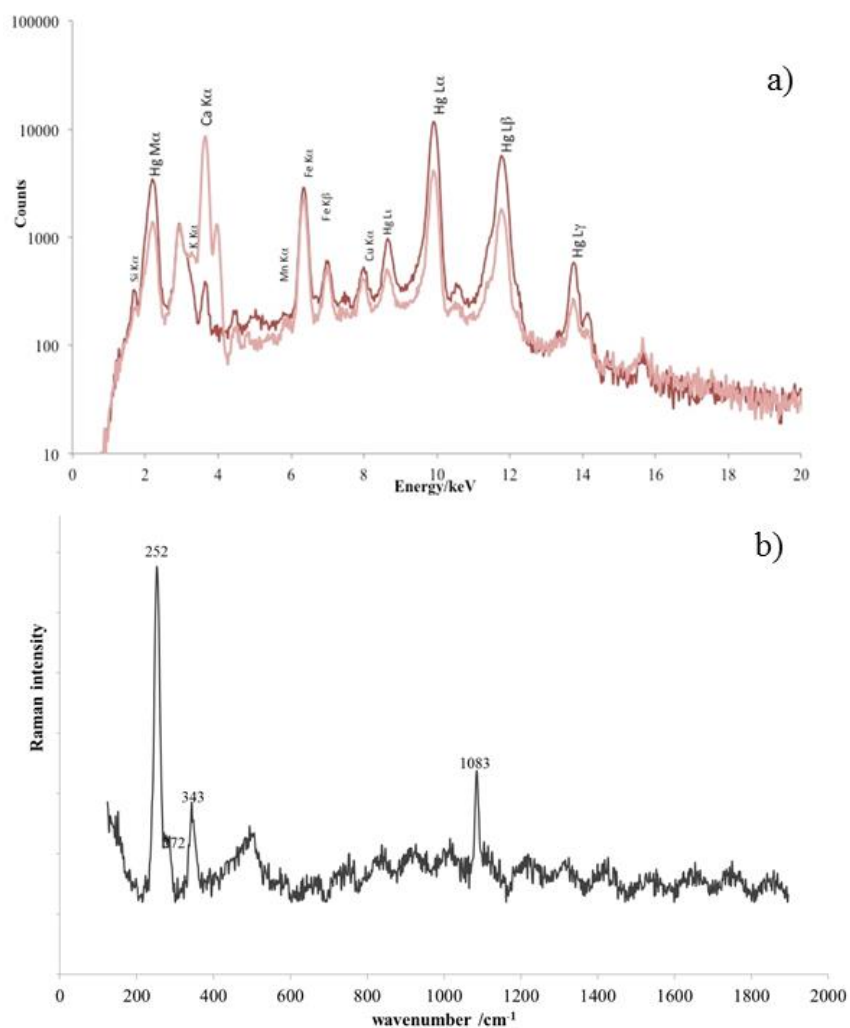
Fig. 5.4.4 -a) XRF spectra obtained for red and pink areas. Spectra acquired at 30 kV, 90μA during 200s. b) Raman spectra obtained for pink micro-sample, acquired with 638 nm laser, 300 μm hole, 100 μm slit, 50x obj., during 5x15s and 5s.

Regarding the yellow color, all the analyzed areas presented Cr, Fe, Ba and Pb in the XRF spectra (Fig. 5.4.5a). In Fig. 5.4.5b, the Raman spectra obtained from the yellow sample analyzed with the 638, 532 and 514 nm laser sources are shown. In all spectra, the presence of lead chromate, commonly called chrome yellow ($PbCrO_4$), was found. Furthermore, the

presence of barium sulfate (BaSO$_4$), often used as an extender for chrome yellow [139] was also detected.

The orange areas presented similar composition in the XRF spectra, but sometimes Hg was also detected. Raman measurements identified the presence of chrome yellow-orange (PbCrO$_4$.PbO) (Fig. 5.4.5c), sometimes mixed with vermillion.
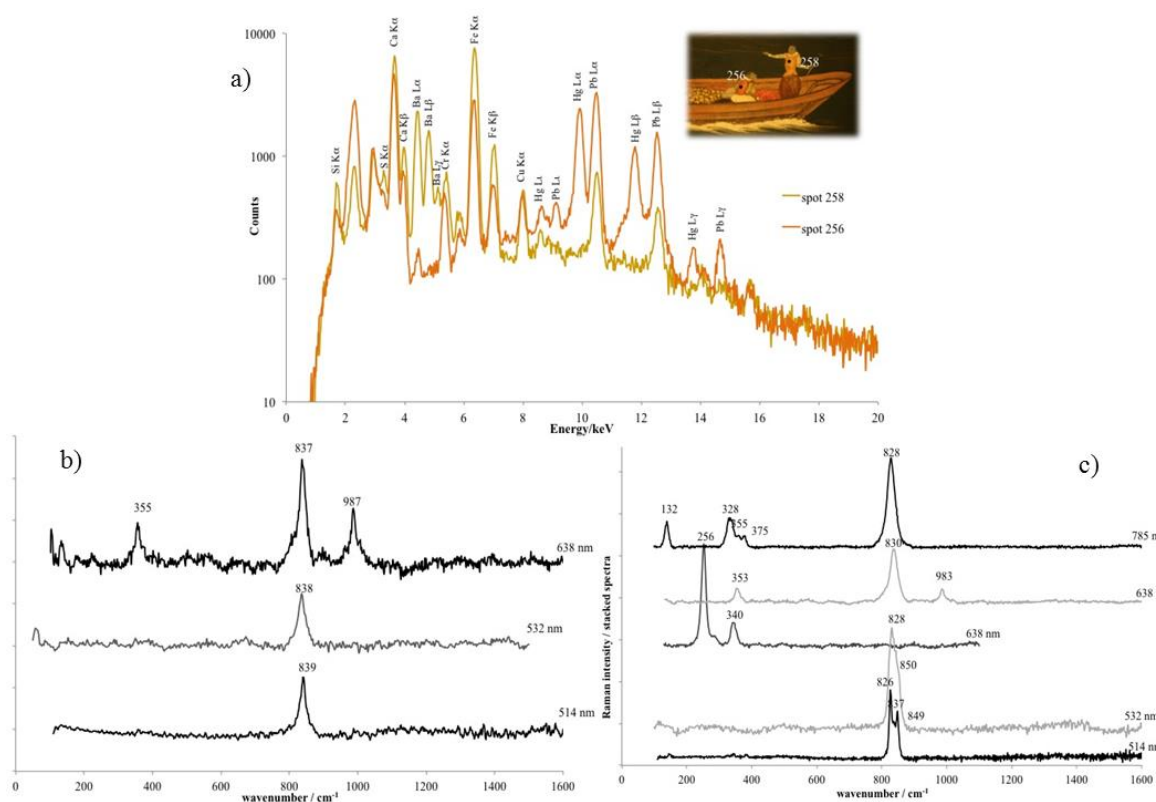
Fig. 5.4.5 a) Comparison of the XRF spectra obtained for yellow and orange areas. Spectra acquired at 30 kV, 90μA during 200s. b) Raman spectra obtained for a yellow sample collected from spot 258. From top, spectrum acquired with 638 nm laser, 300 µm hole, 100 µm slit, 100x objective during 4x6s; acquired with 532 nm laser, 300 µm hole, 100 µm slit, 50x objective during 5x5s; and spectrum acquired with 514 nm laser, 700 µm hole, 100 µm slit, 100x obj., during 10s.

c) Rama spectra obtained for an orange sample collected on spot 256. Spectra acquired with 638 and 532 nm lasers, 300 µm hole, 100 µm slit, 50x obj., during 5x5s, 5x10s, 3x5s and 5x6s, respectively. Bottom spectrum acquired with 514 nm laser, 700 µm hole, 100 µm slit, 100x obj., during 20s.

Also in the case of brown, two very different elemental compositions were found for two shades of brown, one presenting mainly Fe and Ca, as well as Si, and another one presenting high amounts of Cr, Hg and Pb (Fig. 5.4.6a). Raman spectra obtained with all laser sources from the sample collected at spot 498 were identified as chrome-yellow orange (Fig. 5.4.6b). Furthermore, with lasers 785, 638 and 532 nm, it was also possible to identify bands corresponding to vermillion. Regarding the lighter shade of brown, corresponding to the sample collected at spot 507, hematite and carbon black were put in evidence using in both cases the 514 and 638 nm lasers (Figs. 5.4.6c). Moreover, using the 638 nm laser, it was possible to identify calcite and silica. This means that the brown color was obtained by mixing hematite, carbon black, calcite and silica together. On the other hand, a band is observable at around 1450 cm^{-1} that could be indicative of the use of an organic compound in the mixture. According to Winter [127] different organic substances are known to have been employed in Asian paintings, such as madder or lac dye for a red shade, gamboge as a yellow coloring agent or even an organic brown. However, other bands that could be assigned to these compounds are not visible. If present, they could be hidden by the carbon broad bands centered at 1300 and 1500 cm^{-1} [42].
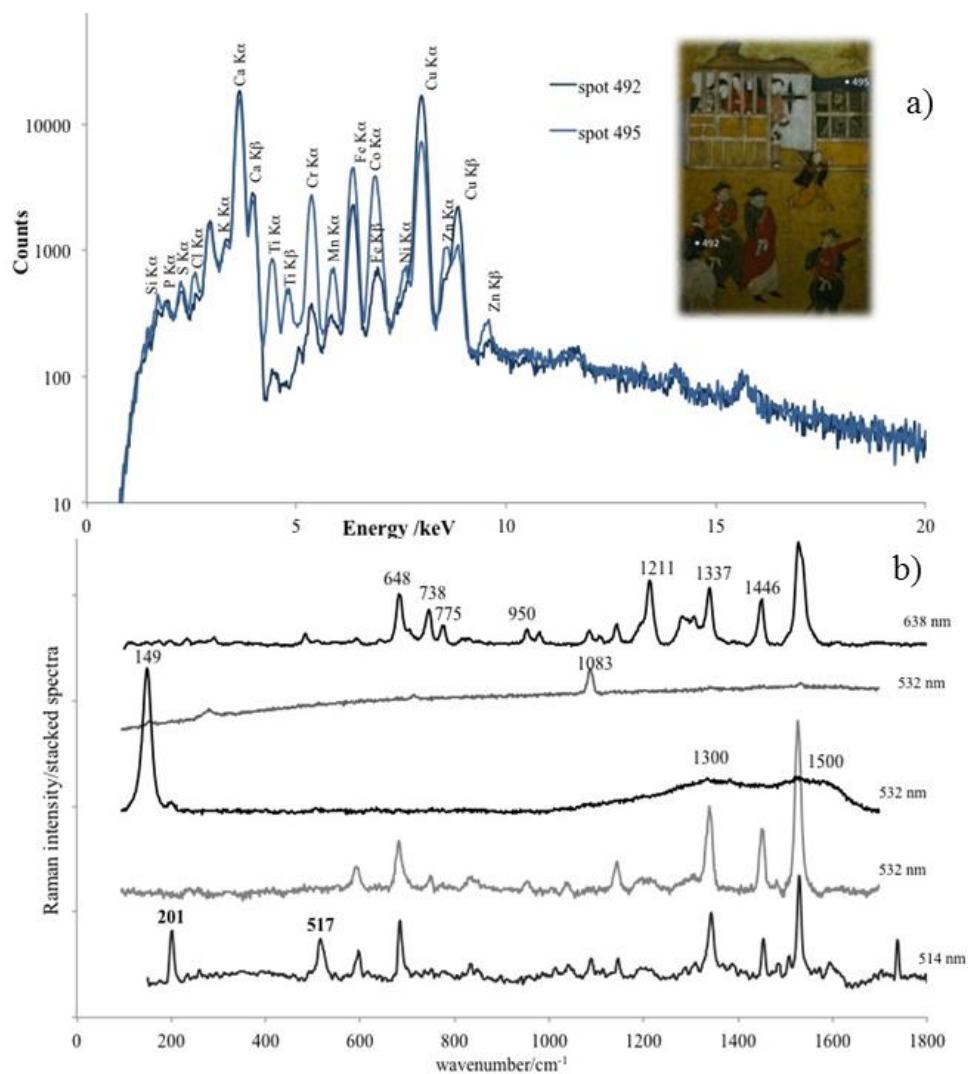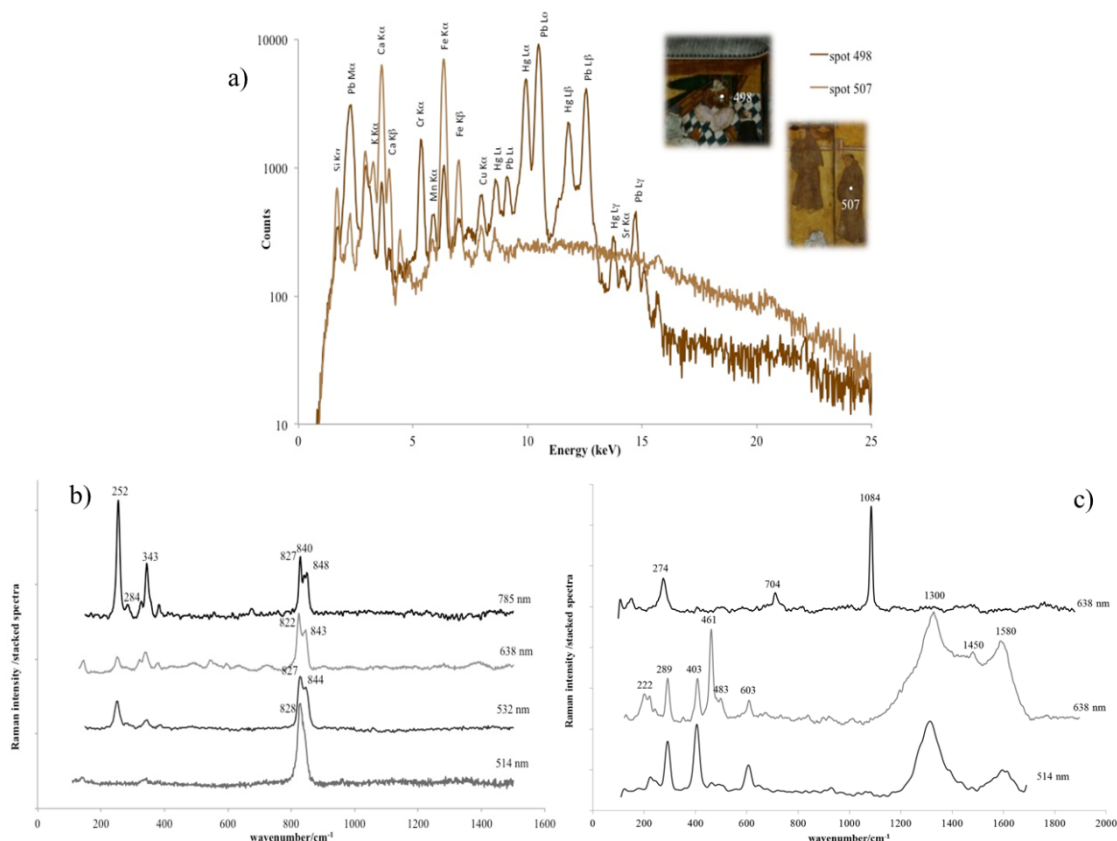
Fig. 5.4.6 a) Comparison of the XRF spectra obtained for brown areas. Spectra acquired at 30 kV, 90µA during 200s. b) Raman spectra obtained for a dark brown sample collected from spot 498. Spectra acquired with 785, 638 and 532 nm lasers, 300 µm hole, 100 µm slit, 50x obj., during 3x8s, 10x30s, and 5x10s, respectively. Bottom spectrum acquired with 514 nm laser, 700 µm hole, 100 µm slit, 100x obj., during 10s. c) Raman spectra obtained for a light brown sample collected on spot 507. Spectra acquired with 638 nm laser, 300 µm hole, 100 µm slit, 100x obj., during 4x5s and 5x15s, respectively. Bottom spectrum acquired with 514 nm laser, 700 µm hole, 100 µm slit, 100x obj., during 30s.

The XRF spectra of white areas presented mainly Ca indicating the presence of $CaCO_3$ (Fig. 5.4.7a). This was confirmed by the presence of a very strong band at around 1086 cm^{-1} in all Raman spectra. As was mentioned before, this band appeared in other Raman spectra indicating the use of this white pigment to lighten other colors. As mentioned in the previous case study, $CaCO_3$, is attributed to the used of oyster-shell white, *gofun* in Japanese.
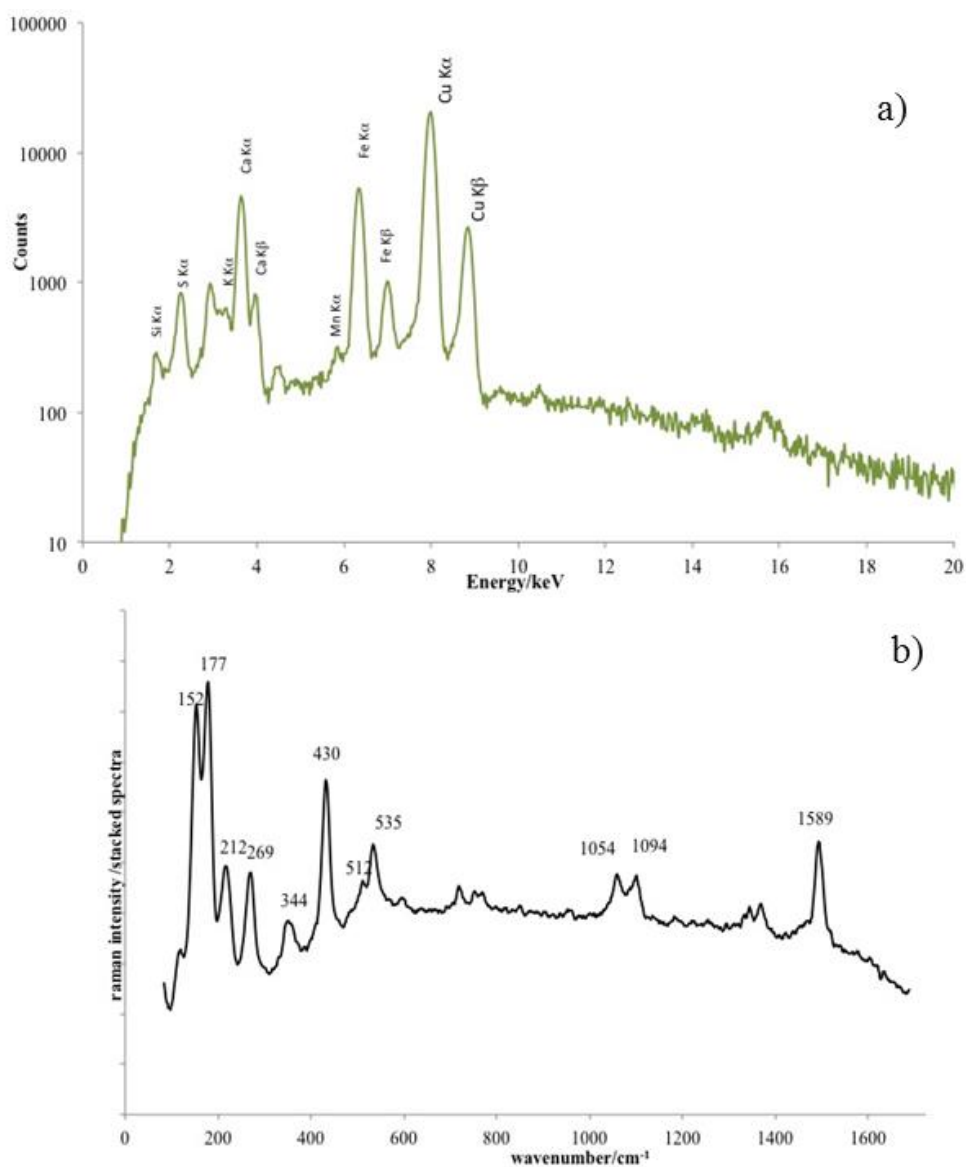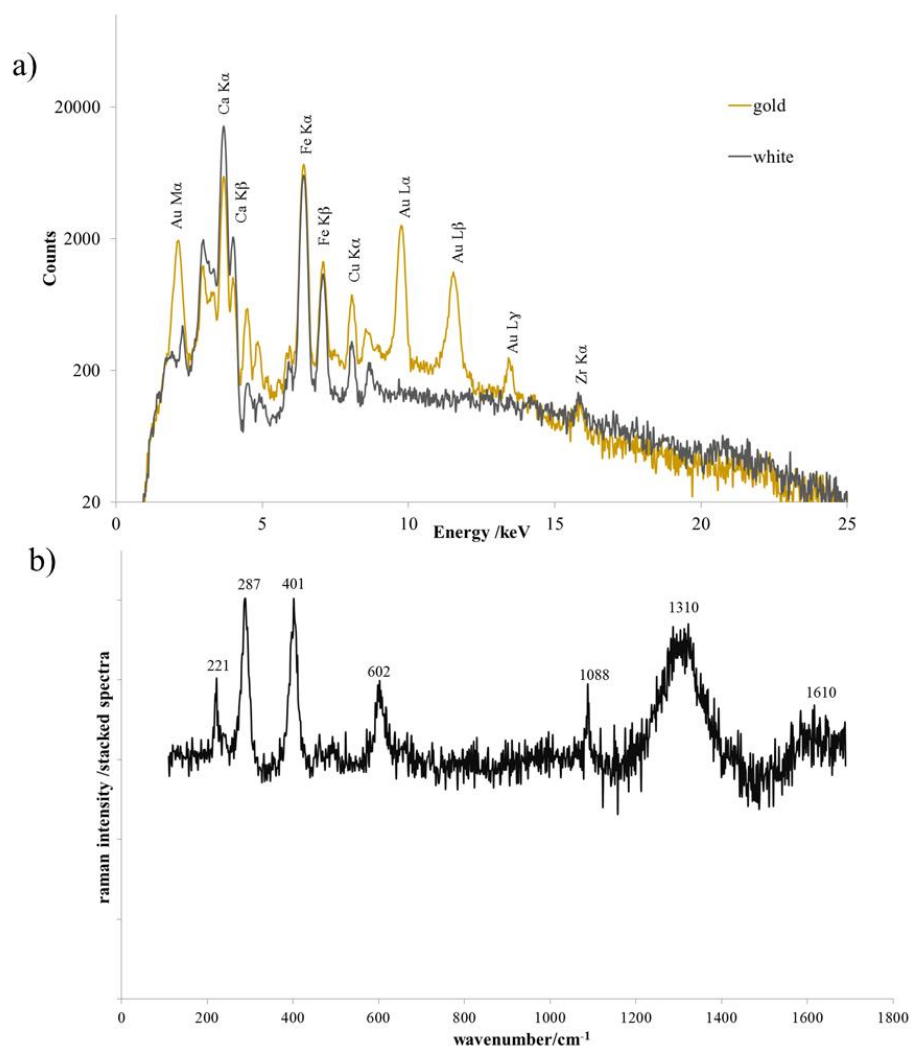
Fig. 5.4.7 – a) XRF spectra obtained for white and golden areas. Spectra acquired at 30 kV, 90μA during 200s. b) Raman spectrum obtained for a grey micro-sample. Spectrum acquired with the 514 nm laser 700 and 20s μm hole, 100 μm slit, 100x obj., during 30s.

Regarding the black and grey areas, the XRF was not so different from the ones of white areas leading us to believe that the black color might be produced with a carbon-based pigment and the grey color, with a mixture of carbon-based pigment and *gofun*. However, Raman spectrum obtained for the grey sample presented the band for calcite, but also presented the bands for hematite (Fe_2O_3) (Fig. 5.4.7b).

Regarding the golden areas, as expected, Au was found covering the background of the screens (Fig. 5.4.7a). Silver was not detected, although the use of an X-ray tube with Ag anode might disguise the characteristic line of Ag (if in small amount), and Cu seems to present in all extent of the screens, most likely as an artifact from the setup. This means that we are in the presence of a a high quality gold, if not a 24 ct gold, consistent with the practice of Japanese artists in the Momoyama and Edo periods [124].

Intervention performed "in the western countries"

The use of azurite, malachite, vermillion, red ochre, carbon black, calcite (*gofun*), or a mixture of vermillion, *gofun* and carbon black to obtain brown, is consistent with the pigments known to be used by Japanese painters in the Momoyama (1573-1603) and Edo (1603-1868) periods [124, 127, 130] and also with the pigments found by Raman and XRF in similar artworks [11]. Most of these pigments were found in pieces as ancient as 4th century BC and are still in use nowadays. The presence of these pigments leads us to assume that they are part of the original painting or, at least, that they are not conclusive in terms of characterizing the later intervention performed on the screens. Regarding the blue pigments, beside azurite, cobalt blue and Phthalocyanine blue were found. Cobalt blue was discovered in 1802 [135] and there is only records of its use in traditional Japanese painting after the II World War [136], so we can consider that this pigment was not part of the original artwork. The same can be said regarding the Phthalocyanine blue, a organic dyestuff with a color considered very strong, about twice as strong as Prussian blue, and very resistant to fading at light exposure. Phthalocyanine blue and copper phthalocyanine were developed by chemists of the Imperial Chemical Industries, Ltd, in the mid-1930s only becoming commercially available at the beginning of 1938 [135]. This way, we can conclude that the 'western' intervention mentioned in the NRICPT report could not have been performed before this date.

Regarding the yellow colors, usually yellow ochre or gamboge was used [124]. In the studied screens, chrome yellow was the pigment found. It is a modern pigment that only appeared in the traditional Japanese paintings in the Meiji era (1868-1912) [136]. Chrome yellow could be found as the rare mineral crocoite or in its synthetic form, and could assume a lighter or darker shade according to the conditions of precipitation. Discovered by

Vauquelin in 1809 (137) it did not come into commercial production before 1818. Regarding the orange shades, they were usually obtained mixing red lead (Pb_3O_4) with vermillion (138) but it was not the case in these screens. Again, a basic lead chromate was found. These lead chromate-based pigments are very unstable, even the best grades are not permanent and the pigment tends to oxidize and darken on exposure to air over time (139). Systematic studies about the degradation mechanisms of lead chromate were carried out until ca. 1950 coinciding with the progressive replacing of chrome yellow pigments by others, such as cadmium yellow (CdS) which was assumed to be more stable (134).

This means that the intervention must have been performed just before the lead chromate pigments (chrome yellow and chrome orange) came in disuse, somewhere in the 1940s or in the very early 1950s, just before the Portuguese state acquired the Namban screens in 1955.

5.5. The Namban folding screen at Museu Oriente (see ANNEX)

5.5.1. Specimen description

The Namban screens described in the previous case studies date from ca 1600, the Momoyama period, but the theme fascinated the Japanese, and the Kano-school atelier, as well as other professional painting studios in Kyoto, have made numerous versions throughout the 17th and 18th centuries. Namban screens typically portrayed the long-nosed Portuguese and their ships, Christian churches and missionaries with a skill and detail that could only be gained from personal observation [140]. Art patrons who saw the early screen masterpieces became interested in Namban themes and commissioned the painters, or colleagues in the Kano school to do other works of identical composition. This way, generations of similar screens were copied out, to the extent of artists that, having no knowledge of Portuguese ships and no understanding of missionaries, would merely imitate previous screen paintings, but the artworks would lack spontaneity and vitality [140]. A large number of works painted in such a stereotyped fashion is unique in Japanese art, and many examples must have been lost during Japanese isolation (1641-1853).

The screen, belonging to the collection of Museu do Oriente (MO) in Lisbon and acquired without a pair (Fig. 5.5.1), constitutes a magnification of the scenes and characters presented in a screen from the Momoyama Period belonging to the collection of MNAA

(Fig. 5.3.1) that bears the Kano Naizen stamp. The ship's arrival at the port of Nagasaki, with the sails collected and the disembarkation of its cargo, with far less detail, as well as the procession headed by the "capitão-mor" and greeted by the missionaries, always with the natives observing. One of the most interesting characteristics of this screen is that in addition to the two types of gold application seen in the previous case studies: as metal leaf, or *Kin-haku,* (covering almost the entire extension of the screen, corresponding to the land where the figures stand and to the sky) and as ground gold mixed with a vehicle, usually animal glue (*nikawa*), and applied as paint, or *Kin dei,* (used for enhancing the sinuous and rounded outlines of the clouds or the limits of the Nagasaki Bay) the artist used flakes of gold sprinkled over the burnished metal leaf, or *Sunago,* in lower part of each panel, giving a textured effect and a specific contrast between the polished and mate coatings [130].

In this case study we investigated the materials used in this screen belonging to the Edo Period in order to understand if the materials and techniques employed in the artwork are similar with the ones used in screens from the Momoyama period, or if they suffered more influence from the materials used in the west.

Fig. 5.5.1- Photographies of the screens belonging to MO (bottom) and MNAA (top) collection.

It can be seen how one was made as an amplification of the scenes present in the other.

5.5.2. Results

Regarding the red pigments, the use of Vermilion (HgS) was suggested in the XRF analysis (Fig. 5.5.2a) Furthermore, a lighter shade, more orange was obtained by mixing Vermilion and Red Lead (Pb_3O_4). These results were confirmed using Raman spectroscopy with characteristic bands at 250, 280 and 341 cm^{-1} and 118 and 549 cm^{-1}, [43] respectively (Fig.5.5.2b).
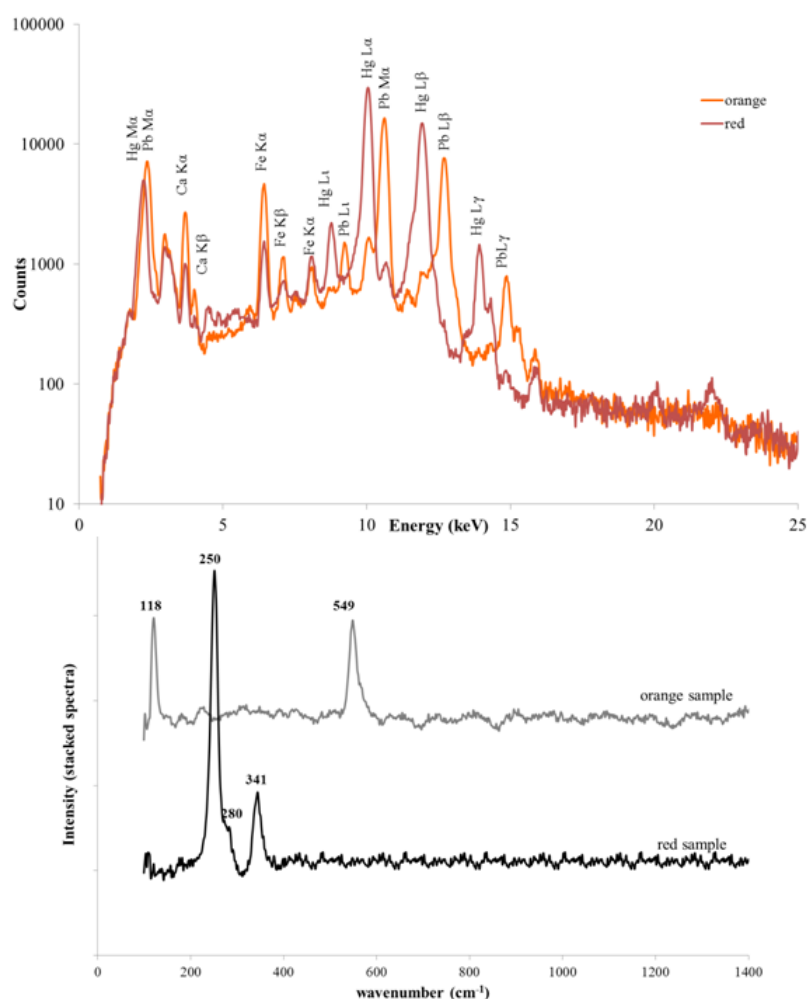
Fig. 5.5.2 -a) XRF spectra obtained for red and orange areas. Spectra acquired at 30 kV, 100µA during 300s. b) Raman spectra obtained for grains in the red and orange samples. Spectra acquired with 638 nm laser, 300 µm hole, 100 µm slit, 50x obj., during 5x5s and 5x10s, respectively.

XRF measurements on white areas presented high amounts of Ca (Fig. 5.5.3a), while the Raman spectra of white micro-samples in both screens was identified as $CaCO_3$ due to the

presence of a strong band at 1084 cm^{-1} (Fig.5.5.3b). Again, CaCO$_3$ is indicative of the use of white oyster-shell or *Gofun*.
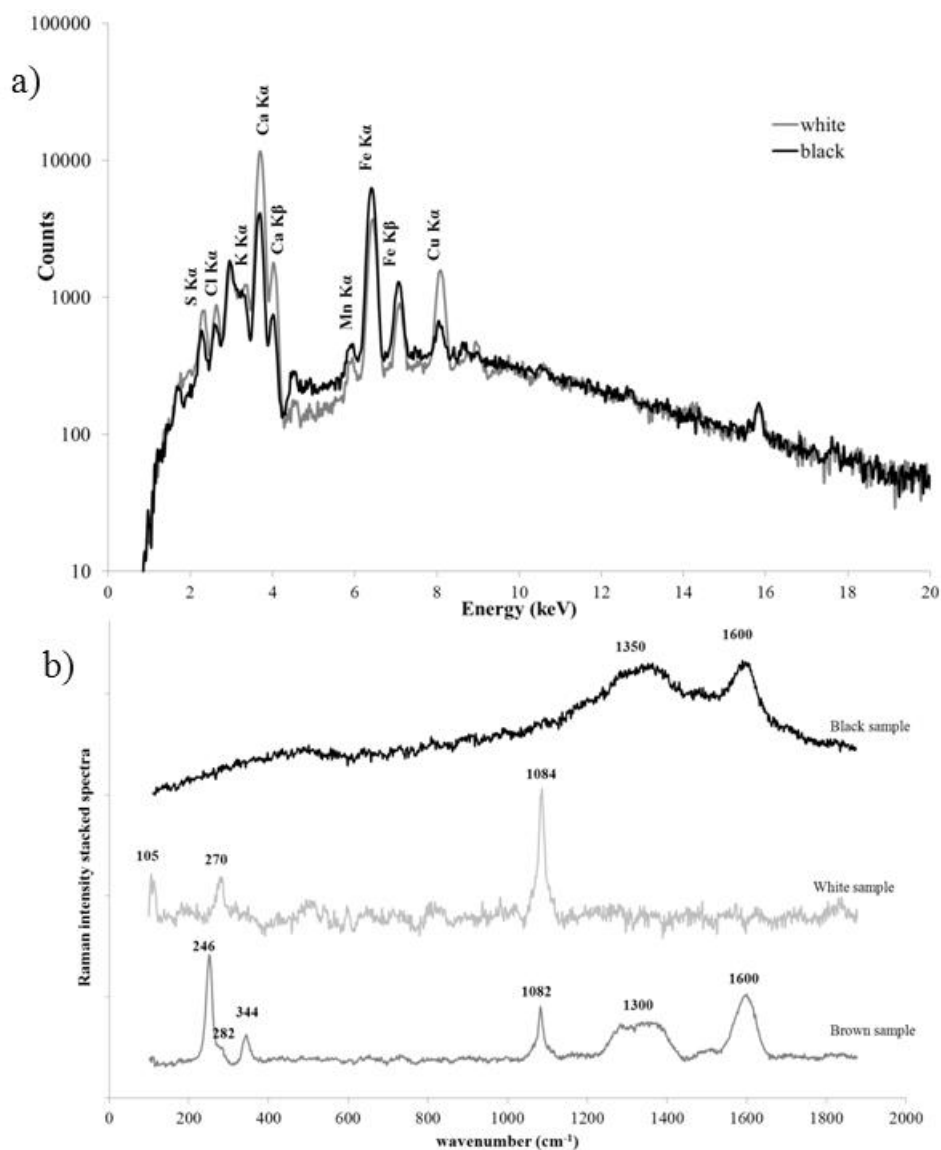
Fig. 5.5.3 -a) XRF spectra obtained for white and black areas. Spectra acquired at 30 kV, 100μA during 300s. b) Raman spectra obtained for white and black samples. Spectra acquired with 638 nm laser, 300 μm hole, 100 μm slit, 50x obj., during 2x5s, 5x10s and 15x3s, respectively.

Regarding the black areas and comparing with a spectrum obtained for a white area, we can see that they are very similar (Fig. 5.5.3a). The Raman analysis obtained for black micro-

samples, a carbon based black pigment was identified by the two broad bands centered at 1350 and 1600 cm^{-1} [43] (Fig.5.5.3.b).

The XRF spectra of the brown areas presented Hg suggesting a mixture using vermillion, and the Raman measurements obtained from a micro-sample collected from a brown area allowed also the identification of vermillion with bands at 246, 282 and 344 cm^{-1}, calcium carbonate with a strong band at 1082 cm^{-1} and carbon black with two broad bands centered at 1320 and 1590 cm^{-1} (Fig. 5.3.5b). This way we can conclude that the brown color was obtained by mixing Vermilion, *Gofun* and Carbon Black.

XRF of green areas of the screen presented mostly Cu, however the intermittent presence of Cl suggested the presence of different compounds (Fig. 5.5.4 a). Raman spectra of different samples of green areas showed the presence of Malachite ($CuCO_3.Cu(OH)_2$) with bands at 151, 174, 220, 268, 355, 424, 1074 and 1092 cm^{-1} (Fig. 5.5.4 b) sometimes mixed with Atacamite ($Cu_2(OH)_3Cl$), identified in the Raman spectrum by the bands at 112, 143, 356, 393, 440, 496, 810, 893 and 960 cm^{-1} and explaining the appearance of Cl [43].
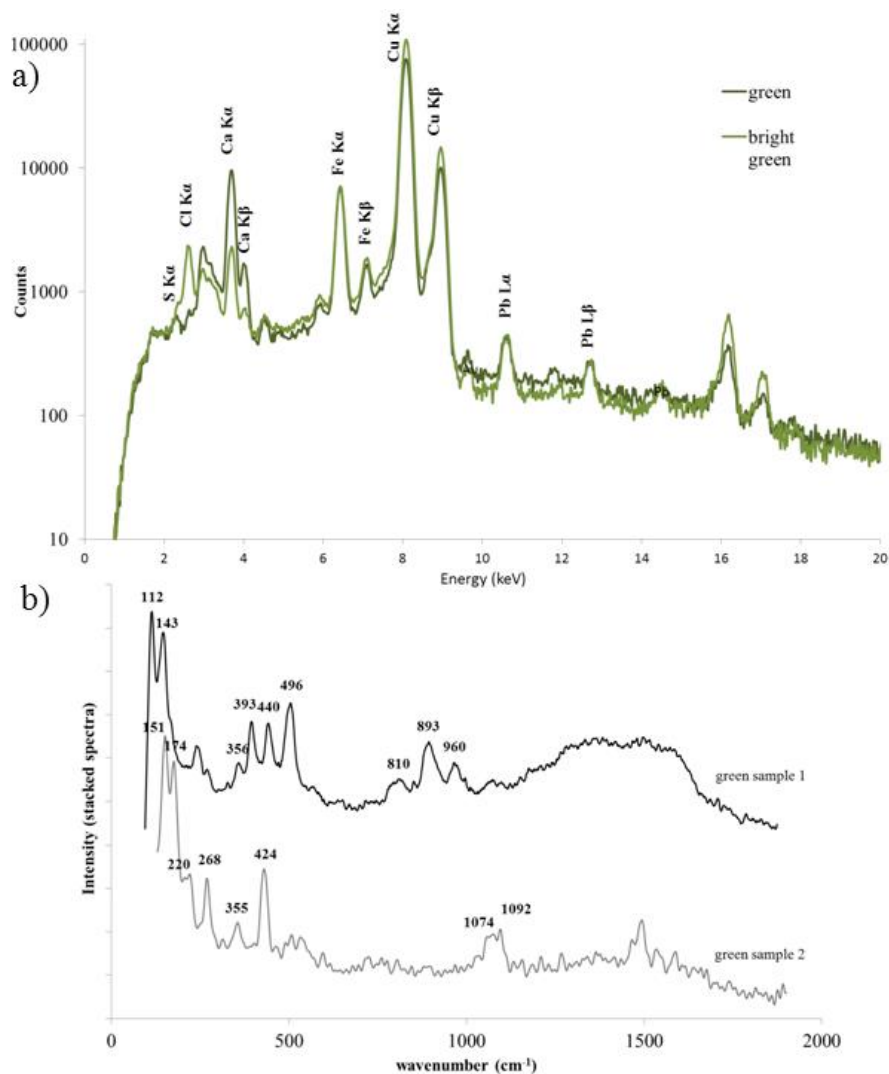
Fig. 5.5.3 - a) XRF spectra obtained for green areas. Spectra acquired at 30 kV, 100µA during 300s. b) Raman spectra obtained for blue samples. Spectra acquired with 638 nm laser, 300 µm hole, 100 µm slit, 50x obj., during 6x25s and 10x40s, respectively.

When comparing the XRF spectra obtained for areas of dark and light blue, a very different elemental composition was obtained (Fig. 5.5.5a). The dark blue areas presented high amounts of Cu, suggesting the presence of Azurite ($2CuCO_3.Cu(OH)_2$), confirmed by Raman spectroscopy as seen in Figure 5.5.5.b with bands at 135, 244, 395, 836, 1091, 1421 and 1574 cm^{-1} [43] .As for the light blue areas, the reduced Cu, suggested the use of other pigment. Raman spectra of samples from the light blue area identified the presence of indigo with bands present at 256, 281, 304, 544, 597, 621 and 1577 cm^{-1} [11].
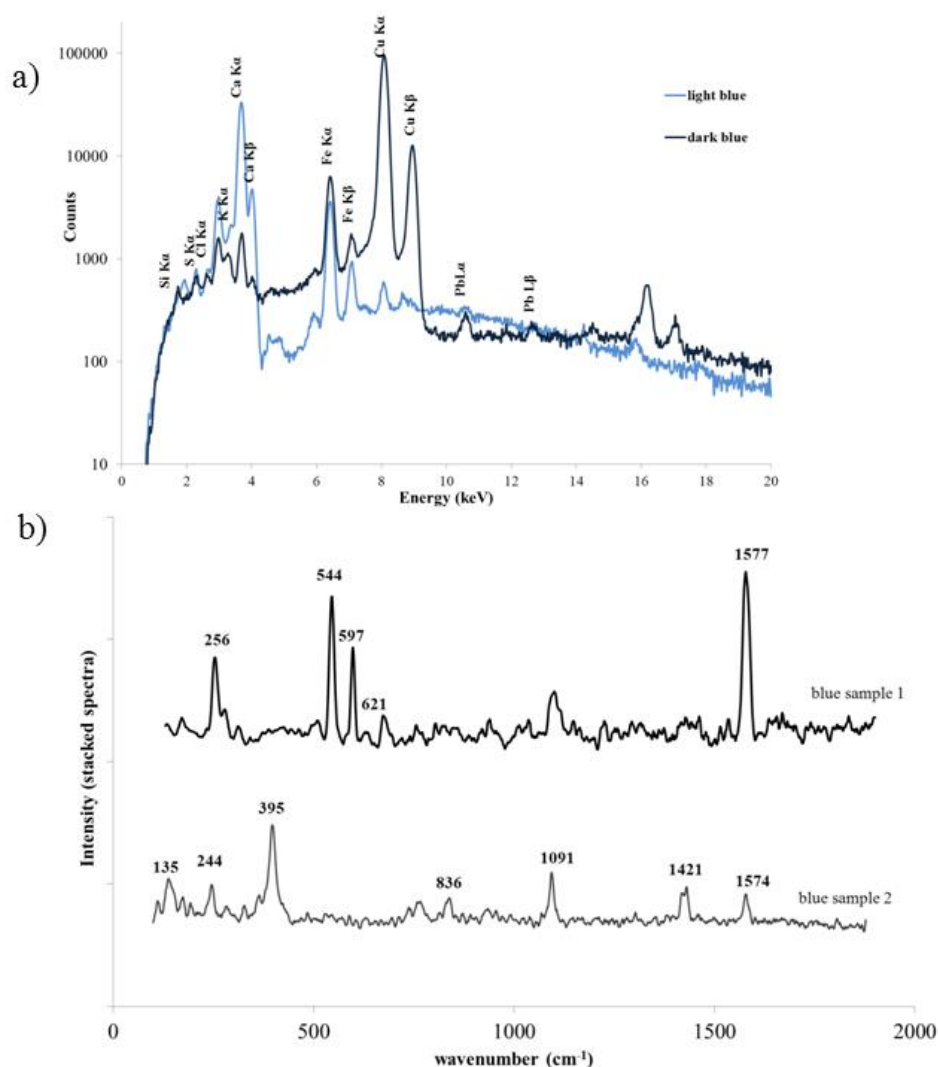
Fig. 5.5.4 - a) XRF spectra obtained for blue areas. Spectra acquired at 30 kV, 100µA during 300s. b) Raman spectra obtained for blue samples. Spectra acquired with 638 nm laser, 300 µm hole, 100 µm slit, 50x obj., during 2x30s and 20x10s, respectively.

The pigments found, malachite, azurite, indigo, vermillion, red lead, carbon black, gofun are consistent with the materials found in screens from the Momoyama period, as seen in previous case-studies. However, in this screen the artist resorted to mixtures that were not seen in the other screens: orange shade obtained through vermilion and red lead and brown obtained by mixing vermillion, Gofun and carbon black. The presence of Atacamite on

artworks on paper support and the discussion whether it was used as a pigment or if it is a degradation product is not new [10, 11]. It is known that this compound appears on East Asian artworks since the 4th century [130] and that it exists naturally in Japan, however the fact that it does not appear dissociated from Malachite seems to be an indication that it is an alteration product of Malachite.

5.6. The two-paneled Namban folding screen belonging to private collections- the boat scene

5.6.1. Specimen description

This screen (Fig. 5.6.1.) was selected to be part of the exhibition: Giappone. Terra di incanti - Di linea e di colore (Japan. Land of enchantment - The line and color) at Museo degli Argenti in the Pitti Palace in Florence (Italy). Before attending this exhibition, the screen in Fig. 5.6.1 had already been displayed, among others, in the Európália exhibition in Brussels [133], so its authenticity was not questioned. If the screen belonging to the MO collection is a magnification of the original screens from the Momoyama period, this screen is an even greater magnification. And, more peculiarly, it is only composed by two panels. This screen is a depiction of the Portuguese *Nao* enclosed in a golden background with brown sea. The sails are collected so we assume they are arriving, to the port believed to be Nagasaki.

Only XRF measurements were performed on this screen.

Fig. 5.6.1 – a) Photography of the Namban screen belonging to a private collection (BAB).

5.6.1. Results

Regarding the red areas, three different shades can be distinguished (Fig. 5.6.2). The brighter shade of red revealed the presence of Cd, S and Se, suggesting the use of the pigment Cadmium Red ($CdS(Se)$). On the other hand, the orange shade observed in the clothes and parcels revealed high amounts of Pb, indicative of the presence of red lead, and also Hg, indicative of vermillion. Considering the darker shade of red, Hg was the main element detected indicative of vermillion. Iron put in evidence in the three spectra could be due to the contribution of an iron-based oxide, such as Hematite (Fe_2O_3), however it is present throughout the screen. Despite these differences, Se is observed in all spectra,

allowing to infer that Cadmium red is always part of the color paints; even though Cd was not detected because of the highest efficiency of the detector for the energies around 10 keV (Kα Se $= 11.2$ keV).
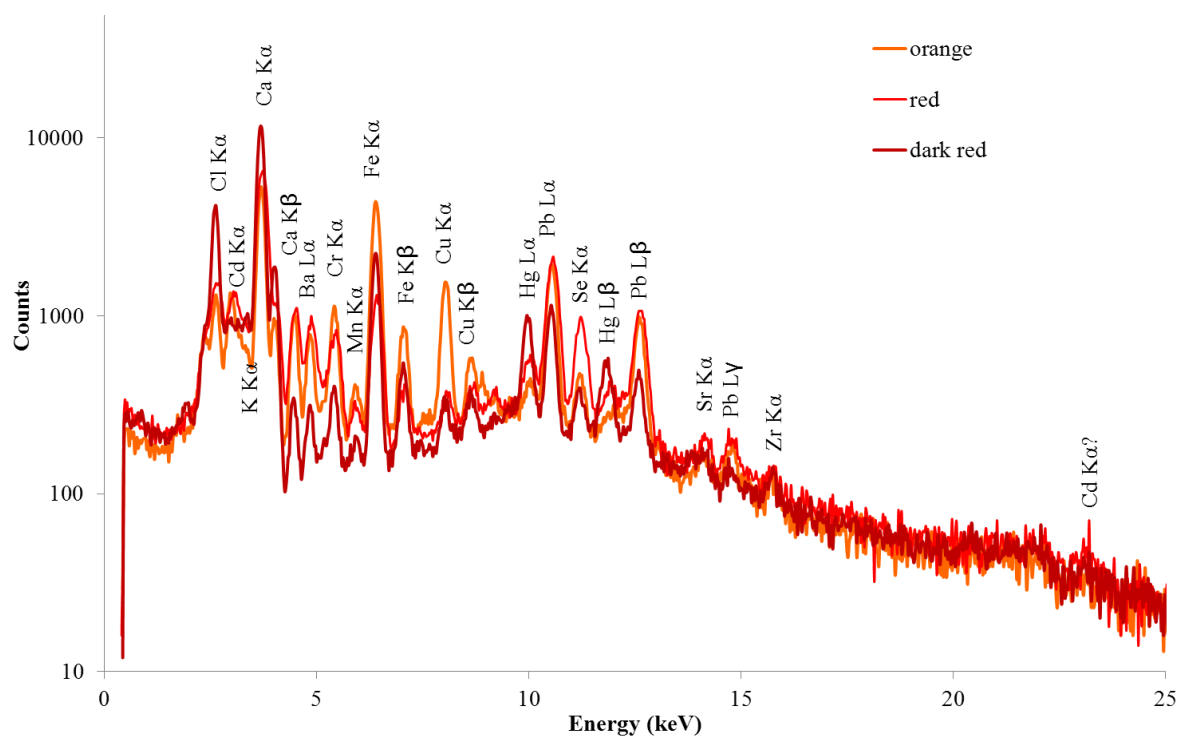
Fig. 5.6.2 -a) XRF spectra obtained for red areas. Spectra acquired at 30 kV, 100µA during 300s.

Regarding the XRF analysis of the green areas, Cu was found (Fig. 5.6.3.a), most likely associated to Malachite. However, the noteworthy presence of Cr in all green areas, indicated the presence of a chromium-based green, probably Chrome green, the name given to the pigment made by co-precipitating Prussian blue [Fe$_4$(Fe[CN]$_6$)$_3$] and Chrome yellow (PbCrO$_4$) [137]. Iron appears also with great intensity in the spectrum, however it is unclear if its presence is due to the same origin as in the background or from the presence of Prussian blue. The presence of Ba and Zn is probably due to the addition of a white opaque pigment to lighten the color, most likely lithopone (ZnS + BaSO$_4$).

Regarding the blue areas, Fe was put in evidence in the XRF spectra (Fig. 5.7.5a), suggesting the presence of Prussian blue, however confirmation would be in order. The presence of Zn, without Ba could be due to the addition of ZnS, also as an opaque white pigment.

91
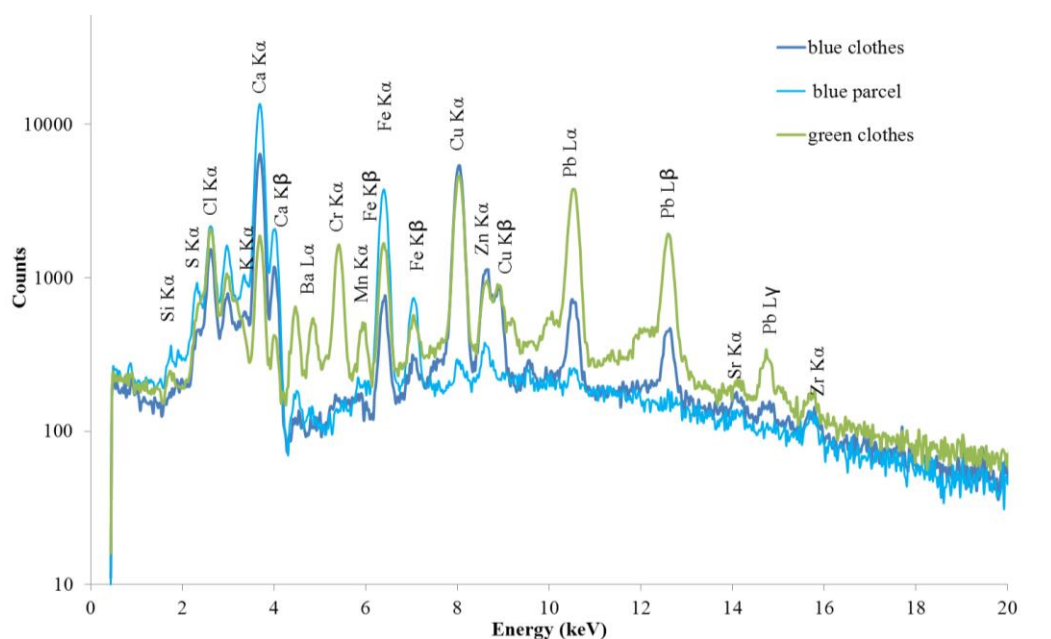
Fig. 5.6.3 -a) XRF spectra obtained for green and blue areas. Spectra acquired at 30 kV, 100µA during 300s.

Regarding the white areas, two different elemental compositions were obtained: the first mainly composed by Ca, corresponding to $CaCO_3$ as expected in this kind of artwork. When analyzing the white sails, a high content of Zn and Ba was detected, again probably due to the use of the white opaque pigment lithopone.
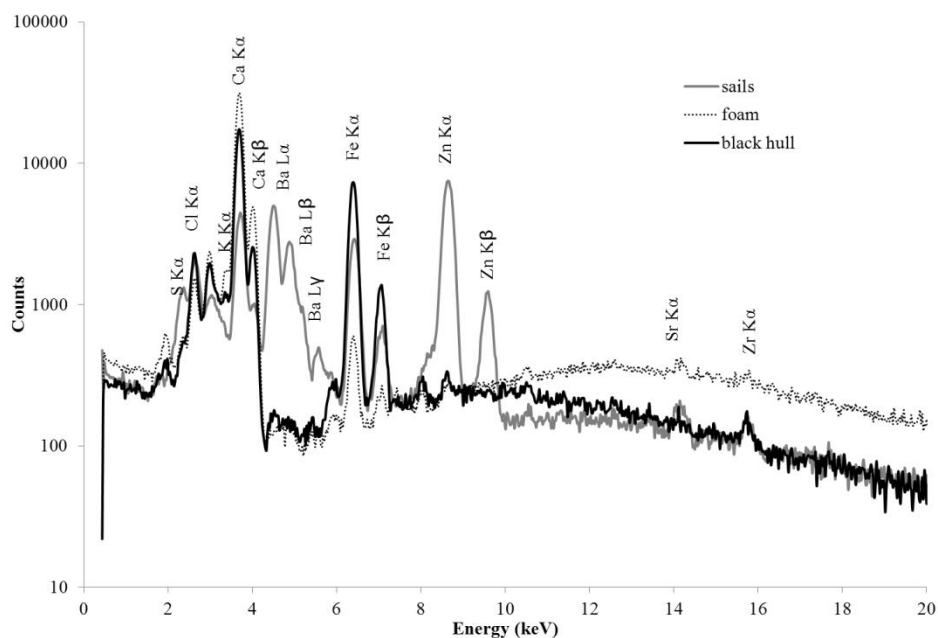
Fig. 5.6.4 -a) XRF spectra obtained for black and white areas. Spectra acquired at 30 kV, 100μA during 300s.

As expected, in folding screens from the Edo period, the golden background was gilded with gold leaf while the brown sea was painted with silver (Fig. 5.6.4). The brown color is probably due to the oxidation of silver, as happened to the screen attributed to Kano Domi belonging to MNAA (section 5.3)
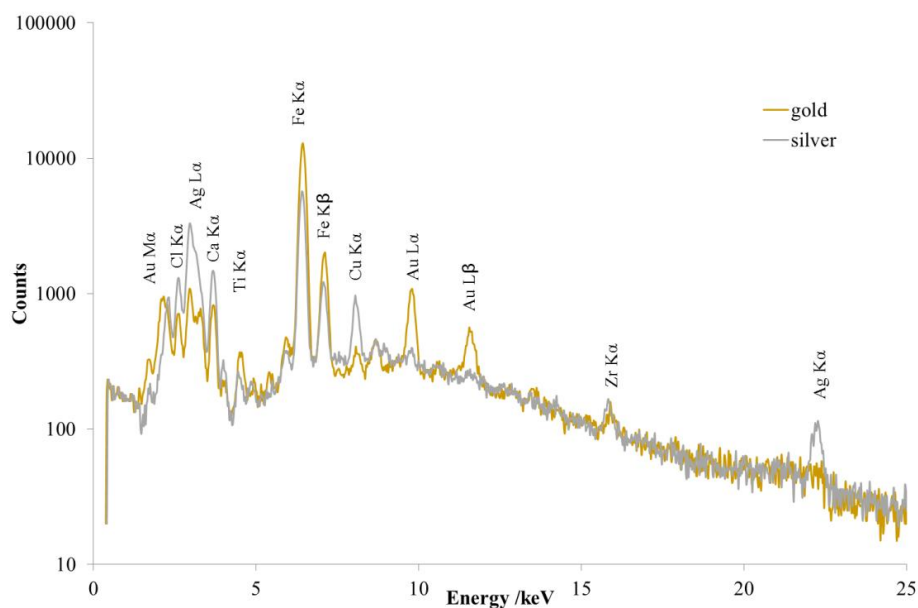
Fig. 5.6.5 -a) XRF spectra obtained for the golden background and brown sea. Spectra acquired at 30 kV, 100μA during 300s.

5.7. The two-paneled Namban-type folding screen belonging to private collection – the parasol scene (see ANNEX)

5.7.1. Specimen description

This screen (Fig. 5.7.1.) was also selected to be part of the exhibition: Giappone. Terra di incanti - Di linea e di colore. In the meantime, doubts were raised regarding its authenticity and dating of screen and it was decided that this artwork would not be presented. Although the figure composition was coherent with the Namban theme: «The alterity of the Portuguese is (…) visible in their thick curling mustaches (…), billowing pantaloons (…), as do the dogs kept on leashes. The Portuguese traders are served by darked-skinned Indian (and possible African) slaves, who can be seen carrying parasols over the capitão-mor (…)» [122], the screen did not have a narrative spirit. Furthermore, it was only composed by two panels, unlike the traditional six-paneled screens, usually displayed in pairs. Another unusual characteristic of the screen was the brownish-grey background contrasting with the shimmer effect of the gilded background of other Namban screens. In order to shed some light on the origin of this artwork, the characterization of the materials used in its composition was performed.

Fig. 5.7.1 – a) Photography of the Namban-type screen belonging to a private collection (BAP).

5.7.2. Results

The most unusual aspect of this screen is the brownish-grey appearance of the background. After examination of the obtained XRF spectra, the Fe content is noteworthy as well as other elements that appear distributed quite heterogeneously (Fig. 5.7.2a). Some of the analyzed areas present high amounts of Cu, Zn and Pb, while others present Ti and Mn, or even high amounts of S. As for the existence of Au, it was rapidly rejected. The brown background recalled the oxidized silver observed in screen attributed to Kano Domi belonging to MNAA collection (Fig. 5.3.1b). The anode of the X-ray tube primarily used was Ag, so the presence of this metal, if in in small amounts is difficult to put in evidence. Therefore, new measurements were performed using the eclipse-IV x-ray tube with Rh anode and the presence of Ag was confirmed throughout the screen (Fig. 6.7.2 b). Because the Kα line of Ag (22.101 keV) is overlaid with the Rh Kβ Compton scattering (~22.3

keV), the obtained spectra were compared with the one of a paper sample without Ag. The shift of the line to the left is perfectly visible, so we can conclude Ag is present.
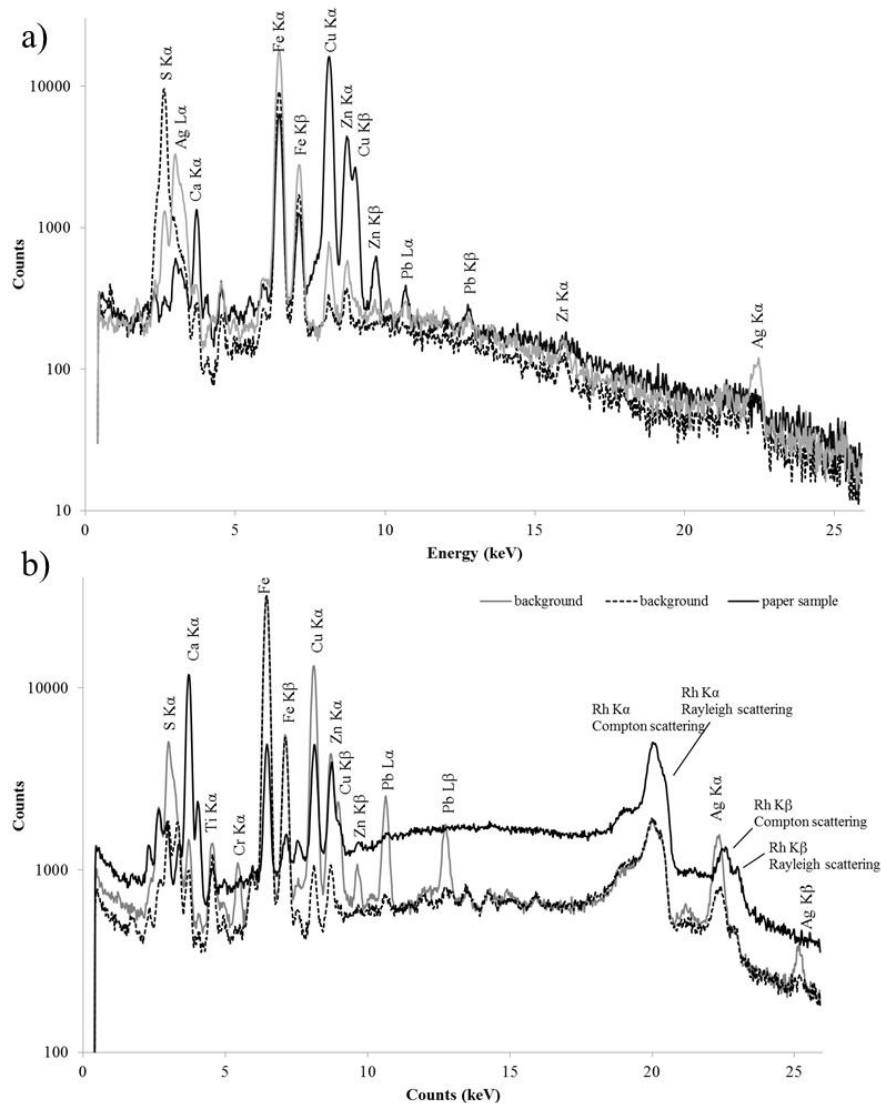
Fig. 5.7.2 - a) XRF spectra obtained for background areas with the Eclipse II (Ag anode). Spectra acquired at 30 kV, 95μA during 300s. b) XRF spectra obtained for background areas with the Eclipse IV (Rh anode). Spectra acquired at 40 kV, 40μA during 300s. Paper spectrum acquired at 40 kV, 40μA during 1200s.

Regarding the red areas, and alike the screen in section 5.6 three different shades can be distinguished (Fig. 5.7.3). The brighter shade of red revealed the presence of Cd, S and Se, suggesting the use of the pigment Cadmium Red (CdS(Se)). On the other hand, the orange shade observed in the parasol revealed higher amounts of Hg in comparison to Pb. This is quite unusual because according to the results obtained in the previous artworks, Pb was

always in higher concentrations for this color. Considering the darker shade of red, the high amount of Fe put in evidence in the spectrum could again be due to the contribution of the material used in the background or to the use of an iron-based oxide, such as Hematite (Fe_2O_3), which has a drabber hue compared to that of vermilion. Selenium was also observed in all spectra, allowing to infer that Cadmium red is always part of the color paints; Furthermore, the S-Kα is exactly in the same energy for the three spectra (2.31 keV), no shift was observed from the contributions of the Hg-Mα (2.195 keV) or Pb-Mα (2.342 keV), meaning that these elements are present in under layers and the Mα lines were attenuated in the sample.
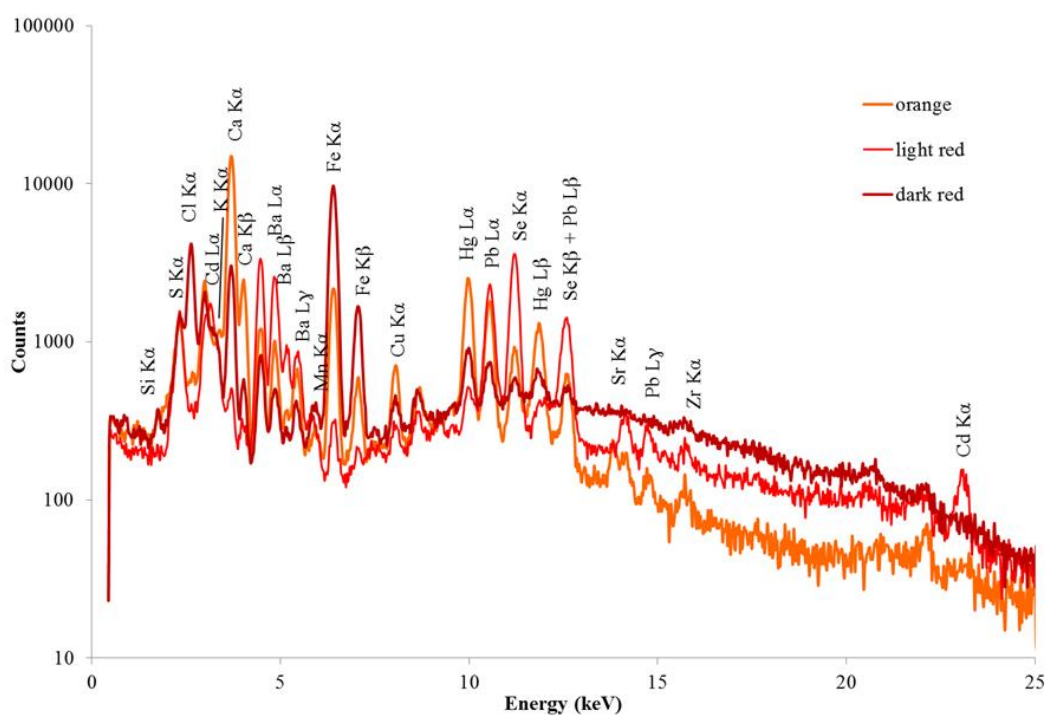
Fig. 5.7.3 - a) XRF spectra obtained for red areas. Spectra acquired at 30 kV, 95µA during 300s.

The yellow color is scarce in this artwork. It is only present in the cross of the parasol, the leash of the dog and the flowers that ornament the clothes of the "Capitão-mor". Figure 5.7.4 presents the XRF spectra obtained for these areas. Iron was, again, found in all spectra. Keeping in mind the Fe found in the background, it is still very likely the use of an iron-based yellow such as yellow ochre ($Fe_2O_3.H_2O$). Regarding the color of the parasol, it should be noted that Au was detected as well, leaving no doubt on the fact that this

97

accessory was painted with gold. Regarding the yellow color of the dog's leash, the measurements also attested the elements Cr and Pb, thus indicating again the use of chrome yellow.
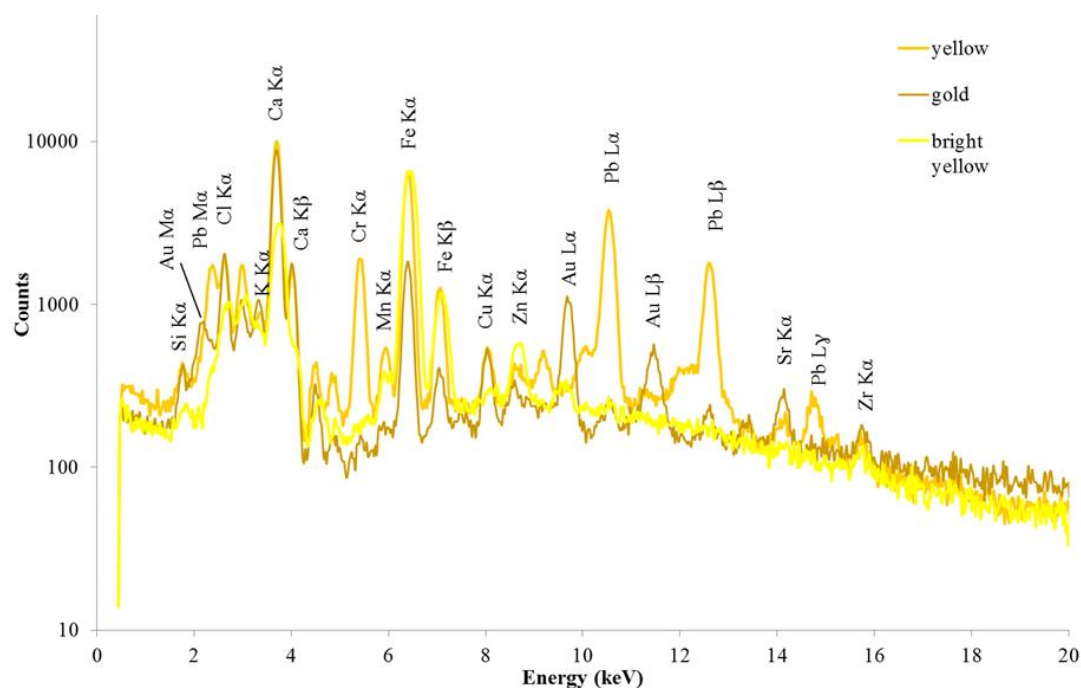
Fig. 5.7.4 - a) XRF spectra obtained for red areas. Spectra acquired at 30 kV, 95µA during 300s.

Regarding the XRF analysis of the green areas, Cu was also found (Fig. 5.7.5.a), but no corroboration of Malachite was obtained with Raman. Again the presence of Cr, indicated the presence of Chrome green. Iron appears also with great intensity in the spectrum, however it is unclear if its presence is due to the same origin as in the background or from the presence of Prussian blue. In fact, Raman analysis of green samples pointed out the presence of lead chromate (Fig. 5.7.5.b) with a strong band at 846 cm^{-1}. However, instead of the characteristic bands of Prussian blue, the typical spectrum of an organic dye was found, with bands at 230, 415, 444, 534, 807, 917, 1181, 1217, 1293, 1378, 1451, 1492, 1597 and 1627 cm^{-1}. This corresponds to a triarylmethane blue dye, most likely Victoria blue [141]. Regarding the blue areas, Fe was put in evidence in the XRF spectra (Fig. 5.7.5a), and Fe mixed with Ba and Zn to obtain a grayish shade of blue on the trousers of the slave. The possibility of the presence of Prussian blue was again raised, however, Raman spectra of the blue samples collected from the screen corresponded to Ultramarine

blue, ($3Na_2O3Al_2O36SiO_22Na_2S$) with bands at 262, 545, 590(sh), 1102 and 1660 cm^{-1} [142]. Again, the presence of Ba and Zn is probably due to the addition of a white opaque pigment to lighten the color, most likely lithopone.
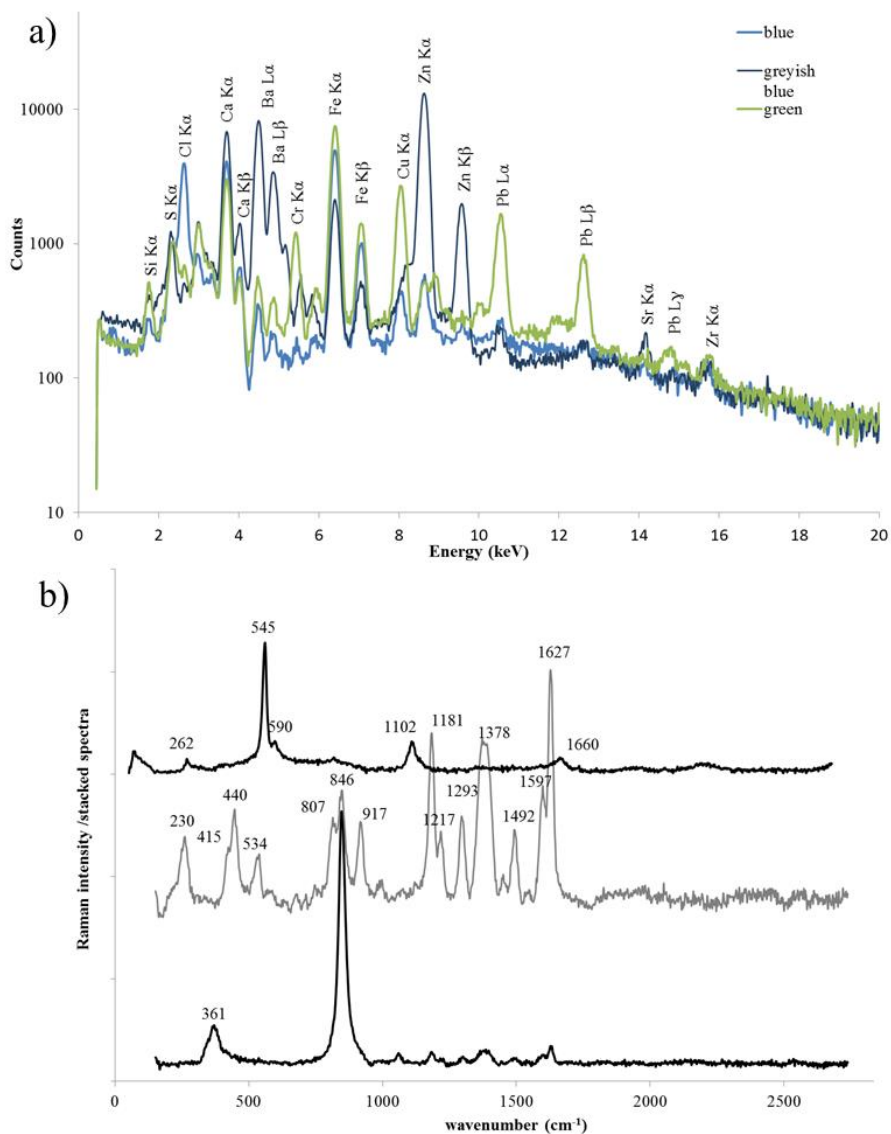
Fig. 5.7.3 - a) XRF spectra obtained for blue and green areas. Spectra acquired at 30 kV, 95μA during 300s. b) Raman spectra obtained for blue (top) and green micro-samples. Spectra acquired with 532 nm laser, 300 μm hole, 100 μm slit, 100x obj., during 6x6s, 6x5 and 6x6s, respectively.

Regarding the white and black areas, again, no substantial differences were detected in the elemental composition (Fig. 5.7.7a). Looking at the XRF spectrum of the whitish tone applied on the chair, the high content of Ca is indicative of the presence of $CaCO_3$. As far as

the black color is concerned, carbon black was the only pigment identified by Raman spectroscopy with two broad bands at ca 1300 and 1600 cm^{-1} (Fig.5.7.7b).
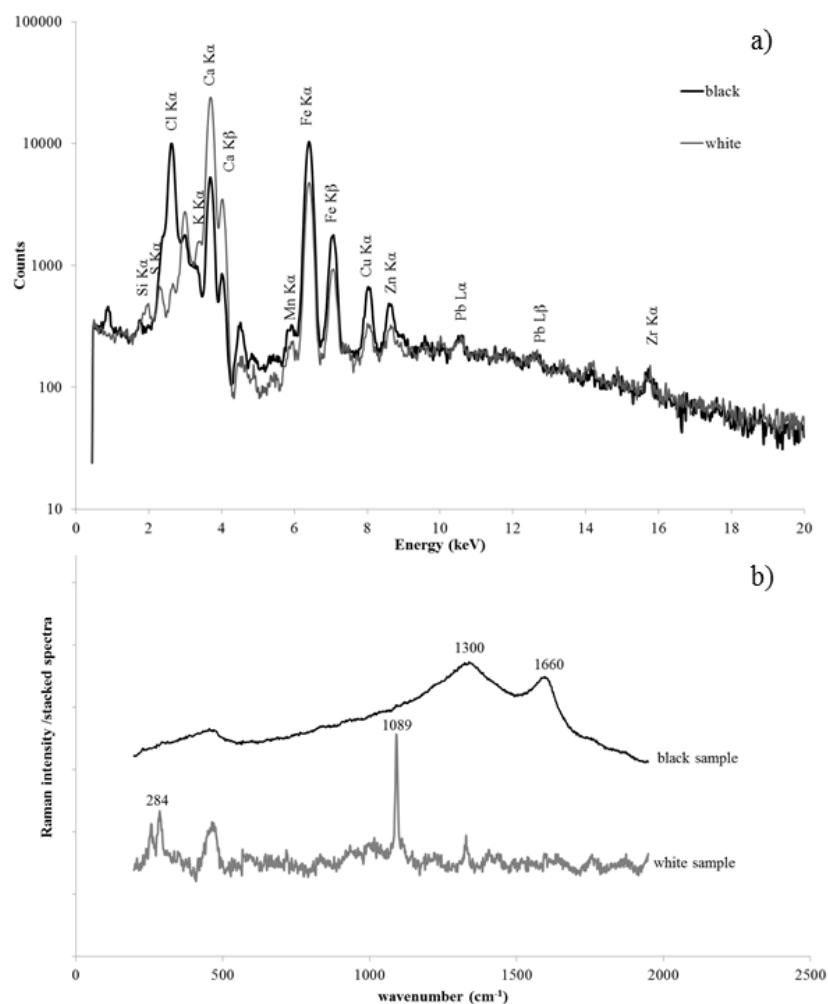
Fig. 5.7.3 - a) XRF spectra obtained for black and white areas. Spectra acquired at 30 kV, 95µA during 300s. b) Raman spectra obtained for black and white samples. Spectra acquired with 532 nm laser, 300 µm hole, 100 µm slit, 100x obj., during 3x6s and 6x10s.

Unlike the traditional six-paneled golden screens attributed to the Namban period, here we are in the presence of a two-paneled screen with silver background. However, as seen in the previous case-study, there is a two-paneled screen attributed by specialists to the Edo period. Furthermore, Namban, or Namban-type screens depicted with silver background, in the form of two or four-paneled artworks can also be found in auction [143, 144] as belonging to the 19th century, which suggests a revival of the Namban style. A broad set of

materials were obviously part of the background, taking into consideration the more or less recurrent presence of S, Ca, Ti, Mn, Fe, Cu and Zn. The provenience of these elements, in such an heterogeneous manner, whether from a ground layer or from materials applied over the background, is hard to interpret. Particularly Fe, because its presence could always be explained by the existence of a pigment with the desired color. Regarding the pigments found, and considering the palette employed by painters in the Momoyama and Edo periods, as seen in the previous case studies, the use of azurite, indigo, malachite, vermillion, red and yellow ochre, carbon black and *gofun* were expected. However these could still be found nowadays, so we could assume that they are part of the original painting but they are not conclusive in terms of dating and characterizing the intervention(s) performed on the screen. In what concerns the green areas, Cu was found in the XRF spectra, indicating the presence of Malachite but no evidence was found with Raman. Instead, chrome yellow mixed with a blue organic dye was the choice for green. Chrome yellow was discovered by Vauquelin in 1809 [137] and it did not come into commercial production before 1818, so it could never belong to an original 17th century artwork. Furthermore, the blue dyes used in Japanese traditional paintings are indigo and blue paper dayflower. Regarding the blue areas, no evidence was found of the use of azurite. The XRF spectra presented Fe, but there were no evidence of Prussian blue in the Raman spectra. Instead, ultramarine blue was detected. Discovered by Jean Baptiste Guimet in 1826, this pigment was a surpassing pigment regarding as much its remarkable properties (identical to those of the substance prepared from lapis-lazuli) as its lower cost [137]. To lighten the colors, lithopone, patented by John Orr in 1874 [135] seem to have been employed. Regarding the red areas, different mixtures were found in the different shades of red. Vermillion was found in all shades and coming from an underlayer, what could correspond to the original painting. Moreover, cadmium red (CdS(Se)) was found. This is one of the most recent of the inorganic colors produced on an industrial scale. Introduced by Haen en 1907, it came into use in England soon after [139]. The use of these compounds obviously resulted from at least two different interventions over time: the first one corresponding to the original coloring scheme, the second one to a later refurbishment, most likely performed in Europe, with materials synthetized from the 19th century onwards. One thing is certain, is that at least a partial intervention took place in the 20th century.

CHAPTER VI. DETERMINATION OF GOLD LEAF THICKNESS

6. DETERMINATION OF GOLD LEAF THICKNESS IN ARTWORKS USING A NON-DESTRUCTIVE APPROACH

6.1. Experimental

6.1.1. X-Ray Fluorescence

The EDXRF equipments used in the following case studies was described in section II as CFAUL-portable-eclipse II and CFAUL-portable-eclipse IV. The eclipse-IV x-ray tube output was filtered using 2 mm Al and 25 µm Ag filters in order to partially monochromatize the beam.

Spectrum deconvolution and evaluation was performed using WinAXIL© software package by Camberra and PyMCA© software package developed by the European Synchrotron Radiation Facility (ESRF) software group.
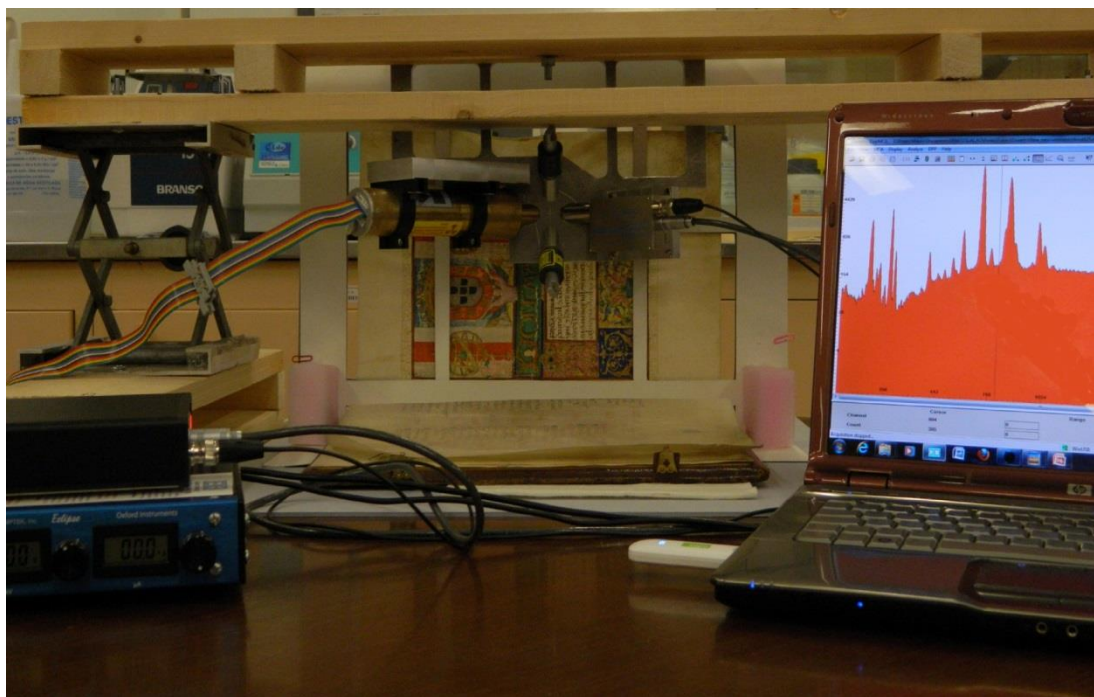
Fig. 6.1.1 – Photography of the CFAUL-portable eclipse IV, *in situ* at Torre do Tombo.

6.1.2. Raman spectroscopy

The Raman confocal microscopes used in these case studies were described in section III as CFAUL-XploRA. Only one sample was removed from foral de Murça in order to confirm the presence of lead white in the underlayer

6.2. Introduction

When dealing with gilded artworks, especially the ones using gold leaf, one of the main objectives is to determine the composition of the gold alloy. Furthermore, the thickness of the applied leaf is of great importance when we want to characterize the gilding technique. Gilding is the attaching of a gold layer on to a surface of another material, and it has been in use since 3000 BC. Several gilding techniques have been discovered in human history, the most important are gilding with gold leaf, gilding with gold foil, gilding with ground gold mixed with a vehicle, and fire gilding [145]. The process of pounding fine gold into leaf is known as goldbeating and has undergone little change since Antiquity. It began with a small ingot that was hammered until a long ribbon was obtained. The ribbon was then cut into squares corresponding to foils, and these were placed between sheets of heavy paper and hammered in their turn, repacked between parchment, and hand-beaten again, with the process repeated successively until the foils of gold have been reduced to dozens of extremely thin leaves. According to several art technological sources, in the early 16th century, more than 150 leaves might be expected from an ingot [146]. The gold leaf could then be applied with a water technique to different kinds of artworks.

There are several strategies to evaluate gilding of an artwork. Pessanha *et al.* [145] used SEM-EDS to determine the composition of the gold alloy applied in 17th-18th century folding screens and found a 100 nm order of magnitude for the thickness of the leaf by obtaining a quasi-transversal view in the backscattered electron image of the sample. Le Gac *et al.* also used SEM imaging to determine the thickness of the gold leaf of the main altarpiece of the Coimbra Old Cathedral [146]. These strategies involve the precise positioning of the sample, slight deviations can be sufficient to modify the apparent thickness of the layers. X-ray fluorescence techniques are non-destructive and often used to determine the thickness of coatings. Fiorini *et al.* [147] and Trojek *et al.* [148] studied the substrate under different angles in order to determine the thickness of the coating layer. By tilting the object around the X axis, the path length increases the intensities of the Au characteristic lines while the characteristic lines of the elements of the under layer are more attenuated. Instead of rotating the sample, one single measurement with at least two detectors at different angles can be attempted, like Kataoka *et al.* [149] performed when studying Zn-Fe alloy coatings. Cesareo *et al.* [150-152] evaluated the gilding of several

artworks by determining the intensity ratio of $L\alpha/L\beta$ lines of the substrate and compared it with the intensity ratio for an infinitely thick sample of the same material. The difference in intensities is due to the attenuation in the gold layer.

6.3. The gilding of Manueline charter of Murça

6.3.1. Specimen description

In the early 16th century, King D. Manuel I of Portugal promoted a large restructuration of the historical written memory of the realm. Within this restructure, the foral charters produced since the 12th century – regulating the juridical relation between a master, such as the king, and a collective entity, such as a village – were copied into renewed codices in the contemporary language and adjusted to the present community rules. This was the most ambitious work carried out by D. Manuel for whom the aesthetics of the charters was as important as the message they carried in. In this context, forals were written on parchment in gothic style characters and illuminated with precious ornaments such as the coat of arms and the armillary sphere used to express the authority of the realm. The Manueline foral charters, as they became known, represent the most important written heritage of the Portuguese Art during the Renaissance [153]. The following case study aims the characterization of the gilding in the frontispiece of the Manueline foral charter of *Murça* (illuminated in 1512) (Fig. 6.3.1).

Usually layer of vermillion or red ochre, called bolus, was applied to ease the burnishing of the gold. However this was not the case, as careful observation through optical microscope lead to believe, as well as reports on the similar foral charter of Vila Flor [154]. In this case, the capital D was gilded using gold leaf over a priming made of lead white, as Raman measurements on a micro-sample confirmed (Fig. 6.3.4). The characteristic lines of Pb, are still visible in the XRF spectra although attenuated in the Au layer. This Au layer is assumed to be of a very high grade, most likely pure gold. By determining the Pb intensity ratio $L\alpha/L\beta$ and comparing it with the corresponding ratio for an infinitely thick sample, we can determine the thickness of the gold leaf.

Fig. 6.3.1 – Photography of the foral charter of Murça belonging to the collection of Banco de Portugal.

6.3.2. Methodology

In a multilayered system, characteristic lines of the elements present in the under layer are attenuated in the upper layer and, most importantly, the different energies are attenuated in a different way. When photons of L lines of an element, *a*, cross a layer of another element, *b*, their ratio is further attenuated in the following manner [150]:

$$\left(\frac{L\alpha}{L\beta}\right) = \left(\frac{L\alpha}{L\beta}\right)_{s.a.} e^{-(\mu_1-\mu_2)\rho_b d_b} \qquad \text{eq.(6.1)}$$

Where:

μ_1 is the mass attenuation coefficient of the material b at energy of Lα;

μ_2 is the mass attenuation coefficient of the material b at energy of Lβ;

ρ_b is the density of material b;

d_b is the thickness of the layer.

$(L\alpha/L\beta)_{s.a.}$ is the intensity ratio of the characteristic lines of the element in the underlayer due to self-attenuation effects.

In the case of lead white covered with gold leaf equation 1 becomes:

$$Pb\left(\frac{L\alpha}{L\beta}\right) = Pb\left(\frac{L\alpha}{L\beta}\right)_{s.a.} e^{-(\mu_1-\mu_2)\rho_{Au} d_{Au}} \qquad \text{eq.(6.2)}$$

Where:

μ_1 is the mass attenuation coefficient of Au at 10.55 keV;

μ_2 is the mass attenuation coefficient of Au at 12.6 keV;

ρ_{Au} is the density of the Au;

d_{Au} is the thickness of the gold layer.

$(L\alpha/L\beta)_{s.a.}$ is the intensity ratio of the characteristic lines of Pb in lead white due to self-attenuation effects.

This last parameter is unknown and has to be determined. Lα/Lβ intensity ratios are very well documented [79, 84] however, they refer, to infinitely thin, elemental samples, where the emitted lines are not interacting with matter. Intensity ratio Lα/Lβ of Pb depends, therefore on the thickness of the layer [152].

$$\left(\frac{L\alpha}{L\beta}\right) = \left(\frac{L\alpha}{L\beta}\right)_0 \left(\frac{\varepsilon(L\alpha)}{\varepsilon(L\beta)}\right) \left[\frac{(\mu_0+\mu_4)}{(\mu_0+\mu_3)}\right] \left[\frac{1-e^{-(\mu_0+\mu_3)d}}{1-e^{-(\mu_0+\mu_4)d}}\right] \qquad \text{eq. (6.3)}$$

Where,

$\left(\frac{L_\alpha}{L_\beta}\right)_0$ is the ratio for an infinitely thin sample;

ε(E) is the detector efficiency for a given energy;

μ_0 is the linear attenuation coefficient of Pb at incident energy E_0;

μ_3 is the linear attenuation coefficient of Pb at energy of Lα (10.55 keV);

μ_4 is the linear attenuation coefficient of Pb at energy of Lβ (12.6 keV);

d is the thickness of the layer.

If considering the detector placed in 45º geometry orthogonal to the sample a correction must be made to eq. 3:

$$\left(\frac{L_\alpha}{L_\beta}\right) = \left(\frac{L_\alpha}{L_\beta}\right)_0 \left(\frac{\varepsilon(L_\alpha)}{\varepsilon(L_\beta)}\right) \left[\frac{(\mu_0+\mu_2)}{(\mu_0+\mu_1)}\right] \left[\frac{1-e^{-(\mu_0+\mu_1)\frac{d}{\cos45º}}}{1-e^{-(\mu_0+\mu_2)\frac{d}{\cos45º}}}\right] \qquad \text{eq.(6.4)}$$

In order to determine the self-attenuation parameter for Pb, we plotted the intensity ratio Lα/Lβ (eq. 4) for a layer of pure Pb, for lead carbonate ($PbCO_3$) and lead white ($2PbCO_3.Pb(OH)_2$) (Fig. 6.3.2). The first conclusion to be drawn is that the behavior is very similar for all the samples and from a thickness of around 30 μm the intensity ratio Lα/Lβ becomes constant (~0.867) for all the samples. This means that the samples can be considered bulk or infinitely thick. According to Mantler *et al.* that thickness should be 24 μm for lead white [2].

In order to evaluate the influence of the binder in the attenuation of Pb characteristic lines, $PbCO_3$ standards of different thicknesses were prepared by grinding $PbCO_3$ in a mortar and mixing with rabbit-skin glue (5%) to an adequate consistency. They were then applied over Whatman paper with a pigment applicator to establish thicknesses of 50, 100, 150 and 200 μm and analyzed with our XRF setup. Figure 6.3.2 shows the experimental values for the Pb Lα/Lβ intensity ratios. In this figure we can see that the Lα/Lβ intensity ratio has reached a plateau at these thickness values as the theoretical calculations predicted, however the value is slightly lower (mean value of 0.847).
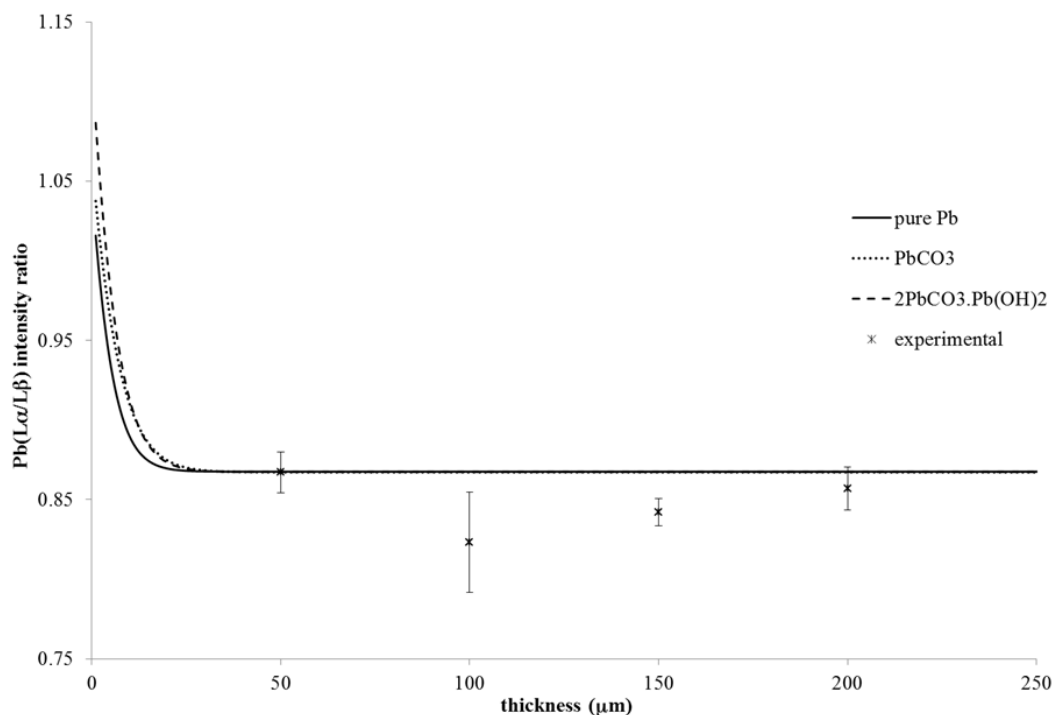
Fig. 6.3.2 – Plot of the intensity ratio Lα/Lβ for a layer of pure Pb (full line), $PbCO_3$ (dotted line) and lead white - $2PbCO_3.Pb(OH)_2$ (dashed line). Experimental values obtained for $PbCO_3$ standards.

Observations made with optical microscope of a sample collected from the charter of *Murça* indicated a lead white layer greater than 30 μm and so, we can consider our sample as an infinitely thick layer of lead white. According to these results, eq. 6.2 can be simplified, considering the self-attenuation Lα/Lβ intensity ratio corresponding to an infinitely thick layer, and the thickness of the gold leaf applied over it can be determined.

6.3.3. Results

Figure 6.3.3 presents the comparison of the EDXRF spectrum obtained for a gilded spot and the parchment for charter of *Murça*. The presence of Ni, Cu and Zn in the spectra are contributions from the experimental setup. Iron, was a constant presence throughout the illuminated area of the charter, probably a contamination from the iron-gall ink. Lead is identified in the spectrum and becomes from the priming layer, identified as lead white through Raman measurements of a collected micro-sample.
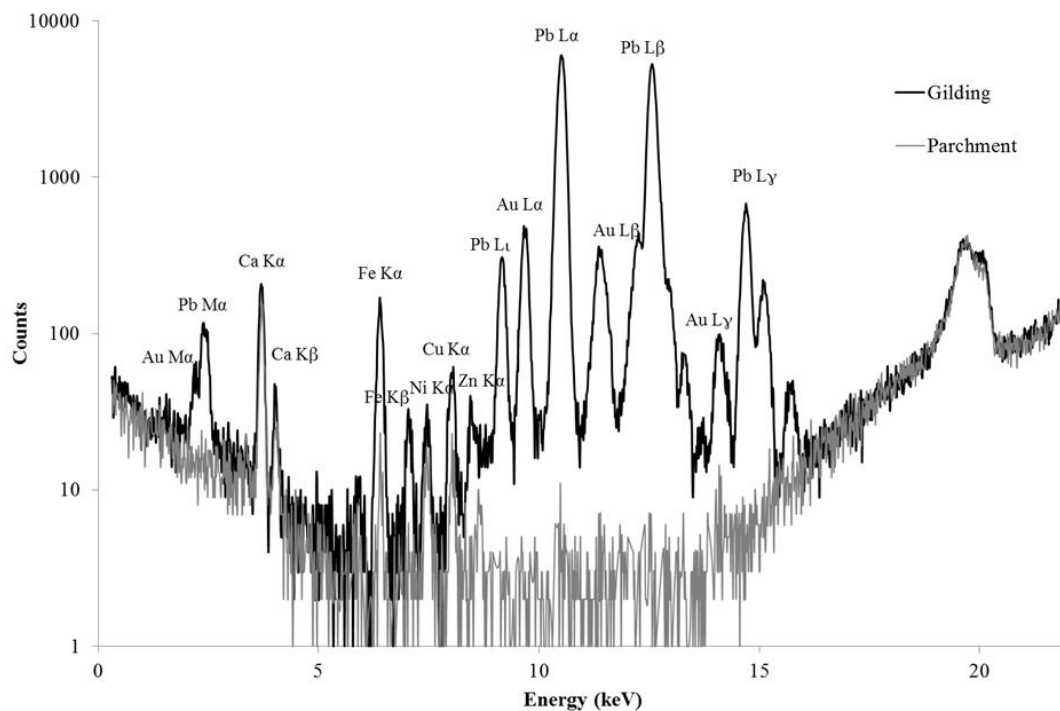
Fig. 6.3.3 – EDXRF spectra obtained for the gilded capital D charter of Murça (black line), for the parchment (gray line).

Figure 6.3.4. shows the characteristic Raman bands of lead white at 671 and 1050 cm^{-1} [43]. The spectrum was acquired transversely and not in a cross-section so we also have information from the parchment (between 1100-1700 cm^{-1} [155], like the presence of calcite ($CaCO_3$) and gypsum ($CaSO_4$) and some sort of unidentified organic binder [154] [156]. Gypsum is formed by Ca^{2+} ions displaced from $CaCO_3$ (used in parchment making [155] in the presence of metal sulfates coming from the ink [157].
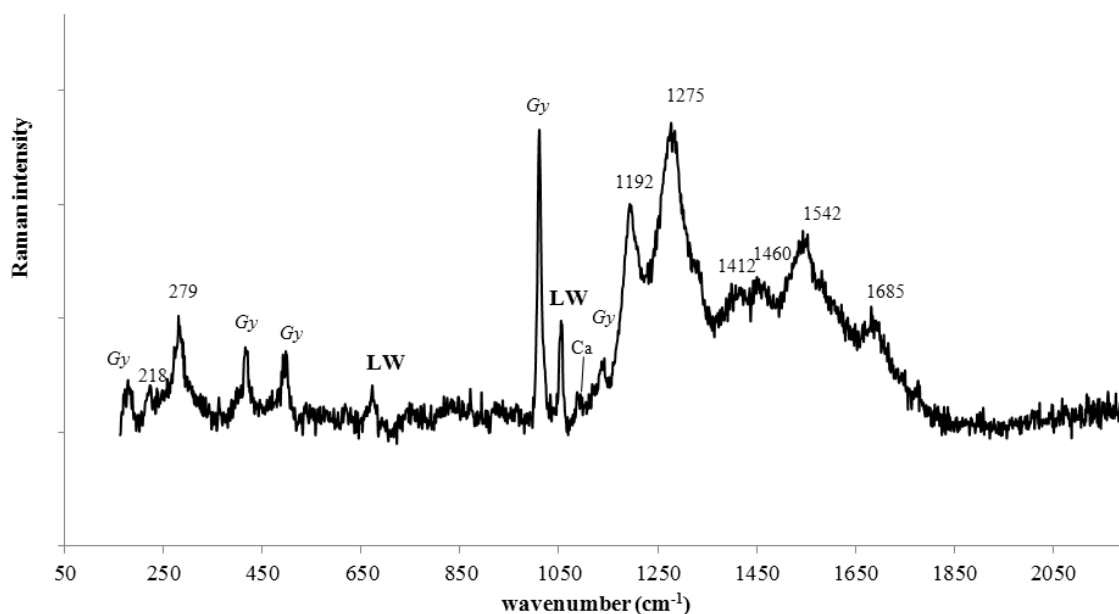
Fig. 6.3.4 –Raman spectrum obtained for the collected micro-sample. LW – lead white, Gy – gypsum, Ca – Calcite. Spectrum obtained with 785 nm laser, 300 µm hole, 100 µm slit, 50x obj., acquisition time 16x30s.

The Pb Lα/Lβ intensity ratios of the XRF spectra performed on the gilding of the charter of *Murça* were determined and the corresponding thicknesses were calculated (eq. 6.2) using both the theoretical and the experimental values for (Lα/Lβ)$_{s.a.}$. Results are presented in table 7.3.1.

	Spot 1		Spot 2		Spot 3		Spot 4			
Pb (Lα/Lβ)	1.07 ±0.01		1.11 ±0.01		1.15 ±0.06		1.07 ±0.05		mean	
(Lα/Lβ)$_{s.a}$	theor.	exp.	theor.	exp.	theor.	exp.	theor.	exp.	theor.	exp.
Au thickness (µm)	1.42± 0.01	1.58± 0.01	1.63± 0.01	1.79± 0.01	1.89± 0.06	2.04± 0.06	1.42± 0.05	1.57± 0.05	**1.6 ±0.4**	**1.7 ±0.4**

Table 6.3.1. Results obtained for the thickness of the gold leaf according to eq. 7.2, using both theoretical and experimental values for Pb Lα/Lβ due to self-attenuation.

Figure 6.3.5 shows a plot of the dependence of Lα/Lβ intensity ratios as a function of the Au thickness, according to eq. 6.2, as well as the thickness values obtained using the (Lα/Lβ)$_{s.a.}$ obtained experimentally. The results obtained using both self-attenuation values

are very similar and within the uncertainties of the calculation, 1.6 ± 0.4 and 1.7 ± 0.4 µm, therefore, we can assume that they are valid even for a different composition of the lead white layer.
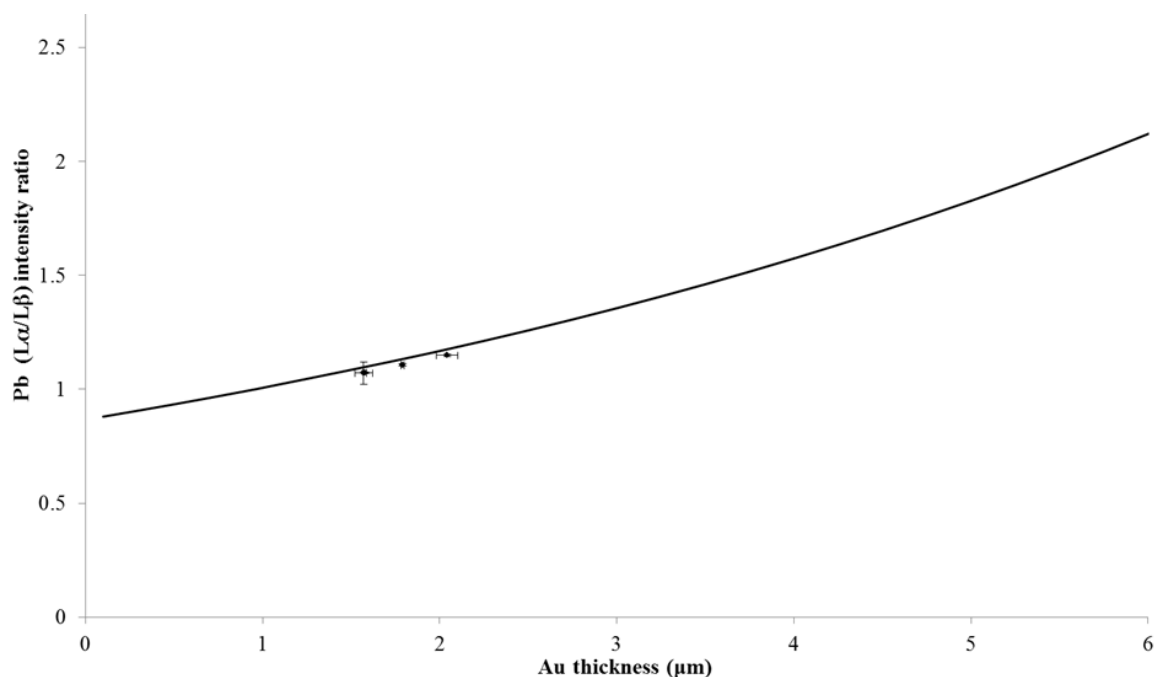
Fig. 6.3.5. - Plot of the intensity ratio of Pb Lα/Lβ as a function of the thickness of the gold layer considering theoretical $(L\alpha/L\beta)_{s.a.}$. In dots, the calculated Au layer thicknesses considering $(L\alpha/L\beta)_{s.a.}$ determined experimentally.

6.4. The gilding of Namban folding screens

6.4.1. Specimen description

The Namban folding screens under study were described in sections 5.3, 5.5 and 5.6 of this work. In the case of Namban screens, the gold leaf was not applied over a layer of lead white, as Pb was not present in the screens. In this case we believe that there could be a bolus layer made of red or yellow ochre, however, Fe is a constant presence throughout the screens and it could be due to some sizing of the paper.

6.4.2. Methodology

As seen in the previous case study, the different lines of an element are attenuated differently as the thickness of the layer increases so the intensity ratio of Lα/Lβ (and Mα/Lα) varies until we can consider the sample infinitely thick and it remains constant. Analogously as in eq. 6.3, the intensity ratio of Mα/Lα lines of Au are dependent of the thickness of the layer by means of:

$$\left(\frac{M_\alpha}{L_\alpha}\right) = \left(\frac{M_\alpha}{L_\alpha}\right)_0 \left(\frac{\varepsilon(M_\alpha)}{\varepsilon(L_\alpha)}\right) \left[\frac{(\mu_0+\mu_2)}{(\mu_0+\mu_1)}\right] \left[\frac{1-e^{-(\mu_0+\mu_1)d}}{1-e^{-(\mu_0+\mu_2)d}}\right] \qquad \text{eq. (6.5)}$$

Where,

$\left(\frac{M_\alpha}{L_\alpha}\right)_0$ is the ratio for an infinitely thin sample;

$\varepsilon(E)$ is the detector efficiency for a given energy;

μ_0 is the linear attenuation coefficient of Au at incident energy E_0;

μ_1 is the linear attenuation coefficient of Au at energy of Mα (2.12 keV);

μ_2 is the linear attenuation coefficient of Au at energy of Lα (9.71 keV);

d is the thickness of the layer.

Again, if considering the detector placed in 45º geometry to the orthogonal to the sample a correction must be made to eq. 6.5:

$$\left(\frac{M_\alpha}{L_\alpha}\right) = \left(\frac{M_\alpha}{L_\alpha}\right)_0 \left(\frac{\varepsilon(M_\alpha)}{\varepsilon(L_\alpha)}\right) \left[\frac{(\mu_0+\mu_2)}{(\mu_0+\mu_1)}\right] \left[\frac{1-e^{-(\mu_0+\mu_1)\frac{d}{\cos 45º}}}{1-e^{-(\mu_0+\mu_2)\frac{d}{\cos 45º}}}\right] \qquad \text{eq. (6.6)}$$

The x-ray tube used in the analysis of the Namban screens had a silver anode so the evaluation of the presence of Ag, if in low concentrations, is challenging. This way, we investigated the influence of the presence of Ag in the Au alloy in the Au(Mα/Lα) and Au(Lα/Lβ) intensity ratios considering different alloy compositions. Figures 6.4.2 and 6.4.3 are plot of these dependences with the thickness considering a pure Au layer, an alloy of 99% Au and 1% Ag; an alloy of 97% Au and 3% Ag and an alloy of 95% Au and 5% Ag. It is visible that, taking into account the uncertainties related with the determination of the peak areas, the layers can be considered identical concerning the attenuation of the Au-Mα Au-Lα and Au-Lβ lines.

Other important consideration to be gathered from this plot is that a layer of pure Au can only be considered infinitely thick if it has more than 10-15 μm, which is much thicker than these artworks [158]. We are therefore in the presence of intermediate thick samples, which would make quantification quite challenging.
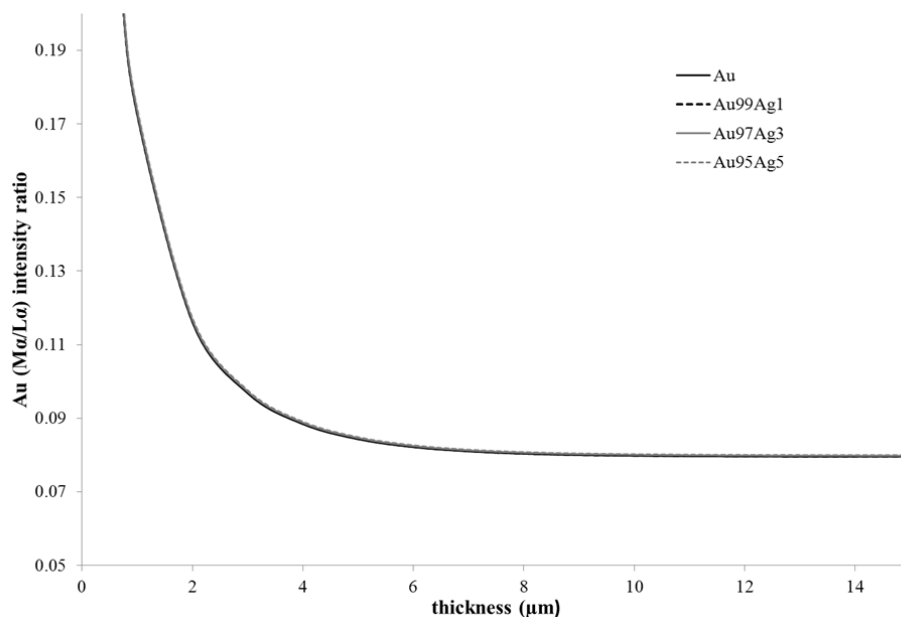
Fig. 6.4.2 – Plot of the intensity ratio Mα/Lα for a layer of pure Au, Au99%-Ag1%, Au97%-Ag3% and Au95%Ag5%.
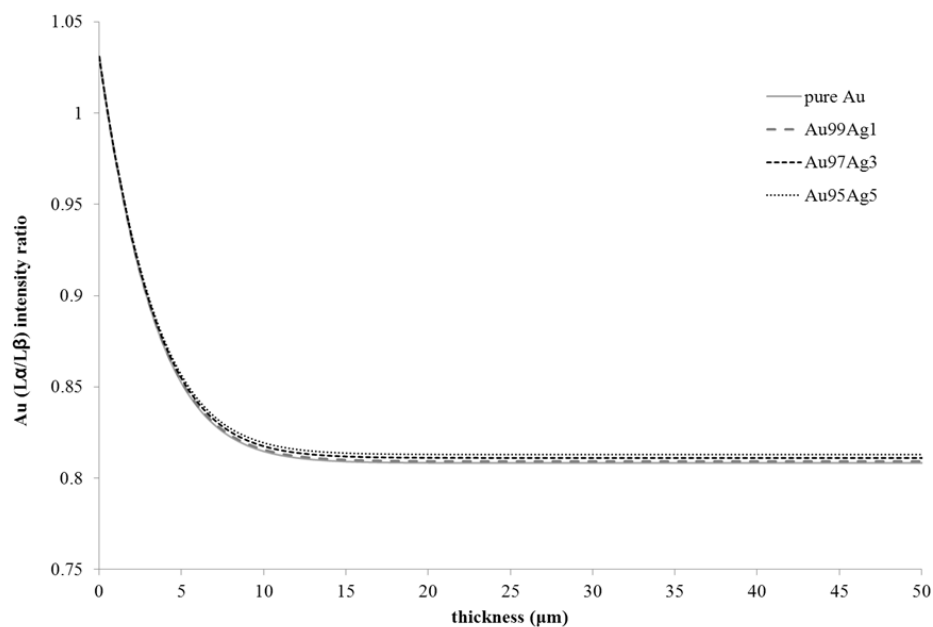
Fig. 6.4.3 – Plot of the intensity ratio Lα/Lβ for a layer of pure Au, Au99%-Ag1%, Au97%-Ag3% and Au95%Ag5%.

The measurements on the screens were performed with no filters and using the bremsstrahlung from the tube and the plotted curves contemplate a 20 keV incident radiation, so we cannot determine the thickness as performed for the previous case study. However, these results show that we can compare the intensity ratios obtained for the screens to gain an idea of the comparative thicknesses of the gold leafs applied on the different screens.

6.4.3. Results

The comparison of the Au(Mα/Lα) and the Au(Lα/Lβ) intensity ratios is presented in table 6.4.1. There were no differences found in the Au(Lα/Lβ) intensity ratios for the different screens, which could mean that the thickness is too small for this different attenuation factors to be taken into account, however, the comparison of the Au(Mα/Lα) intensity ratios rendered more interesting results. The intensity ratios and therefore the thickness of the gold leaf seem to be similar for both pairs of screens at MNAA as well as the screen belonging to the private collection. Interestingly, the screen belonging to MO presents a higher mean value for the intensity ratio meaning that the Au-Mα line is less attenuated and therefore the layer is thinner. A quasi-transversal view obtained with scanning electron microscope of a sample collected from this screen indicated a thickness of 100 nm order of magnitude [145], which is consistent with the testimony of Koyano that the Japanese leaf is the thinnest in the world [159].

	MNAA1	MNAA2	MO	private
Au (Mα/Lα)	0.31 ±0.04	0.28 ±0.05	0.41 ±0.05	0.32 ±0.01
Au (Lα/Lβ)	1.87±0.04	1.91±0.03	1.88±0.03	1.94±0.02

Table 6.4.1. Results obtained for the Au (Mα/Lα) and Au(Lα/Lβ)intensity ratio for four studied screens.

7. CONCLUSIONS AND OUTLOOK

7. CONCLUSIONS

With the work here presented we demonstrated the efficacy of X-ray fluorescence (XRF) with portable setups, aided by Raman spectroscopy, in providing answers to actual issues of characterization, conservation and authentication related with artworks in paper and parchment support. Sometimes however, the information gathered from XRF analysis were not enough and micro-sampling was performed and Raman microscopy was employed.

The first part of the work concerned the use of μ-XRF to the study of paper discolorations. The use of the micro beam was fundamental, especially when dealing with the small size foxing stains (few millimeters in diameter). The micro beam was obtained by using a polycapillary lens to focus the x-ray beam. Furthermore, by taking advantage of the vacuum chamber and reduction of air path, it became possible to improve the detection limits for light Z elements, such as Al, Si and P.

The elemental quantification of stained and unstained areas of paper was obtained through the compare mode method, which compares the net peak areas of the elements of the unknown samples with the areas of standard reference materials with the same matrix and similar elemental composition. The results showed similar behavior in the two kinds of analyzed stains, as we observed that the K content increased in the stain, as was already reported (123) (118). Regarding the foxing stains, it was also determined that whenever Cl was present in paper it will be likely to disappear in the stain.

A different equipment, more compact and light, was used to study all the Namban paper folding screens existing in both private and public Portuguese collections. This equipment is much easier and faster to assemble and can be carried in two suitcases, making the visits to the museums much pleasant. This equipment has a larger spot size, however it is perfectly suitable for analyzing characters and features in the centimeter scale. Furthermore, we took advantage of the 90º geometry to reduce bremsstrahlung and Compton scattering. Six of the studied six-panel folding screens are attributed to the Kano School painters of the Momoyama period (~1573-1603) while, two screens, due to their lack of detail an even great magnification of the scenes and characters are attributed to the Edo period (~1603-1868). One screen, very peculiar because it did not present the typical gilded background belonged, most likely, also to the Edo period. The specimens belonging

to MNAA are extremely well preserved and present the original materials representing an important opportunity for characterizing the pigments used during the Momoyama period by the Kano school workshops. These pigments were malachite, azurite, indigo, vermillion, red lead, white oyster shell, and carbon black. As for the screen belonging to MO collection, the same pigments as the original folding screen were found, however we also found different mixtures such as vermillion, carbon black and calcium carbonate for the brown, and vermillion and red lead for the orange. The use of these mixtures was already discovered in the 16th century copy of the Tale of Genji (11). Furthermore, the presence of atacamite was discovered in this screen, most likely a degradation product of malachite.

On the other hand we studied screens that were subject of vast restoration interventions and modern materials were found throughout the artworks: the screens belonging to MNSR presented pigments such as cobalt blue and phthalocyanine blue, this last one only commercially available in 1938, pigment such as chrome yellow and chrome yellow-orange that were replaced in the 1950's by cadmium yellow and cadmium red pigments. This means that these pigments were subjected to an intervention somewhere between these two dates, probably in the beginning of the 1950's just before the Portuguese state acquired them.

An even greater magnification of the boat arriving to the port of Nagasaki is depicted in a two-paneled screen belonging to a private collector. The authenticity of this screen was not in question, however modern material were discovered together with the original ones. These pigments were zinc white and lithopone, chrome green and cadmium red. This last pigment was only introduced in 1907 meaning that this screen was subjected to a conservation intervention after this date.

The other two-paneled screen investigated had the particularity of not having a gilded background. Instead, silver was found, although covered with an unknown substance. Again, pigments that were not accessible in the 17th century were found together with the pigments commonly used in the Namban screens attributed to the Kano school. However, it is unclear whether the insinuation of malachite and the presence of vermillion, carbon black and $CaCO_3$ are compelling evidences of an original painting from the 17th century, then improved or modified during the last century, or if these materials, together with the choice

of a silver background and the use of chrome yellow, ultramarine blue and lithopone, are rather an indication of an artwork created during a 19th century Namban revival.

The third part of the work focused on the evaluation of the thickness of the gold leaf applied in gilded artworks in paper and parchment support. Two similar methodologies were used: the first one is based on the differences in attenuation coefficients of the characteristic lines of the substrate on which the gold leaf is applied. This methodology is dependent of the determination of the intensity ratio of the characteristic lines of the element in the underlayer due to self-attenuation effects. This factor was determined both theoretically and experimentally using model samples of different thicknesses. This methodology was applied to the gilding of the frontispiece of the Manueline charter of Murça, applied of a layer of lead white, where a thickness of 1.6 μm was determined, and can also be applied to the gilding of similar artworks. Regarding the gilding in the Namban folding screens, and because there was no lead white underlayer, we used the differences in attenuation coefficients for the different lines of Au itself. Using this methodology we were able to compare the thickness of the gold leaf applied in Namban folding screens and conclude that the leaf applied in the screen from Museu Oriente is the thinnest.

OUTLOOK

The case studies here presented are successful examples of how analytical techniques can be very useful to unveiling an artist technique or artwork journey in what concerns interventions. However, sometimes a deeper knowledge of the stratigraphy of the piece is fundamental. This can be obtained by applying methodologies based on the differences in attenuation coefficients of the characteristic lines, similarly to the ones applied here for gilding. In order to establish these methodologies model samples of known stratigraphies with commonly used pigments should be created and evaluated.

Bibliography

1. M Schreiner, B Frühmann, D Jembrih-Simbürger, R Linke. *x-rays in art and archaeology – an overview.* 2004, Advances in X-ray Analysis, Vol. 47, pp. 1-17.

2. M Mantler, M Schreiner. *X-ray fluorescence spectrometry in art and archaeology.* 2000, X-Ray Spectrometry, Vol. 29, pp. 3-17.

3. A Duran, M L Franquelo, M A Centeno, T Espejo, J L Perez-Rodriguez. *Forgery detection on an Arabic illuminated manuscript by micro-Raman and X-ray fluorescence spectroscopy.* 2011, Journal of Raman spectroscopy, Vol. 42, pp. 48-55.

4. A Galli, L Bonizzoni. *True versus forged in the cultural heritage materials: the role of PXRF analysis.* 2013, x-ray spectrometry DOI 10.1002/xrs.2461

5. B Wehling, P Vandenabeele, L Moens, R Klockenkamper, A von Bohlen , G Van Hooydonk , M de Reu. *Investigation of Pigments in Medieval Manuscripts by Micro Raman Spectroscopy and Total Reflection X-Ray Fluorescence Spectrometry.* 1999, Mikrochim. Acta, Vol. 130 , pp. 253-260.

6. J L Ferrero, C Roldán, D Juanes, J Carballo, J Pereira, M Ardid, J L Lluch, R Vives. *Study of inks on paper engravings using portable EDXRF spectrometry.* 2004, Nuclear Instruments and methods in physics research B, Vol. 213, pp. 729-734.

7. K Castro, N Proietti, E Princi, S Pessanha, M L carvalho, S Vicini, D Capitani, J M Madariaga. *Analysis of a coloured Dutch map from the eighteenth century: The need for a multi-analytical spectroscopic approach using portable instrumentation.* 2008, Analytica Chimica Acta, Vol. 623, pp. 187-194.

8. N Mendes, C Lofrumento, A Migliori, E M Castelluci. *Micro-Raman and particle-induced X-ray emission spectroscopy for the study of pigments and degradation products present in 17th century coloured maps.* 2008, Journal of Raman spectroscopy, Vol. 39, pp. 289-294.

9. K Proost, K Janssens, B Wagner, E Bulska, M Schreiner. *Determination of localized Fe2+/Fe3+ ratios in inks of historic documents by means of l-XANES.* 2004, Nuclear Instruments and Methods in Physics Research B, Vol. 213, pp. 723-728.

10. K Castro, S Pessanha, N Proietti, E Princi, D Capitani, M L Carvalho, J M Madariaga. *Noninvasive and nondestructive NMR, Raman and XRF analysis of a Blaeu coloured map from the seventeenth century.* 2008, Analytical and Bioanalytical Chemistry, Vol. 391, pp. 433-441.

11. K Eremin, J Stenger, M Li Green. *Raman spectroscopy of Japanese artists' materials: The Tale of Genji by Tosa Mitsunobu.* 2006, Journal of Raman spectroscopy, Vol. 37, pp. 1119-1124.

12. K D Charleton, A E Smith, D M Goltz. *Microsampling and Determination of Metals in Iron Gall Ink.* 2009, Analytical Letters, Vol. 42, pp. 2533-2546.

13. A Adriaens, *Non-destructive analysis and testing of museum objects: An overview of 5 years of research.* 2005, Spectrochimica Acta Part B: Atomic Spectroscopy, Vol. 60, pp. 1503-1516.

14. S Piorek, *Principles and applications of man-portable X-ray fluorescence spectrometry.* 1994, Trends in Analytical Chemistry, Vol. 13, pp. 286-293.

15. R Cesareo, G Gigante, A Castellano, S Ridolfi. *Portable and handheld systems for energy-dispersive x-ray fluorescence analysis.* In R A Meyers. *Encyclopedia of analytical chemistry*. John Wiley & sons Ltd, 2009.

16. G L Bosco, *Development and application of portable, hand-held X-ray fluorescence spectrometers.* 2013, Trends in Analytical Chemistry, Vol. 45, pp. 121-134.

17. T Pantazis, J Pantazis, A Huber, R Redus. *The historical development of the thermoelectrically cooled x-ray detector and its impact on the portable and hand-held XRF industries (February 2009).* 2010, X-ray spectrometry, Vol. 39, pp. 90-97.

18.. T Cechac, T Trojek, L Musilek, H Paulusova. A*pplication of x-ray fluorescence in investigations of Bohemian historical manuscripts* 2010, Applied Radiation and Isotopes, Vol. 68, pp. 875-878.

19. T D Chaplin, R J H Clark, M Martinón-Torres. *A combined Raman microscopy, XRF and SEM-EDX study of three valuable objects - A large painted leather screen and two illuminated title pages in 17th century books of ordinances of the Worshipful company of barbers, london.* 2010, Journal Of Molecular Structure, Vol. 976, pp. 350-359.

20. G Van der Snickt, W de Nolf, B Vekemans, K Janssens. *micro-XRF/micro-RS VS SR micro-XRD for pigment identification in illuminated manuscripts.* 2008, Applied Physics A, Vol. 92, pp. 59-68.

21. A Duran, J L Perez-Rodriguez, T Espejo, M L Franquelo, J castaing, P Walter. *Characterization of illuminated manuscripts by laboratory made portable XRD and micro-XRD systems.* 2009, Anal Bioanal Chem , Vol. 395, pp. 1997-2004.

22. Institute for scientific instruments website - http://www.ifg-adlershof.de/index.php?id=51&L=6. (september 2013)

23. M Ardid, J L Ferrero, C Roldán, D Juanes, J L Lluch, R Vives, P Punter. *Design of EDXRF equipment for the nondestructive study of prints.* 2004, Advances in X-ray analysis, Vol. 47, pp. 70-75.

24. M. Manso, A. Le Gac, S. Longelin, S. Pessanha, J. C. Frade, M. Guerra, A. J. Candeias, M. L. Carvalho. *Spectroscopic characterization of a masterpiece: The Manueline foral charter of Sintra* 2013, Spectrochimica Acta Part A: Molecular and Biomolecular Spectroscopy, vol.105, pp.288–296

25. R Cesareo, A Brunetti. *X-ray fluorescence - analysis of 19th century stamps.* 2008, x-ray spectrometry, Vol. 37, pp. 260-264.

26. K Trentelman, M Bouchard, M Ganio, C Namowicz, C S Patterson, M Walton. *The examination of works of art using in situ XRF line and area scans.* 2010, X-Ray Spectrom., Vol. 39, pp. 159–166.

27. Bruker website http://www.bruker.com/en/products/x-ray-diffraction-and-elemental-analysis/handheld-xrf/tracer-iii/overview.html. (september 2013)

28. K Trentelman, N Turner. *Investigation of the painting materials and techniques of the late-15th century manuscript illuminator Jean Bourdichon.* 2009, Jornal of Raman Spectroscopy Vol. 40, pp. 577-584.

29. C Miguel, A Claro, A P Gonçalves, V S F Muralha, M J Melo. *A study on red lead degradation in a medieval manuscript Lorvao Apocalypse (1189).* 2009, Journal of Raman spectroscopy, Vol. 40, pp. 1966-1973.

30. L Burgio, R J H Clark, V S F Muralha, T Stanley, P*igment analysis by Raman microscopy of the non-figurative illumination in the 16th to 18th century islamic manuscripts.* 2008, journal of Raman Spectroscopy, Vol. 39, pp. 1482-1493.

31. L Burgio, Robin J H Clark, R R Hark. *Spectroscopic investigation ofmodern pigments on purportedly medieval miniaturesby the 'Spanish Forger'.* 2009, Journal of Raman Spectroscopy, Vol. 40, pp. 2031-2036.

32. M Aceto, A Agostino, E Boccaleri, F Crivello, A Cerutti Garlanda. *Evidence for the degradation of an alloy pigment on an ancient Italian manuscript.* 2006, Journal of Raman spectroscopy, Vol. 37, pp. 1160-1170.

33. Assing website - http://www.assing-group.it/eng/divisione_strumenti.html?ID_o=93&d=5&m=1&ms=3&mss=3. (september 2013)

34. M Aceto, A Agostino, G Fenoglio, P Baraldi, P Zannini, C Hofmann, E Gamillscheg. *First analytical evidences of precious colourants on Mediterranean illuminated manuscripts.* 2012, Spectrochimica Acta Part A: Molecular and Biomolecular Spectroscopy, Vol. 95, pp. 235-245.

35. Niton website - http://www.niton.com/en/niton-analyzers-products/xl3/xl3t. (september 2013)

36. S Bruni, S Caglio, V Gugliemi, G Poldi. *The joined use of n.i. spectroscopic analyses FTIR, Raman, visible reflectance spectrometry and EDXRF to study drawings and illuminated manuscripts.* 2008, Applied Physics A, Vol. 92, pp. 103-108.

37. M Mantler, J Klikovits. *Analysis of art objects and other delicate samples: is XRF really non-destructive?* 2004, advances in x-ray analysis, Vol. 47, pp. 42-46.

38. M Mantler, M Schreiner. *X-ray analysis of objects of art and archaeology.* 2001, Journal of Radioanalytical and Nuclear Chemistry, Vol. 247, pp. 635-644.

39. R J H Clark, *Raman microscopy: sensitive probe of pigments on manuscripts paintings and other artefacts.* 1995, Journal of Molecular Structure, Vol. 347, pp. 417-428.

40. D Bersani, P P Lottici, F Vignali, G Zanichelli. *A study of medieval illuminated manuscripts by means of portable Raman equipments.* 2006, Journal of Raman Spectroscopy, Vol. 37, pp. 1012-1018.

41. G D Smith, R J H Clark. R*aman microscopy in archaeological science.* 2004, Journal of archaeological science, Vol. 31, pp. 1137-1160.

42. I M Bell, R J H Clark, P J Gibbs. *Raman spectroscopic library of natural and synthetic pigments.* 1997, spectrochimica acta a, Vol. 53, pp. 2159-2179.

43. L Burgio, R J H Clark. *library of FT-Raman spectra of pigments, minerals, pigment media and varnishes, and supplement to existing library of raman spectra.* 2001, spectrochimica acta a, Vol. 57, pp. 1491-1521.

44. K Castro, M Pérez-Alonso, M D Rodriguez-Laso, L A Fernandez, J M Madariaga. *On-line FT-Raman and dispersive Raman spectra database of artists materials (e-VISART database).* 2005, Analytical and Bioanalytical Chemistry, Vol. 382, pp. 248-258.

45. S P Best, R J H Clark, R Withnall. *Non-destructive pigment analysis of artefacts by Raman microscopy,* 1992, Endeavour, Vol. 16, pp. 66-73.

46. R J H Clark, *Raman Microscopy: Application to the identification of pigments on medieval manuscripts,* 1995, Chemical Society Reviews, Vol. 24, pp. 187-196.

47. R J H Clark, *Raman microscopy: sensitive probe of pigments on manuscripts.* 1999, Journal of Molecular Structure, Vols. 480-481, pp. 15-20.

48. R J H Clark, *Pigment identification by spectroscopic means.* 2002, C R Chimie, Vol. 5, pp. 7-20.

49. R J H Clark, *The scientific investigation of artwork and archaeological artefacts: Raman microscopy as a structural, analytical and forensic tool,* 2007, Appl. Phys. A, Vol. 89, pp. 833-840.

50. L. Burgio, D. A. Ciomartan, R. J. H. Clark. *Pigment identification on medieval manuscripts, paintings and other artefacts by Raman spectroscopy: applications to the study of three german manuscripts.* 1997, J. Mol. Struct, Vol. 405, pp. 1-11.

51. A Jurado-López, O Demko, R J H Clark, D Jacobs. *Analysis of the palette of a precious 16th century illuminated Turkish manuscript by Raman microscopy.* 2004, Journal of Raman Spectroscopy, Vol. 35, pp. 119-124.

52. T D Chaplin, R J H Clark, D Jacobs, K Jensen, G D Smith, *The Gutenberg Bibles: Analysis of the illuminations and inks using Raman spectroscopy.* 2005, Analytical Chemistry, Vol. 77, pp. 3611-3622.

53. K L Brown, Robin J H Clark. *The Lindisfarne Gospels and two other 8th century.* 2004, Journal of Raman Spectroscopy, Vol. 35, pp. 4-12.

54. R J H Clark, L Cridland, B M Kariuki, K D M Harris, R Withnall,. *Synthesis, structural characterisation and Raman Spectroscopy of the inorganic pigments lead tin yellow types I and II and lead antimonate yellow: their identification on medieval paintings and manuscripts.* 1995, Journal of Chemical Society Dalton Trans, Vol. 16, pp. 2577-2582.

55. L Burgio, R J H Clark, R R Hark. *Raman microscopy and x-ray fluorescence analysis of pigments on medieval and Renaissance Italian manuscript cuttings.* 2010, Proc. Nat. Acad. Sci , Vol. 107, pp. 5726-5731.

56. T D Chaplin, A Jurado-López, R J H Clark, D R Beech. *Identification by Raman microscopy of pigments on early postage stamps: distinction between original 1847 and*

1858–1862, forged and reproduction postage stamps of Mauritius. 2004, Journal of Raman Spectroscopy , Vol. 35, pp. 600-604.

57. M Aceto, A Agostino, E Boccaleri, F Crivello A C Garlanda. E*vidence for the degradation of an alloy pigment on an ancient italian manuscript.* 2006, journal of raman spectroscopy, Vol. 37, pp. 1160-1170.

58. S. Bruni, F. Cariati , F. Casadio , L. Toniolo. *Spectrochemical characterization by micro-FTIR spectroscopy of blue pigments in different polychrome works of art.* 1999, Vibrational Spectroscopy , Vol. 20 , pp. 15–25.

59. S Bruni, F Cariati, F Casadio, V Guglielmi. *Micro-Raman identification of the palette of a precious XVI century illuminated Persian codex.* 2001, Journal of Cultural Heritage , Vol. 4, p. 291−296.

60. S Pessanha, A Guilherme, M L Carvalho, M I Cabaço, K Bittencourt, J L Bruneel, M Besnard. *Study of a XVIII century hand-painted Chinese wallpaper by multianalytical non-destructive techniques* 2009, Spectrochimica acta part B: Atomic spectroscopy, Vol. 64, pp. 582-586.

61. A. Jurado-López, O. Demko R. J. H. Clark, D. Jacobs. *Analysis of the palette of a precious 16th century illuminated Turkish manuscript by Raman microscopy.* 2004, J. Raman Spectrosc., Vol. 35, pp. 119-134.

62. S. Bruni, F. Cariati , F. Casadio , L. Toniolo. *Identification of pigments on a XV century illuminated parchment by Raman and FTIR microspectroscopies.* 1999, Spectrochimica Acta Part A, Vol. 55 , pp. 1371−1377.

63. Kaiser optical systems website http://www.kosi.com/Raman_Spectroscopy/is-modularramanspectrometer.php?ss=600. (september 2013)

64.. K Eremin, J Stenger, J Huang, A Aspuru-Guzik, T Betley, L Vogt, I Kassal, S Speakman, N Khandekar. *Examination of pigments on Thai manuscripts: the first identification of copper citrate* 2008, Journal of Raman spectroscopy, Vol. 39, pp. 1057-1065.

65.   bruker   website   http://www.bruker.com/en/products/infrared-and-raman-spectroscopy/raman/senterra/overview.html. (september 2013)

66. M Bicchieri, M Monti, G Piantanida, A Sodo. *All that is iron-ink is not always iron-gall!* 2008 , Journal of Raman Spectroscopy, Vol. 39 , pp. 1074–1078.

67. Renishaw website .renishaw.com/en/invia-raman-microscope--6260. (september 2013)

68. F Magistro, D Majolino, P Migliardo, R Ponterio, M T Rodriquez. *Confocal Raman spectroscopic study of painted medieval manuscripts.* 2001, journal of cultural heritage, Vol. 2, pp. 191-198.

69. M Bicchieri, M Nardone, A Sodo. *Application of micro-Raman spectroscopyto the study of illuminated medieval manuscript.* 2000, Journal of Cultural Heritage, Vol. 1, pp. s277-s279.

70. A. Deneckere, M. De Reu, M.P.J. Martens , K. De Coene, B. Vekemans, L. Vincze, Ph. De Maeyer, P. Vandenabeele, L. Moens. *The use of a multi-method approach to identify the pigments in the 12th century manuscript Liber Floridus.* 2011, Spectrochimica Acta Part A , Vol. 80, pp. 125– 132.

71.   Horiba   website.   http://www.horiba.com/us/en/scientific/products/raman-spectroscopy/raman-spectrometers/raman-microscopes/details/xplora-tm-124/. (September 2013)

72. J L Shi, T Li. *Technical investigation of 15th and 19th century Chinese paper currencies: Fiber use and pigment identification.* 2013, Journal of Raman spectroscopy, Vol. 44, pp. 892–898.

73. P. Vandenabeele, K. Castro, M. Hargreaves , L. Moens, J.M. Madariaga , H.G.M. Edwards. *Comparative study of mobile Raman instrumentation for art analysis.* 2007 , Analytica Chimica Acta, Vol. 588 , pp. 108-116.

74. G. Van der Snickt, W. de Nolf, B. Vekemans, K. Janssens. *Micro-XRF/Micro-RS vs SR micro-XRD for pigment identification in illuminated manuscripts.* 2008, Appl. Phys. A: Mater. Sci. Process, Vol. 92, pp. 59-68.

75. S Bioletti, R Leahy, J Fields, B Meehan, W Blau. *The examination of the Book of Kells using micro-Raman spectroscopy.* 2009, , J. Raman Spectrosc., Vols. 40,, pp. 1043–1049.

76. Renishaw website [Online] http://www.renishaw.com/en/ra100-raman-analyser--6643. (september 2013)

77.. K Castro, M Pérez-Alonso, M D Rodríguez-Laso, J M Madariaga. *Pigment analysis of a wallpaper from the early 19th century: Les Monuments de Paris* 2004, Journal of Raman Spectroscopy, Vol. 35, pp. 704-709.

78. K Castro, M Pérez-Alonso, M D Rodríguez-Laso, N Etxebarria, J M Madariaga. *Non-invasive and non-destructive micro-XRF and micro-Raman analysis of a decorative wallpaper from the beginning of the 19th century.* 2007, Analytical and Bioanalytical Chemistry, Vol. 387, pp. 847-860.

79. A Markowicz R van Grieken. *Handbook of x-ray spectrometry: methods and techniques*: Marcel Dekker, 1993, New York

80. R Klockenkamper. *Total-reflection x-ray fluorescence analysis*: Wiley, 1996, New York

81. Amptek website http://www.amptek.com. (september 2013)

82. M Guerra, M Manso, S Pessanha, S Longelin, M L Carvalho. *Theoretical and Experimental Study on the Angular Dependence.* 2013, X ray spectrometry, Vol. 7.

83. S Pessanha, A Guilherme, M L Carvalho. *Comparison of matrix effects on portable and stationary XRF spectrometers for cultural heritage samples.* 2009, Appl Phys A, Vol. 97, pp. 497-505.

84. R Cesareo, R. X-ray physics: interaction with matter, production, detection. *la Rivista del Nuovo Cimento della Società Italiana di Fisica.* 2000, Vol. 23, 7.

85. R Van Grieken K Janssens. *Non-destructive Micro Analysis of Cultural Heritage Materials.* Elsevier, 2004, New York.

86. R Jenkins, J L de Vries. *Practical x-ray spectrometry.*: Springer-verlag, 1969, New York

87. oxford-instruments website http://www.oxford-instruments.com/products/x-ray-tubes-and-integrated-sources/x-ray-tubes. (september 2013

88. varian website http://www.varian.com/us/xray/. (september 2013)

89. moxtek website http://www.moxtek.com/. (september 2013)

90.. A Migliori, P Bonanni, L Carraresi, N Grassi, P A Mandò. *A novel portable XRF spectrometer with range of detection extended to low-Z elements*, 2011, X-ray Spectrometry, Vol. 40, pp. 107-112.

91. S Bichlmeier, K Janssens, J Heckel, D Gibson, P Hoffmann, H M, Ortner. *Component selection for a compact micro-XRF spectrometer.* 2001, X-ray spectrometry, Vol. 30, pp. 8-14.

92. S Pessanha, A Le Gac, T I Madeira, M Guerra, M L Carvalho. *Elemental analysis by portable Ag and Rh X-ray sources of a Namban type folding screen.* 2013. Nuclear instruments and Methods in physics research B, Vol. 309, pp. 254-259

93. A Gianoncelli, J Castaing, L Ortega, E Dooryhée, J Salomon, P Walter, J L Hodeau, P Bordet. *A portable instrument for in situ determination of the chemical and phase compositions of cultural heritage objects.* 2008, x-ray spectrometry, Vol. 37, pp. 418-423.

94. http://www.xraylamp.webd.pl/files/podzial_lamp_rentgenowskich_3%284%29en.pdf. (september 2013)

95. A Longoni, C Fiorini. X-ray detectors and signal processing. [book auth.] B Kanngiesser, N Langhoff, R Wedell, H H Wolff B Beckhoff. *Handbook of practical x-ray fluorescence analysis.* Springer-Verlag, 2006, pp. 203-226. Berlin

96. Vortex website http://www.hitachi-hitec-science.us/vortex.php. (september 2013)

97. ketek website http://www.ketek.net/. (september 2013)

98. P van Espen,. spectrum evaluation. in R Markowicz R van Grieken. *handbook of x-ray spectrometry: methods and techniques.* Marcel Dekker, 1993, New York

99. Camberra website http://www.canberra.com/products/438012.asp. (september 2013)

100. PyMCA website http://pymca.sourceforge.net/index.html. (september 2013)

101. V A Solé, E Papillon, M Cotte, Ph Walter, J Susini. *A multiplatform code for the analysis of energy-dispersive X-ray fluorescence spectra.* 2007, Spectrochim. Acta Part B, Vol. 62, pp. 63-68.

102. P van espen, P Lemberge. *EDXRF spectrum evaluation and quantitative analysis using multivariate and nonlinear techniques.* 2000, Advances in x-ray analysis, Vol. 43, pp. 560-569.

103. R Tertian, F Claisse. *Principles of quantitative x-ray fluorescence analysis.* Heyden, 1982, London

104. A. Rindby. *Software for Energy-Dispersive X-Ray Fluorescence,* 1989, X-Ray Spectrometry, Vol. 18, pp. 113-118.

105. R Jenkins, R W Gould, D Gedcke. *Quantitative X-ray spectrometry.* Marcel dekker, 1981, New York

106. XOS optics website http://www.xos.com/products/x-ray-optics-excitation-systems-x-beam/optics/polycapillary-optics/x-tra-polycapillary-focusing-optics/.

107. Dupont website http://www2.dupont.com/Kapton/en_US/. (september 2013)

108. J R Ferraro, K Nakamoto, C W Brown. *Introductory Raman Spectroscopy.* Elsevier, 2003, Waltham USA

109. P Larkin, *Infrared and Raman spectroscopy: principles and spectral interpretation.* Elsevier, 2011. Waltham USA

110. R L McCreery, *Raman spectroscopy for chemical analysis.* Wiley interscience, 2000, New York

111. O Hollricher, J Toporski T Dieing. *Confocal Raman microscopy.* Springer-Verlag, 2010, Berlin.

112. Horiba website http://www.horiba.com/us/en/scientific/. (september 2013)

113. P J Custodio, M L Carvalho, F Nunes, S Pedroso, A Campos. *Direct analysis of human blood (mothers and newborns) by energy dispersive X-ray fluorescence.* 2005, Journal of Trace Elements in Medicine and Biology , Vol. 19, pp. 151-158.

114. NL Rebrikova, NV Manturovska. *Foxing: a new approach to an old problem.* 2000, Restaurator, Vol. 21, pp. 85-100.

115. M Bicchieri, G Pappalardo, FP Romano, FM Sementilli, R Acutis. *Characterization of foxing stains by chemical and spectrometric methods.* 2001, Restaurator, Vol. 22, pp. 1-9.

116. M bicchieri, S Ronconi, FP Romano, L Pappalardo, M Corsi, G Cristoforetti, S Legnaioli, V Palleschi, A Salvetti, E Tognoni. *Study of foxing stains on paper by chemical methods, infrared spectroscopy, micro-x-ray fluorescence spectrometry and laser induced breakdown spectroscopy.* 2002, Spectrochimica Acta A, Vol. 57, pp. 1235-1249.

117. M-LE Florian, L Manning. *SEM analysis of irregular fungal fox spots in an 1854 book: population dynamics and species identification.* 2000, International Biodeteriotarion and Biodegradation, Vol. 46, pp. 205-220.

118. H Arai, *Foxing caused by fungi: twenty-five years of study.* 2000, International biodeterioration and biodegradation, Vol. 46, pp. 181-188.

119. JL Pedersoli, FJ Ligterink, M van Bommel. *Investigation into fluorescence changes accompanying paper discoloration.* 2001, Helsinki (Finland) ICOM-CC Interim meeting of the working group on graphic documents at EVTEK institute of art and design. pp. 7-10.

120. M Manso, S Pessanha, ML Carvalho. *Artificial aging processes in modern papers: x-ray spectrometry sudies.* 2006, Spectrochimica acta A, Vol. 61, pp. 922-928.

121. P Carneiro, *The voyage of the southern barbarians at the Soares dos Reis National Museum:an iconographic analysis.*2006, Bulletin of Portuguese/Japanese studies, Vol. 12, pp. 41-56.

122. Y Lippit, *Japan's southern barbarian screens.* Encompassing the globe: Portugal and the world in the 16th and 17th centuries. MNAA, 2009, Lisbon.

123. T Takamizawa, *Biombos namban, exhibition catalogue.* Calouste Gulbenkian foundation, 1981, Lisboa.

124. S Grantham, *Japanese painted screens: manufacturing materials and painting techniques.* Proceeding of the conference: works of art in paper: books, documents and photographs: techniques and conservation 2002, Baltimore pp. 83-87.

125. P Willis, *Far eastern pictorial art: form and function.* 1985, The Paper Conservator, Vol. 9, pp. 5-12.

126. T K McClintock, *Japanese folding screens in a Western collection: Notes on a representative treatment.* 2006, The paper conservator, Vol. 30, pp. 25-42.

127. J Winter, *Paints and supports in far eastern pictorial art.* 1985, Paper conservator, Vol. 9, pp. 24-31.

128. *Exhibition catalogue: Enconpassing the globe: Portugal and the world in the 16th and 17th centuries.* MNAA, 2009, Lisbon.

129. C Coutry, G Sagon, P Gorguet-Ballesteros. *Raman spectroscopy of blue contemporary textiles.* 1997, Journal of raman spectroscopy, Vol. 28, pp. 85-89.

130. J Winter, *East Asian paintings.* Archetype, 2008, Washington.

131. L D Kock, D De Waal. *Raman analysis of ancient pigments on a tile from the Citadel of Algiers.* 2008, Spectrochimica acta a, Vol. 71, pp. 1348-1354.

132. NIST website http://physics.nist.gov/Phys RefData/XrayMassCoef/tab3.html. september 2013)

133. *Art namban - catalogue of the Európália89 exposition.* Musées Royaux d'art et d'histoire, 1989, Brussels.

134. L Monico, G van der Snickt, K Janssens, W de Wolf, C Miliani, J Verbeeck, H Tian, H Tan, J Dik, M Radepont, M Cotte. *Degradation process of lead chromate in paintings by Vincent Van Gogh studies by means of Synchrotron x-ray spectromicroscopy and related methods 2- original paint layer samples.* 2011, Analytical Chemistry, Vol. 83, pp. 1224-1231.

135. R J Gettens, G L Sout. *Painting materials, a short encyclopaedia.* Dover publications, 1966, New York.

136. M Koyano, m Yoneda, R Tojo, M Okawa, M Saito. *Conservation of modern nihonga (traditional japanese paintings) on paper.* 1985, The paper conservator, Vol 4 pp. 114-117.

137. B Guineau, *Glossaire des matériaux de la couleur,* Brepols publisher, 2005, Turnhout.

138. R R Ersnt, *In situ Raman microscopy applied to large central Asian paintings.* 2010, Journal of raman spectroscopy, Vol. 41, pp. 275-287.

139. R Mayer, *The artists handbook of materials and techniques.* faber&faber, 1982, London.

140. Y Okamato, *The art of Japan,* Wheatherhill, 1972, New York.

141. M R Marcelino, V S F Muralha. *Synthetic organic pigments in contemporary Balinese painting: a Raman microscopy study.* 2012, Journal of Raman Spectrosc., Vol. 43, pp. 1281-1292.

142. I. Osticioli, N.F.C. Mendes, A. Nevin, Francisco P.S.C. Gi, M. Becuccia, E. Castellucci, *Analysis of natural and artificial ultramarine blue pigments using laser.* 2009, Spectrochimica Acta Part A: Molecular and, Vol. 73, pp. 525-531.

143. http://www.pcv.pt/lot.php?ID=4889. (September 2013)

144. http://www.cinoa.org/antiques/d/namban-screen/97634. (september 2013)

145. S Pessanha, A le Gac, T I Madeira, A Guilherme, M Manso, M L Carvalho. *Characterization of a namban foding screen from the Edo period by means of EDXRF, SEM-EDS and raman spectroscopy.* 2013, x-ray spectrometry, Vol. 42, pp. 128-133.

146. A Le Gac, A I Seruya, M Lefftz, A Alarcão. *The main altarpiece of the Old Cathedral of Coimbra (Portugal)* 2009, Revue d'Archéométrie - ArcheoSciences, Vol. 33, p. 423-432

147. C Fiorini, A Gianoncelli, A Longoni, F Zaraga. *Determination of the thickness of coatings by means of a new XRF spectrometer* 2002, X-ray spectrometry, Vol. 31, pp. 92-99.

148. T Trojek, M Hlozek. 2012, *X-ray fluorescence analysis of archaeological finds and art objects: Recognizing gold and gilding.* Appl. Rad. Isotopes, Vol. 70, p. 1420-1423.

149. Y Kataoka, H Kohno, E Furusawa, M Mantler, *XRF analysis of Zn–Fe alloy coatings by using measurements at two take-off angles* 2007, x-ray spectrometry, Vol. 36, p. 221-225.

150. R Cesareo, A Brunetti, S Ridolfi. *Pigment layers and precious metal sheets by energy-dispersive x-ray fluorescence analysis.* 2008, X-ray spectrometry, Vol. 37, p. 309-316.

151. R Cesareo, *Non-destructive EDXRF-analysis of the golden haloes of Giotto's frescos in the Chapel of the Scrovegni in Padua*, 2003, Nuclear Instruments and methods B, Vol. 211, p. 133-137.

152. R Cesareo, M A Rizzutto, A Brunetti, D V Rao. *Metal location and thickness in a multilayered sheet by measuring Kα/Kβ, Lα/Lβ and Lα/Lγ X-ray ratios*, 2009, nuclear instruments and methods B, Vol. 267, p. 2890-2896.

153. M Manso, A Le Gac, S Longelin, S Pessanha, J C Frade, M Guerra, A J Candeias, M L Carvalho, S*pectroscopic characterization of a masterpiece:the manueline foral charter of sintra.* 2013, Spectrochimica acta A, Vol. 105, pp. 288-296.

154. L Moura, M J Melo, C Casanova, A Claro. *A study on Portuguese manuscript illumination: The Charter of Vila Flor (Flower town), 1512.* 2007, Journal of Cultural Heritage , Vol. 8. pp. 299-306

155. HGM Edwards, DW Farwell, EM Newton, F R Perez, S J Villar. *Application of FT-Raman spectroscopy to the characterisation of parchment and vellum, I; novel information for paleographic and historiated manuscript studies,* 2001, spectrochimica acta A, Vol. 57, p. 1223-1234

156. P Vandenabeele, B Wehling, L Moens, H Edwards, M De Reu, G Van Hooydonk. *Analysis with micro-Raman spectroscopy of natural organic binding media and varnishes used in art*, 2000, Analytica Chimica Acta, Vol. 407, p. 261-274.

157. M Bicchieri, M Monti, G Piantanida, F Pinzari, A Sodo. *Non-destructive spectroscopic characterization of parchment documents.* 2011, Vibrational Spectroscopy, Vol. 55, pp. 267–272.

158. E Darque-Ceretti, M Aucouturier. *Dorure: décor et sublimation de la matière.* Mines ParisTech, 2012, Paris.

159. M Koyano, *Gilding and gilding conservation in Japan.* Gilded wood: conservation and history, Sound view press, 1991, Madison.

ANNEXES

Contents lists available at SciVerse ScienceDirect

Spectrochimica Acta Part B

Application of spectroscopic techniques to the study of illuminated manuscripts: A survey

S. Pessanha, M. Manso, M.L. Carvalho *

Atomic Physics Center of the University of Lisbon, Physics Department, Av. Professor Gama Pinto, 2 1649-003, Lisboa, Portugal

ARTICLE INFO

ABSTRACT

This work focused on the application of the most relevant spectroscopic techniques used for the characterization of illuminated manuscripts. The historical value of these unique and invaluable artworks, together with the increased awareness concerning the conservation of cultural heritage, prompted the application of analytical techniques to the study of these illuminations. This is essential for the understanding of the artist's working methods, which aids conservation–restoration. The characterization of the pigments may also help assign a probable date to the manuscript. For these purposes, the spectroscopic techniques used so far include those that provide information on the elemental content: X-ray fluorescence, total reflection X-ray fluorescence and scanning electron microscopy coupled with energy-dispersive spectroscopy and laser-induced breakdown spectroscopy. Complementary techniques, such as X-ray diffraction, Fourier transform infrared and Raman spectroscopy, reveal information regarding the compounds present in the samples. The techniques, suitability, technological evolution and development of high-performance detectors, as well as the possibility of microanalysis and the higher sensitivity of the equipment, will also be discussed. Furthermore, issues such as the necessity of sampling, the portability of the equipment and the overall advantages and disadvantages of different techniques will be analyzed.

© 2012 Elsevier B.V. All rights reserved.

1. Introduction

An illuminated manuscript is a document in which the text is supplemented by the addition of decoration, such as initials, borders and miniature illustrations. The term "illumination" originally denoted the embellishment of the text with gold or, more rarely, silver, giving the impression that the page had been literally illuminated. These illuminations were often as important and carried as much information as the text itself [1]. The majority of the surviving manuscripts and books are from the Middle Ages, although many illuminated manuscripts survived from the Renaissance, along with a very limited number from Late Antiquity. The rising awareness in the scientific community of the importance of the preservation of cultural heritage, as well as the establishment of multidisciplinary teams combining scientists with restorers and conservators, prompted an increased interest in the application of analytical techniques to the study of illuminations. These studies are essential for the understanding of the artist's work methods, which aids in the restoration process when cleaning and retouching; this understanding also helps in conservation because, depending on the nature of the pigments, specific storage conditions may be required. The characterization of the pigments may also help assign a probable manuscript age. Over the past

decades, enormous advances in the technology contributed to the more reliable, sensitive, nondestructive *in situ* techniques that are now being used in the study of many significant, well-documented artworks from public and private collections. In this review, we will discuss the suitability, advantages and disadvantages of the techniques used in the study of illuminated manuscripts.

2. X-ray fluorescence

X-ray fluorescence (XRF) spectrometry is a well-established technique for elemental analysis at the micro and trace levels. The technique is mostly nondestructive in nature and has sensitivities at the level of parts per million (ppm). XRF has continuously evolved either in the form of conventional energy-dispersive X-ray fluorescence (EDXRF) techniques or in the form of wavelength-dispersive X-ray fluorescence (WDXRF) techniques. In EDXRF, the dispersion and detection of fluorescence photons are performed using a solid-state X-ray detector and a multichannel pulse height analyzer (MCA). This technique produces an accumulating digital spectrum that can be processed further to derive the concentrations of the different elements present in a sample.

2.1. Energy-dispersive X-ray fluorescence

EDXRF is among the most cited analytical methods in the literature dealing with cultural heritage investigations. The major advantages of

---

* Corresponding author.
E-mail address: luisa@cii.fc.ul.pt (M.L. Carvalho).

X-ray spectrometric measurements include simple spectra, spectral coverage for most elements, minimal sample preparation, nondestructive and fast analysis and good precision and accuracy. The fact that analyses need to be performed in a nondestructive and, more importantly, noninvasive way is extremely important, as removing samples is sometimes unacceptable. Furthermore, with the development of portable and handheld XRF spectrometers, the quantity and types of objects that can be analyzed have increased dramatically. The development of low-power X-ray tubes allows the instrument to be used safely without external shielding. The main characteristics of these tubes are air cooling, low weight and stability. On the other hand, several types of noncryogenic miniaturized detectors that use Si-PIN photodiodes and SDD (Silicon Drift Detector) technology can be employed. Because these spectrometers can be taken directly to the artwork, immovable or otherwise inaccessible objects, such as valuable or fragile illuminated manuscripts that cannot be moved from museums or libraries, can now be analyzed [2–14]. There are, of course, several degrees of portability, ranging from the equipment used by Čechác et al. [8], an annular radio-nuclide source and a Si(Li) detector cooled with liquid nitrogen, to the ultra-compact, handheld equipment used by Chaplin et al. [2]. There are also equipment that combine different techniques, such as the PRAXIS (trans)portable equipment used by Van der Snickt [7], where a Raman probe is combined with the EDXRF system using a polycapillary X-ray lens to focus the beam and a SDD detector cooled by the Peltier effect (Fig. 1). The characterization of illuminated manuscripts was also performed by Duran using a laboratory-made portable X-Ray Diffraction/X-Ray Fluorescence (XRD/XRF) system [9]. To reduce the background and improve the detection limits by using nearly monochromatic radiation, Bruni et al. [6] placed a Zr transmission filter between the sample and the X-ray tube (with Mo target).

All these works used single-spot or micro-spot analyses, but sometimes the distribution of elements across a region is of particular interest; the elemental mapping can help identify an artist's characteristic palette and painting technique or even reveal a hidden painting. Trentelman et al. [15] used the ARTAX800 XRF spectrometer commercialized by Bruker to perform line and area scans of 15th century illuminated manuscripts by Jean Bourdichon to determine the order in which some pigments were applied.

On the other hand, when analyzing illuminated manuscripts, we are usually in a multiple-layer system, and it is not possible to distinguish the information coming from the different layers. Trojek et al. [16] studied the $K\alpha/K\beta$ and $L\alpha/L\beta$ ratios of characteristic X-rays of the pigment layers in model samples created to simulate illuminated

manuscripts. The principle of this technique lies in the different absorption coefficients for the $K\alpha$ and $K\beta$ lines (and also for the $L\alpha$ and $L\beta$ lines). If an element is deposited on a surface, the emitted X-rays are only slightly affected by the absorption in the specimen. However, if an element is present at some depth in a bottom layer of the specimen, its characteristic radiation has to penetrate through an upper layer, and the characteristic X-ray fluxes are significantly changed. The $K\alpha/K\beta$ ratio is usually reduced because the attenuation coefficient for a $K\alpha$ line is higher than for $K\beta$. The ratio can be increased only if another element with an absorption edge between the set two lines is present in the specimen. This technique was applied to a set of Bohemian books dating back to the 14th and the 15th centuries.

Although a nonsampling strategy is always preferable, there are cases where sampling is possible. Deneckere et al. [17] used a benchtop system equipped with a Si(Li) detector and a polycapillary lens to focus the X-rays to a minute spot size of 25 μm. This equipment also allows one to work under vacuum, facilitating the detection of low-Z elements; however, this feature was not used in this work.

Synchrotron radiation XRF (SR-XRF) has also started to play an increasingly important part in cultural heritage analyses. The specific features of synchrotron radiation include energy tunability, a higher photon flux, and a higher resolution. Another major advantage is the application of synchrotron μ-beam XRF to selectively identify areas of analyses. Kanngießer et al. [18] investigated the oxidation and migration processes of Fe, Cu and Zn in ink-corroded manuscripts by performing 2D mappings using the KMC-2 beamline at the BESSY synchrotron facilities. Faubel et al. [19] also used synchrotron radiation at the ANKA facilities to study the iron-gall ink corrosion in an 18th century manuscript. With the advent of new X-ray optics and the technological development of polycapillary lenses, a new tool for microanalysis arose: three-dimensional micro-X-ray fluorescence spectroscopy (3D micro-XRF). This technique is based on the use of two polycapillary optics in a confocal arrangement. The overlap of the foci of the two X-ray optics forms a probing volume from which fluorescence and scattered radiation is exclusively derived. Mantouvalou et al. [20] used this technique and obtained lateral- and depth-resolved measurements of samples gathered from the Dead Sea Scrolls.

2.2. Total reflection X-ray fluorescence

Total reflection X-ray fluorescence (TXRF) spectrometry is a variation of the EDXRF method in which the specimen is excited by the
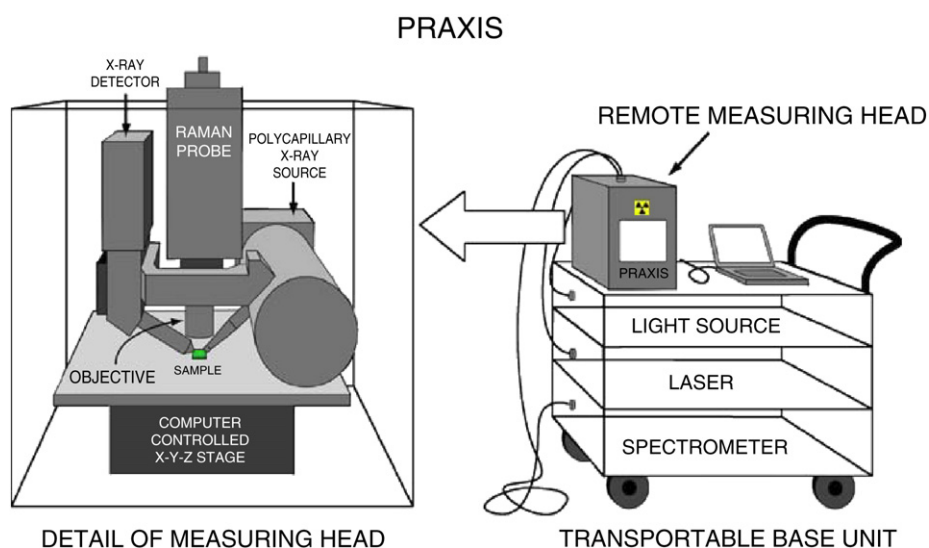

Fig. 1. Non-commercial equipment where a Raman probe is combined with the EDXRF system using a polycapillary X-ray lens. An excitation–detection scheme was designed to allow both Raman and XRF spectroscopy to be performed simultaneously on the same location of a macroscopic sample [7].

primary X-ray beam at a glancing angle that is less than the critical angle at which total external reflection occurs; the primary exciting radiation is incident on a plane-polished surface, which serves either as a sample support or is itself the object to be examined. This mode of excitation almost completely eliminates the large Compton scattering of the primary X-ray beam from the sample bulk, which usually limits the detection sensitivities in the conventional EDXRF method. The reduced Compton scattering in the TXRF mode and the enhancement of the analyte's fluorescence intensity due to the twofold excitation during incident and reflected beams result in the improvement of the elemental-detection sensitivities at the level of a few parts per billion (ppb).

The application of total reflection X-ray fluorescence (TXRF) to the study of illuminated manuscripts has been primarily performed by Von Bohlen and Klockenkämper [21–28], where a minute amount of paint was wiped off the surface by means of a cotton-wool tip or a Q-tip. This technique is nearly noninvasive. Different Q-tips were applied to different spots of the painting and were transported in bottle caps. For analysis, the Q-tips were dabbed onto a glass carrier by a single tip. The quantitative information provided by TXRF allows knowledge regarding the pigment mixing ratios. Different brands or provenances of the same pigments can be identified based on minor and/or trace element impurities that are detected in addition to the main constituents. Van Hooydonk et al. [29] used multivariate analysis on the elemental concentrations obtained by TXRF in a set of Late-Medieval Mercatelli manuscripts to classify them into groups according to the impurity content of some of the pigments.

3. Scanning electron microscopy coupled with energy-dispersive spectrometry

Scanning electron microscopy (SEM) is also a very powerful tool in cultural heritage research because it provides knowledge about the surface topography of the studied samples. This microscope uses electrons rather than light to form an image, and if it is coupled with an energy-dispersive detector, the information regarding the elemental composition is also obtained.

Kautek et al. [30] performed the morphological diagnostics of the laser cleaning of pigments on parchment using SEM. Della Gatta et al. [31] used the SEM images to assess the damage resulting from the environmental impact on parchments. Bicchieri et al. [32] also used SEM images and energy dispersive spectrometry (EDS) to differentiate parchment manufacturing procedures. SEM–EDS was used by Aceto et al. [33] to perform elemental micro-analysis on a 9th century Italian manuscript to study the degradation of an alloy pigment.

4. Laser-induced breakdown spectroscopy

Laser-induced breakdown spectroscopy (LIBS) is an atomic-emission technique in which an intense nanosecond laser pulse incident on the surface of a sample results in the formation of a plasma that, upon being allowed to cool, emits radiation characteristic of the elements present there. This technique has high sensitivity and selectivity, and only a minute amount of the sample is consumed during each pulse. Successive pulses probe deeper into the artwork, so that depth profiling becomes possible. LIBS strongly depends on matrix effects, pulse-to-pulse fluctuations, plasma–solid interactions, etc., which makes quantification challenging. LIBS spectroscopy can be produced from a variety of lasers, but pulsed Nd:YAG lasers are typically used. In particular, when dealing with cultural heritage, LIBS instruments require small and compact lasers (with a portable power supply) and miniaturized broad-band spectrometers. Advances in optical configurations (such as fiber optics, beam optics and telescopes) for guiding and collecting the plasma radiation have resulted in the development of compact instrumentation.

Dolgin et al. [34,35] used LIBS to find specific elemental markers for rapid, simple and reliable characterization of historical parchment. The laser was focused on the sample with a quartz lens, and the emission of the plume was then collected by a quartz optical fiber bundle and delivered to the entrance slit of a monochromator that was coupled with a gated intensified charge-coupled device. A spectral resolution of 0.2 nm is obtained using a 1200 grooves/mm grating. Discriminant analysis based on Ca, Fe and Mg enabled the distinction between historical and modern parchments. Furthermore, Dolgin et al. performed depth profiles of the samples by repeatedly probing the same spot with the laser and discovered that the Mg depth profile made possible the identification of the animal that was used.

The most commonly used blue pigments in medieval manuscripts are azurite and lapis-lazuli, so Bicchieri et al. [36] applied different mixtures of these pigments to parchment samples to simulate the study of an illuminated manuscript. Utilizing a new technique of LIBS spectra analysis that was recently developed and patented by the Institute of Atomic and Molecular Physics in Pisa (IFAM), Bicchieri et al. obtained precise quantitative information on the elemental composition without the need for reference samples or calibration curves.

According to Melessanaki et al., they performed the first study of pigment identification on a real illuminated manuscript using LIBS [37]. In view of the piece's fragility and to optimize the measurements, the operating conditions were tested on model samples of paint in parchment and then applied to the real samples.

Laser ablation can also provide a method for removing layers that are untreatable using conventional methods. Furthermore, it prevents the use of various chemical substances that present a potential hazard to the conservators. Melessanaki et al. demonstrated the value of an ultraviolet (excimer) laser not only as a restoration tool for the removal of surface material but also as a non-contact diagnostic tool, providing important information regarding the chemical and physical structure of the artwork [38,39].

5. Proton-induced X-ray emission

Proton-induced X-ray emission (PIXE) is another powerful elemental-analysis technique used in cultural-heritage applications. This technique uses a proton beam to excite the inner shell electrons in the target atoms. The expulsion of these inner shell electrons results in the production of X-rays. The energies of the X-rays, which are emitted when the created vacancies are filled again, are uniquely characteristic of the elements from which they originate, and the number of X-rays emitted is proportional to the mass of that corresponding element in the sample being analyzed.

Budnar et al. investigated iron-gall inks in documents using an in-air PIXE arrangement [40,41]. In this type of setup, the beam is exposed to the atmosphere; the target is hit and analyzed with no need to place it in vacuum. Due to the high sensitivity of PIXE, extended information on materials can be obtained with a very low beam current; as a result, the analysis does not produce any visible damage to the work. Remazeilles et al. [42] used this technique to perform mapping and spot analysis using external microprobe equipment at the Louvre Museum facilities to study original manuscripts damaged by ink corrosion. Kakuee et al. [43] also used external PIXE to study the ink and pigments used in a 15th century illuminated manuscript.

6. Raman spectroscopy

It is argued [44–46] that Raman spectroscopy is the best technique for singlehandedly studying and identifying inorganic solids, especially when they are in heterogeneous mixtures at a micrometer scale. Raman spectroscopy probes molecular and crystal-lattice vibrations and is therefore sensitive to the composition, bonding, chemical environment, phase and crystalline structure of the sample material.

Raman Spectroscopy is a fingerprinting technique, and materials are identified by comparing their characteristic vibrational spectra with those in databases [47–49].

Clark and his coworkers have been strong advocates of the application of Raman spectroscopy to the study of cultural heritage, particularly as it pertains to illuminated manuscripts, with over 15 publications. These publications comprise review articles on the application and developments of Raman spectroscopy, including the study of illuminated manuscripts [46,50–54] and case studies where Raman microscopy alone [44,55–58] or in combination with other techniques [2,59–61] could characterize an artist's palette or even detect forgeries [3]. These case studies focused mainly on pigment characterization and included the inedited analysis of the King George III copy of the Gutenberg bible and the study of several manuscripts of European Medieval, Persian and Islamic origins. The pigments found are basically the same and are extensively described in a previous publication [53].

The characteristics of the Raman technique that make it so well qualified for the analysis of these materials include its molecular specificity, nondestructiveness, applicability to samples of large or non-uniform shapes and relative immunity to interference. If we couple a standard optical microscope to a Raman spectrometer, we obtain high-magnification visualization of a sample and Raman analysis with a microscopic spot. In a typical setup, a microscope is coupled with a spectrometer with an intensified diode array or CCD detector. Laser radiation is focused on each grain via the microscope objective (up to x100). The Raman scattering by the sample retraces the path of the incident beam, which is collected by the same objective and directed to the monochromator and then to the detector [44]. Raman microscopy has been used to investigate pigments in illuminated manuscripts either by collecting micro-samples [21,33,62,63] or by placing the manuscript directly under the microscope [4,56,57,60,63–66]. This strategy was also used to study the inks present in an 18th century Italian manuscript [5].

Spatial resolution can be further improved by the use of confocal geometries. Traditional confocal Raman microscopes use a pinhole aperture placed in front of the spectrograph entrance slit. The Raman light is focused onto the pinhole, and the diverging beam after the pinhole is then refocused onto the entrance slit of the spectrograph. Different pinhole apertures can be used to control the degree of confocality, whereas the entrance slit is used to control the spectral resolution of the spectrometer. Raman microscopes with a confocal geometry (Fig. 2) have been applied to the study of pigments in illuminated manuscripts by Magistro et al. [67], Bicchieri et al. [68] and Deneckere et al. [17]. Aceto et al. [33] used a confocal Raman microscope to characterize the inks that had undergone a severe degradation process in a 9th century Italian manuscript. Lee et al. [69] also used a confocal Raman microscope to study the corrosive nature of different inks and ink solutions that were prepared in a laboratory using four different historic recipes and written on new and naturally aged parchments.

Recently, the appearance of compact, portable Raman equipment with probe heads that are connected to the excitation laser source and base Raman analyzer by fiber optic cables made possible the *in situ* use of Raman spectroscopy in the study of cultural heritage. Vandenabeele et al. compared different spectroscopic aspects of these existing instruments, including spectral resolution, wavelength calibration, laser cut-off and general spectral quality, to evaluate their suitability for this purpose [70]. These equipments have also been employed in the study of pigments in illuminated manuscripts, especially when the value of the codices does not allow them to be moved from museums or libraries or when sampling, even gentle micro-sampling, cannot be performed [6,7,17,45,57,71].

Unfortunately, Raman analysis can be greatly frustrated by naturally fluorescent organic materials (such as parchment or paper), by atomic fluorescence in some materials or by fluorophores that have become incorporated in the pieces from handling.

The use of excitation in the near-infrared region was the strategy used by Mannucci et al. [72], by Bicchieri et al. [32] and by Edwards et al. [73] to overcome this obstacle in the study of ancient parchment and vellum.

Other possible strategies include the application of spectral manipulations, such as subtracted-shifted Raman (SSRS) analysis, to mathematically eliminate the background fluorescence signal. The SSRS technique consists of taking the difference of two Raman spectra acquired at two different grating positions. The Raman bands follow the shift, which is chosen to be sufficiently small enough to leave
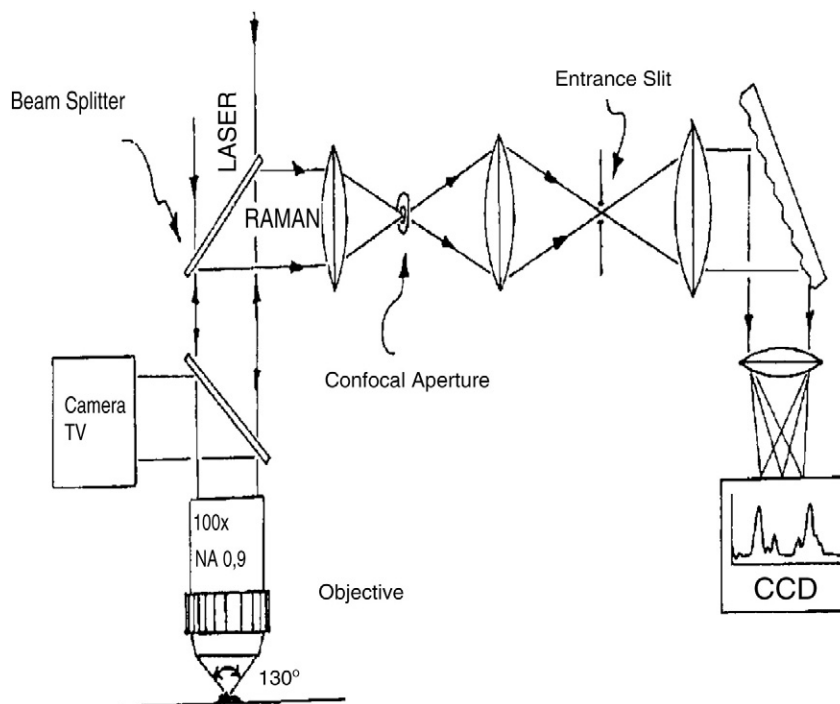

Fig. 2. Scheme of confocal Raman apparatus [67].

the fluorescence background almost unchanged. As a result, the final subtracted spectrum will contain only Raman information expressed as derivative-like peaks, whereas the fluorescence background will be strongly reduced or eliminated. Rosi et al. [74] applied this mathematical treatment of spectra to analyze organic dyes and lakes in colored parchments. Whitney et al. also studied the lakes commonly used in parchment coloring by resorting to another method of spectral manipulation: Surface Enhanced Raman Spectrometry (SERS) [75]. SERS is normally performed using a silver or gold colloid or a substrate containing silver or gold. The surface of the silver or gold is excited by the laser, resulting in an increase in the electric fields surrounding the metal. Given that Raman intensities are proportional to the electric field, there is a significant increase in the measured signal. SERS was used by Centeno et al. [76] for the characterization of the sepia melanin pigment extracted from the cuttlefish or *Sepia officinalis*, a material used for writing purposes.

Degradation of hydrocerussite (lead white $2Pb(CO_3).Pb(OH)_2$) after exposure to H_2S gas has been studied using Raman spectrometry by Clark et al. [77]. Miguel et al. [4] studied naturally aged red lead pigment (Pb_3O_4) from a 12th century set of illuminated manuscripts and discovered the bands corresponding to galena (PbS). The same compound as well as lead arsenate appeared when the model sample of the same pigment was submitted to accelerated degradation.

Advances in instrumentation for generating, sorting, and detecting Raman-scattered light have overcome many of the limitations. These obstacles included the intrinsic weakness of the Raman-scattering phenomenon, the scale and cost of the requisite instrumentation, and the tendency of the weak Raman signal to be overwhelmed by broadband fluorescence from some samples. The introduction of high-throughput optical configurations, efficient Rayleigh rejection filters and high quantum yield CCD detectors have improved tremendously the sensitivity of modern Raman instruments while simultaneously reducing their cost.

7. Fourier transform infrared spectroscopy

Although the vibrational information obtainable by Raman spectroscopy is similar to that obtained by infrared spectroscopy (IR), it is not identical but rather complementary due to the different selection rules governing vibrational Raman scattering (mandatory change in the polarization) and IR absorption (mandatory change in the dipole moment). The Fourier transform infrared (FTIR) spectroscopy technique offers a fast analysis of micro-samples and is able to provide information on the nature of the organic and inorganic materials used by an artist.

This technique has been used regularly over the last decades in pigment and binding-media characterization in illuminated manuscripts, often in combination with other techniques, both in transmission [4,62,11] and reflection mode [6,32,62,64]. Furthermore, it has been used in the study of inks. For instance, Senvaitiene et al. [78] performed the systematic investigation of eight historical writing ink samples recording the spectra through three different techniques (KBr pellet, Si substrate and ZnSe cell). The KBr method was used for the characterization of evaporated-to-dryness ink samples, whereas Si substrate and ZnSe cell techniques were used for the analysis of ink aqueous solutions or suspensions. According to the authors, the KBr and ZnSe cell techniques used for the characterization of historical writing ink samples were successful, whereas the Si substrate method was unsuccessful. Centeno et al. [76] studied the sepia melanin pigment extracted from the cuttlefish or *Sepia officinalis*, a material used for writing purposes. The FTIR spectra of sepia samples that were prepared in the laboratory following recipes recommended in an artist's materials reference source and of commercial sepia were obtained. In this work, the samples were mounted between the windows of a diamond anvil cell and observed in the transmission mode. Synchrotron radiation FTIR micro-spectroscopy at Australian synchrotron facilities was used by Creagh et al. [79] to perform the mapping of both the surface and cross sections to the surface to elucidate details of the binding of the ink to the parchment.

Bicchieri et al. [32] used attenuated total reflectance (ATR) FTIR spectrometry to study parchment manufacturing procedures. This technique allowed western (with lime) parchments to be distinguished from eastern (with enzymatic treatment) parchments. Incrustations of salts on the surface as well as superficial treatment with tannin were also detected.

Gonzalez et al. [80] also used ATR-FTIR to study the extent of the gelatinization of historical parchments in a noninvasive way. Badea et al. [81] studied a set of 14th- to-16th century parchment bookbindings using the FTIR spectra recorded with a spectrophotometer equipped with a KBr beam splitter. The samples were prepared by grinding approximately 1 mg parchment with KBr and pressing the mixture into very thin disks. The maximum resolution of the measurements was $1 cm^{-1}$. The changes in the measured physical and chemical parameter values of the parchment due to the interaction with the environment were used to identify possible deterioration pathways.

Mannucci et al. [72] also used this method to study parchment samples before and after restoration to understand, at a molecular level, the structural changes associated with damaged and restored materials.

8. X-ray diffraction

X-ray diffraction (XRD) is a technique used to characterize the crystal composition, grain size, and preferred orientation in polycrystalline or powdered solid samples. XRD detects the molecular or mineralogical composition and can distinguish between the various phases of a given chemical compound—for example, calcite, aragonite, and vaterite, which all have the same formula ($CaCO_3$). X-ray diffraction (XRD) in conventional diffractometers allows all the phases to be determined for specimens in powder.

Miguel et al. [4] studied the 1-year reaction of red lead with orpiment to simulate the degradation reaction that occurred in 12th century illuminated manuscripts and discovered arsenic trioxide (As_2O_3) as a product using X-ray powder diffraction. Cucos et al. [82] observed different XRD patterns and crystallinity degrees in new and old (14th-to-17th century) parchment, and Gonzalez [80] used XRD to study the nanoscopic structural changes and the extent of the gelatinization of historical parchments as collagen degrades into gelatin.

Recently, the need to perform *in situ* analysis of art objects that cannot be removed easily from their location has led to the development of portable XRD diffractometers. This technological advancement was facilitated by the development of X-ray beam control (polycapillaries and collimators) and by the adaptation of devices that were initially designed for synchrotron radiation, such as 2D imaging plate detectors. However, only a few portable XRD systems are available for phase identification. XRD requires careful alignment and reproducibility of the incidence and reflection angles, source sample-detector distances, etc. In addition, XRD analyses usually require long acquisition times due to the low intensities of the diffracted beam. Duran et al. used laboratory-made portable XRD equipment to study the pigment used in illuminated manuscripts [9,10] (Fig. 3). With this equipment, the measurements are performed directly on the manuscript, without sampling, in reflection mode. In one of these works [9], the authors also used a μ-XRD system in transmission mode, obtaining a measurement area of 0.2 mm² by means of a 200 μm collimator.

Kennedy et al. [83] made use of the microfocus beamline ID18F at the European Synchrotron Radiation Facility (ESRF), Grenoble, to perform surface-to-surface scans of thin sections of parchment. This allowed X-ray diffraction analysis of features that were present only in specific areas of the parchment, such as at the surface. The orientation of collagen fibrils in the plane of the parchment, the effects of laser cleaning, mineral phases and crystalline lipids present in samples, and
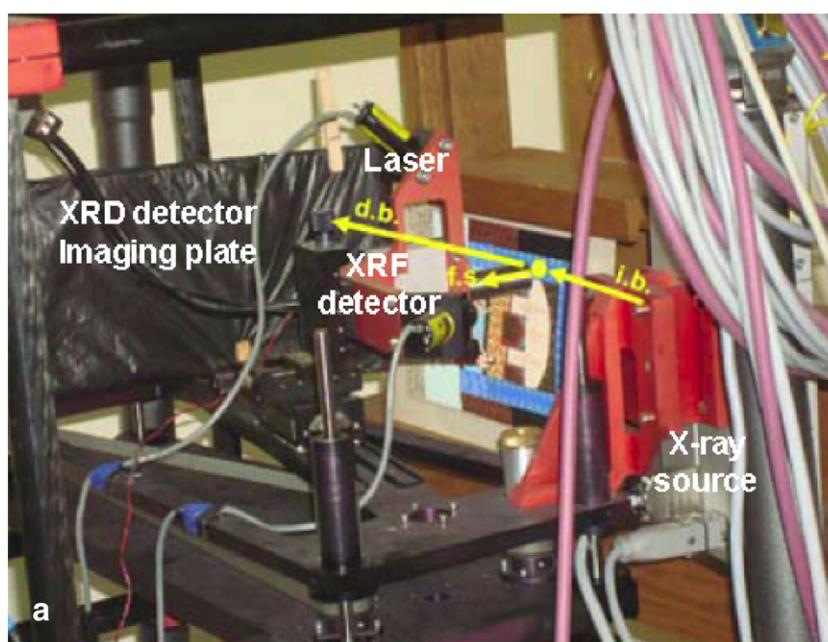
Fig. 3. Non-commercial portable equipment combining EDXRF and XRD techniques. Analysis is performed directly on the manuscript, without sampling [9].

Table 1
Summary of the main features of each technique.

	Manuscript characterization			Equipment features			
	Pigment	Ink	Parchment	Nondestructiveness	Portability	Micro-analysis	Synchrotron radiation
EDXRF	✓	✓		✓	✓✓	✓	✓
TXRF	✓	✓					
SEM–EDS		✓	✓			✓	
LIBS	✓		✓				
PIXE	✓	✓				✓	
Raman	✓✓		✓	✓	✓	✓	
FTIR	✓	✓	✓	✓		✓	
XRD	✓		✓	✓	✓	✓	✓

the parchment structure under an inked region were investigated. It is shown that the long collagen fibril axis lies parallel to the parchment surface throughout the sections. Van der Snickt et al. [7] also used SR μ-XRD (HASY-LAB, beam line L) in transmission mode to study the fillers in the parchment and the pigments used in illuminated manuscripts.

9. Conclusions

In this paper, the most relevant techniques used for the characterization of illuminated manuscripts are described. A comparison of the major advantages of each mentioned technique is presented in Table 1. In most situations, these manuscripts must not leave the controlled environment where they are kept; therefore, their study often requires *in situ* analysis, ideally without causing any damage to the artwork. EDXRF is undoubtedly the most suitable technique in these circumstances. Furthermore, using 3D micro-XRF and SEM–EDS, it was possible to distinguish information coming from different layers. When quantification is relevant for the study of pigments and inks, TXRF is a technique that should be considered. However, when elemental information is not enough to proceed with a complete characterization of the manuscripts, the complementary techniques XRD, Raman and FTIR, which reveal information on the compounds present in the samples, were used in the cited works. These techniques, with the exception of FTIR, have been used *in situ* for nondestructive analysis or for micro-sampling. Whereas Raman spectroscopy was used more for pigment identification, FTIR was used more for binders and parchment

characterization. The degradation of the materials employed in the illuminated manuscripts was also covered by this study. Whereas parchment-degradation processes were achieved by the SEM–EDS, LIBS, FTIR and XRD techniques, the study of pigment degradation was performed using Raman spectroscopy.

References

[1] D.V. Thompson, The Materials and Techniques of Medieval Painting, Dover, New York, 1956.
[2] T.D. Chaplin, R.J.H. Clark, M. Martinón-Torres, A combined Raman microscopy, XRF and SEM–EDX study of three valuable objects—a large painted leather screen and two illuminated title pages in 17th century books of ordinances of the Worshipful company of barbers, London, J. Mol. Struct. 976 (2010) 350–359.
[3] L. Burgio, R.J.H. Clark, R.R. Hark, J. Raman Spectrosc. 40 (2009) 2031–2036.
[4] C. Miguel, A. Claro, A.P. Gonçalves, V.S.F. Muralha, M.J. Melo, A study on red lead degradation in a medieval manuscript Lorvão apocalypse (1189), J. Raman Spectrosc. 40 (2009) 1966–1973.
[5] M. Bicchieri, M. Monti, G. Piantanida, A. Sodo, All that is iron-ink is not always iron-gall! J. Raman Spectrosc. 39 (2008) 1074–1078.
[6] S. Bruni, S. Caglio, V. Guglielmi, G. Poldi, The joined use of n.i. spectroscopic analyses—FTIR, Raman, visible reflectance spectrometry and EDXRF—to study drawings and illuminated manuscripts, Appl. Phys. A: Mater. Sci. Process. 92 (2008) 103–108.
[7] G. Van der Snickt, W. de Nolf, B. Vekemans, K. Janssens, micro-XRF/micro-RS VS SR micro-XRD for pigment identification in illuminated manuscripts, Appl. Phys. A: Mater. Sci. Process. 92 (2008) 59–68.
[8] T. Cechac, T. Trojek, L. Musilek, H. Paulusova, Application of x-ray fluorescence in investigations of Bohemian historical manuscripts, Appl. Radiat. Isot. 68 (2010) 875–878.
[9] A. Duran, J.L. Perez-Rodriguez, T. Espejo, M.L. Franquelo, J. Castaing, P. Walter, Characterization of illuminated manuscripts by laboratory made portable XRD and micro-XRD systems, Anal. Bioanal. Chem. 395 (2009) 1997–2004.

[10] A. Duran, M.L. Franquelo, M.A. Centeno, T. Espejo, J.L. Perez-Rodriguez, Forgery detection on an Arabic illuminated manuscript by micro-Raman and X-ray fluorescence spectroscopy, J. Raman Spectrosc. 42 (2011) 48–55.

[11] L. Moura, M.J. Melo, C. Casanova, A. Claro, A study on Portuguese manuscript illumination: the Charter of Vila Flor (Flower town), 1512, J. Cult. Herit. 8 (2007) 299–306.

[12] K. Trentelman, N. Turner, Investigation of the painting materials and techniques of the late-15th century manuscript illuminator Jean Bourdichon, J. Raman Spectrosc. 40 (2009) 577–584.

[13] O. Hahn, W. Malzer, B. Kanngiesser, B. Beckhoff, Characterization of iron-gall inks in historical manuscripts and music compositions using x-ray fluorescence spectrometry, X-Ray Spectrom. 33 (2004) 234–239.

[14] M. Aceto, A. Agostino, E. Boccaleri, A. Cerutti Garlanda, The Vercelli Gospels laid open: an investigation into the inks used to write the oldest Gospels in Latin, X-Ray Spectrom. 37 (2008) 286–292.

[15] K. Trentelman, M. Bouchard, M. Ganio, C. Namowicz, C.S. Patterson, M. Walton, The examination of works of art using in situ XRF line and area scans, X-Ray Spectrom. 39 (2010) 159–166.

[16] T. Trojek, T. Cechak, L. Musílek, Recognition of pigment layers in illuminated manuscripts by means of Ka/Kb and La/Lb ratios of characteristic X-rays, Appl. Radiat. Isot. 68 (2010) 871–874.

[17] A. Deneckere, M. De Reu, M.P.J. Martens, K. De Coene, B. Vekemans, L. Vincze, Ph. De Maeye, P. Vandenabeele, L. Moens, The use of a multi-method approach to identify the pigments in the 12th century manuscript Liber Floridus, Spectrochim. Acta Part A 80 (2011) 125–132.

[18] B. Kanngisser, O. Hahn, M. Wilke, B. Nekat, W. Malzer, A. Erko, Investigation of oxidation and migration processes of inorganic compounds in ink-corroded manuscripts, Spectrochim. Acta Part B 59 (2004) 1511–1516.

[19] W. Faubel, S. Staub, R. Simon, S. Heissler, A. Pataki, G. Banik, Non-destructive analysis for the investigation of decomposition phenomena of historical manuscripts and prints, Spectrochim. Acta Part B 62 (2007) 669–676.

[20] I. Mantouvalou, T. Wolff, O. Hahn, I. Rabin, L. Luhl, M. Pagels, W. Malzer, B. Kanngiesser, 3D Micro-XRF for cultural heritage objects: new analysis strategies for the investigation of the dead sea scrolls, Anal. Chem. 83 (2011) 6308–6315.

[21] B. Wehling, P. Vandenabeele, L. Moens, R. Klockenkamper, A. von Bohlen, G. Van Hooydonk, M. de Reu, Investigation of pigments in medieval manuscripts by micro Raman spectroscopy and total reflection X-ray fluorescence spectrometry, Mikrochim. Acta 130 (1999) 253–260.

[22] A. von Bohlen, Total reflection x ray fluorescence spectrometry—a versatile tool for ultra-micro analysis of objects of cultural heritage, e-PS.1, 2004, pp. 23–34.

[23] P. Vandenabeele, B. Wehling, L. Moens, M. de Reu, G. van Hooydonk, A. Von Bohlen, R. Klokenkämper, Characterization of pigments in mercatellis manuscripts by TXRF and Raman microscopy, Achaeometry 98 Proceedings of the 31st symposium, 2002, pp. 825–827.

[24] R. Klockemkämper, A. von Bohlen, L. Moens, Analysis of pigments and inks on oil paintings and historical manuscripts using total reflection X ray fluorescence spectrometry, X-Ray Spectrom. (2000) 119–129.

[25] W. Devos, L. Moens, A. von Bohlen, R. Klockenkämper, Ultra-microanalysis of inorganic pigments on painted objects by TXRF analysis, Stud. Conserv. 40 (1995) 153–162.

[26] L. Moens, W. Devos, R. Klockenkämper, A. von Bohlen, TXRF in the ultramicro analysis of artists pigments, Trends Anal. Chem. 13 (1994) 198–205.

[27] L. Moens, W. Devos, R. Klockenkämper, A. von Bohlen, Application of TXRF for the ultramicro analysis of artists pigments, J. Trace Microprobe Tech. 13 (1995) 119–139.

[28] A. von Bohlen, Total reflection X-ray fluorescence and grazing incidence X-ray spectrometry—tools for micro- and surface analysis. A review, Spectrochim. Acta Part B 64 (2009) 821–832.

[29] G. Van Hooydonk, M. De Reu, L. Moens, J. Van Aelst, L. Milis, A TXRF and micro-Raman spectrometric reconstruction of palettes for distinguishing between scriptoria of related medieval manuscripts, Eur. J. Inorg. Chem. (1998) 639–644.

[30] W. Kautek, S. Pentzien, M. Röllig, P. Rudolph, J. Krüger, C. Maywald-Pitellos, H. Bansa, H. Grösswang, E. König, Near-UV laser interaction with contaminants and pigments on parchment: laser cleaning diagnostics by SE-microscopy, VIS-, and IR-spectroscopy, J. Cult. Herit. 1 (2000) s233–s240.

[31] G. Della Gatta, E. Badea, R. Ceccarelli, T. Usacheva, A. Maši, S. Coluccia, Assessment of damage in old parchments by DSC and SEM, J. Therm. Anal. Calorim. 82 (2005) 637–649.

[32] M. Bicchieri, M. Monti, G. Piantanida, F. Pinzari, A. Sodo, Non-destructive spectroscopic characterization of parchment documents, Vib. Spectrosc. 55 (2011) 267–272.

[33] M. Aceto, A. Agostino, E. Boccaleri, F. Crivello, A.C. Garlanda, Evidence for the degradation of an alloy pigment on an ancient Italian manuscript, J. Raman Spectrosc. 37 (2006) 1160–1170.

[34] B. Dolgin, Y. Chen, V. Bulatov, I. Schechter, Use of Libs for rapid characterization of parchment, Anal. Bioanal. Chem. 386 (2006) 1535–1541.

[35] B. Dolgin, V. Bulatov, Y. Chen, I. Schechter, Characterization of historical parchment using laser induced breakdown spectroscopy, Am. Lab. 40 (2008) 24–27.

[36] M. Bicchieri, M. Nardone, P.A. Russo, A. Sodo, M. Corsi, G. Cristoforetti, V. Palleschi, A. Salvetti, E. Tognoni, Characterization of azurite and lazurite based pigments by laser induced breakdown spectroscopy and micro-Raman spectroscopy, Spectrochim. Acta Part B 56 (2001) 915–922.

[37] K. Melessanaki, V. Papadakis, C. Balas, D. Anglos, Laser induced breakdown spectroscopy and hyper-spectral imaging analysis of pigments on an illuminated manuscript, Spectrochim. Acta Part B 56 (2001) 2337–2346.

[38] W. Kautek, S. Pentzien, P. Rudolph, J. Krüger, E. König, Laser interaction with coated collagen and cellulose fibre composites: fundamentals of laser cleaning of ancient parchment manuscripts and paper, Appl. Surf. Sci. 127–129 (1998) 746–754.

[39] M. Strlic, J. Kolar, V.-S. Selih, M. Marincek, Surface modification during Nd:YAG (1064 nm) pulsed laser cleaning of organic fibrous materials, Appl. Surf. Sci. 207 (2003) 236–245.

[40] M. Budnar, J. Simčič, Z. Rupnik, M. Uršič, J. Kolar, M. Strlič, Determination of elemental concentrations of iron gall ink components by PIXE, proceeding of the international conference. Application of accelerators in research and industry, 2003, pp. 436–439.

[41] M. Budnar, J. Simčič, M. Uršič, Z. Rupnik, P. Pelicon, J. Kolar, M. Strlič, In-air PIXE set-up for automatic analysis of historical document inks. analysis, In-air PIXE set-up for automatic, Nucl. Instrum. Methods Phys. Res. B 219–220 (2004) 41–47.

[42] C. Remazeilles, V. Quillet, T. Calligaro, J.C. Dran, L. Pichon, J. Salomon, pixe elemental mapping on original manuscripts with an external microbeam. Application to manuscripts damaged by iron ink corrosion, Nucl. Instrum. Methods Phys. Res. B 181 (2001) 681–687.

[43] O.R. Kakuee, V. Fathollahi, P. Oliaiy, M. Lamehi-Rachti, R. Taheri, H.A. Jafarian, External PIXE analysis of an Iranian 15th century poetry book, Nucl. Instrum. Methods Phys. Res. B 273 (2012) 178–181.

[44] R.J.H. Clark, Raman microscopy: sensitive probe of pigments on manuscripts paintings and other artefacts, J. Mol. Struct. 347 (1995) 417–428.

[45] D. Bersani, P.P. Lottici, F. Vignali, G. Zanichelli, A study of medieval illuminated manuscripts by means of portable Raman equipments, J. Raman Spectrosc. 37 (2006) 1012–1018.

[46] G.D. Smith, R.J.H. Clark, Raman microscopy in archaeological science, J. Archaeol. Sci. 31 (2004) 1137–1160.

[47] I.M. Bell, R.J.H. Clark, P.J. Gibbs, Raman spectroscopic library of natural and synthetic pigments, Spectrochim. Acta Part A 53 (1997) 2159–2179.

[48] L. Burgio, R.J.H. Clark, Library of FT-Raman spectra of pigments, minerals, pigment media and varnishes, and supplement to existing library of Raman spectra, Spectrochim. Acta Part A 57 (2001) 1491–1521.

[49] K. Castro, M. Pérez-Alonso, M.D. Rodríguez-Laso, L.A. Fernández, J.M. Madariaga, On-line FT-Raman and dispersive Raman spectra database of artists' materials (e-VISART database), Anal. Bioanal. Chem. 382 (2005) 248–258.

[50] S.P. Best, R.J.H. Clark, M.A.M. Daniels, R. Withnall, Endeavour 16 (1992) 66–73.

[51] R.J.H. Clark, Raman microscopy: application to the identification of pigments on medieval manuscripts, Chem. Soc. Rev. 24 (1995) 187–196.

[52] R.J.H. Clark, Raman microscopy: sensitive probe of pigments on manuscripts, J. Mol. Struct. 480–481 (1999) 15–20.

[53] R.J.H. Clark, Pigment identification by spectroscopic means, C. R. Chim. 5 (2002) 7–20.

[54] R.J.H. Clark, The scientific investigation of artwork and archaeological artefacts: Raman microscopy as a structural, analytical and forensic tool, Appl. Phys. A: Mater. Sci. Process. 89 (2007) 833–840.

[55] L. Burgio, D.A. Ciomartan, R.J.H. Clark, Pigment identification on medieval manuscripts, paintings and other artefacts by Raman spectroscopy: applications to the study of three German manuscripts, J. Mol. Struct. 405 (1997) 1–11.

[56] A. Jurado-López, O. Demko, R.J.H. Clark, D. Jacobs, Analysis of the palette of a precious 16th century illuminated Turkish manuscript by Raman microscopy, J. Raman Spectrosc. 35 (2004) 119–124.

[57] T.D. Chaplin, R.J.H. Clark, D. Jacobs, K. Jensen, G.D. Smith, The Gutenberg bibles: analysis of the illuminations and inks using Raman spectroscopy, Anal. Chem. 77 (2005) 3611–3622.

[58] K.L. Brown, R.J.H. Clark The, Lindisfarne Gospels and two other 8th century, J. Raman Spectrosc. 35 (2004) 4–12.

[59] R.J.H. Clark, L. Cridland, B.M. Kariuki, K.D.M. Harris, R. Withnall, Synthesis, structural characterisation and Raman Spectroscopy of the inorganic pigments lead tin yellow types I and II and lead antimonate yellow: their identification on medieval paintings and manuscripts, J. Chem. Soc. Dalton Trans. 16 (1995) 2577–2582.

[60] L. Burgio, R.J.H. Clark, V.S.F. Muralha, T. Stanley, Pigment analysis by Raman microscopy of the non-figurative illumination in the 16th to 18th century Islamic manuscripts, J. Raman Spectrosc. 39 (2008) 1482–1493.

[61] L. Burgio, R.J.H. Clark, R.R. Hark, Raman microscopy and x-ray fluorescence analysis of pigments on medieval and Renaissance Italian manuscript cuttings, Proc. Nat. Acad. Sci. 107 (2010) 5726–5731.

[62] S. Bruni, F. Cariati, F. Casadio, L. Toniolo, Spectrochemical characterization by micro-FTIR spectroscopy of blue pigments in different polychrome works of art, Vib. Spectrosc. 20 (1999) 15–25.

[63] S. Bruni, F. Cariati, F. Casadio, V. Guglielmi, Micro-Raman identification of the palette of a precious XVI century illuminated Persian codex, J. Cult. Herit. 4 (2001) 291–296.

[64] S. Bruni, F. Cariati, F. Casadio, L. Toniolo, Identification of pigments on a XV century illuminated parchment by Raman and FTIR microspectroscopies, Spectrochim. Acta Part A 55 (1999) 1371–1377.

[65] K. Turner, N. Trentelman, Investigation of the painting materials and techniques of the late-15th century manuscript illuminator Jean Bourdichon, J. Raman Spectrosc. (2009) 577–584.

[66] A.S. Lee, V. Otieno-Alego, D.C. Creagh, Identification of iron-gall inks with near-infrared Raman microspectroscopy, J. Raman Spectrosc. 39 (2008) 1079–1084.

[67] F. Magistro, D. Majolino, P. Migliardo, R. Ponterio, M.T. Rodriquez, Confocal Raman spectroscopic study of painted medieval manuscripts, J. Cult. Herit. 2 (2001) 191–198.

[68] M. Bicchieri, M. Nardone, A. Sodo, Application of micro-Raman spectroscopy to the study of an illuminated medieval manuscript, J. Cult. Herit. 1 (2000) s277–s281.

[69] A.S. Lee, P.J. Mahon, D.C. Creagh, Raman analysis of iron gall inks on parchment, Vib. Spectrosc. 41 (2006) 170–175.

[70] P. Vandenabeele, K. Castro, M. Hargreaves, L. Moens, J.M. Madariaga, H.G.M. Edwards, Comparative study of mobile Raman instrumentation for art analysis, Anal. Chim. Acta 588 (2007) 108–116.

[71] S. Bioletti, R. Leahy, J. Fields, B. Meehan, W. Blau, The examination of the Book of Kells using micro-Raman spectroscopy, J. Raman Spectrosc. 40 (2009) 1043–1049.

[72] E. Mannucci, R. Pastorelli, G. Zerbi, C.E. Bottani, A. Facchini, Recovery of ancient parchment: characterization by vibrational spectroscopy, J. Raman Spectrosc. 31 (2000) 1089–1097.

[73] H.G.M. Edwards, F.R. Perez, Application of Fourier transform Raman spectroscopy to the characterization of parchment and vellum. Effect of biodeterioration and chemical deterioration on spectral interpretation, J. Raman Spectrosc. 35 (2004) 754–760.

[74] F. Rosi, M. Paolantoni, C. Clementi, B. Doherty, C. Miliani, B. Brunetti, A. Sgamellotti, Subtracted shifted Raman spectroscopy of organic dyes and lakes, J. Raman Spectrosc. 41 (2010) 452–458.

[75] A.V. Whitney, R.P. Van Duyne, F. Casadio, An innovative surface-enhanced Raman spectroscopy (SERS) method for the identification of six historical red lakes and dyestuffs, J. Raman Spectrosc. 37 (2006) 993–1002.

[76] S.A. Centeno, J. Shamir, Surface enhanced Raman scattering (SERS) and FTIR, J. Mol. Struct. 873 (2008) 149–159.

[77] R.J.H. Clark, P.J. Gibbs, Identification of lead(ii) sulfide and pararealgar on a 13th century manuscript by Raman microscopy, Chem. Commun. (1997) 1003–1004.

[78] J. Senvaitiene, A. Beganskiene, A. Kareiva, Spectroscopic evaluation and characterization of different historical writing inks, Vib. Spectrosc. 37 (2005) 61–67.

[79] D. Creagh, A. Lee, V. Otieno-Alego, M. Kubik, Recent and future developments in the use of radiation for the study of objects of cultural heritage significance, Rad. Phys. Chem. 78 (2009) 367–374.

[80] L. Gonzalez, T. Wess, Use of attenuated total reflection-Fourier transform infrared spectroscopy to measure collagen degradation in historical parchments, Appl. Spectrosc. 62 (2008) 1108–1114.

[81] E. Badea, L. Miu, P. Budrugeac, M. Giurginca, A. Masic, N. Badea, G. Della Gatta, Study of deterioration of historical parchments by various thermal analysis techniques complemented by sem, ftir, uv–vis–nir and unilateral nmr investigations, J. Therm. Anal. Calorim. 91 (2008) 17–27.

[82] A. Cucos, P. Budrugeac, L. Miu, S. Mitrea, G. Sbarcea, Dynamic mechanical analysis (DMA) of new and historical parchments and leathers: correlations with DSC and XRD, Thermochim. Acta 516 (2011) 19–28.

[83] C.J. Kennedy, J.C. Hiller, D. Lammie, M. Drakopoulos, M. Vest, M. Cooper, W.P. Adderley, T.J. Wess, Microfocus X-ray diffraction of historical parchment reveals variations in structural features through parchment cross sections, Nano Lett. 4 (2004) 1373–1380.

ORIGINAL PAPER

Characterisation of foxing stains in eighteenth to nineteenth century drawings using non-destructive techniques

M. Manso · S. Pessanha · F. Figueira · S. Valadas ·
A. Guilherme · M. Afonso · A. C. Rocha ·
M. J. Oliveira · I. Ribeiro · M. L. Carvalho

Abstract The reddish-brown, brown or yellowish stains of circular or irregular shape known as foxing spots have been fully described in conservation literature but still, this phenomenon does not find any scientific agreement since many hypotheses have been raised concerning their origin. In this work a contribution to foxing definition not only focussed on its appearance but also reported on its chemical information. For this purpose foxing stains present in drawings from two Portuguese artists dated from the eighteenth to nineteenth centuries were observed under ultra-violet light and optical microscope and analysed by three non-invasive spectroscopy techniques. The observations carried out on the stains provided information on their surface morphology. The use of energy-dispersive X-ray fluorescence revealed a variation on the elemental content between foxing and paper region. Although the results from X-ray diffraction analysis showed no signs of cellulose degradation in foxing stains, Fourier-transformed infrared analysis revealed the presence of oxide groups. Both the information on the chemical nature and surface morphology of the stains achieved in this study will contribute to increase foxing formation information and develop future protocols for conservation purposes.

M. Manso · S. Pessanha · A. Guilherme · M. L. Carvalho (✉)
Departamento de Física da Faculdade de Ciências,
Centro de Física Atómica da Universidade de Lisboa,
Av. Prof. Gama Pinto, 2,
1649-003 Lisbon, Portugal
e-mail: luisa@cii.fc.ul.pt

F. Figueira · S. Valadas · M. Afonso · A. C. Rocha ·
M. J. Oliveira · I. Ribeiro
Instituto Português dos Museus,
Rua das Janelas Verdes, 37,
1249-018 Lisbon, Portugal

Introduction

Foxing on paper has been actively researched since the 1930s by conservation scientists and conservators to elucidate its causes and to establish protocols for detection, prevention and treatment. Foxing stains can be seen on different kinds of papers dating from the beginning of the sixteenth to the twentieth century. They are more pronounced on paper produced in the end of eighteenth up to the beginning of twentieth century. In spite that a large amount of research has been published on the origin and characterisation of foxing, there are still no conclusive results. According to Derow and Choi [1, 2], the main difficulty of this subject may lie in the vague definition of foxing. The term foxing generally refers to small, roundish spot stains of reddish or yellowish brown colour, generally of small dimensions, with sharp or irregular edges, found in paper or other fibre-based materials. This term only vaguely describes the size, shape and colour of certain stains, of which interpretation may depend on each viewer's subjectivity. Due to the lack of specific criteria for definition, confusion sometimes occurs about whether a certain local stain may or may not be called foxing. Although the causes of foxing are not yet completely understood, they are usually ascribed to mould growth and/or heavy-metal-induced degradation of cellulose and sizing. New hypotheses have developed on foxing formation including preferential cellulose oxidation or moisture condensation related to the non-homogeneity of the paper [3]. Metal has been considered one of the major causes of foxing. It may arise either from the papermaking process or from airborne dust [4]. Metals found in foxing spots

include iron, tin, copper, copper–mercury or copper–zinc or brass and were typically identified using scanning electron microscopy and energy-dispersive X-ray (SEM or SEM/ EDX), X-ray fluorescence (XRF) and atomic absorption analysis [4–6]. Fungal infection of foxing had been reported as early as 1917. Published research making use of light microscopy and SEM for examining foxing visually proved the presence of fungi in the affected areas [7–10]. However it is still difficult to determine whether mould is the causal agent of degradation or if the mould growth is opportunistic in nature, taking advantage of the weakening of paper due to chemical factors [11]. Currently the only common characteristic found in foxing stains is localised cellulose oxidation [4, 5]. Oxidation occurs by a reaction between a cellulose molecule and oxygen that forms hydrogen peroxide radicals as a reactive intermediate. Metals or acids from various origins, e.g. fungal metabolites or cellulose degradation products, can accelerate the oxidation process. Oxidation compounds have been detected using infrared spectroscopy on foxing stains [5, 12]. Regardless of the direct causes of oxidation, a prevailing agreement is that UV fluorescence is detected in the early stage of foxing. As foxing formation progresses, UV fluorescence decreases and visible colour increases instead [4, 13]. In order to contribute to a consensus on a new definition of foxing not only based on the appearance of the stains, physical and chemical analysis has been performed in our research. In the present article we report on the analysis of foxing stains by energy-dispersive X-ray fluorescence (EDXRF), X-ray diffraction (XRD) and Fourier-transformed infrared (FTIR) analysis and observation under UV light and optical microscope as non-invasive tools for foxing characterisation in respect to their nature. The article investigates both the chemical nature and the surface morphology of the stains with the aim of getting a new insight into the microscopic mechanisms causing damage to paper.

Experimental

Foxing stains in 14 drawings belonging to the collection of the Museu Nacional de Arte Antiga in Lisbon were analysed in situ with μ-EDXRF, μ-XRD and μ-FTIR spectrometers. Observations of the drawings under optical microscopic lens and UV light were also carried out. Out of the 14 studied drawings, 11 belong to the artist Domingos Sequeira (1768–1823), while the remaining three belong to the artist Cirilo Wolkmar Machado (1748–1823). The 14 drawings have been subdivided into four groups (A, B, C and D). These groups integrate batches of papers, whose texture, tone, density, grammage (Table 1) and elemental (Fig. 1) composition are closely the same. The 14 drawings have been subdivided into groups A and B and

are respectively composed of four tinted greenish-brown and five tinted brown-reddish medium thick wove papers from Domingos Sequeira. These nine drawings depict the 1810 royal court representatives. Group C, also belonging to Domingos Sequeira, is composed of two cream white wove papers that present a strong discolouration in some of its areas suggesting of having been in contact with extremely high temperatures through the contact of a glazing glass and dating from 1796. Cirilos drawings date from 1798 (group D) and were executed on thin white laid paper.

Optical microscopic lens

The foxing stains were observed on a Leica MZ6 microscopic lens, which supports a magnification of ×6.3–40. For a stain dimension comparative purpose, a magnification of ×25 was chosen. This amplification was chosen in order to be able to encompass most of the stains encountered. Lower amplifications were used for larger dimensioned stains only present in groups A and B. A ×40 magnification was chosen to document the paper surface topography. The images were captured using an incorporated Leica DC200 camera with raking light Leica CLS ×100 at no. 3 exposure. The colour correction circle was kept constant.

UV illumination

The macro-images were taken with a Nikon Coolpix 8700 on a photographic column stand. The machine was held on the stand at 0 cm height; zoom was adjusted until the macro-symbol became activated and the white balance was adjusted for fluorescent light. These conditions were kept constant throughout the photographic session. A UV Waldmann W portable lamp with two Philips TL 4 W/08 F4 T5/BLB was used and the distance was also held constant.

μ-EDXRF analysis

All the samples were analysed in situ with a portable μ-EDXRF spectrometer. EDXRF technique is completely non-destructive, and it is sensitive to a great number of elements, typically those with atomic number $Z>13$. The equipment used for foxing stain and paper elemental analysis was a portable instrument consisting of an Oxford X-ray generator (Model XTF 5011) with Mo anode (50 kV, 1 mA). The detector used was a Vortex-EX SDD (Si) thermoelectrically cooled with a nominal area of 50 mm^2 and a Be window. The X-ray generator and detector were coupled to a vacuum chamber [14] in 45° geometry. The spot size of the used polycapillary was 90 μm, which is

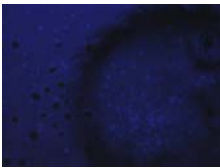**Table 1** Batches of the studied papers grouped according to tone and texture
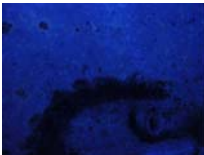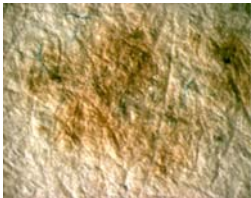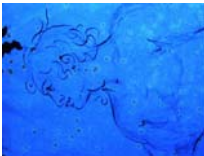
Groups of drawings	Tone	Image detail in a photographic stand using the same condition parameters to show the paper and foxing tones as well as the stain dimension and occurrence.	Microscopic image in raking light at 25X magnification showing colour and dimension of foxing stain	Microscopic image in raking light at 40X magnification showing paper topography	Image detail under UV light
Group A Inv. 1613 Inv. 1617 Inv. 1624 **Inv. 1625**	Green-brown paper				
Group B Inv. 1603 Inv. 1604 Inv. 1605 **Inv. 1615** Inv. 1620	Brown-red paper				
Group C Inv. 1924 **Inv. 1925**	Cream paper				
Group D **Inv. 2945** Inv. 2946 Inv. 2947	White paper				

Image details from drawings in bold are shown under raking light and under UV light

Fig. 1 Batches of papers according to the elemental concentration of the papers from the 14 studied drawings

particularly suited to analysing stains with dimensions in the order of 1 mm or less. The chamber also possesses a camera, allowing the visualisation of the analysed area and thus the capture of the image and the spot of analysis, which was highlighted by the two lasers. All spectra were collected using the polycapillary mode in vacuum, operating conditions of 40 kV, 0.5 mA and 300 s. The spectra analyses were performed using the WinAXIL (analysis of X-ray spectra by iterative least-squares fitting) software package, and the quantification was made through the compare mode, using three standard reference materials (poplar leaves GBW 07604, bush branches GBW 07603 and tea leaves GBW 07605). The accuracy of the method was checked by analysing a fourth standard reference material orchard leaves NBS1571 and is presented in Table 2. The detection limits (DL) obtained by EDXRF were calculated according to:

$$DL = \frac{3c_i\sqrt{N_b}}{N_p}$$

where C_i is the concentration of the element i, N_b is the counting rate for the background and N_p is the counting rate for the corresponding peak. The results for orchard leaves

Table 2 Mean elemental concentration and standard deviation (μg g^{-1}) obtained in this work for orchard leaves NBS1571 and certified values

	P	S	Cl	K	Ca	Mn	Fe	Zn	Cu
Present work	2,300±400	3,000±1000	760±90	16,000±2,000	18,000±3,000	80±10	260±60	19±7	8±2
Certified value	2,100±100	2,300±100	700±10	14,700±300	20,900±300	91±4	300±20	25±3	12±1

(NBS standard reference material 1571) are presented in Table 3.

μ-XRD analysis

The main purpose of the XRD measurements was to achieve information on the crystallinity of the cellulose component. μ-XRD analysis was performed directly on the samples, without previous preparation, using a Bruker D8 Discover diffractometer equipped with Cu Kα radiation, a Gobel mirror assembly and a GADDS detector. To allow the analysis of relatively small areas of interest in the stains, a 1-mm-diameter pinhole collimator was used. The angular range (2θ) was scanned from 6.4° to 71.4° at a step size of 0.02°, and the working voltage and current were, respectively, 40 kV and 40 mA.

μ-FTIR analysis

Infrared analysis was carried out using a Nicolet Nexus spectrometer coupled to a Nicolet CONTINUμM microscope. The spectrometer has a Ge-on-KBr beam splitter and an Ever-Glo infrared source. The microscope was equipped with a ×15 Reflachromat objective and condenser pair and fitted with a Nicolet mercury–cadmium–telluride (MCT-A) detector cooled with liquid nitrogen (working range of 4,000–650 cm^{-1}). Samples were removed from the papers and compressed in a Spectra-Tech μSample Plan micro-compression diamond cell and analysed in transmission mode. The area of analysis of the sample was defined by the double aperture contained in the microscope. For each spectrum, 256 scans were acquired with a spectral resolution of 4 cm^{-1}. No spectral processing other than removal of the carbon dioxide bands was performed.

Table 3 Detection limits (μg g^{-1}) obtained by EDXRF in orchard leaves, NBS standard reference material 1571

	P	S	Cl	K	Ca	Mn	Fe	Cu	Zn
DL	63	23	31	71	88	2	5	2	2

Detection limits obtained for orchard leaves sample

Discussion and results

Stain form and appearance under optical microscope and UV illumination

Microscopic images

Out of the 14 papers observed, the tones of the foxing stains range from brown-red on groups A and B to orange on group D (Table 1). The inverse foxing found on the discoloured areas of group C seems to be the result of a local intrinsic immunity system towards the oxidative process. These stains consist of a very circular whiter spot inserted within the brown discoloured areas (Table 1). The centre of these inverse foxing stains may sometimes present a dark-coloured spot. Observing the topography of the papers at the foxed and unfoxed areas, it does not seem to show a significant alteration in the fibre surface disposition. Groups A, B and D present a more irregular surface when compared with group C. Although some foxing spots do seem to appear as a result of a local difference of the surface topography as is suggested in the literature [3], the authors did not always find that correlation.

UV illumination

When observed under UV light, some of the examined stains fluoresce quite well while others do not. Fluorescent areas are reported to be usually larger than the visibly stained areas, and in some cases, fluorescence occurs without any visible discolouration (Table 1). It has been suggested that the formation of fluorescent species is an intermediate stage in the degradative process of paper that culminates in brown discolouration [4, 13].

Physical and chemical studies on the stains

μ-EDXRF measurements

By pointing the beam at different points of the papers, it was possible to compare EDXRF spectra obtained from foxing stains and those obtained from the unstained paper. The elements measured during the non-destructive analysis in both areas were Al, Si, P, S, Cl, K, Ca, Mn, Fe and Cu. Dendrogram analysis

Table 4 Mean elemental concentration (μg g^{-1}) for unstained paper and foxing stain present in the studied drawings

Sample	Description	Al	Si	P	S	Cl	K	Ca	Mn	Fe	Cu
Inv. 1624	Paper	2,000±400	2,500±500	600±100	2,100±400	BDL	800±100	1,300±200	30±5	2,800±500	40±5
	Foxing	2,500±400	2,400±450	600±100	2,200±450	BDL	1,800±200	1,500±200	30±5	2,700±500	40±5
Inv. 1613	Paper	1,400±280	1,900±350	700±100	2,300±400	BDL	1,100±100	1,100±200	20±3	1,900±380	25±5
	Foxing	1,500±300	2,200±400	900±100	2,100±400	BDL	1,700±200	900±100	25±4	2,000±400	25±5
Inv. 1605	Paper	1,400±280	2,800±500	700±100	2,000±400	BDL	810±100	1,000±200	40±5	1,000±200	20±4
	Foxing	1,600±300	3,000±600	600±100	2,100±400	BDL	1,000±100	900±100	50±8	1,300±200	30±6
Inv. 1924	Paper	1,000±200	1,200±200	340±60	1,900±380	720±80	260±30	4,000±600	14±2	50±10	BDL
	Inverse foxing	1,100±200	1,000±200	330±50	1,900±380	BDL	190±20	4,100±600	11±2	40±8	BDL
Inv. 2945	Paper	600±100	1,800±300	600±90	1,900±350	1,000±100	80±10	2,100±300	BDL	40±8	BDL
	Foxing	600±100	2,000±400	600±100	1,900±350	BDL	580±70	3,100±500	BDL	50±10	BDL

taking into account the measured elemental content present in the unstained areas of the 14 studied papers is shown in Fig. 1. The hierarchical cluster analysis dendrogram was obtained using *Statistica 8*. Single linkage method and Euclidian distances were used. According to this analysis, the 14 papers were grouped into five clusters (A1, A2, B, C and D). When taking account of the elemental content, group A was further divided into two groups. The elemental content of the foxing stains present in each paper cluster was also quantified and it is presented in Table 4. Here we can compare the mean elemental content of unstained areas of one paper sample representative of each cluster and the respective mean elemental content of the foxed areas. The μ-EDXRF results showed that whenever Cl was present in paper (group C and D) it tended to vanish in the stains (Fig. 2). It is important to observe that Ca is always present in the paper, and it is not directly related to foxing stains. Potassium revealed a different behaviour between groups of drawings. While in group B and C its concentration in paper and stain remained fairly constant, in groups A1, A2 and D, a remarkable growth in the stain was shown. The authors had already observed an increase of K levels accompanied by an intense decrease of Cl levels when studying artificial aged model papers by cellulosomes, *Clostridium cellulolyticum* [15]. Bicchieri et al. [5] also reported an increase of K values in foxing stains when compared to paper unstained areas in seventeenth century documents. The levels of Al, Si, P, S, Mn and Fe between stain and unstained area in paper are similar as can be seen in Table 4.

μ-XRD measurements

Cellulose I is the common variety in nature and hence in paper. It has a distinct and well-defined XRD pattern, which is due to the crystalline nature of the cellulose molecules. The crystallinity of cellulose is a function of its source and the degree of degradation of the fibres due to grinding, beating or other treatment. The XRD pattern of cellulose I is characterised by a well-defined principal peak at 22.5° (2θ) and two secondary peaks at 14.5° and 16.3° (2θ). As the cellulose fibre is degraded, the two secondary peaks first of all merge and are then destroyed; simultaneously the principal peak becomes smaller [16]. Eventually a hump-backed curve is formed with a maximum at about 17° (2θ). The positions of the peaks are reasonably constant although they do occasionally shift by up to approximately 0.2° (2θ) about the mean position. Despite the changes in the elemental content of K and Cl, no phase differences between paper and stain were detected by μ-XRD for any of the studied groups of drawings (Fig. 3).

Fig. 2 EDXRF spectra of paper
and foxing stain in drawing
from group D
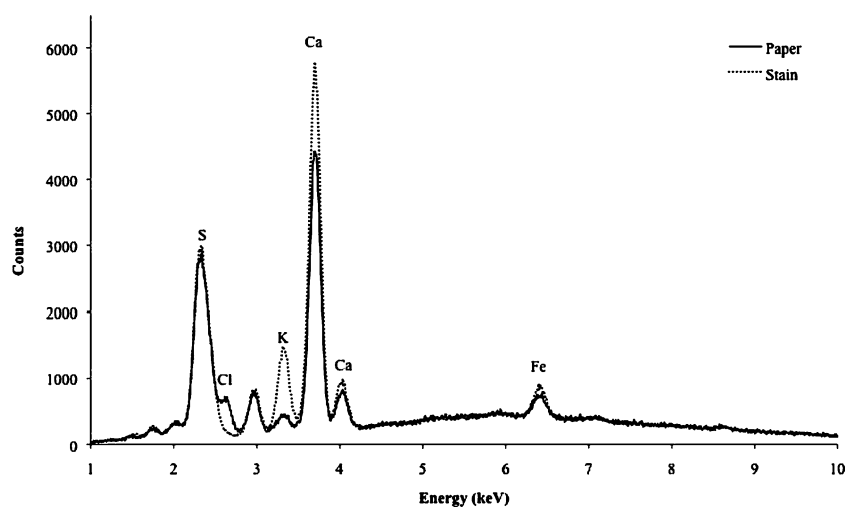
μ-FTIR measurements

FTIR spectra of samples were collected from areas that presented foxing stains and those that were not damaged in order to highlight and characterise degradation compounds related to foxing. The identification was accomplished either by assigning chemical groups to the peaks in the spectra or by comparing each spectrum to those of known compounds and making the identification by the best match. No differences were found between paper and stain for spectra obtained for drawings from groups A, B and C. The differences obtained for paper and stain for drawings from group D are displayed in Fig. 4, and the spectra interpretation is presented in Table 5. Paper spectrum revealed typical assignment of cellulose (β-D-glycopyranose conformation), and stain spectrum differed from paper spectrum on only two peaks, which appear at 1,686 and 1,600 cm^{-1}. These two shoulders are usually associated with C=O and the COO$^-$ stretching of the carboxyl group,

respectively [17], probably sourced from the degradation of cellulose [18]. According to the most recent researches, the mechanisms of degradation of cellulose should be associated with mixed oxidative and hydrolytic processes. The oxidation process affects various C–OH groups on the glycopyranose rings, producing various carbonyl groups (ketones, esters and carboxylic acid salts), which cause acidic environment and induces the hydrolysis of cellulose by producing mainly aldehydic groups on terminal rings [6]. Attribution of bands is not very easy because different structures can coexist in the same part of paper, unmodified, differently oxidised cellulose, hydrocellulose, etc., and some functional groups evidence the same spectral regions. For example, carbon–carbon double bonds on the ring and carbonyl groups are usually masked by the broad bands of bonded water. As a result, we only can indicate two peaks, which can be associated to cellulose degradation, and it is not enough to indicate with precision which mechanisms are related.

Fig. 3 XRD spectra of paper
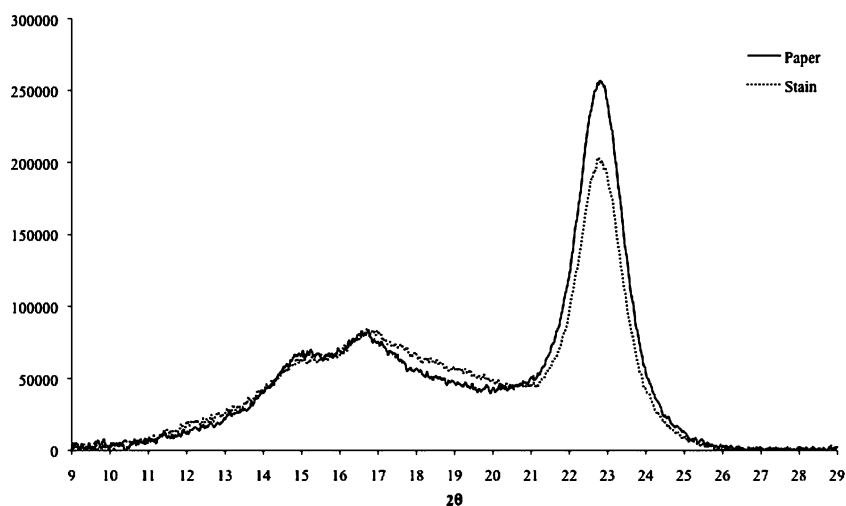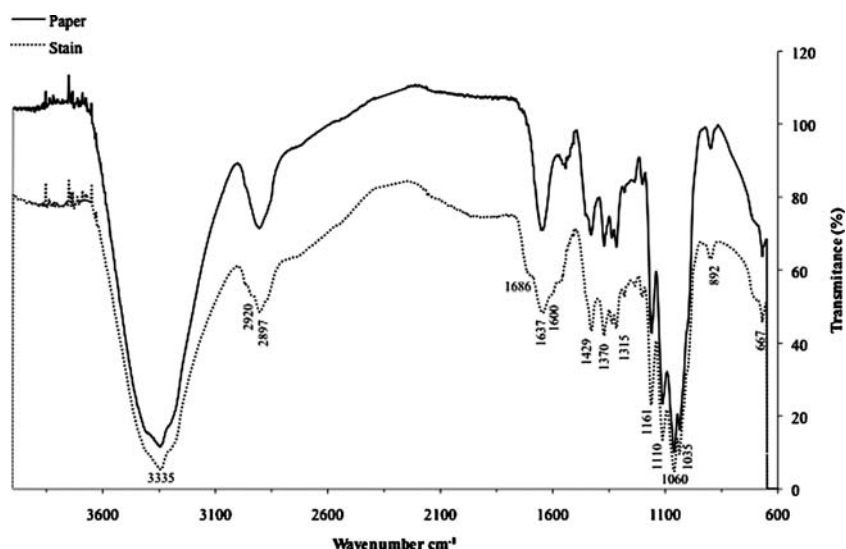and foxing stain in drawing
from group D

Fig. 4 FTIR spectra of paper and stain in drawing 2945 from group D

Conclusion

A combination of non-destructive spectroscopy and observation techniques were applied to the characterisation of foxing stains present in papers used for these drawings. Observations of the foxing stains under optical microscopic lens that revealed no significant alterations in the fibre surface disposition were observed between foxed and unfoxed areas of the drawings, and hence no correlation was found between the localisation of the foxing spots and the surface topography of the papers. UV imaging showed fluorescence not only around foxing spots but also in non-

foxed areas. Some foxing spots did not show fluorescence. The use of μ-EDXRF equipment turned out to be outstanding for the performance of this research. It allows in situ non-destructive analysis, and since it is coupled to a vacuum chamber, it allows the detection of lighter elements, which is fundamental in the analysis of paper-based artworks. The video camera allowed the visualisation of the analysed area and ensured the capture of the analysed spots, in which elemental content was measured by micro-beam particularly suited to analysing stains with dimensions in the order of 1 mm. By means of this equipment, variation on the elemental content between foxing and paper region was formally achieved. Metals have been considered as one of the major causes of foxing, and at the moment, the most frequent ones found in these spots include Fe and Cu. In this work a metal not so often found in foxing stains—K—was detected and measured in much higher concentrations than in the unstained parts of the analysed documents (groups A and D). Alkaline metals such as K can have a catalysing effect on oxidation reaction [5]. The disappearance of Cl in the foxing stains of the documents from group C and D reveals that the formation mechanism of foxing stains may be related not only with metallic elements but also with non-metals. The results obtained in [15] in artificially aged papers with cellulosomes may suggest that the foxing stains in documents from group D have been originated from enzymes. Although the results from X-ray diffraction analysis showed no signs of cellulose degradation, i.e. all cellulose I characteristic peaks were well defined in the spectra obtained from foxing stains, Fourier-transformed infrared analysis revealed the presence of carboxyl groups that are reported to be responsible for the hydrolysis of cellulose.

Table 5 Peak table and interpretation of paper and stain (italic) from group D [12, 17, 18]

Wavenumber (cm^{-1})	Interpretation
3,335	O–H stretching vibration
2,920	C–H$_2$ stretching vibration
2,897	C$_6$–H stretching vibration (C–H, C–H$_2$)
1,686	C=O stretching vibration
1,637	O–H stretching vibration, water in cellulose
1,600	COO$^-$ stretching vibration
1,429	C–H$_2$ bending vibration
1,370	CO–H bending vibration
1,315	C–H$_2$ bending vibration
1,161	C–O stretching vibration
1,110	C–O–C symmetric stretching vibration
1,060	C–O–C asymmetric stretching vibration
1,035	O–H bending vibration (primary alcohol)
892	Skeletal vibration—anomeric cellulose
665	C–OH bending vibration

References

1. Derow J, Owen A (1992) In: Paper conservation catalog, American Institute for Conservation Book and Paper Group, Foxing, Washington, D.C.: AIC. Chap.13:1–39

2. Choi S (2007) Foxing on paper: a literature review. J Am Inst Conserv 46:37–152

3. Ligterink FJ, Porck HJ, Smith WJ Th (1991) Foxing stains and discolouration of leaf margins and paper surrounding printing ink: elements of a complex phenomenon in books. The Paper Conservator, IPC, 15:45–52

4. Rebrikova NL, Manturovskaya NV (2000) Foxing: a new approach to an old problem. Restaurator 21:85–100

5. Bichieri M, Pappalardo G, Romano FP, Sementilli FM, Acutis R (2001) Characterisation of foxing stains by chemical a spectrometric methods. Restaurator 22:1–19

6. Bicchieri M, Ronconi S, Romano FP, Pappalardo L, Corsi M, Cristoforetti G, Legnaioli S, Palleschi V, Salvetti A, Tognoni E (2002) Study of foxing stains on paper by chemical methods, infrared spectroscopy, micro-X-ray fluorescence spectrometry and laser induced breakdown spectroscopy. Spectr Acta B 57:1235–1249

7. Florian M-LE (1996) The role of the Conidia of fungi in fox spots. Stud Conserv 41:65–75

8. Florian M-LE, Manning L (2000) SEM analysis of irregular fungal fox spots in an 1854 book: population dynamics and species identification. Int Biodeterior Biodegrad 46:205–220

9. Arai H (2000) Foxing caused by Fungi: twenty-five years of study. Int Biodeterior Biodegrad 46:181–188

10. Zotti M, Ferroni A, Calvini P (2008) Microfungal biodeterioration of historic paper: preliminary FTIR and microbiological analyses. Int Biodeterior Biodegrad 62:186–194

11. Rakotonirainy MS, Heude E, Lavédrine B (2008) Isolation and attempts of biomolecular characterization of fungal strains associated to foxing on a 19th century book. J Cult Herit 8:126–133

12. Choisy P, De La Capelle A, Thomas D, Legoy DT (1997) Non invasive techniques for the investigation of foxing stain of graphic art material. Restaurator 18:131–152

13. Pedersoli JL, Ligterink FJ, van Bommel M (2001) Investigation into fluorescence changes accompanying paper discoloration. In: ICOM—CC's Interim meeting of the working group on graphic documents at EVTEK Institute of Art and Design, pp. 7–10. Vantaa (Helsinki), Finland

14. Pessanha S, Manso M, Guilherme A, Costa M, Carvalho ML (2009) Investigation on historical documents for forensic purposes by X ray fluorescence analysis. Surface and Interface Analysis doi:10.1002/sia.3085

15. Manso M, Pessanha CML (2006) Artificial aging processes in modern papers: X-ray spectrometry studies. Spectr Acta B 61:922–928

16. Foner HA, Adan N (1983) The characterisation of papers by X-ray diffraction (XRD): measurement of cellulose crystallinity and determination of mineral composition. J- forensic Sci Soc 23:313–321

17. Lojewska J, Lubanska A, Miskowiec P, Lojewski T, Proniewicz LM (2006) FTIR in situ transmission studies on the kinetics of paper degradation via hydrolytic and oxidative reaction paths. Appl Phys A 83:597–603

18. Laguardia L, Vassallo E, Cappitelli F, Mesto E, Cremona A, Sorlini C, Bonizzoni G (2005) Investigation of the effects of plasma treatments on biodeteriorated ancient paper. Appl Surf Sci 252:1159–1166

Study of Air-Induced Paper Discolorations by Infrared Spectroscopy, X-ray Fluorescence, and Scanning Electron Microscopy

ADRIANA FERREIRA, FRANCISCA FIGUEIRA, SOFIA PESSANHA, INGELISE NIELSEN, and MARIA LUISA CARVALHO*

Arquivo Municipal de Lisboa, Rua B ao Bairro da Liberdade, Portugal (A.F.); Instituto dos Museus e Conservação, Rua das Janelas Verdes, Portugal (F.F.); Centro de Física Atómica da Universidade de Lisboa and Departamento de Física da Faculdade de Ciências, Av. Prof. Gama Pinto, 2, 1649–003 Lisboa (S.P., M.L.C.); and Portugal, School of Conservation- Royal Danish Academy of Fine Arts, Denmark (I.N.)

Air-induced paper discoloration is described as being different from other discoloration morphologies. It seems to be the result of prolonged exposure to air in a humid and polluted environment without appropriate protecting coverage. In this work, three folios from the same eighteenth century book, presenting three degrees of discoloration and opacity and subjected to different environmental conditions, were examined and compared. Samples were analyzed and compared by three different instrumental techniques, mid-infrared spectroscopy, X-ray fluorescence (XRF), and scanning electron microscopy (SEM). Chemical and physical changes were confirmed from the data collected by these techniques. The absence of the secondary amide band characteristic of proteins in the infrared spectra of the two discolored folios, accompanied by the appearance and increase of white mineral-like deposits visible in the SEM micrographs, support the idea that oxidation reactions occurred and that these two folios were subjected to more severe degradation hazard.

Index Headings: **Art conservation; Discoloration; Oxidation; Paper; Fourier transform infrared spectroscopy; FT-IR spectroscopy; X-ray fluorescence; XRF; Scanning electron microscopy; SEM.**

INTRODUCTION

A paper presented at the IIC Congress in 2002[1] described the observation of paper artifacts presenting partial or total discoloration sometimes associated with an increase in opacity. In the conservation literature consulted at the time, no mention was made of air exposure provoking discoloration and opacity, although many research papers on the effect of air pollution, and its control and effects on air quality inside museums, have been published previously. More specifically related to the phenomenon of the gain in opacity, Johansson mentions that the presence of NO_2 allows for a greater pick-up rate of SO_2 on the paper and promotes the formation of gypsum.[2] Since then, Letnar and Muck found that paper samples submitted to accelerated aging registered a decrease of brightness and an increase in yellowness as well as an increase in opacity. They attribute this to an altered gelatine sizing.[3]

Porck et al. reported on a study regarding the differences between identical book copies stored in two different libraries, respectively located in a highly polluted urban area and a less polluted area.[4] They concluded that the paper in the more polluted environment registered a larger amount of sulfur and a greater level of acidity; no mention was made of discoloration. In 2002 Havermans and Pork carried out further tests on the same books and concluded that the margins were not only more acidic but also considerably more discolored.[5]

Although ozone had been overlooked in indoor pollution parameters until quite recently because of its high reactivity and low time existence indoors (6 minutes), it has been more recently studied and published in non-conservation literature.[6,7] Synergetic effects produced by different air contaminants have also started to be considered. Weshler investigated ozone concentration levels in indoor and outdoor areas[8] and concluded that the ozone levels tend to be larger in homes with natural ventilation and that the higher the relative humidity, the larger the deposition velocities to different surfaces. The author also states that ozone can synergistically react with nitrogen dioxide and form nitrate radical, which can accumulate indoors in the absence of direct sunlight.[8] The nitrate radical is short-lived and is ultimately converted to nitric acid in typical indoor environments.[8] Dahlin and Grontoft agree with this and state that the reactions involving NO_2 and O_3 increase in the summer in towns with heavy traffic.[9] Ferm et al. speak of new multi-pollutant situations provoked by the decreasing sulfur dioxide levels in most parts of Europe and the increasing automobile traffic causing an increase of nitrogen compounds, ozone, and particulate matter. Although the dominant reaction for the formation of HNO_3 is between NO_2 and OH radicals, HNO_3 can also be formed by a dark reaction involving O_3 and NO_2.[10]

Relating the present findings with the discoloration study presented in 2002,[1] it seems plausible that papers exposed for prolonged periods to polluted and humid air, without glazing protection in a naturally ventilated dark room overlooking a street with dense traffic, should develop a strong oxidizing process.

Parallel to this, reactions responsible for an increase of opacity also take place. As explained by Johanssons[2] SO_2 from the surrounding environment is physically adsorbed on the paper surface and converted into sulfite S(IV). This thermodynamically unstable substance is further oxidized into sulfate S(VI)[2] in the presence of NO_2. The sulfate further reacts with calcium, present in the paper, to form gypsum ($CaSO_4 \cdot 2H_2O$), which then acts as a filler and the paper increases in opacity.

Preliminary studies through visual characterization and simple analytical tests, namely surface pH measurements and colorimetric tests, have already been published.[1] It was found that pH values on air-induced discolored paper areas were only slightly different from the non-discolored areas, presenting pH values of 4.58 and 4.64, respectively. Measurements on the relative lightness and darkness of the papers (L* value) confirmed that the oxidized C folio became considerably darker than the non-oxidized A folio, presenting an L* value of approximately 88 and 62, respectively.

FIG. 1. Folios A, B, and C under normal light.

In the present study we intend to characterize and detect differences between the discolored and non-discolored paper samples using chemical and physical analytical instruments, namely mid-infrared (MIR) spectroscopy, energy dispersive X-ray fluorescence (XRF), and scanning electron microscopy (SEM). This article presents some of the results collected.

The use of MIR spectroscopy is not new in the conservation field and in the last decades has been extensively described in the specialized literature; Fourier transform infrared (FT-IR) spectroscopy has been employed in the qualitative study of organic materials such as paper.[11–19]

X-ray fluorescence is also a technique widely used to identify and quantify the elements present in historical documents and aged paper samples.[19–24] This is an analytical technique that provides multi-elemental information in a completely nondestructive way, without sampling or other damage to the artwork. Furthermore, technological advances have allowed such a miniaturization that portable spectrometers are available to provide quality measurements on location. This way, documents of important value or in a severe state of degradation can be analyzed without removal from the museum or archive.

Scanning electron microscopy is also a valuable technique that has been used in the qualitative characterization and degradation of paper.[24,25] SEM has been used for morphological characterizations of fibers, identification of filling materials, and for comparison of physical differences on paper artifacts.

MATERIALS AND METHODS

Specimen Description. The paper samples selected for this study are three folios pertaining to an unbound and incomplete glossarium printed in 1766, donated in 1983 by the Portuguese National Library for experimental conservation treatments. The folios, designated as A, B, and C, are rag, gelatine sized handmade papers (Fig. 1). Having in mind the printed date period and the observed light extinction in transmitted light, the paper leaf does not seem to have had china clay incorporated into its paper mesh. Collins and Milner state that the use of china clay was first suggested in 1733 but was in general use only in 1780.[25] From 1983 to 1997, the folios were stored in different environments and were not submitted to any type of treatment. Folio A, which exhibits a light tone, was protected by a folder of tracing paper inside a metal archive drawer in the Paper Conservation Department. Folio C, which corresponds to the brown paper, was shown in 1986 during a six-month exhibition, as an example of a document extremely attacked by insects. It was secured with metal pins onto white painted low density fiberboard. No glass was present. It is interesting to note that the exhibition room was located next to a heavy traffic street with no trees and a narrow sidewalk. After the exhibition, folio C remained in the same position, in the same room, in total darkness, for at least another year and remained on the same exhibition board, unprotected from direct contact with air, for another 10 years in a dim corridor of the building. Folio B was exhibited inside a showcase in the same exhibition room

TABLE I. Mean elemental concentration and standard deviation ($\mu g \cdot g^{-1}$) obtained in this work for orchard leaves NBS1571 and certified values.

	P	S	Cl	K	Ca	Mn	Fe	Zn	Cu
Present work	2300 ± 400	3000 ± 1000	760 ± 90	16000 ± 2000	18000 ± 3000	80 ± 10	260 ± 60	19 ± 7	8 ± 2
Certified value	2100 ± 100	2300 ± 100	700 ± 10	14700 ± 300	20900 ± 300	91 ± 4	300 ± 20	25 ± 3	12 ± 1

as folio C and followed the same time path except for the last 10 years, when it was returned to its folder in a metal drawer cabinet.

Comparing the three folios by means of optical properties, it is possible to see that folio A after remaining inside a drawer is non-oxidized and retains its original cream color, while folio C, which had been in direct contact with air, in the conditions stated above, not only became very brown but also acquired a gain in opacity. Folio B also seems oxidized although its tone is mildly intense when compared with the tone presented by C.

Experimental Setup. *Mid-Infrared Spectroscopy.* Infrared spectra obtained in the range from 4000 to 650 cm^{-1} were acquired with a Perkin Elmer 1600 FT-IR spectrometer. Paper samples were analyzed in transmission, with accumulations of 64 scans and a resolution of 4.0 cm^{-1}. The data obtained were further analyzed on a separate work station using Omnic 5.2 software.

The samples were previously prepared by mixing 0.5 mg of defibered paper with 50 mg of anhydrous potassium bromide (Merck, spectroscopy grade). The mixture was ground in an agate mortar and transferred to a die and pressed into a pellet 7 mm in diameter using a press of 8–10 tonnes for 5 minutes, in order to obtain transparent disks.

Energy Dispersive X-ray Fluorescence. The equipment used in this study is a portable instrument consisting of an Oxford X-Ray generator (Model XTF 5011) with Mo anode. The detector used is a Vortex-EX SDD (Si) thermoelectrically cooled with a nominal area of 50 mm^2 and a Be window. The X-ray generator and detector are coupled to a vacuum chamber in 45° geometry. By using a polycapillary lens to collimate the beam, a spot size of 90 μm is obtained. The chamber also possesses a camera, allowing the visualization of the analyzed area and thus the capture of an image.[26]

All spectra were collected using the polycapillary mode in vacuum, operating conditions of 40 kV, 1 mA, and 300 s. The spectral analyses were performed using the WinAXIL (Analysis of X-ray spectra by Iterative Least-squares fitting) software package and the quantification was made using the compare mode, using three Standard Reference materials (Poplar leaves GBW 07604; Bush branches GBW 07603; Tea leaves GBW 07605).

The accuracy of the method was checked by analyzing a fourth Standard Reference Material, orchard leaves NBS1571, and the results are presented in Table I.

Scanning Electron Microscopy. A Jeol JSM-5310LV SEM with a high voltage of 20 kV was used. Square samples of ~1 cm^2 were removed from all the samples on equivalent paper sections where no printing ink was present. After metallization of the paper specimens with a very thin layer of graphite to assure a good conductivity, they were placed inside the sample holder compartment. SEM images were recorded using the secondary electron detector at two different magnifications: 150× and 500×.

RESULTS AND DISCUSSION

Mid-Infrared Spectroscopy. For the spectra obtained in the range of 4000 to 650 cm^{-1}, a special emphasis was given to the analyses of the region below 2000 cm^{-1}, which normally contains the most interesting and valuable information of the material we are studying. The identification was accomplished either by assigning chemical groups to the peaks in the spectra or by comparing each spectrum to those of known compounds and making the identification by the best match.

Infrared spectra are shown in Fig. 2. The spectra of folios A and B present great similarity and their cellulose character is strongly confirmed by the presence of specific bands identified and listed in Table II. Bands located at 898 cm^{-1} and 1060 cm^{-1} are due to vibration of cellulose structure and to C–O–C glycosidic ether group, respectively. In folio A, the presence of gelatine sizing is revealed by the amide I and II bands at 1545 cm^{-1} and 1648 cm^{-1}, respectively.[15] The band at 1648 cm^{-1} seems to be a superimposition of the amide I band and the H–O–H bending mode of hydrogen-bonded water in the cellulose. In the folio B spectrum, the band at 1545 cm^{-1} is missing, meaning that the original sizing was subjected to deterioration as there are less peptidic bonds. Here the band at 1639 cm^{-1} must be due to absorbed water.

As for folio C some differences can be pointed out in the region of 1700 cm^{-1} when compared with the other two spectra. Small, sharp bands are observed in this region, leading us to conclude that they are constituents from degradation products such as ketones, aldehydes, and carboxylic acids. The absence of the three characteristic amide bands of proteins in folio C, associated with the loss of the absorption band at 898 cm^{-1} attributed to the cellulose skeletal vibration, reinforces the idea that folio C was subjected to a more severe degradation
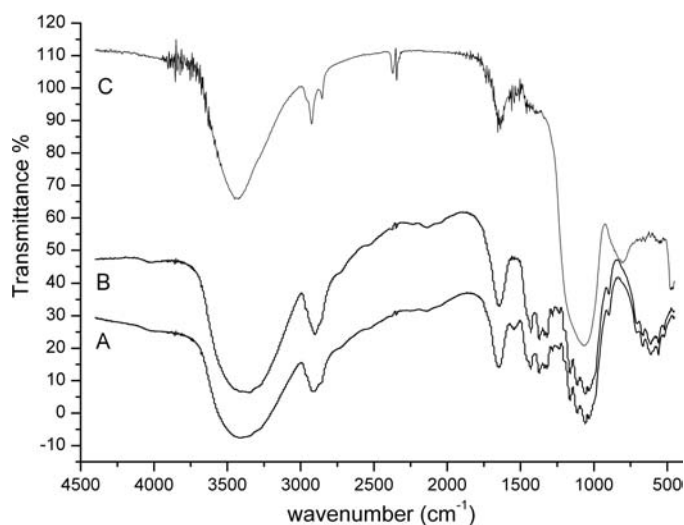

FIG. 2. FT-IR spectra obtained for paper samples of folios (**A**) A, (**B**) B, and (**C**) C.

TABLE II. Peak wavenumber (cm^{-1}) and interpretation for folios A, B, and C.

Folio A	Folio B	Folio C	Assignment	Interpretation
3406	3345		O–H stretching	Hydroxyl group of cellulose
			N–H stretching	
2902	2902	2927	C–H stretching	Aliphatic hydrocarbons
		2854		
		1777	C=O stretching	Acetones, aldehydes and/or carboxylic acids
		1753		
		1721		
		1709		
1648	1639		C=O stretching	Amide I
			COO$^-$ stretching	Carboxilic groups/ions
			O–H stretching	Water in cellulose
1545			C–N stretching	Amide II
			N–H bending	
1373	1372		CO–H bending	
1318	1318			
1282	1282		–CH$_3$ stretching	
1163	1163		C–OH stretching	
1113	1113		C–O–C symmetric stretching	
1060	1060	1060	C–O–C asymmetric stretching	Cellulose, aliphatic ethers -glucose
898	898		Skeletal vibration	Cellulose
704			CH$_2$ rocking	Cellulose
665	664	669	C–OH bending	Out of plane

hazard. The formation of carbonyl groups points to an oxidation process induced by air pollutants as the main reaction responsible for discoloration, as previously hypothesized.

Furthermore, in the region of 2800–3000 cm^{-1}, attributed to the stretching vibration of CH, CH$_2$ groups, folio C presents two peaks at 2927 cm^{-1} and 2854 cm^{-1}, revealing that this folio contained more methylene groups than the other two folios.

X-ray Fluorescence. The mean elemental concentrations of Al, Si, K, S, Ca, Mn, and Fe for the three folios are presented in Table III. A slight increase of the potassium content was observed for the stained folios (B and C) when compared with folio A, as shown in Fig. 3. This behavior has already been found in studies regarding paper degradation.[21] No other elemental variation was found, namely for Ca, leading us to believe that the formation of gypsum was due to a rearrangement of the elements constituting the paper.

Scanning Electron Microscopy. Scanning electron microscopy results corroborate the conclusions made from the MIR spectra: micrographs show the presence of a cellulosic matrix for all three samples; however, the three samples show

different stages of deterioration. The results of the inner surface of the paper samples, shown in Fig. 4, show that the fibrous structure is still pristine in folio A while in folios B and C the fibrous structure is progressively more flattened. Fibers in folio C are not only more flat but also appear to be considerably more fibrillated and therefore shorter in length. They also have blunter ends.

In the micrograph of folio A short white thin lines are observed within the fiber filaments. This differs from the small, white mineral-like deposits agglomerated on the surface or between the fibers in the other two folios. These same mineral-like deposits are quite numerous on folio C.

The thin lines may be attributed to the presence of calcium carbonate within the fiber structure. Dabrowski et al.[27] spoke of early European handmade papers as having a buffer of calcium carbonate natural filler conveyed by the manufacturing process, which added lime to the beating process.

TABLE III. Mean elemental concentration and standard deviation (μg·g^{-1}) in the three studied folios (A, B and C).

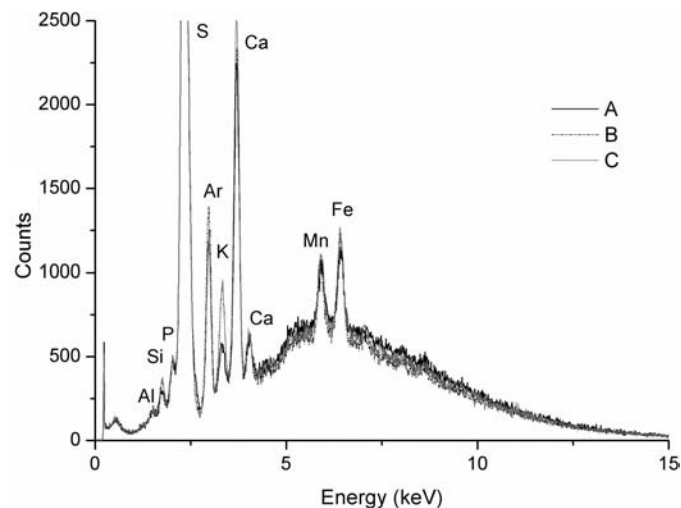|	A	B	C
Element	Mean ± SD	Mean ± SD	Mean ± SD
Al	2480 ± 420	2250 ± 150	2600 ± 100
Si	4500 ± 600	4400 ± 700	5500 ± 500
P	1200 ± 100	1400 ± 100	1300 ± 100
S	3000 ± 100	3000 ± 100	3000 ± 100
K	250 ± 50	400 ± 50	400 ± 80
Ca	1250 ± 250	1100 ± 100	1100 ± 1000
Mn	60 ± 10	50 ± 10	60 ± 10
Fe	70 ± 10	80 ± 10	70 ± 10

FIG. 3. Comparison of the obtained XRF spectra for folios A, B, and C.

Fig. 4. SEM observation on the surface structure of paper folios A, B, and C at 500× magnification.

As for the other two folios, the presence of the small white mineral-like deposits outside the fiber filaments may suggest the presence of fillers. As these forms are only observed in these folios and are absent in folio A, it is plausible to consider that their formation occurred parallel to or after the air-induced oxidation and that they may be responsible for the increase in opacity.

CONCLUSION

This work is a successful combination of several analytical techniques in the characterization of paper degradation. The results obtained in this study are of importance in preventive conservation and can bring new perspectives to the role of science in artwork conservation.

Chemical and physical changes were confirmed from the data collected using the different analytical methods. The detection of progressively stronger carbonyl bands for folio C, together with the absence of the secondary amide band characteristic of proteins in folios B and C, support the idea that oxidation reactions occurred and that these two folios were subjected to a more severe degradation hazard, not only by presenting a loss of their original gelatine sizing but also by presenting a greater intensity of oxidation.

The appearance and increase of white mineral-like deposits visible in the SEM micrographs of folios B and C seem to confirm the degradation of cellulose structure and the transformation and rearrangement of the original calcium carbonate into gypsum. The thin white straight lines previously visible within the fiber filaments give space to the mineral-like deposits scattered within the fiber structure. The maintenance of the calcium elemental content also supports the rearrangement hypothesis. Gypsum when deposited between the fibers acts as filler and can be responsible for the increase in opacity in folio C. Furthermore, the XRF technique confirmed that no elemental changes occurred in the paper during the discoloration process, except for a slight increase in potassium, confirming that the discoloration progression is not due to metallic ions present in either paper or the environment.

1. F. Figueira, A. M. Fernandes, and A. Ferreira, in *Works of Art on Paper, Books, Documents, and Photographs: Techniques and Conservation*, D. Daniels, A. Donnithorne, and P. Smith, Eds. (IIC, London, 2002), pp. 65–68.
2. A. Johansson, P. Kolseth, and O. Lindqvist, Restaurator **21,** 117 (2000).
3. M. C. Letnar and T. Muck, Restaurator **24,** 240 (2003).
4. H. Porck, W. J. T. Smit, J. Heijst, and I. Leeuwen, in *Paper Preservation Symposium* (Tappi Press, 1988), 74–80.
5. J. Havermans and H. Porck, *La Conservation à l'Ère du Numérique* (ARSAG, Paris, 2002), pp. 173–179.
6. G. Thomson, *The Museum Environment* (Butterworth-Heinemann, Oxford, 1986), 2nd ed., p. 146.
7. M. Cernic Letnar and V. Kropar Vancina, Restaurator **23,** 118 (2002).
8. C. Weschler, Indoor Air **10,** 269 (2000).
9. E. Dahlin, T. Grontoft, S. Rentmeister, C. Calnan, J. Czop, K. Hallett, D. Howell, C. Pitzen, and A. S. Larsen, The 14th Triennial Meeting, ICOM-CC (James and James, London, 2005), pp. 617–624.
10. M. Ferm, F. De Santis, and C. Varotsos, Atmos. Environ. **39,** 6664 (2005).
11. J. L. Pedersol and F. J. Ligterink, Restaurator **22,** 133 (2001).
12. G. Bitossi, R. Giorgi, M. Mauro, B. Salvadori, and L. Dei, Appl. Spectrosc. Rev. **40,** 187 (2005).
13. L. M. Proniewicz, C. Paluszkiewicz, A. W. Birczyńska, H. Majcherczyk, A. Baránski, and A. Konieczna, J. Mol. Struct. **596,** 163 (2001).
14. K. Castro, S. Pessanha, N. Proietti, E. Princi, D. Capitani, M. L. Carvalho, and J. M. Madariaga, Anal. Bioanal. Chem. **391,** 433 (2008).
15. P. Garside and P. Wyeth, Stud. Conserv. **48,** 269 (2003).
16. M. Baker, D. Reyden, and N. Ravenel, Book Paper Group Annu. **8,** 177 (1989).
17. N. V. Ivanova, E. V. Korolik, R. G. Zhbankov, and N. I. Insarova, J. Appl. Spectrosc. **38,** 937 (1983).
18. R. J. Koestler, N. Indictor, and B. Fiske, Restaurator **13,** 58 (1992).
19. M. Bicchieri, S. Rinconi, F. P. Romano, L. Pappalardo, M. Corsi, G. Cristoforetti, S. Legnaiolo, V. Palleschi, A. Salvetti, and E. Tognoni, Spectrochim. Acta, Part B **57,** 1235 (2002).
20. M. Manso, M. Costa, and M. L. Carvalho, Nucl. Instrum. Meth. A **580,** 732 (2007).
21. M. Manso, S. Pessanha, and M. L. Carvalho, Spectrochim. Acta, Part B **61,** 922 (2006).
22. J. L. Ferrero, C. Roldan, D. Juanes, J. Carballo, J. Pereira, M. Ardid, J. L. Lluch, and R. Vives, Nucl. Instrum. Meth. Phys. Res. B **213,** 729 (2004).
23. K. Castro, N. Proietti, E. Princi, S. Pessanha, M. L. Carvalho, S. Vicini, D. Capitani, and J. M. Madariaga, Anal. Chim. Acta **623,** 187 (2008).
24. E. Princi, S. Vicini, E. Marsano, and V. Trefiletti, Thermochim. Acta **468,** 27 (2008).
25. T. Collings and D. Milner, Paper Conservator **14,** 58 (1990).
26. M. Manso, S. Pessanha, F. Figueira, S. Valadas, A. Guilherme, M. Afonso, A. C. Rocha, M. J. Oliveira, I. Ribeiro, and M. L. Carvalho, Anal. Bioanal. Chem. **395,** 2029 (2009).
27. J. Dabrowski and J. Simmons, Fibres Textiles Eastern Eur. **11,** 8 (2003).

Characterization of two pairs of 16th century Nanbam folding screens by Raman, EDXRF and FTIR spectroscopies[†]

**Sofia Pessanha,[a] Maria Luisa Carvalho,[a*] Maria Isabel Cabaço,[a,b]
Sara Valadas,[c] Jean-Luc Bruneel,[d] Marcel Besnard[d] and Maria Isabel Ribeiro[c]**

Two pairs of hand-painted Japanese folding screens were analyzed by Raman, energy dispersive X-ray fluorescence (EDXRF) and Fourier transform infrared (FTIR) spectroscopy, in order to characterize the materials used in their production. Japanese folding screens, called *byobu,* are one of the oldest and most highly refined forms of Japanese art, where paper and silk were used as materials for the artists to paint on. The two pairs of folding screens studied in this work also exhibit a golden background to create a luminous effect. These screens depict some of the Portuguese who arrived to Japan during the 16th century, initiating active commercial and cultural exchange between Japan and the West, called the Nanban Trade. Nowadays, only about 60 examples of this Namban genre remain, so the study of these two pairs is of utmost importance to the knowledge of this precious craft. The materials identified, such as gold, silver, malachite, azurite, vermillion, red lead, red madder, yellow ochre, white oyster shell, and carbon black, are part of the traditional Japanese palette. Copyright © 2010 John Wiley & Sons, Ltd.

Keywords: confocal Raman; EDXRF; FTIR; cultural heritage

Introduction

The exhibition 'Encompassing the Globe – Portugal and the world in the 16th and 17th centuries' was produced by the Smithsonian Institution, through the A. M. Sackler and Freer Gallery, in Washington DC, where it was held between June and September 2007. This exhibition, of about 200 pieces from several of the most prestigious collections, traveled the world and is currently in Lisbon at the National Museum of Fine Arts.[1]

This prompted the interest of studying for the first time two pairs of Japanese folding screens from the 16th century, which are among the central pieces of the exhibition. In 1543, the Portuguese arrived in Japan and from that date onwards a process of commercial and cultural exchange began. It was in such a context that these screens were commissioned, recording the special atmosphere of festivity and novelty that was represented by the arrival of the black boat of the *namban jin* (the barbarians from the south, as the Portuguese were known), at the port of Nagasaki. The great care and attention to detail with which all the different people are represented, the depiction of the ship and its precious cargo, and, above all, the decisive presence of the Jesuit missionaries elevate this screen to a level of meaning far beyond that of a simple visual record, making these pieces a unique document in the context of Portuguese–Japanese relations.

Folding screens, called *byobu,* have been used by the Japanese for hundreds of years to create intimate spaces, as room dividers, as well as to add beauty to any room. Traditional *byobu* are usually two or six panel screens with a lacquered wood edge. Both paper and silk were used as materials for the artists to paint on.[2,3]

Before the painting is executed, the support may be prepared in a number of ways, which include sizing, beating, dyeing, application of grounds, and application of metal leafs. Usually, Japanese screens have large areas of gold leaf as part of the design 'field', and this might also be regarded as a further method of decorating the support. Painted elements of small extent are usually done over the leaf, which then functions as a ground, but the latter does not usually extend far under larger, opaquely painted areas; no doubt this was to avoid the unnecessary use of expensive metals, but also because of possible poor adhesion between the paint and gold.[4]

Material characterization and pigment identification on paintings, ceramics, and manuscripts are essential in finding solutions to problems of restoration, conservation, dating, and authentication in the art world. Determination of the artist's original materials as well as materials applied afterwards (by the artist or the conservator) is essential for providing support for conservation choices. This is important because the alternatives may be liable to react

Figure 1. (a) Picture of the pair of screens signed by Kano Naizen. Microsampling spots marked from A1–A8; (b) pair of screens attributed to Kano Domi. Microsampling spots marked from B1–B8.

with contiguous pigments with disastrous visual effects. Moreover, the identification of any degradation products of pigments must be appraised in order to suggest possible treatments in a conservation intervention.

In order to proceed to the characterization of an artwork, a multianalytical approach is needed, by combining techniques of elemental and molecular analysis,[5,6] and by joining spectroscopic techniques with optical techniques.[7–9]

Energy dispersive X-ray fluorescence (EDXRF) analysis has been demonstrated to be of great power for the noninvasive characterization of the artist's palette, being the technique of excellence for performing preliminary studies. Furthermore, the identification of the key elements supports an educated identification of the pigment composition.[10–14]

The suitability of Raman and Fourier transform infrared (FTIR) spectroscopies in the study of pigment in all sorts of artworks, alone or combined, is well established,[15–19] but more reliable and complete results are obtained when both techniques are combined.[20–22]

Measurements with an EDXRF portable equipment were carried out in the museum facilities, and an extensive screening of the pieces was made. Furthermore, a total of 16 microsamples were taken with a surgical scalpel for Raman, FTIR, and optical microscopy (OM) analysis, in order to fully characterize the used technique and the used pigments as well.

Specimen description

In this pair of screens (Fig. 1(a)), marked with the seal of the painter Kano Naizen, the story is related from left to right, narrating the preparations for the departure of the ship from a port that is supposed to be Goa, an intention that is underlined by the representation of elephants and another type of architecture. In the second screen, we can see a representation of the ship's arrival at the port of Nagasaki and the disembarkation of its precious goods, depicted in great detail. The Chinese silks can be perfectly identified, as well as the exotic animals and all the other

products traded by the Portuguese at various points around the Far East, transported in a procession that is headed by the ship's commander. Further to the right, members of various missionary orders have gathered in front of a church to await the arrival of this committee.

In the second pair of screens (Fig. 1(b)), attributed to the painter Kano Domi, a similar theme is repeated, although in a different scale. In the left-hand screen, trading negotiations are being conducted aboard a ship without sails, whilst on land the unloading of the precious cargo is being carefully supervised, once again with an abundance of rich Chinese silks in the form of either bundles or rolls. In the right-hand screen, the procession led by the ships' commander can be seen walking in the direction of the house of the Jesuits. This is followed by a group of people dressed in rich costumes, and the parade also contains representations of the Chinese litter, exotic animals, and the famous glazed pots used for transporting spices.

Experimental

Energy dispersive X-ray fluorescence
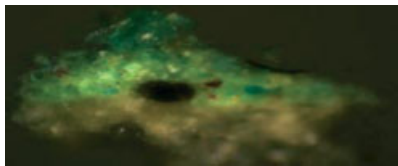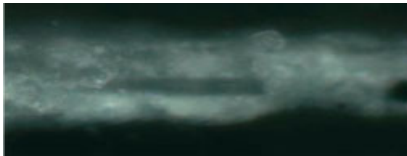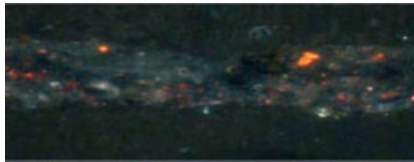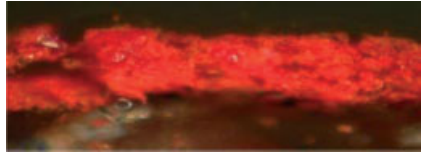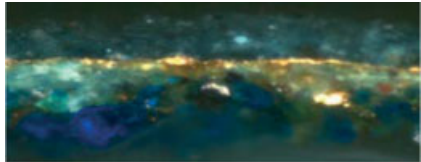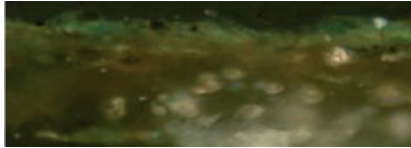
The EDXRF equipment used in this study consists on an X-ray generator from Amptek, the ECLIPSE III with a Ag anode and an Amptek XR-100CR of Si-PIN thermoelectrically cooled detector.[14]

The components are assembled on an aluminum structure (in 90° geometry) and mounted in a tripod that allows a range of 1.5 m. Once assembled, the sample position is identified by two laser beams. A macroscopic screening of the pieces was made, and about 250 measurements were performed *in situ*. All spectra were acquired during 300 s under working conditions of 30 kV and 100 µA.

Confocal Raman spectrometry

In this work, a Dilor-Jobin Yvon Labram 1B spectrometer equipped with an Olympus BH2 microscope system in a confocal geometry

Table 1. Description of the microsamples removed from Kano Naizen screens. Cross-section thickness determined by OM. Pictures are not to scale
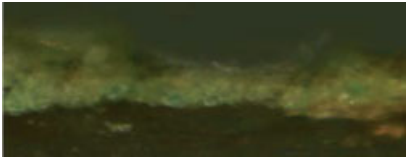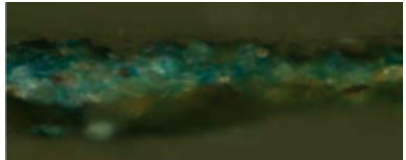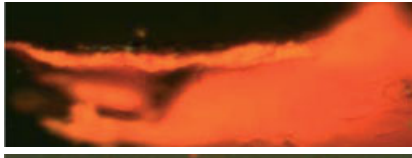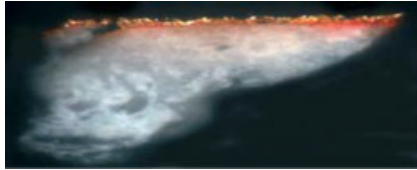
Sample	Color	Cross-section layers thickness	Photomicrograph
A1	Green	First layer to 76 µm	
A2	White	Second layer to 72 µm 67 µm	
A3	Black	67 µm	
A4	Red	75 µm	
A5	Pink	First layer to 72 µm	
A6	Blue	Second layer to 6 µm First layer to 68 µm	
A7	Green	Second layer to 6 µm Third layer to 45 µm Fourth layer to 40 µm First layer to 32 µm	
A8	Yellow	Paper support 31 µm	

was used. Two sources were used: a helium–neon laser (632.8 nm) and a Spectra Physics argon–krypton model 2018 laser (514.5 nm), with power on the sample ranging from 100 µW to 2.5 mW. The scattered light collected by the objective was dispersed onto an air-cooled CCD array by a 1800 lines/mm grating giving a resolution of about 4 cm^{-1}. The magnification of the objective was 50×.

Infrared microspectroscopy

Infrared analysis was carried out using a Nicolet Nexus spectrometer coupled to a Nicolet CONTINUµM microscope.[22] The small samples were compressed in a Spectra-Tech µSample Plan microcompression diamond cell and analyzed in transmission

Table 2. Description of the microsamples removed from Kano Domi screens. Cross-section thickness determined by OM. Pictures are not to scale

Sample	Color	Cross-section layers thickness	Photomicrograph
B1	Brownish gray	First layer to 15 µm	
		Paper support	
B2	Green	28 µm	
B3	Bluish green	67 µm	
B4	Black	Paper support	
B5	Orange	31 µm	
B6	Brown	18 µm	
B7	White	First layer to 123 µm	
		Second layer to 48 µm	
B8	Gold	First layer to 6 µm	
		Second layer to 7 µm	
		Third layer to 20 µm	
		Paper support	

mode over just one part of the cell. The area of analysis of the sample was defined by the double aperture contained in the microscope. For each spectrum, 256 scans were acquired with a spectral resolution of 4 cm^{-1}. No spectral processing other than removal of the carbon dioxide bands was performed.

Optical microscopy

The samples were prepared as cross-sections, being embedded in an epoxy polymeric resin. After curing of the resin, the cross-sections were roughly polished with silicon carbide and then repolished with an alumina–water slurry over a cloth wheel.
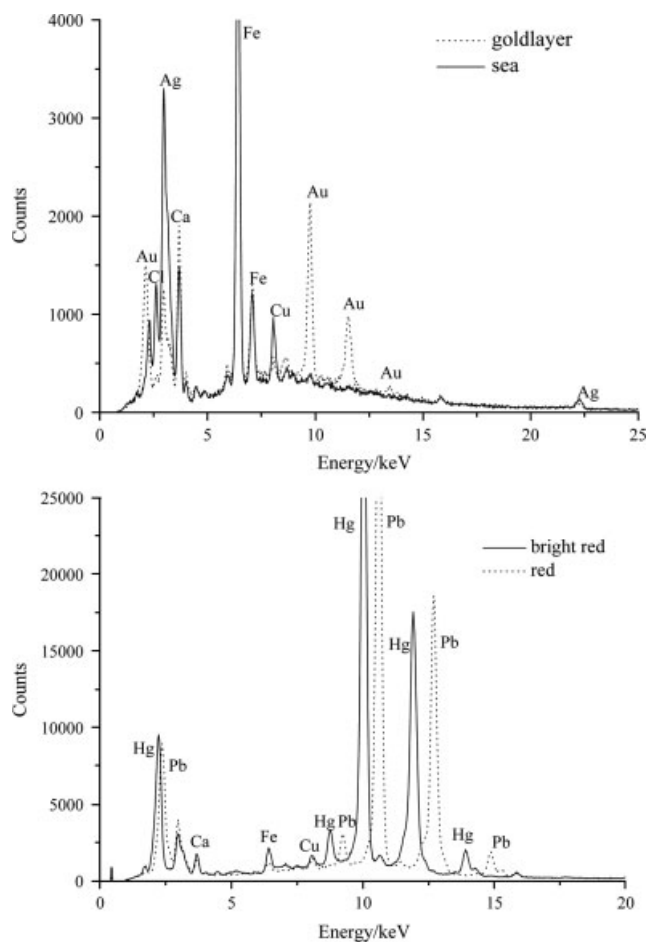
Figure 2. EDXRF spectra obtained for the gold layer and the sea of one of the screens attributed to Kano Domi.

Figure 3. Confocal Raman spectra obtained for (a) white sample (b) green sample, and (c) blue sample.
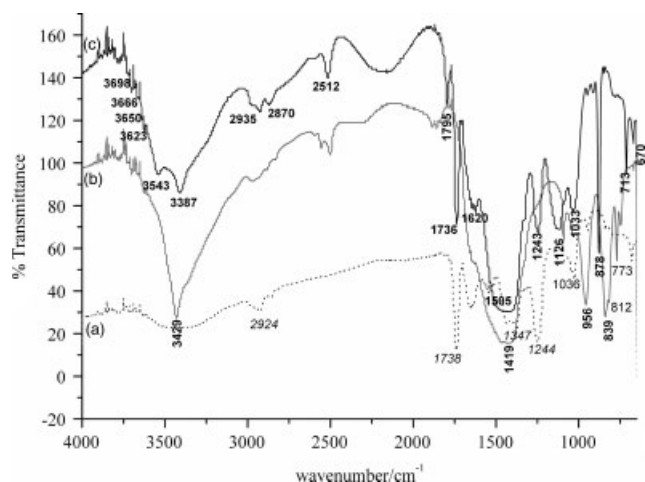
Figure 4. FTIR spectra obtained for (a) red sample, (b) blue sample, and (c) yellow sample.

Examination by OM was carried out using a Leitz Wetzlar microscope (10× ocular) with a 11× or 22× objective, under visible light. Image acquisition was carried out with a coupled Leica DC500 digital camera and IM1000 software.

Results and Discussion

A wide screening of the pieces was made *in situ* by EDXRF technique. Furthermore, 16 microsamples were removed from the screens, as indicated in Fig. 1, and analyzed by Raman, FTIR, and OM.

Photomicrographs of the analyzed cross-sections are shown in Tables 1 and 2. The examination of the cross-sections by OM provided valuable information about the samples, such as layer dimensions, pigment color distribution, and existence of gold beneath the paint. The observation of these micrographs reveals that, in most cases, only one layer of pigment was applied; the exceptions are samples A1, B7, and B8 where different shades of the same color are present, and samples A5 and A6 were a layer of gold leaf is present. On the other hand, we can observe that no preparation layer was used before applying the paint to the paper.

Gold and silver

As expected, precious materials such as gold and silver were found in the screens (Fig. 2(a)). Silver was found in several EDXRF

measurements in the brownish sea and sky of Kano Domi screens. On the other hand, high amounts of Au mixed with Cu were found through EDXRF analysis of golden areas: gold leaf and golden painted with brush.

Green and blue pigments

The green areas, in the vegetation and clothing, presented a high level of Cu in the EDXRF measurements, which suggests the use of copper-based green pigment. In Fig. 3(b), we can see the Raman spectrum obtained for the sample A1 with the identification of the characteristic bands of malachite at 153, 179, 220, 271, 350, 432, 509, 1063, and 1492 cm^{-1}.[23] A few bands are not clearly identified, but two of them (at 1098 and 1461 cm^{-1}) might correspond to azurite contamination which usually occurs with malachite. Malachite, a basic copper carbonate, ($CuCO_3Cu(OH)_2$) is the main green pigment used in Japan from the 7th until today.[24] The blue areas of the screens also presented high amount of Cu in the EDXRF measurements. Figure 4(b) presents the FTIR spectrum of sample B3, where azurite ($Cu(OH)_2.2CuCO_3$) was identified through the characteristic bands at 3429, 1419, 956,
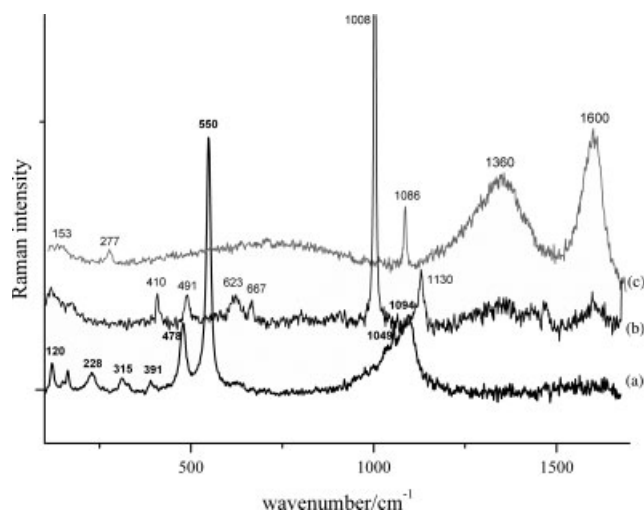
Figure 5. Confocal Raman spectra obtained for (a) red sample, (b) yellow sample, and (c) black sample.

and 839 cm^{-1}.[25] Characteristic peaks of azurite were also found in the Raman spectrum of sample A6, together with the ones corresponding to indigo at 1698, 1584, 1464, 1361, 1310, 1250, 759, 598, 545, and 252 cm^{-1}[26] (Fig. 3(c)).

Yellow pigments

Regarding the yellow pigments, EDXRF analysis detected Fe, suggesting the use of a iron-based yellow pigment, probably yellow ochre. Yellow ochre is a natural earth pigment, which consists of silica and clay – most likely in aluminosilicate form such as kaolinite – and owes its color to various hydrated forms of iron oxide, in particular the mineral goethite, FeOOH.

Figure 4(c) shows the FTIR spectrum obtained for sample A7, where the peaks of kaolinite at 3698, 3666, 3650, and 3623 cm^{-1} appear.[7] Furthermore, the band at 1033 cm^{-1} also is in agreement with the one found in database for yellow ochre, whereas the strong band centered at 3387 cm^{-1} is the signature of the OH vibration of goethite.[27] The remaining bands present in the spectrum are a mixture of calcite (3397, 2512, 1795, 1506, 878, and 713 cm^{-1}) gypsum (3543, 1620, 1126, and 670 cm^{-1}), and shellac type resin (2935, 2870, 1736, 1243, and 1033 cm^{-1}). This resin was also found in other samples and is probably due to a protection layer.[28]

Figure 5(b), shows the spectrum obtained by confocal Raman from the same yellow sample, where the bands at 410, 491, 623, 667, 1008, and 1130 cm^{-1} indicative of gypsum are present.[29]

Red pigments

Red was the color that presented more variety of the used pigments. In Fig. 2(b), we present the EDXRF spectra obtained for the two different shades of red present in the screens. The high amount of Hg in the bright red areas implies the use of vermillion (HgS), whereas the deeper red implies red lead (Pb$_3$O$_4$). The existence of red lead in the second shade of red was confirmed by the presence of a strong band at 550 cm^{-1} followed by bands at 478, 391, 315, 228, and 120 cm^{-1}, which are characteristic of red lead[23] found in the Raman spectrum of the sample B5 (Fig. 5(a)). Furthermore, a different shade of red, a kind of red dye, was visible in agglomerates at the microscope in sample A4

(Table 1). In Fig. 4(a), we can see that the spectrum obtained for the agglomerates is in good agreement with the one in our database for red madder (alizarin, 1,2-dihydroxyanthraquinone, C$_{14}$H$_8$O$_4$) with characteristic peaks at 2924, 1738, 1347, and 1244 cm^{-1}.

White pigment

The EDXRF spectra obtained for the several white areas revealed essentially the presence of Ca. Calcium carbonate (CaCO$_3$) was unequivocally detected by a very strong peak at 1088 cm^{-1} in the Raman spectrum of sample B7 (Fig. 3(a)). Until the 15th century, clay was always used as the white pigment for paintings, but between the 15th and 16th centuries, powdered oyster shell took the place of clay and continued to be used throughout the Edo period until today. In fact, Japan seems to be the only country that has used oyster shell as a white pigment, leading us to believe that this was the case of the white pigment in the screens.

Black pigment

The Raman spectrum obtained for the black sample B4 revealed two broad bands at approximately 1360 and 1600 cm^{-1}, which are characteristic of black pigments made up of disordered carbon, such as charcoal or bone black (Fig. 5(c)). The spectrum also presents a strong band at 1086 cm^{-1} together with bands at 153 and 277 cm^{-1} attributed to CaCO$_3$, which may occur as an impurity of carbon black.[30] This explains the high amount of Ca encountered in the black areas in the EDXRF analysis.

Gold leaf application technique

In contrast to the expectations of the museum curator, that the whole screens were covered with gold leaf and the paint applied afterwards, the experimental results obtained by EDXRF did not show Au in the majority of the analyzed spots. Gold was hardly ever detected in the black and white areas (lighter materials) even for the small details, e.g. figures, animals, and plants, leading us to conclude that the gold leaf did not cover the whole surface of the screens. To further confirm the experimental results, a theoretical study was performed to calculate the absorption of X-rays considering an incident radiation beam, assuming a monochromatic beam of 25 keV (crossing a maximum thickness of 100 μm) and the emitted Au L lines (∼10 keV) crossing again the same layer of CaCO$_3$. The calculated transmitted radiation would be approximately 50% of the incident one. Under these conditions, if a gold layer beneath the pigment layer existed, we should be able to detect it in the spectra obtained by EDXRF, which was not the case.

Conclusions

This paper emphasizes the need of having a multianalytical approach for studying cultural heritage. Noninvasive elemental analysis is sometimes not enough to fully characterize the materials used by the artist, and it is necessary to resort to techniques that provide molecular information. This work shows the importance of having portable equipment in the study of artworks, because exhaustive noninvasive measurements can be taken to all sections of the artwork in order to fully understand how the artist worked.

From the analysis of the obtained results, we find that the artist used the traditional Japanese palette: gold, silver, malachite, azurite, vermillion, red lead, red madder, yellow ochre, white oyster

shell, and carbon black. Gypsum and not white oyster shell was found in the yellow sample. One could speculate about the choice of the artist in using this different white pigment only in the yellow areas, or suggest the presence of gypsum as a decaying of calcite after SO_2 attack. Nevertheless, gypsum was not found in the remaining white areas, so the theory of the use of gypsum to lighten the yellow must prevail.

Furthermore, as a remarkable consequence of this work, in contrast to what historians surmised, we arrive at the conclusion that the screens are not fully covered in gold leaf, and even small areas like figures and animals were not painted over gold. It is likely that the artist first drew the elements to decorate the screens prior to applying the cut-out gold leaf, meaning that he had the artwork idealized in his/her mind beforehand and not much space was left for improvisation.

Acknowledgements

References

[1] http://www.mnarteantiga-ipmuseus.pt/pt-PT/destaques/Content Detail.aspx?id=319 **2009**.

[2] S. Grantham, Japanese painted screens: manufacturing materials and painting techniques, in Works of art on paper: books, documents and photographs: techniques and conservation: contributions to the Baltimore Congress, 2–6 September **2002**, 2002 pp 83.

[3] P. Wills, *Paper Conservator* **1985**, *9*, 5.

[4] J. Winter, *Paper Conservator* **1985**, *9*, 26.

[5] K. Castro, N. Proietti, E. Princi, S. Pessanha, M. L. Carvalho, S. Vicini, D. Capitani, J. M. Madariaga, *Anal. Chim. Acta* **2008**, *623*, 187.

[6] S. Bruni, S. Caglio, V. Gugliemi, G. Poldi, *Appl. Phys. A: Mater. Sci. Process.* **2008**, *92*, 103.

[7] E. Pavlidou, M. Arapi, T. Zorba, M. Anastasiou, N. Civici, F. Stamati, K. M. Paraskevopoulos, *Appl. Phys. A: Mater. Sci. Process.* **2006**, *83*, 709.

[8] M. Gil, M. L. Carvalho, A. Seruya, I. Ribeiro, P. Alves, A. Guilherme, A. Cavaco, J. Mirão, A. Candeias, *X-Ray Spectrom.* **2008**, *37*, 328.

[9] A. Kriznar, A. Ruiz-Conde, P. J. Sánchez-Soto, *X-Ray Spectrom.* **2008**, *37*, 360.

[10] F. M. Rosi, A. Burnstock, K. Jan Van den Berg, C. Milani, B. G. Brunetti, A. Sgamellotti, *Spectrochim. Acta, Part A* **2009**, *71*, 1655.

[11] J. L. Ferrero, C. Roldán, D. Juanes, J. Carballo, J. Pereira, M. Ardid, J. L. Lluch, R. Vives, *Nucl. Instrum. Methods Phys. Res., Sect. B* **2004**, *213*, 729.

[12] M. Mantler, M. Schreiner, *J. Radioanal. Nucl. Chem.* **2001**, *247*, 635.

[13] L. Bonizzoni, A. Galli, G. Poldi, M. Milazzo, *X-Ray Spectrom.* **2007**, *36*, 55.

[14] S. Pessanha, A. Guilherme, M. L. Carvalho, *Appl. Phys. A: Mater. Sci. Process.* **2009**, *97*, 497.

[15] K. Eremin, J. Stenger, M. L. Green, *J. Raman Spectrosc.* **2006**, *37*, 1119.

[16] L. Burgio, D. A. Ciomartan, R. Clark, *J. Raman Spectrosc.* **1997**, *28*, 79.

[17] F. Casadio, L. Toniolo, *J. Cult. Heritage* **2001**, *2*, 71.

[18] P. Baraldi, C. Fagnano, P. Bensi, *J. Raman Spectrosc.* **2006**, *37*, 1104.

[19] C. Genestar, C. Pons, *Anal. Bioanal. Chem.* **2005**, *382*, 269.

[20] T. Li, Y. Xie, Y. Yang, C. Wang, X. Fang, J. Shi, Q. He DOI: 10.1002/jrs.2340.

[21] S. Pessanha, A. Guilherme, M. L. Carvalho, M. I. Cabaço, K. Bittencourt, J. L. Bruneel, M. Besnard, *Spectrochim. Acta, Part A* **2009**, *64*, 582.

[22] A. M. Correia, M. J. V. Oliveira, R. J. Clark, M. I. Ribeiro, M. L. Duarte, *Anal. Chem.* **2008**, *80*, 1482.

[23] L. Burgio, D. A. Ciomartan, R. Clark, *J. Raman Spectrosc.*, **1997**, *28*, 79.

[24] J. Winter, *East Asian Paintings*, Archetype Publications Ltd: London, **2008**.

[25] J. A. Goldsmith, S. D. Ross, *Spectrochim. Acta, Part A* **1968**, *24*, 2131.

[26] C. Coutry, G. Sagon, P. Gorguet-Ballesteros, *J. Raman Spectrosc.* **1997**, *28*, 85.

[27] P. Cambier, *Clay Mater.* **1986**, *21*, 191.

[28] M. T. Doménech-Carbó, *Anal. Chim. Acta* **2008**, *621*, 109.

[29] I. M. Bell, R. J. H. Clark, P. J. Gibbs, *Spectrochim. Acta, Part A* **1997**, *53*, 2159.

[30] L. D. Kock, D. DeWaal, *Spectrochim. Acta, Part A* **2008**, *71*, 1348.

Evaluation of the intervention of a folding screen belonging to the Momoyama period by Raman spectroscopy using different wavelengths[†]

Sofia Pessanha,[a] Agnès Le Gac,[a,b] Teresa Isabel Madeira,[a] Jean-Luc Bruneel,[c] Stéphane Longelin[a] and Maria Luisa Carvalho[a]*

Museu Nacional Soares dos Reis (Oporto) owns a pair of Japanese folding screens belonging to the early 17th century – Namban genre. As the pieces manifested structural conservation issues, they were subjected to an intervention between 2000 and 2002 in the National Research Institute for Cultural Properties in Tokyo. According to the restoration report, an unknown substance had been applied to the overall surface, adding a glossy finish, as well as some colors inconsistent with the original painting. These materials seem to correspond to a restoration work conducted *in the Western countries*, but this intervention does not appear neither in the museum records nor in other historical sources.

The aim of this work is to determine the materials used in this restoration work of which very little is known and to understand why these new materials appear in a worse condition of preservation than some of the original ones. Preliminary, *in situ* , Energy Dispersive X-ray Fluorescence analyses were performed, and right from the beginning, elements such as Cr, Ba, and Co appear in the spectra of orange, yellow, brown, and blue areas, accusing the anachronism of the used materials. Nineteen microsamples were collected to be analyzed with two different confocal Raman equipments using 514, 532, 638, and 785-nm laser sources. Interesting results were obtained for the blue decoration of one of the houses: whereas the energy dispersive X-ray fluorescence spectrum showed the odd combination of Cr, Fe, Co, Cu, and Zn, the Raman spectra indicated mostly the use of Phthalocyanine blue. Copyright © 2012 John Wiley & Sons, Ltd.

Keywords: Raman; EDXRF; Japanese; Namban genre

Introduction

In 1955, the Portuguese state acquired the third pair of Namban screens for the country's collection. In addition to their aesthetic value, these screens are of extreme importance because they represent the Portuguese expansion in the Orient during the 16th century.[1]

According to Japanese specialist Tadao Takamizawa, there are three types of compositions for the Namban screens.[2] The set at Museu Nacional Soares dos Reis belongs to the more common category, with the representation of the Portuguese *Nao* at a port in the left hand screen along with a panorama of the shire, whereas the right hand screen depicts a perspective of the city of Nagasaki, a group of Portuguese sailors, and a Christian church (Fig. 1). According to the same author, this typology of screens would have been executed between 1593 and 1605, following the compositional scheme created by the painter Kano Mitsunobu. As these screens were works of an unusual historical and artistic value, they were often requested in various national and international exhibitions for artistic, historical, and commemorative purposes. At the end of the 1980s, an exhibition entitled *Art Namban, les Portugais au Japon* was part of the Európalia89 festival held in Brussels. The screens were then studied by specialists and attributed to the Kano School and were tentatively dated to between 1600 and 1610, a classification that still stands as of today.

As the pieces had been revealing some structural conservation problems for several years, they were subjected to a thorough restoration intervention at the National Research Institute for Cultural Properties in Tokio (NRICPT) between 2000 and 2002. According to the restoration report, a restoration procedure, *performed in the Western countries*, had been carried out previously, in which a glossy coating had been applied along with some color retouching. Very little is known about these treatments. Conservators at NRICPT dismounted the screens and substituted the frame, removed the glossy coating,

* Correspondence to: Maria Luisa Carvalho, Departamento de Fisica, Centro Fisica Atómica da Universidade de Lisboa, Av. Prof. Gama Pinto, 2 1649-003, Lisboa, Portugal. E-mail: luisa@cii.fc.ul.pt

[†] This article is part of the Journal of Raman Spectroscopy special issue entitled "Raman spectroscopy in art and archaeology" edited by Juan Manuel Madariaga and Danilo Bersani.

a Centro Fisica Atómica da Universidade de Lisboa (CFAUL), Departamento de Fisica, Av. Prof. Gama Pinto, 2 1649-003 Lisboa, Portugal

b Departamento de Conservação e Restauro, Faculdade de Ciências e Tecnologia da Universidade Nova de Lisboa, 2829-516 Monte de Caparica, Portugal

c Institut des Sciences Moléculaires (UMR CNRS 5255) Université Bordeaux I, Groupe de Spectroscopie Moléculaire, 351, cours de la libération, 33405 Talence, France

1699

Figure 1. Photographs of the pair of Namban screens in *Museu Soares dos Reis*.

and consolidated the paint layers to prevent further detaching. With the following research, we intend to characterize the restoration procedure *performed in the Western countries* and understand why the new colors appear more degraded than the original ones.

To achieve these goals, *in situ*, noninvasive Energy Dispersive X ray Fluorescence (EDXRF) was carried out in all extensions of the two folding screens to assess the elemental content of the chromatic layers of the screens. This way, an educated and aware choice of the sampling areas for posterior Raman measurements was made, ensuring the representativeness of the Raman results. Raman measurements were performed using two equipments and four laser wavelengths to select the most appropriate laser and take more advantage of each sample. The combined use of these two analytical techniques to studies in cultural heritage is not innovative but has proven to be a suitable and successful approach in other works[3–6] – namely pigments in paper[7–9] in a nondestructive, nearly non invasive way.

Experimental

The portable EDXRF equipment used in this study consists of an X-ray generator ECLIPSE II from Amptek (Amptek Inc., 14 De Angelo Drive, Bedford, MA. 01730 U.S.A.), with a Ag anode and an Amptek XR-100CR of Si-PIN thermoelectrically cooled detector with a 7-mm^2 detection area and 300-μm thick and 25-μm Be window. The energy resolution is 190 eV at 5.9 keV, and the acquisition system is Amptek PMCA. A Ta collimator is used to obtain a spot size of nearly 0.5 cm. This spot size is perfectly suitable to the analysis of this artwork because the characters and features are in the centimeter scale. The angle between the incident and emitted beam is 90°. This geometry allows for a minor background reduction due to Compton scattering. The components are placed in an aluminum structure mounted on a tripod with 1.5-m vertical amplitude. The operating conditions were 30 kV, 90 μA, and 200 s.

Two Raman microscopes were used in this work.

At Centro de Fisica Atomica da Universidade de Lisboa (CFAUL) facilities, measurements were made using a HORIBA Jobin Yvon Xplora confocal spectrometer (HORIBA Jobin Yvon S.A.S., 5 avenue Arago, Z. A. de la Vigne aux Loups, 91380 Chilly Mazarin France), equipped with three laser diode sources operating at 532, 638, and 785 nm; the power on the samples was reduced with neutral density filters up to 1 mW. The scattered light collected by the objective was dispersed onto an air cooled charge-coupled device array by 1200 grooves/mm grating. A 50× objective numerical aperture 0.75 with a pinhole of 300 μm was used to optimize the spatial resolution and the signal intensity.

At Institut des sciences moleculaires–centre national de la recherche scientifique (ISM-CRNS), a Horiba-Jobin Yvon Labram 1B spectrometer (HORIBA Jobin Yvon S.A.S., 5 avenue Arago, Z.A. de la Vigne aux Loups, 91380 Chilly Mazarin France) equipped with an Olympus BH2 microscope system in a confocal geometry was used. A Spectra Physics argon–krypton model 2018 laser (514.5 nm) was used to avoid degradation; the power on the samples was reduced with neutral density filters up to 2.5 mW. The scattered light collected by the objective was dispersed onto an air-cooled charge-coupled device array by a 1800 grooves/mm grating giving a spectral resolution of 4 cm^{-1}. The confocal aperture was adjusted to 700 μm, and a 50× objective of 0.75 numerical aperture was used.

The number and durations of scans varied from sample to sample to obtain a reliable peak to background ratio in each spectrum.

Results and discussion

The results obtained by *in situ* EDXRF and Raman spectroscopies are summarized in Table 1,[10–12] together with the Raman shift for each investigated pigment.

Blue

The EDXRF spectra obtained for blue areas rendered different elemental composition (Fig. 2(a)). Whereas some features appear to be painted using a copper-based pigment, further identified as azurite ($2CuCO_3.Cu(OH)_2$) by Raman spectroscopy, some clothes of characters presented Ti, Cr, Co, Ni, and Zn in their composition. Figure 2(b) shows the Raman spectra obtained from a sample collected in spot 495 using the 514, 532, and 638 wavelengths. The pigment phtalocyanine blue ($CuC_{32}H_{16}N_8$) was put in evidence as well as calcite ($CaCO_3$) with all lasers. Cobalt blue ($CoO.Al_2O_3$) was identified with the 514-nm laser. Furthermore, titanium dioxide in the anatase mineral form (TiO_2) and two broad bands centered at 1330 and 1500 cm^{-1} corresponding to carbon black were found with the 532-nm laser.

Green

The *in situ* spectra obtained with EDXRF from the green areas presented high amounts of Cu (Fig. 3), indicating the presence of a copper-based green pigment. Malachite ($CuCO_3.Cu(OH)_2$) was identified by Raman spectroscopy with the use of all the laser sources (Fig. 4(b)) sometimes mixed with calcite ($CaCO_3$) to produce a lighter shade and sometimes mixed with hematite (Fe_2O_3) to produce a darker shade.

Red and pink

With regard to the red areas, Hg was found in great amount in the EDXRF spectra (Fig. 3, spot 479), confirming the presence of vermillion (HgS) by Raman spectroscopy. (Fig. 4(c)). This pigment was also found to be mixed with white calcite to obtain the pink color.

Table 1. Results obtained by *in situ* EDXRF and Raman spectroscopy, together with the Raman shift for each investigated pigment

Color	XRF	Raman bands (cm⁻¹) 514	532	638	785	Pigments [10–12]	Notes [12]
Blue	Fig. 2(a) Spot 492 – Cu Spot 495 – Ti, Cr, Co, Ni, Cu, Zn	Fig. 2(b) 230; 589; 684; 775; 1103; 1303; 1337; 1446; 1525.	Fig. 2(b) 230; 589; 681; 748; 775; 1103; 1303; 1339; 1450; 1526.	Fig. 2(b) 230; 589; 682; 738; 773; 950; 1103; 1211; 1303; 1338; 1449; 1527.	Fig. 2(b) —	Phthalocyanine blue	Synthetic [19]
		1083.	1083.	1083.		Calcite (CaCO₃)	Mineral
		201; 517				Cobalt blue (CoO·Al₂O₃)	Synthetic 1802 [20]
			149.			Anatase (TiO₂)	Synthetic 1923
			1300; 1500			Carbon black	Mineral
Green	Fig. 3 Cu	—	Fig. 4(b) 152; 177; 0212; 269; 344; 430; 512; 535; 1059; 1049;1489.	—	—	Malachite (CuCO₃·Cu(OH)₂)	Mineral
Yellow	Fig. 5(a) Cr, Fe, Ba, Pb	Fig. 5(b) 839.	Fig. 5(b) 838.	Fig. 5(b) 837; 355. 987.	Fig. 5(b) —	Chrome yellow (PbCrO₄) Barium sulfate (BaSO₄)	Synthetic 1818 [19] Mineral
Orange	Fig. 5(a) Cr, Fe, Ba, Pb	Fig. 5(c) 826;837;849.	Fig. 5(c) 828; 850(sh)	Fig. 5(c) 830. 250; 340.	Fig. 5(c) 828; 375; 355; 328; 137.	Chrome yellow orange (PbCrO₄.PbO) Vermillion (HgS)	Synthetic 1818 [19] Mineral
Red	Fig. 3 Hg	—	—	—	Fig. 4(c) 254; 279; 340.	Vermillion (HgS)	Mineral
Brown	Fig. 6(a) Spot 498: Cr, Hg, Pb Spot 507 Si, Ca, Fe	Fig. 6(b) 828.	Fig. 6(b) 827; 844. 252; 343. Fig. 6 c) 222; 289; 408; 606.	Fig. 6(b) 822; 843. 254; 340. Fig. 6(c) 222; 290; 403; 603. 201; 461. 1300; 1500. 1450.	Fig. 6(b) 827; 840; 848. 253; 284; 344. Fig. 6(c) 274; 704; 1084.	Chrome yellow orange (PbCrO₄,PbO) Vermillion (HgS) Hematite Calcite (CaCO₃) Silica (SiO₂) Carbon black Organic compound	Synthetic 1818 [19] Mineral Mineral Mineral Mineral Mineral
Gray	Fig. 7 Ca	Fig. 4(a) 1088. 221; 287; 401; 602.	Fig. 4(a) —	—	—	Calcite (CaCO₃) Hematite (Fe₂O₃)	Mineral Mineral
White	Fig. 7 Ca	—	—	—	—	—	—
Black	Fig. 7 Ca	—	—	—	—	—	—

EDXRF, energy dispersive X-ray spectroscopy; XRF, X-ray fluorescence.

wileyonlinelibrary.com/journal/jrs

Figure 2. a) Comparison of the EDXRF spectra obtained from two different shades of blue (spot 492 and 495); b) Raman spectra obtained from the sample collected at spot 495.

Figure 3. Comparison of the EDXRF spectra obtained from green (spot 251), red (spot 479) and golden (spot 502) areas.
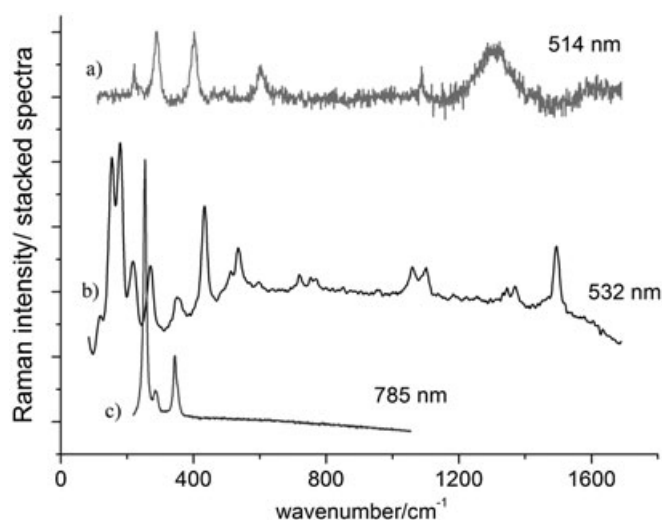
Figure 4. Raman spectra obtained from: a) grey sample; b) – green sample; c) – red sample.

Yellow and orange

Regarding the yellow color, all the analyzed areas presented Cr, Fe, Ba, and Pb in the EDXRF spectra (Fig. 5(a)). In Figure 5(b), the Raman spectra obtained from the yellow sample analyzed with the 638, 532, and 514-nm laser sources are shown. In all spectra, the presence of lead chromate, commonly called as chrome yellow ($PbCrO_4$), was found. Furthermore, the presence of barium sulfate ($BaSO_4$), often used as an extender for chrome yellow,[13] was also detected.
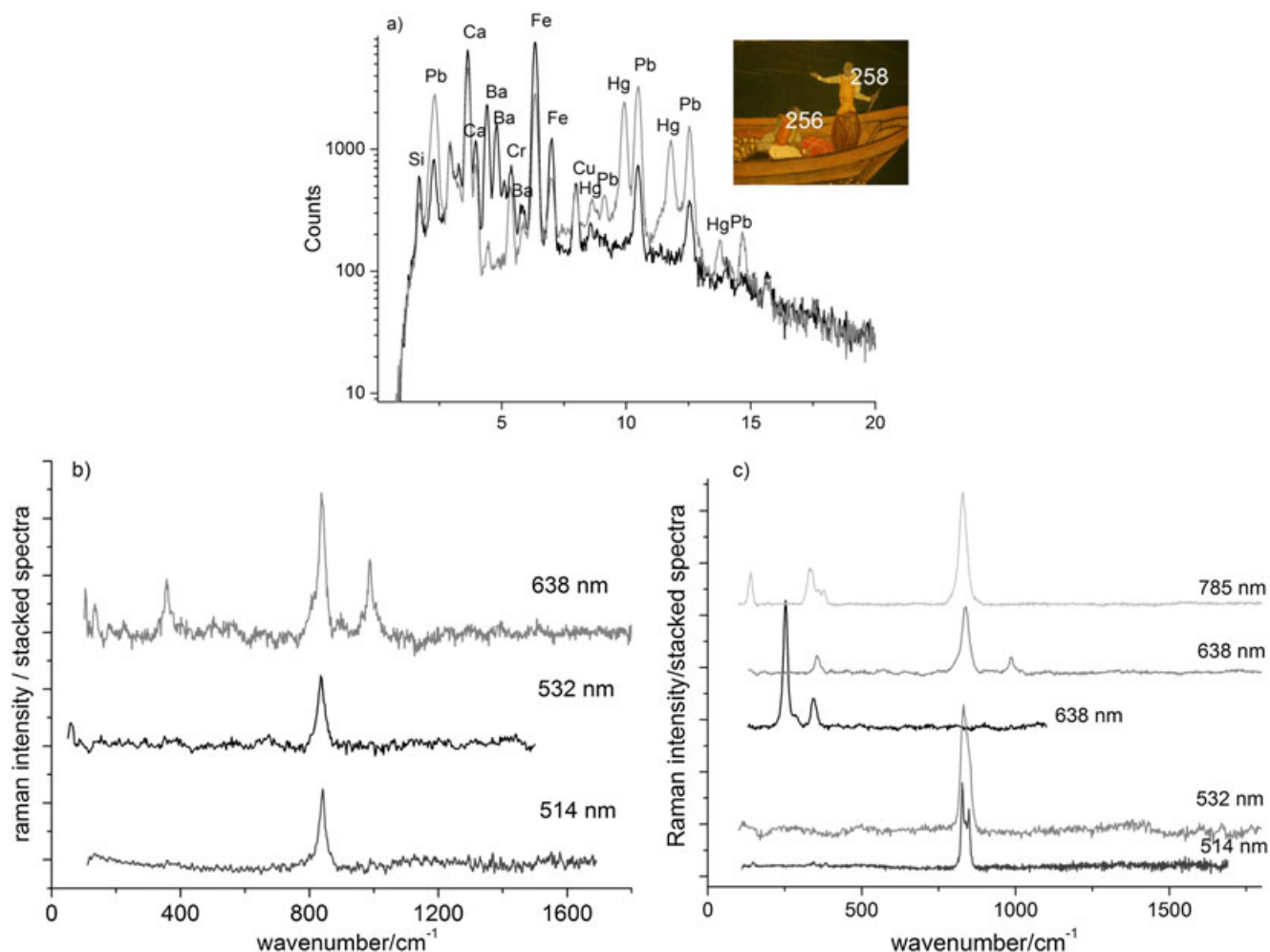
Figure 5. a) EDXRF spectra obtained from yellow (spot 258) and orange (spot 256) areas of the screens. b) Raman spectra obtained from a yellow sample; c) Raman spectra obtained from an orange sample.

The orange areas presented similar composition in the EDXRF spectra, but sometimes, Hg was also detected. Raman measurements identified the presence of chrome yellow-orange ($PbCrO_4.PbO$) (Fig. 5(c)) sometimes mixed with vermillion.

Brown

Also, in this case, two very different elemental compositions were found for two shades of brown: one presenting mainly Fe and Ca, as well as Si, and another presenting high amounts of Cr, Hg, and Pb (Fig. 6(a)). Raman spectra obtained with all laser sources from the sample collected at spot 498 were identified as chrome yellow-orange. Furthermore, with lasers 785, 638, and 532 nm, it was also possible to identify bands corresponding to vermillion. With regard to the lighter shade of brown, corresponding to the sample collected at spot 507, red ochre and carbon black were put in evidence using, in both cases, the 514 and 638 nm lasers (Fig. 6(c)). Moreover, with the use of the 638-nm laser, it was possible to identify calcite and silica. This means that the brown color was obtained by mixing red ochre, carbon black, and calcite together. The presence of SiO_2 is unusual. It could be used as an extender to modify the covering power of the paint or as a white material to modify the optical property of the brown hue.[14]

On the other hand, a band is observable at around 1450 cm^{-1} (Fig. 6(c) – 638-nm laser) that could be indicative of the use of an organic compound. According to Winter,[15] different organic substances are known to have been employed in Asian paintings, such as madder or lac dye for a red shade, gamboge as a yellow-coloring agent, or even an organic brown. Nevertheless, other bands that could be assigned to these compounds are not visible. If present, they could be hidden by the carbon broad bands centered at 1300 and 1500 cm^{-1}.[11]

White, black, and gray

The EDXRF spectra of white areas presented mainly Ca indicating the presence of calcite (Fig. 7). This was confirmed by the presence of a very strong band at around 1086 cm^{-1} in all Raman spectra. As was mentioned before, this band appeared in other Raman spectra indicating the use of this white pigment to lighten other colors. Calcite, especially when dealing with 17th-century Japanese artworks is attributed to the use of oyster-shell white, *gofun* in Japanese, a pigment made out of crushed oyster shells.[15] As *gofun* is supposed to contain not only calcite but also aragonite, the analysis was conducted to put it in evidence. Therefore, the band at 1086 cm^{-1} could
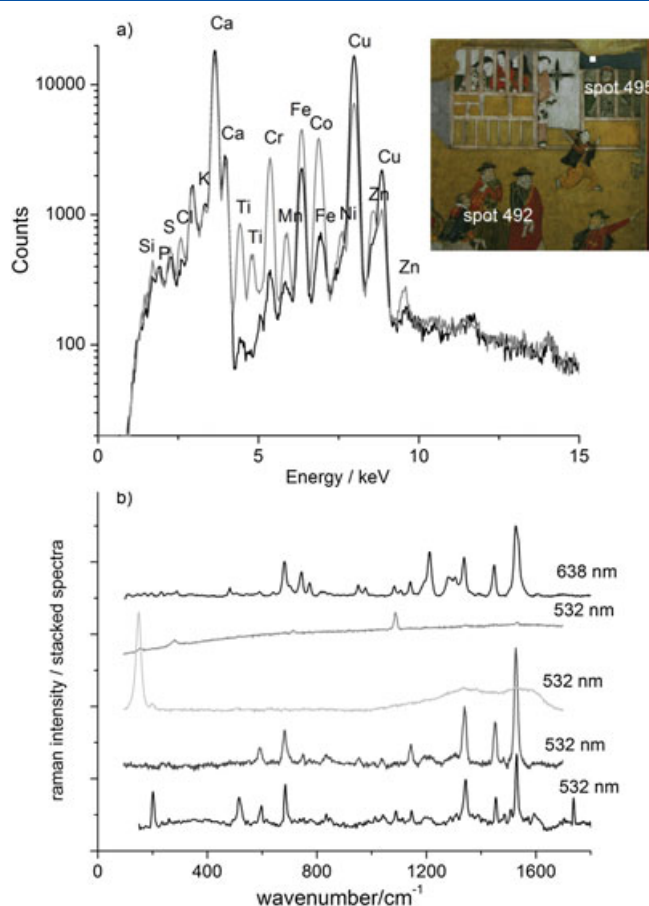
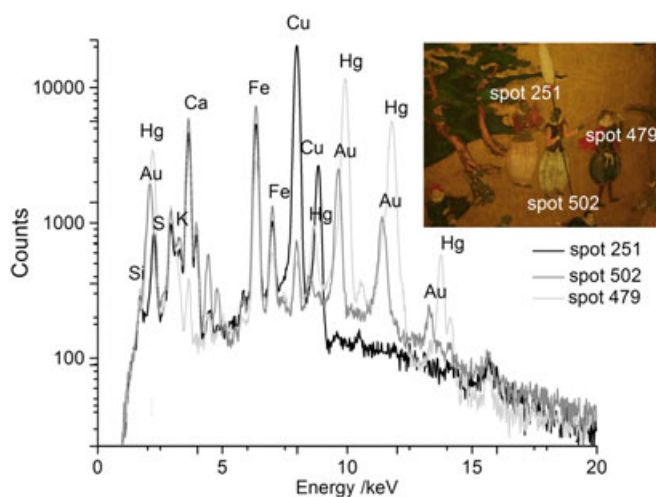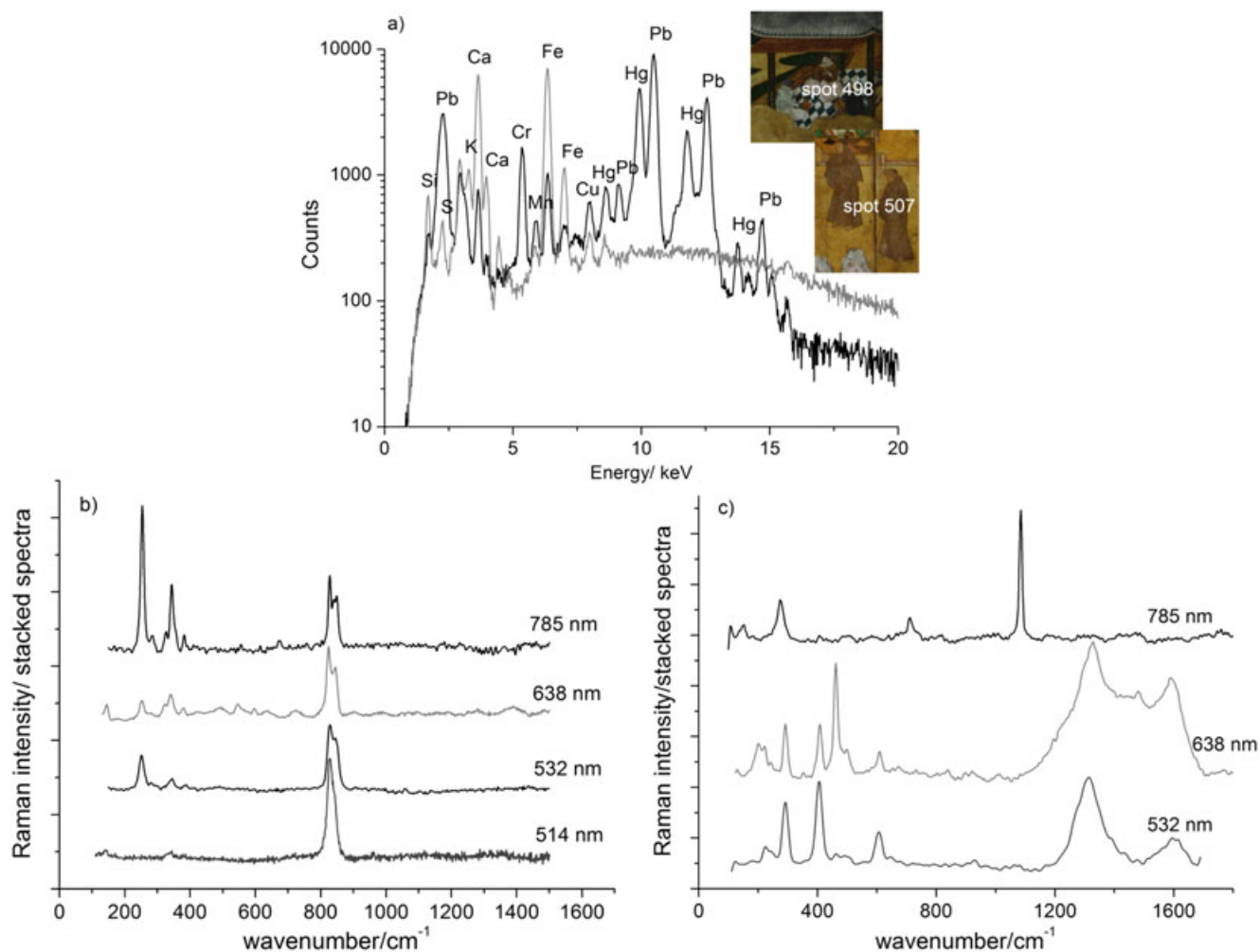**Figure 6.** a) Comparison of the EDXRF spectra obtained from two different shades of brown (spots 498 and 507). b) Raman spectra obtained from the brown sample taken from spot 498; c) Raman spectra obtained from the brown sample taken from spot 507.
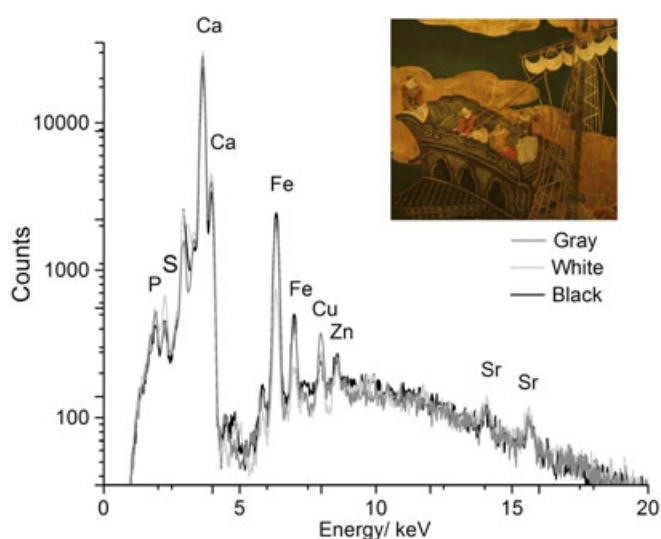
Figure 7. EDXRF spectra obtained from white, black and grey areas of the folding screens.

be attributed to $CaCO_3$ in both crystal forms calcite and aragonite. Furthermore, the small peak at $714\,cm^{-1}$ could be

interpreted as shifted or as an unresolved peak of both species, but what really distinguishes the calcite from the aragonite spectrum is the spectra behavior in the range of 200–$300\,cm^{-1}$. Comparing the results obtained from the sample and the reference spectra from calcite and aragonite, the presence of aragonite could not be confirmed, but the presence of calcite leaves no doubt. Regarding the black and gray areas, the EDXRF was not so different from the ones of white areas (Fig. 7), leading us to believe that the black color might be produced with a carbon-based pigment and the gray color with a mixture of carbon-based pigment and *gofun*. However, Raman spectrum obtained for the gray sample presented the band for calcite and also presented the bands for hematite (Fe_2O_3) (Fig. 4(a)).

Golden

Regarding the golden areas, as expected, Au was found covering the background of the screens (Fig. 3, spot 502). The fact that the Cu content is very low could be indicative of the use of a high quality gold, consistent with the practice of Japanese artists in the Momoyama and Edo periods.[16]

Intervention performed *in the Western countries*

The use of azurite, malachite, vermillion, red ochre, carbon black, calcite (*gofun*), or a mixture of vermillion, *gofun*, and carbon black to obtain brown is consistent with the pigments known to be used by Japanese painters in the Momoyama and Edo periods [15–17] and also with the pigments found by Raman and EDXRF in similar artworks.[7,8,18,19] Most of these pigments were found in pieces as ancient as 4th century BC[15] and are still in use nowadays. The presence of these pigments leads us to assume that they are part of the original painting or, at least, that they are not conclusive in terms of characterizing the intervention performed on the screens. Regarding the blue pigments, besides azurite, cobalt blue and phthalocyanine blue were found. Cobalt blue was discovered in 1802,[20] and the only records of its use is in traditional Japanese painting after the World War I;[21] so, we can consider that this pigment was not part of the original artwork. The same can be said with regard to the phthalocyanine blue, an organic dyestuff with a color considered very strong, about twice as strong as Prussian blue and very resistant to fading at light exposure. Phthalocyanine blue or copper phthalocyanine was developed by chemists of the Imperial Chemical Industries, Ltd, in the mid-1930s, only becoming commercially available at the beginning of 1938.[20] This way, we can conclude that the *Western* intervention mentioned in the NRICPT report could not have been performed before this date.

Regarding the yellow colors, usually yellow ochre or gamboge were used.[16,17] In the studied screens, chrome yellow was the pigment found. It is a modern pigment that only appeared in the traditional Japanese paintings in the Meiji era (1868–1912).[21] Chrome yellow could be found as the rare mineral crocoite or in its synthetic form and could assume a lighter or darker shade according to the conditions of precipitation. Discovered by Vauquelin in 1809,[14] it did not come into commercial production before 1818.[19] Regarding the orange shades, they were usually obtained by mixing red lead (Pb_3O_4) with vermillion,[22] but it was not the case in these screens. Again, a basic lead chromate was found. These lead chromate-based pigments are very unstable, even the best grades are not permanent, and the pigment tends to oxidize and darken on exposure to air over time.[23] Systematic studies about the degradation mechanisms of lead chromate were carried out until ca. 1950, coinciding with the progressive replacing of chrome yellow pigments by others, such as cadmium yellow that was assumed to be more stable.[24]

This means that the intervention must have been performed just before the lead chromate pigments (chrome yellow and chrome orange) came in disuse, somewhere in the 1940s or in the very early 1950s, just before the Portuguese state acquired the Namban screens in 1955, or immediately after, especially in the perspective of their incorporation into the museum collection.

Noteworthy is the fact that the areas that turned out to be more recent were the ones that present the worse state of preservation as can be seen in Fig. 8. The orange areas systematically presented a stained effect. Several colors show that they have suffered different mechanisms of degradation conducing to more or less pronounced loss of paint or to its modification to a darker hue. The dark blue color applied to the clothes of the European characters (also in architectonic elements) reveals a loss of cohesion. This state of pulverulence made visible the brownish tone of the substrate underneath, leaving heterogeneous surfaces. Its optical and aesthetical properties are not questioned in this

Figure 8. Detail of one of the screens. The degradation of the orange and blue colors is put in evidence.

artwork because its brightness and covering power are satisfactory. It seems that the main issue is related with the suitability of the binder and the way the paint layer has been applied.

When this intervention took place, in the second third of the 20th century, two different conservation philosophies could be considered: in the first one, the restorers sought to respect the original palette, limiting the restoration to the restitution of the damaged areas of the color that characterized them. In the second, rather corresponding to a refurbishment, the restorers did not hesitate to apply a new color or nuances in the same tone to give the artwork a brighter look.[25–29] In this study, we could not identify the pigment used prior to the restoration. Nevertheless, from the investigation conducted on another pair of folding screens belonging to the same period,[7] it is known that the colors more often applied for the clothing of the Portuguese sailors and slaves were: black using carbon black, green using malachite, blue using azurite, and red using vermillion. Taking this into account, it could be assumed that when using the phthalocyanine blue, a deep shade of blue, the restorers were trying to maintain the blue color. On the other hand, the recurrent use of the orange color in the clothes is highly unusual; it seldom appears in the other studied screens[7] and from the observation of other Namban folding screens.[30] In this case, we infer that the restorers invested on a new color scheme. However, it is a fact that the screens were subjected to a significant aesthetical change through the application of the glossy substance on the overall surface, as mentioned in the NRICPT report. Whatever was the chemical nature of the varnish used (resinous, oily, or both) that we may never analyze because it was removed by the NRICPT, this upper layer had been likely used as a protective coating immediately after the retouching process. Indeed, in Western practices, this treatment constituted very often, if not always, the last step in a restoration campaign when intended to paintings or correlated artworks. The application of a final varnish inevitably introduced a uniform brightness. This action was contradictory with the original aesthetic of the screens, where the burnished aspect of the gilded background and the dull aspect of the other colors were intentionally juxtaposed to produce a powerful visual contrast. Despite of this change, this was acknowledged as a legitimate treatment for providing

protection against pollutant agents (such as dust and finger prints and other marks).[26] This conservative function was favored to the detriment of maintaining the original artistic expression.

Conclusions

In this study, we relied on the analytical capabilities of EDXRF and Raman spectroscopy to study and compare the original polychromy and an unknown intervention performed on a pair of 17th-century Namban folding screens. These two techniques proved suitable for this task, in particular Raman spectroscopy. Different wavelengths are used to quench the fluorescence background of some compounds. Apart from differences in spectral resolution, we observed that some compounds were only identified using certain wavelengths. For example, cobalt blue and anatase were only identified with a green laser at 514 or 532 nm, and barium sulfate and silica were only identified with a red laser at 638 nm. The use of several wavelengths means that more information is gathered from each sample, resulting in a lesser need of sampling.

Furthermore, it is interesting to perceive that the restorers took advantage of the chemical novelties that were rising, in what concern polymers and the industrial production of new colors by using always the most publicized in fashion and very promising materials.

References

[1] P. Carneiro, *bulletin of portuguese/japanese studies* **2006**, *12*, 41.
[2] T. Takamizawa, *biombos namban, exhibition catalogue*, Calouste Gulbenkian Foundation, Lisbon, **1981**.
[3] S. Bruni, S. Caglio, V. Gugliemi, G. Poldi, *Applied Physics A* **2008**, *92*, 103.
[4] A. Duran, M. L. Franquelo, M. A. Centeno, T. Espejo, J. L. Perez-Rodriguez, *J. Raman Spectrosc.* **2011**, *42*, 48.
[5] L. Burgio, R. J. H. Clark, R. R. Hark, *Proc. Nat. Acad. Sci.* **2010**, *107*, 5726.
[6] K. Trentelman, N. Turner, *J. Raman Spectrosc.* **2009**, *40*, 577.
[7] S. Pessanha, M. L. Carvalho, M. I. Cabaço, S. Valadas, J.-L. Bruneel, M. Besnard, M. I. Ribeiro, *J. Raman Spectrosc.* **2010**, *41*, 1510.
[8] S. Pessanha, A. Guilherme, M. L. Carvalho, M. I. Cabaço, K. Bittencourt, J. L. Bruneel, M. Besnard, *Spectrochimica Acta B* **2009**, *64*, 582.
[9] K. Castro, N. Proietti, E. Princi, S. Pessanha, M. L. Carvalho, S. Vicini, D. Capitani, J. M. Madariaga, *Anal. Chim. Acta* **2008**, *623*, 187.
[10] K. Castro, e-visart, Raman database. [Cited: 11 7, 2011].
[11] I. M. Bell, R. J. H. Clark, P. Gibbs, *Spectrochimica Acta A* **1997**, *53*, 2159.
[12] L. Burgio, R. J. H. Clark, *Spectrochimica Acta A* **2001**, *57*, 1491.
[13] L. Monico, G. van der Snickt, K. Janssens, W. de Nolf, C. Miliani, J. Verbeeck, H. Tian, H. Tan, J. Dik, M. Radepont, M. Cotte, *Anal. Chem.* **2011**, *83*, 1214.
[14] B. Guineau, *Glossaire des matériaux de la couleur*, Brepols publishers, Turnhout, **2005**.
[15] J. Winter, *East Asian Paintings – Materials, Structures and Deterioration Mechanisms*, Archetype publications, London, **2008**.
[16] S. Grantham, *The Paper Conservator* **1985**, *9*, 83.
[17] J. Winter, *The Paper Conservator* **1985**, *9*, 24.
[18] K. Eremin, J. Stenger, M. L. Green, *J. Raman Spectrosc.* **2006**, *37*, 1119.
[19] K. Yamasaki, K. Nishikawa, *Stud. Conserv.* **1970**, *15*, 278.
[20] R. J. Gettens, G. L. Stout, *Painting Materials, A Short Encyclopaedia*, Dover Publications, Inc., New York, **1966**.
[21] M. Koyano, M. Yoneda, R. Tojo, M. Okawa, M. Saito, *The Paper Conservator* **1985**, *9*, 114.
[22] R. R. Ernst, *J. Raman Spectrosc.* **2010**, *41*, 275.
[23] R. Mayer, *The Artists Handbook of Materials and Techniques (*Ed.: E. Smith), Faber & Faber, London, **1982**.
[24] L. Monico, G. van der Snickt, K. Janssens, W. de Nolf, C. Miliani, J. Dik, M. Radepont, E. Hendriks, M. Geldof, M. Cotte, *Anal. Chem.* **2011**, *83*, 1224.
[25] N. S. Price, K. Jr. Talley, A. M. Vaccaro, *Historical and Philosophical Issues in the Conservation of Cultural Heritage*, The Getty Conservation Institute, Los Angeles, **1996**.
[26] H. Kühn, *Conservation and Restoration of Works of Art and Antiquities*, vol. 2, Butterworths, London, **1986**.
[27] S. Bergeon, *Science et Patience » ou la Restauration des Peintures*, Editions de la Réunion des musées nationaux, Paris, **1990**.
[28] U. Baldini, *Teoria Del Restauro e Unita Di Metodologia*, vol. 2, Nardini Editore, Florence, **1978**.
[29] C. Brandi, *Il Restauro, Teoria E Pratica*, Editori Riuniti, Roma, [1963] **1996**.
[30] http://www.city.kobe.lg.jp/culture/culture/institution/museum/

1706

Characterization of a Namban folding screen from the Edo period by means of EDXRF, SEM-EDS and Raman spectroscopy[†]

S. Pessanha,[a] A. LeGac,[a,b] T. I. Madeira,[a] A. Guilherme,[a] M. Manso[a] and M. L. Carvalho[a]*

In this work, a multianalytical approach is employed to characterize the materials used in a *Namban* folding screen that depicts the arrival of the Portuguese to the port of Nagasaki. Portuguese sailors reached Japan in 1543 and initiated what was to be known as the *Namban* trade. This interaction between Portuguese and Japanese was meticulously recorded by artists in the form of valuable and rare folding screens.

The present screen, attributed to the Edo period (~1603–1868), is what we could consider a second-generation screen, a copy of scenes and characters that appear in screens from the Momoyama period (~1573–1603) but in increased scale and minor detail. The materials used in the screen were identified by means of *in situ* energy dispersive X-ray fluorescence. Complementary results were obtained by Raman and scanning electron microscopy coupled to energy dispersive spectrometry analysis of microsamples taken from the screen.

The palette used in this artwork resorts to gold, malachite, azurite, vermillion, red lead, white oyster shell, and carbon black. Differences were found, when compared with previously studied screens, i.e. the use of mixtures of pigments, namely vermillion with red lead in an orange shade of red and also the mixture of vermillion and carbon black to obtain a brown color. Special emphasis was given to the characterization of the golden areas and study of techniques of gold application. Copyright © 2013 John Wiley & Sons, Ltd.

Introduction

The contacts established between Portugal and Japan from 1543 onwards, with the regular presence of Portuguese ships in the ports of the Island of Kyushu, namely, Nagasaki, were characterized by a climate of cordiality and the development of common interests between the two cultures.[1] This inspired the emergence of a new art style, designated as *Namban*, meaning Southern Barbarians, because these outsiders arrived from the south, in which their social and trade customs are depicted. The earliest *Namban* screens date from ca 1600, but the novel subject fascinated the Japanese, and the Kano school atelier and other professional painting studios in Kyoto have made numerous versions throughout the 17th and 18th centuries. *Namban* screens typically portrayed the long-nosed Portuguese and their ships, Christian churches, and missionaries with a skill and detail that could only be gained from personal observation.[2] Art patrons who saw the early screen masterpieces became interested in *Namban* themes and commissioned the painters or colleagues in the Kano school to do other works of identical composition. This way, generations of similar screens were copied out, to the extent of artists that, having no knowledge of Portuguese ships and no understanding of missionaries, would merely imitate previous screen paintings, but the artworks would lack spontaneity and vitality.[2] A large number of works painted in such a stereotyped fashion are unique in Japanese art, and many examples must have been lost during Japanese isolation, so that only around 90 extant examples are known.

In this work, we investigate the materials used in a screen belonging to the Edo period to understand if the materials and techniques employed in the artwork are similar with the ones used in screens from the Momoyama period or if they suffered more influence from the materials used in the west.

The screen, belonging to the collection of Museu do Oriente in Lisbon, was acquired without its pair (Fig. 1). It constitutes a magnification of the scenes and characters presented in a screen from the Momoyama period belonging to the collection of Museu Nacional de Arte Antiga[3] that bears the Kano Naizen stamp. Kano Naizen was one of the most prestigious artists from this genre, and this pair of screens was classified by experts Tadao Takamizawa and Yoshimoto Okamoto as belonging to the oldest and most refined group of *Namban* folding screens.[4] At least two identical pairs of screens bearing the Kano Naizen stamp are known, one belonging to the Kobe City Museum collection[5] and other recently put to auction by Christie's.[6]

The study here described made use of energy dispersive X-ray fluorescence (EDXRF) spectroscopy to perform the *in situ* survey of the folding screens in all their extension. This way, only the

* Correspondence to: M. L. Carvalho, Centro de Física Atómica da Universidade de Lisboa, Av. Professor Gama Pinto, 2 1649–003, Lisboa. E-mail: luisa@cii.fc.ul.pt

† This article was published online on 12 February 2013. An error in the title was subsequently identified and corrected 29 April 2013.

a Centro de Física Atómica da Universidade de Lisboa, Av. Professor Gama Pinto, 2 1649-003, Lisboa

b Departamento de Conservação e Restauro, Faculdade de Ciências e Tecnologia, Universidade Nova de Lisboa, Quinta da Torre, 2829-516 Caparica, Portugal

Figure 1. Picture of the Namban folding screen belonging to the collection of Museu do Oriente.

necessary microsamples were taken to apply Raman spectroscopy and attain a better characterization of the materials used in the pigments. Special emphasis was given to the characterization of the golden areas and study of techniques of gold application. By mixing gold with silver and copper, the goldsmith could produce a large number of alloys with different mechanical properties (strength, hardness, and ductility) and different colors, meaning that each alloy is tailored to a particular application. Hardness can be improved by alloying gold with copper and silver and by using annealing and quenching. The addition of copper (red) and silver (white) in different proportions to gold (yellow–orange) changes the color of the final alloy. When analyzing the screen, we can see three types of gold application: (1) as metal leaf (*Kin-haku*) covering almost the entire extension of the screen, corresponding to the land where the figures stand and to the sky (Fig. 2(a)). Traditionally, a grid was marked slightly across the paper as a guide for laying the hand-beaten gold leaves (~10 cm × 10 cm) in horizontal rows, starting from the top left-hand corner[7]; (2) as ground gold mixed with a vehicle,

usually animal glue (*nikawa*), and applied as paint (*Kin dei*) used for enhancing the sinuous and rounded outlines of the clouds or the limits of the Nagasaki Bay (Fig. 2(b)); (3) and as flakes of gold sprinkled over the burnished metal leaf (*Sunago*). This use is limited to the very lower part of each panel, giving a textured effect and a specific contrast between the polished and mate coatings[8] (Fig. 2(c)). To further investigate the gold alloys used, scanning electron microscopy coupled to energy dispersive spectrometry (SEM-EDS) was performed. The combination of a technique of elemental analysis, such as EDXRF and EDS, with the ones that provide information on a molecular level, such as Raman spectroscopy, has proven suitable and successful in other studies related with material characterization of Argentinean prehistoric pigments[9] of Polish mural paintings,[10] Medieval vault paintings,[11] and wall paintings from the Ming Dynasty.[12] Raman spectroscopy and EDXRF have been also applied in studies related to the characterization of colored maps[13,14] and illuminated manuscripts[15,16] and more importantly, in the characterization of Japanese folding screen from the Momoyama period.[3,17]

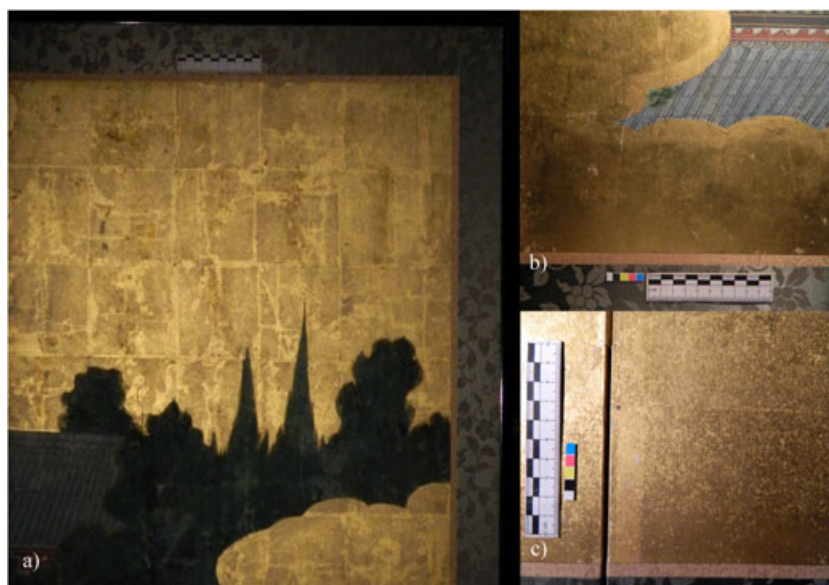**Figure 2.** Photographs of the three types of of gold application: (a) as metal leaf (*Kin-haku*), (b) ground gold mixed with a vehicle and applied as paint (*Kin dei*), and (c) gold flakes sprinkled on the support (*Sunago*).

Experimental

The EDXRF equipment used in this study consists of an X-ray generator ECLIPSE II from Amptek, with Ag anode and an Amptek XR-100CR of Si-PIN thermoelectrically cooled detector. The X-ray tube operated at 30 kV and 100 μA in 300 s acquisitions.

The Raman measurements were carried out using the Xplora confocal Raman microscope by Horiba, using a laser diode source operating at a wavelength of 638 nm and 50× objective. The incident power on the sample ranged from 0.1 to 1 mW, and the scattered light collected by the objective was dispersed onto an air-cooled CCD array by 1200 lines/mm grating. Pigment identification was made by comparison with the literature.[18,19]

The SEM-EDS analyses were carried out using a FEG-SEM model JSM 7001F by JEOL with an Oxford Si(Li) INCA PentaFet-x3 detector. The accelerating voltage was 20 kV and acquisition time of 40 s. For every analyzed sample, an average of three measurements was performed.

Results

Gold

As it can be observed in Fig. 2, the very homogeneous brightness of the gilded surface and the polishing process highlighting the subtle texture of the paper support put in evidence that the gold leaves were thoroughly burnished on the whole ground. In fact, the anarchic orientation of the compressed fibers of the Japanese paper remains slightly exposed, which suggests that a very thin substance was used for the metal leaf application. The water-soluble ground for gold application was usually animal glue (*nikawa*).[7,8,20] In Table 1, we present the semiquantitative evaluation achieved for the metal leaf. A binary alloy containing an average 97.11% of Au and 2.89% of Ag was obtained corresponding to approximately 23.25 ct gold. Silver was likely used to turn the alloy less ductile and better to cover flat surfaces. Because the Japanese gold leaf was said to be the thinnest in the world by Koyano,[20] the assessment of the gold leaf thickness was attempted. As it was not possible to obtain cross-sections from samples of this type of coating because of their extreme thinness and the impossibility of positioning them exactly at 90°, images were used to try to assess the gold leaf thickness (using both secondary and backscattered electrons). Taking advantage of the rise of the leaf from the paper support, we were able to obtain a quasi-transversal view. Considering that the scale the image was taken, we conclude that the gold leaf is in the 100 nm order of magnitude (Fig. 3(a)).

Regarding the gold paint, a high-grade gold was also used, approximately 23 ct, with mean elemental concentrations of 96.49% Au and 3.37% Ag. This technique of gold application was used in the outline of the golden mountains and clouds, presenting a raised effect over the gold leaf. The elemental composition of

Table 1. Semiquantitative results expressed in weight% and standard deviation (SD) obtained for gold samples by EDS analyses

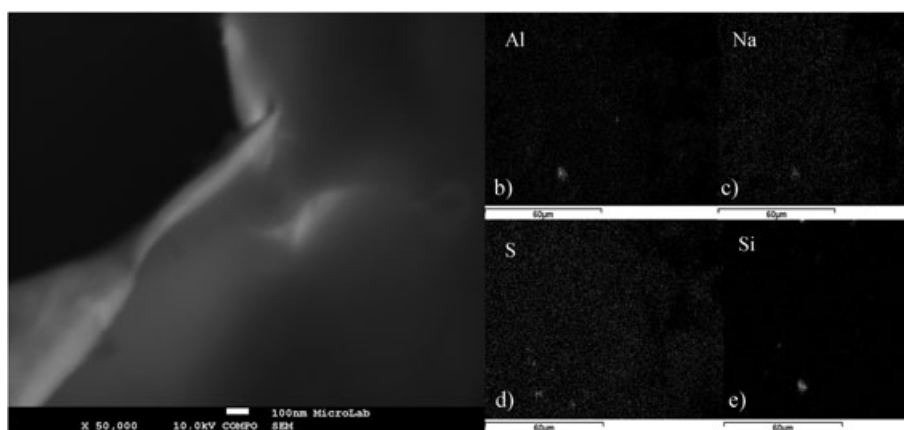| Elements	Leaf Weight% ± SD	Painted Weight% ± SD	Painted White layer Weight% ± SD	Sprinkled Weight% ± SD	Sprinkled Weight% ± SD	Sprinkled Weight% ± SD
Cu	BDL	BDL		0.99 ± 0.07	0.98 ± 0.03	0.79 ± 0.09
Ag	2.89 ± 0.23	3.37 ± 0.45		2.79 ± 0.33	1.97 ± 0.65	3.32 ± 0.67
Au	97.11 ± 0.32	96.49 ± 0.34		96.19 ± 0.36	97.00 ± 0.37	95.89 ± 0.61
C			13.01 ± 1.92			
O			56.04 ± 5.39			
Na			0.36 ± 0.04			
Mg			0.25 ± 0.04			
Al			0.22 ± 0.04			
Si			0.47 ± 0.20			
S			0.35 ± 0.05			
Ca			29.59 ± 3.2			

Figure 3. (a) Backscattered electron image obtained for a gold leaf sample, (b) mapping obtained for Al, (c) mapping obtained for Na, (d) mapping obtained for S, and (e) mapping obtained for Si.

the ground layer over which the paint was applied was also determined (Table 1), and the presence of sodium aluminosilicates is inferred (Fig. 3(b–e)).

Regarding the sprinkled gold, visual records obtained by backscattered electron and secondary electron imaging were fundamental to understand that the gold flakes are aggregates of hand-beaten gold leaves ground separately and then sprinkled over the burnished gilded ground of the folding screen. Different elemental compositions were obtained for different particles ranging from a 23.25 ct gold, with 97% of Au, 1.97 of Ag, and 0.98 of Cu, to a lower grade gold with 95.89% of Au, 3.32% of Ag and 0.79% of Cu (Table 1).

Red

Regarding the red pigments, the use of vermilion (HgS) was suggested in the EDXRF analysis (Fig. 4(a)). Furthermore, a lighter shade, more orange, was obtained by mixing vermilion and red lead (Pb_3O_4) (Fig. 4). The presence of vermillion was confirmed in the Raman spectrum of the red sample 1 with bands at 250, 280, and 341 cm^{-1},[18] and red lead was identified in the red sample 2 with bands at 118 and 549 cm^{-1}[18] (Fig. 5(a)).

Figure 4. (a) Comparison of the EDXRF spectra obtained for two different shades of red and (b) comparison of the EDXRF spectra obtained for white and black areas of the screen.
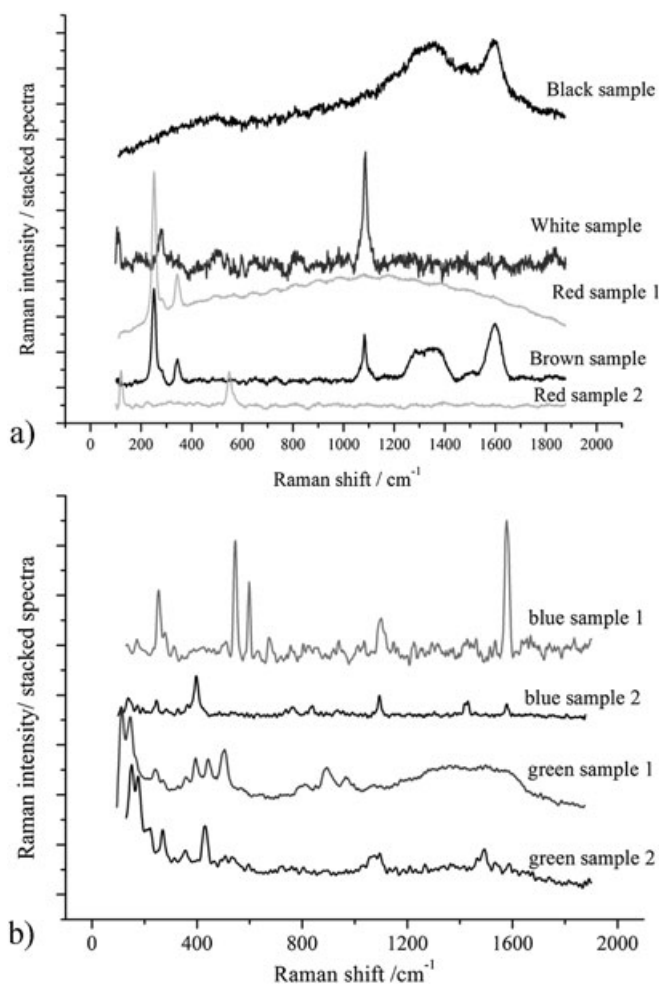
Figure 5. (a) Raman spectra obtained for microsamples collected from black, white, red, and brown areas of the screen and (b) Raman spectra obtained for microsamples collected from blue and green areas of the screen.

White

The EDXRF measurements on white areas presented high amounts of Ca (Fig. 4(b)), whereas the Raman spectra of white microsample was identified as $CaCO_3$ because of the presence of a strong band at 1084 cm^{-1}[18] (Fig. 5(a)). Whether we are in the presence of calcite, aragonite, or both was not possible to assess. Calcium carbonate is indicative of the use of oyster-shell white (*gofun* in Japanese), which has been used widely in Japan since the 15th century.[7]

Black

Regarding the black areas and comparing with a spectrum obtained for a white area, we can see that they are very similar (Fig. 4(b)). The Raman analysis obtained for black microsamples, a carbon-based black pigment, was identified by the two broad bands centered at 1350 and 1600 cm^{-1}[18] (Fig. 5(a)).

Brown

The EDXRF spectra of the brown areas presented Hg, suggesting a mixture using vermillion, and the Raman measurements obtained from a microsample collected from a brown area

allowed also the identification of vermillion with bands at 246, 282, and 344 cm^{-1}, calcium carbonate with a strong band at 1082 cm^{-1}, and carbon black with two broad bands centered at 1320 and 1590 cm^{-1}[18] (Fig. 5(a)). This way we can conclude that the brown color was obtained by mixing vermilion, *gofun*, and carbon black.

Green

The EDXRF of green areas of the screen presented mostly Cu; however, the intermittent presence of Cl suggested the presence of different compounds (Fig. 6(a)). Raman spectra of different samples of green areas showed the presence of malachite ($CuCO_3.Cu(OH)_2$) with bands at 151, 174, 220, 268, 355, 424, 1074, and 1092 cm^{-1}[18] (Fig. 5(b)) sometimes mixed with atacamite ($Cu_2(OH)_3Cl$), identified in the Raman spectrum by the bands at 112, 143, 356, 393, 440, 496, 810, 893, and 960 cm^{-1},[18] explaining the appearance of Cl.

Blue

When comparing the EDXRF spectra obtained for areas of dark and light blue, a very different elemental composition was obtained (Fig. 6(b)). The dark blue areas presented high amounts

of Cu, suggesting the presence of azurite ($2CuCO_3.Cu(OH)_2$), confirmed by Raman spectroscopy as seen in Fig. 5(b) with bands at 135, 244, 395, 836, 1091, 1421, and 1574 cm^{-1}.[18] As for the light blue areas, the reduced Cu suggested the use of other pigment. Raman spectra of samples from the light blue area identified the presence of indigo with bands present at 256, 281, 304, 544, 597, 621, and 1577 cm^{-1}.[19]

Conclusions

The arrival of the Portuguese *nao do trato*, known to the Japanese as the *kurofune* (black ship), gave motto to a period of great development in the pictorial panorama of Japan. Here, we analyzed the materials used in what could be considered a second-generation screen belonging to the Edo period depicting that scene. The pigments found, malachite, azurite, indigo, vermillion, red lead, carbon black, and *gofun*, are consistent with the materials found in screens from the Momoyama period.[3,17] However, in this screen, the artist resorted to mixtures that were not seen in the other screens: orange shade obtained through vermilion and red lead and brown obtained by mixing vermillion, *gofun*, and carbon black. These mixtures are not uncommon and are present, e.g. in the 16th century copy of the *Tale of Genji*.[20]

The presence of atacamite and the fact that it does not appear dissociated from malachite seem to be an indication that it is an alteration product of malachite. This has also been discussed in the literature.[14,19] The presence of Fe and Cu throughout the screen could be explained by some paper-sizing treatment;[21] however, we did not had access to any gap in the screen to study the paper.

This work also focused in the characterization of the three different gold application techniques: leaf, paint, and sprinkled flakes. The later was exclusive of this screen and was not seen in other first-generation screens.[3,17]

The semiquantitative analyses by SEM-EDS of the three kinds of gold revealed the use of a high-grade alloy, as leaves and applied as paint. Regarding the sprinkled gold, different gold alloys were found, thus issued from hand-beaten leaves from different batches to obtain different shades. Our results seem to point out ternary alloys; however, and according to Guerra,[22] an amount of Cu up to 1% may be considered as being part of the natural gold alloy, so in these samples, the presence of Cu would not be intentionally added.

References

[1] P. Carneiro. *Bulletin of Portuguese/Japanese Studies* **2006**, *12*, 41.
[2] Y. Okamoto, *The Art of Japan*, Weatherhill, New York, **1972**.
[3] S. Pessanha, M. L. Carvalho, M. I. Cabaço, S. Valadas, J. L. Bruneel, M. Besnard, M. I. Ribeiro. *J. Raman Spectrosc.* **2010**, *41*, 1510.
[4] Y. Lippit, *Encompassing the Globe: Portugal and the World in the 16th and 17th Centuries*, MNAA, Lisbon, **2009**.
[5] http://www.city.kobe.lg.jp/culture/culture/institution/museum/ . accessed October 2012
[6] http://www.christies.com/features/southern-barbarians-come-to-trade-1281-1.aspx . accessed June 2012
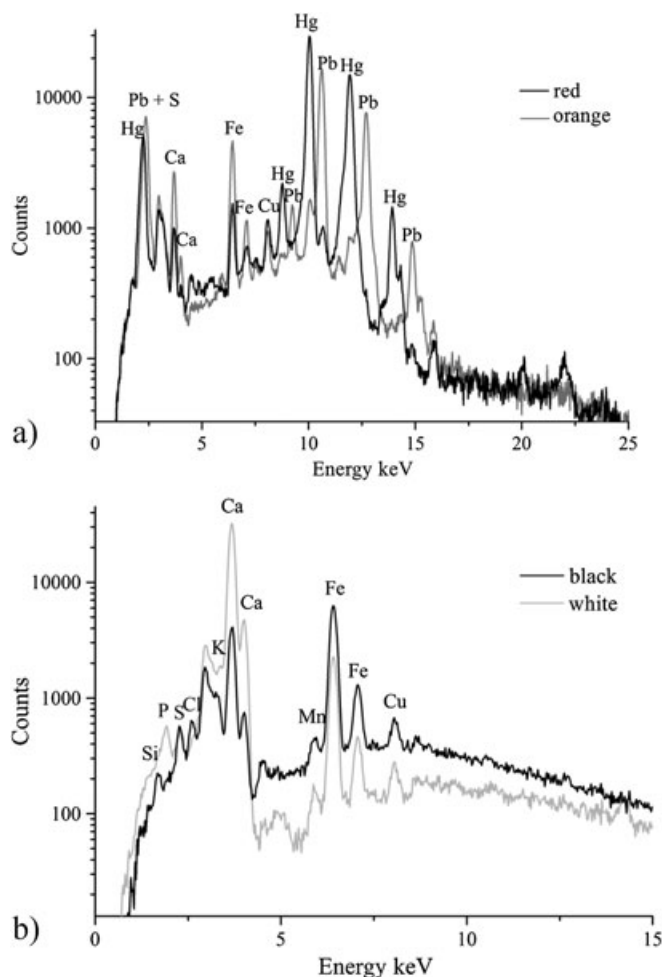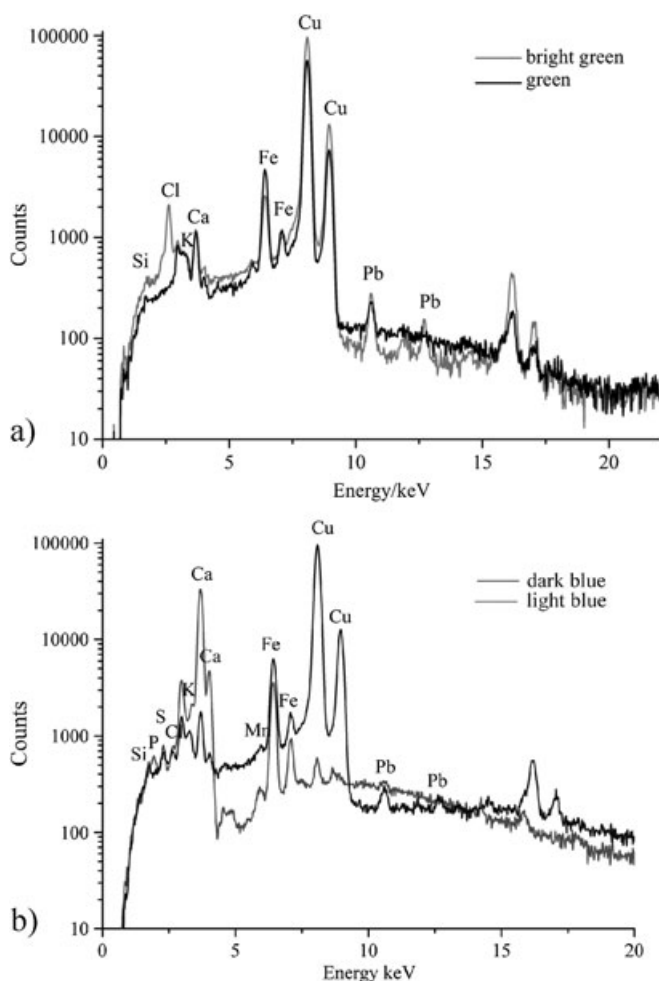
Figure 6. (a) Comparison of the EDXRF spectra obtained for two different shades of green and (b) comparison of the EDXRF spectra obtained for two different shades of blue.

[7] S. Grantham. *The Paper Conservator* **1985**, *9*, 83.

[8] J. Winter, *East Asian Paintings: Materials, Structures and Deterioration Mechanisms*, Archetype Publications, Washington, **2008**.

[9] L. Darchuk, Z. Tsybrii, A. Zorobiec, C. Vázquez, O. M. Palacios, E. A. Stefaniak, G. Gatto Redondo, R. van Grieken. *Spectrochimica Acta Part A* **2010**, *75*, 1398.

[10] M. Sawczak, A. Kaminska, G. Rabczuk, M. Ferretti, R. Jendrzejewski, G. Sliwinski. *Applied Surface Science* **2009**, *255*, 5542.

[11] A. Deneckere, W. Schudel, M. Van Bos, H. Wouters, A. Bergmans, P. Vandenabeele, L. Moens. *Spectrochimica Acta Part A* **2010**, *75*, 511.

[12] Q. G. Zeng, G. X. Zhang, C. W. Leung, J. Zuo. *Microchemical Journal* **2010**, *96*, 330.

[13] K. Castro, N. Proietti, E. Princi, S. Pessanha, M. L. Carvalho, S. Vicini, D. Capinani, J. M. Madariaga. *Anal. Chim. Acta* **2008**, *623*, 187.

[14] K. Castro, S. Pessanha, N. Proietti, E. Princi, D. Capitani, M. L. Carvalho, J. M. Madariaga. *Anal. Bioanal. Chem.* **2008**, *391*, 433.

[15] M. Aceto, A. Agostino, E. Boccaleri, F. Crivello, A. Cerutti Garlanda. *J. Raman Spectrosc.* **2006**, *37*, 1160.

[16] T. D. Chaplin, R. J. H. Clark, M. Martinón-Torres. *J. Mol. Struct.* **2010**, *976*, 350.

[17] S. Pessanha, A. LeGac, T. I. Madeira, J.-L. Bruneel, S. Longelin, M. L. Carvalho. *J. Raman Spectrosc.* **2012**, *43*, 1699.

[18] I. M. Bell, R. J. H. Clark, P. J. Gibbs. *Spectrochim Acta A* **1997**, *53*, 2159.

[19] K. Eremin, J. Stenger, M. L. Green. *J. Raman Spectrosc.* **2006**, *37*, 1119.

[20] M. Koyano, *Gilding and Gilding Conservation in Japan. Gilded Wood: Conservation and History*, Sound view press, Madison, **1991**.

[21] S. Grantham. *The Paper Conservator* **1985**, *9*, 83.

[22] M. F. Guerra, T. Calligaro. *Meas. Sci. Technol.* **2003**, *14*, 1527.

133

wileyonlinelibrary.com/journal/xrs
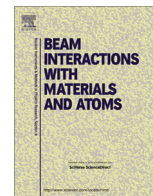
Elemental analysis by portable Ag and Rh X-ray sources of a *Namban* type folding screen

Sofia Pessanha [a], Agnès Le Gac [a,b], Teresa Isabel Madeira [a], Mauro Guerra [a], Maria Luisa Carvalho [a,*]

[a] *Centro de Física Atómica da Universidade de Lisboa, Av. Professor Gama Pinto, 2 1649-003 Lisboa, Portugal*
[b] *Departamento de Conservação e Restauro, Faculdade de Ciências e Tecnologia, Universidade Nova de Lisboa, Quinta da Torre, 2829-516 Caparica, Portugal*

A B S T R A C T

This work focuses on the characterization of the materials used in a Japanese *Namban* type folding screen. *Namban* is the art style inspired by the arrival of the southern barbarians or *Nambanjin* to Japan in 1543, and the commercial trade then initiated. Energy dispersive X ray spectrometry (EDXRF) was used and complemented with Raman spectroscopy. The unexpected aspect about this screen concerns the brownish–grey color over which the characters stand instead of the usual golden color obtained by gilding. To better assess the elemental composition of the background and, most importantly, conclude about the presence of precious metals, an X-ray tube with Rh anode was used supporting the results obtained with the Ag one.

© 2013 Elsevier B.V. All rights reserved.

1. Introduction

Namban is the art style inspired by the arrival of the Portuguese sailors to Japan in 1543 and the commercial trade then initiated. The contacts established between Portugal and Japan from 1543 onwards, were characterized by a climate of cordiality and the development of common interests between the two cultures [1]. This inspired the emergence of a new art style, designated as *Namban* (meaning Southern Barbarians) in which the *Namban*'s social and trade customs are depicted. The earliest *Namban* screens date from ca 1600 but the novel subject fascinated the Japanese and numerous versions were made throughout the 17th century [2]. Examples of these oldest screens are the ones kept at Museu Nacional de Arte Antiga in Lisbon [3] and at Museu Nacional Soares dos Reis in Oporto [4]. As the *Namban* theme became more admired, art patrons who saw the early screen masterpieces became interested in *Namban* themes and commissioned the painters to produce other works of identical composition. This way, second generation screens were created as copy of scenes and characters but in increased scale and minor detail [2]. In this work we studied the composition of the materials present in a folding screen (Fig. 1). This screen was selected to be part of the exhibition: *Giappone. Terra di incanti – Di linea e di colore* (Japan. Land of enchantment – The line and color) at Museo degli Argenti in the Pitti Palace in Florence (Italy) [5]. In the meantime, doubts were raised regarding its authenticity and dating and it was decided that this artwork would not be presented.

Although the figure composition was coherent with the *Namban* theme: "The alterity of the Portuguese is (...) visible in their thick curling mustaches (...), billowing pantaloons (...), as do the dogs kept on leashes. The Portuguese traders are served by darked-skinned Indian (and possible African) slaves, who can be seen carrying parasols over the capitão-mor (...)" [6], the screen did not have a narrative spirit. Furthermore, it was only composed by two panels, unlike the traditional six-paneled screens, usually displayed in pairs. Another unusual characteristic of the screen was the brownish–grey background contrasting with the shimmer effect of the gilded background of other *Namban* screens. In order to shed some light on the origin of this artwork, the characterization of the materials used was carried out by means of portable Energy dispersive X-ray fluorescence (EDXRF) and Raman spectroscopies. Special interest lied in assessing the composition of the background and two different EDXRF setups were used, with X-ray tubes with two different anodes in order to better attest the presence or not of precious metals such as gold or silver. The combination of a technique of elemental analysis, such as EDXRF, with ones that provide information on a molecular level, like Raman spectroscopy, have proven suitable and successful in other studies related with material characterization in Cultural Heritage [7,8], particularly in studies related with the characterization of pigments in artworks on paper support [3,4,9–12].

2. Experimental

The EDXRF equipment used in this study for elemental analysis consists on an Amptek USA XR-100CR Si-PIN thermo electrically

---

Fig. 1. Photograph of the studied screen. Spots of analysis are marked: in black – EDXRF (Ag anode); in black italic – EDXRF (Rh anode); in white – microsamples collected for Raman analysis.

cooled detector coupled either with an X-ray generator ECLIPSE II from Amptek, with Ag anode or an X-ray generator ECLIPSE IV from Amptek, with Rh anode. The X-ray tubes are low power, end window tubes (experimental conditions: 30 kV, 95 μA). The used detector has a 7 mm^2 detection area, 300 μm thick and a 12.5 μm Be window. The energy resolution is 185 eV at 5.9 keV, and the acquisition system is Amptek PMCA. The acquisitions were performed during 300 s. For collimating the X-ray beam an acrylic support with a 2 mm pinhole in tantalum was constructed, which yielded a 5 mm effective spot size on the sample. To allow easy adjustment of the sample position, about 7 mm from the tube, a system of two point lasers is mounted on the tube and detector holder. The sample matrix is the main responsible for the diffusion effects, and the total amount of scattered radiation by Compton and Rayleigh is strongly dependent on the matrix composition. The angle between the incident beam and emitted beam from the sample is 90°. This geometry has been chosen in order to minimize the scattered radiation of the bremsstrahlung radiation on the sample. Both elastic (Rayleigh) and inelastic (Compton) scattering have minimum for 90° due to partial polarization. Furthermore, the probability for Compton scattering exhibits a minimum around 90°.

The Raman measurements were carried out using the XploRA Confocal Raman microscope by Horiba France, with three different laser sources (532, 638, and 785 nm) and the 50× and 100× objectives. Using an entrance slit of 100 μm, the scattered light collected by the objectives was dispersed onto the air cooled CCD array of an Andor iDus detector by a 1200 lines/mm grating. The incident power on the sample ranged from 0.1 to 1 mW.

3. Results

The examination of the open folding screen under UV radiation revealed a very confusing aspect of the whole surface (Fig. 2). Although fluorescence is an imprecise tool for identification, as coatings change as a result of absorbing light energy, it allowed to point out different chemical family for a broad set of materials. Two or more substances were applied in a quite heterogeneous

way as final coatings, since an intense orange fluorescence was mainly observed on the background of the panels, suggesting the use of shellac, and the greenish fluorescence of broad brush strokes applied over it, almost everywhere (but still trying to preserve the characters), likely referring to a natural resinous varnish. This layer seems to have been superimposed to the former, since it partially hides the orange fluorescence underneath. Other brush strokes of a denser yellowish green color were also detected here and there, apparently applied in a random way but in an attempt to give more brilliance from place to place or highlight some figures contours. The brighter fluorescence of the material used in this later intervention refers perhaps to a more complex mixture containing a drying oil and resin [13–18].

4. Background

The most unusual aspect of this screen is the brownish–grey appearance of the background. After examination of the obtained EDXRF spectra, the Fe content is noteworthy as well as other elements that appear distributed quite heterogeneously (Fig. 3). Some of the analyzed areas present high amounts of Cu, Zn and Pb, while others present Ti and Mn, or even high amounts of S. As for the existence of Au, it was rapidly overthrown (Fig. 3). The brown background recalled the oxidized silver observed on other *Namban* screens [3]. The anode of the X-ray tube primarily used was Ag, so the presence of this metal in small amounts was difficult to put in evidence. Therefore, new measurements were performed using an Rh anode and the presence of Ag was confirmed (Fig. 3b). Because the Kα line of Ag (22.101 keV) is overlaid with the Rh Kβ Compton scattering (∼22.3 keV), the obtained spectra were compared with the one of a paper sample without Ag. The shift of the line to the left is perfectly visible when Ag is present.

5. Blue and Green

Regarding the EDXRF analysis of the green areas, Cu was found (Fig. 4a), most likely associated to Malachite ($CuCO_3Cu(OH)_2$), the

Fig. 2. Details of the screen photographed under UV radiation.

Fig. 3. Comparison of the EDXRF spectra obtained for the background (a) with the Ag anode X-ray tube; (b) with the Rh anode X-ray tube.

most widely used green pigment in East Asian paintings [19]. However, the noteworthy presence of Cr, might indicate the presence of Viridian ($Cr_2O_3 2H_2O$), or Chrome green, the name given to the pigment made by co-precipitating Prussian blue [$Fe_4(Fe[CN]_6)_3$] and Chrome yellow ($PbCrO_4$) [20,21]. Iron appears also with great

intensity in the spectrum, however it is unclear if its presence is due to the same origin as in the background or from the presence of Prussian blue. In fact, Raman analysis of green samples pointed out the presence of lead chromate (Fig. 4b) with a strong band at 846 cm^{-1}. However, instead of the characteristic bands of Prussian blue (538, 2102 and 2154 cm^{-1}), the typical spectrum of an organic dye was found, with bands at 230, 415, 444, 534, 807, 917, 1181, 1217, 1293, 1378, 1451, 1492, 1597, and 1627 cm^{-1} (Fig. 4b). When confronting this spectrum with the ones available in databases, a triarylmethane blue dye, most likely Victoria blue, seems to have been used [22]. Regarding the blue areas, Fe was put in evidence in the EDXRF spectra (Fig. 4a), and Fe mixed with Ba and Zn to obtain a grayish shade of blue on the trousers of the slave. The possibility of the presence of Prussian blue was again raised, however, Raman spectra of the blue samples collected from the screen corresponded to ultramarine blue, a complex sulfur-containing sodium-aluminosilicate and polysulfides ($3Na_2O3Al_2O_36SiO_22Na_2S$) with bands at 262, 545, 590(sh), 1102 and 1660 cm^{-1} [23,24]. The presence of Ba and Zn may be interpreted as the addition of a white opaque pigment to lighten the color, probably lithopone ($ZnS + BaSO_4$).

6. Red and yellow

When analyzing the screen, three different shades of red can be distinguished (Fig. 5). The brighter shade of red revealed the presence of Cd, S and Se, suggesting the use of the pigment Cadmium Red ($CdS(Se)$). On the other hand, the orange shade observed in the parasol revealed high amounts of Hg, suggesting the presence of Vermillion (HgS). Considering the darker shade of red, the high amount of Fe put in evidence in the spectrum could again be due to the contribution of the material used in the background or to the use of an iron-based oxide, such as Hematite (Fe_2O_3), which has a drabber hue compared to that of vermilion. Despite these differences, Se is observed in all spectra, allowing to infer that Cadmium red is always part of the color paints; even though Cd was not detected because of the highest efficiency of the detector for the energies around 10 keV (Ka Se = 11.2 keV). The yellow color is scarce in this artwork. It is only present in the cross of the parasol, the leash of the dog and the flowers that ornament the clothes
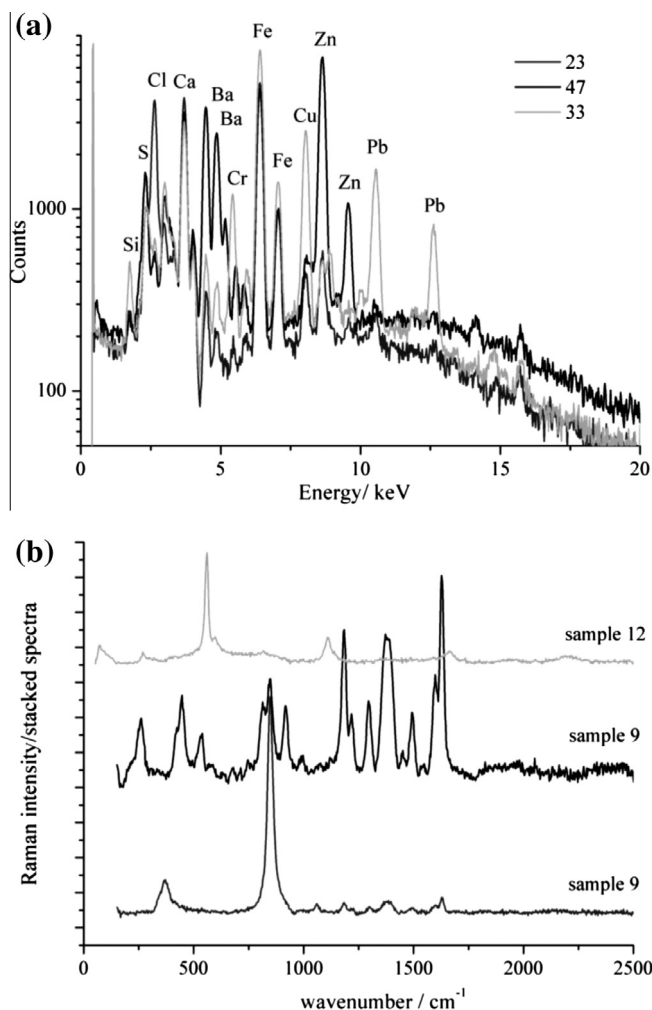
Fig. 4. (a) Comparison of the EDXRF spectra obtained for green (spot 33) and blue (spots 23 and 47) areas; (b) Raman spectra obtained for green (sample 9) and blue (sample 12) samples. (For interpretation of the references to color in this figure legend, the reader is referred to the web version of this article.)

of the "Capitão-mor". Fig. 6 presents the EDXRF spectra obtained for these areas. Iron was, again, found in all spectra. Keeping in mind the Fe found in the background, it is still very likely the
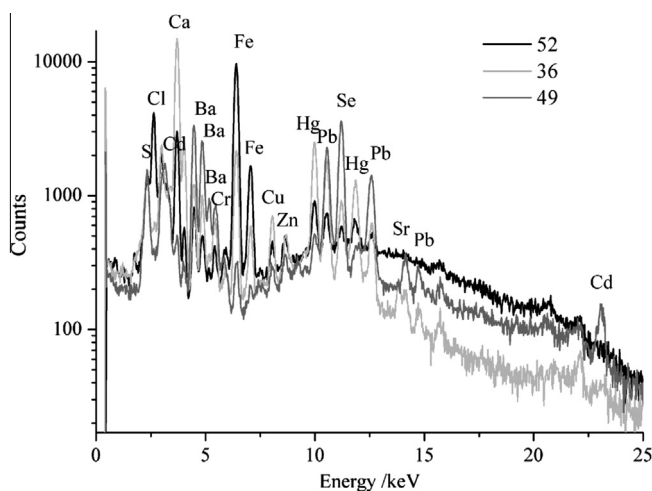

Fig. 5. Comparison of the EDXRF spectra obtained for three different shades of red. (For interpretation of the references to color in this figure legend, the reader is referred to the web version of this article.)
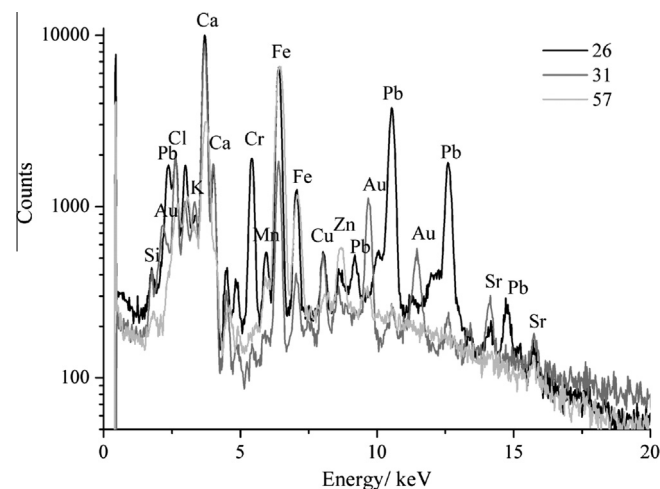

Fig. 6. Comparison of the EDXRF spectra obtained for yellow areas of the screen. (For interpretation of the references to color in this figure legend, the reader is referred to the web version of this article.)

use of an iron-based yellow such as yellow ochre ($Fe_2O_3 \cdot H_2O$). Regarding the color of the parasol, it should be noted that Au was detected as well, leaving no doubt on the fact that this accessory was painted with gold. Regarding the yellow color of the dog's leash, the measurements also attested the elements Cr and Pb, thus indicating again the use of chrome yellow.

7. White and black

Regarding the white and black areas, no substantial differences were detected in the elemental composition (Fig. 7a). Looking at the EDXRF spectrum of the whitish tone applied on the chair, the high content of Ca is indicative of the presence of $CaCO_3$. As far as the black color is concerned, the presence of S, K, Ca, Fe and Cu in the spectrum, seem to refer to several black matters potentially employed in this folding screen. The presence of Cu, could suggest the use of black copper oxide (CuO) in its natural or artificial form [25,26]. Because of the high amounts of both S, Fe and Ca, the presence of 'burnt vitriol' might be considered, since it corresponded to a pigment composed of iron oxide (Fe_2O_3) and anhydrite calcium sulfate ($CaSO_4$) producing a dark brownish red [21]. However, carbon black was the only pigment identified by Raman spectroscopy with two broad bands at ca 1300 and 1600 cm^{-1} (Fig.7b).

8. Discussion

The results obtained in this study, confronted with the available knowledge on *Namban* art are focus of interpretation. Unlike the traditional six-paneled screens attributed to the *Namban* period [2–4,6], we are in the presence of a two-paneled screen. There are records, however, of a two-paneled screen from the Edo period (17th century) which participated to the 'Europália89' exhibition [27]. This screen is a representation of the Portuguese 'Nao' enclosed in a golden background with brown sea (probably a tarnished silvering). Nevertheless, there is no evidence of the use of a golden background in the screen under study. Instead, the background contains Ag mixed with one or more coatings (shellac, resinous varnish and dry oil with resins). *Namban*, or *Namban*-type screens depicted with silver background, in the form of two or four-paneled artworks can be found in auction [28,29] as belonging to the 19th century, which suggests a revival of the *Namban* style. A broad set of materials were obviously part of the background,
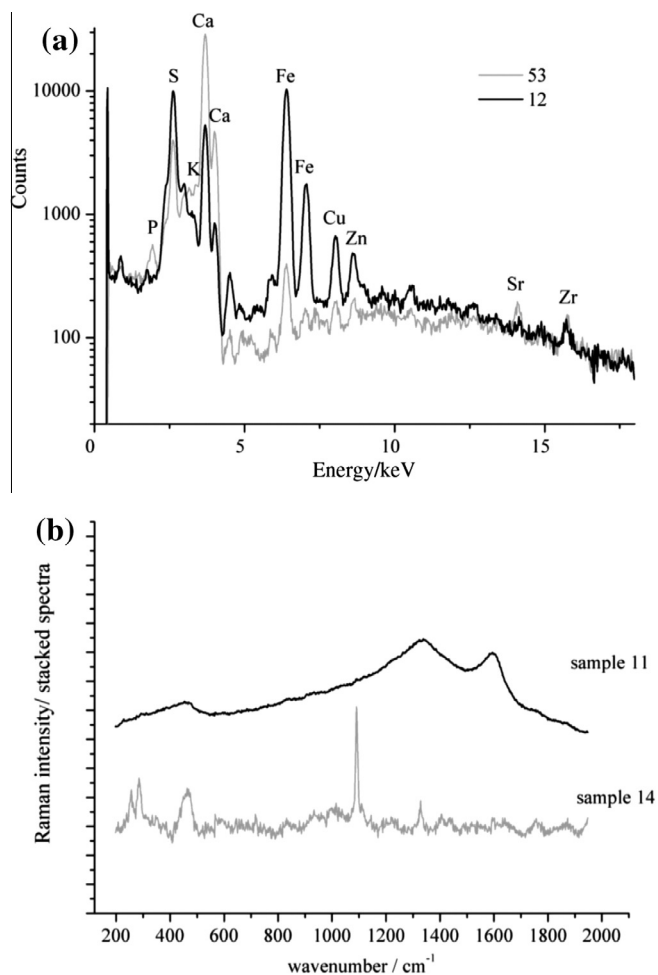
Fig. 7. (a) Comparison of the EDXRF spectra obtained for black and white areas of the screen; (b) Raman spectra obtained for black and white samples. (For interpretation of the references to colour in this figure legend, the reader is referred to the web version of this article.)

taking into consideration the more or less recurrent presence of S, Ca, Ti, Mn, Fe, Cu, and Zn. The application of several organic substances, revealed under ultraviolet light and their oxidation over time, as well as the oxidation of the applied silver may have greatly contributed to the brown color observed nowadays. The provenience of these elements, in such an heterogeneous manner, whether from a ground layer or from materials applied over the background, is hard to interpret. Particularly Fe, because its presence could always be explained by the existence of a pigment with the desired color. Regarding the pigments found, and considering the palette employed by painters in the Momoyama and Edo periods [3,4,19,30,31], the use of azurite, indigo, malachite, vermillion, red and yellow ochre, carbon black and *gofun* ($CaCO_3$) were expected. Regarding the black and white areas, the materials attested by Raman analysis are consistent with the pigments used in Japan during the 17th century, however they could still be found nowadays. We could assume that they are part of the original painting but they are not conclusive in terms of dating and characterizing the intervention(s) performed on the screen. In what concerns the green areas, Cu was found in the EDXRF spectra, indicating the presence of Malachite but no evidence was found with Raman. Instead, chrome yellow mixed with a blue organic dye was the choice for green. Chrome yellow was discovered by Vauquelin in 1809 [21], and it did not come into commercial production before 1818, so it could never belong to an original 17th century artwork.

Furthermore, the blue dyes used in Japanese traditional paintings are indigo and blue paper dayflower. Regarding the blue areas, no evidence was found of the use of azurite. The EDXRF spectra presented Fe, but there were no evidence of Prussian blue in the Raman spectra. Instead, ultramarine blue was detected. Discovered by Jean Baptiste Guimet in 1826, this pigment was a surpassing pigment regarding as much its remarkable properties (identical to those of the substance prepared from lapis-lazuli) as its lower cost [21]. To lighten the colors, lithopone, patented by John Orr in 1874 [20], seem to have been employed. Regarding the red areas, different mixtures were found in the different shades of red. Vermillion was found in all shades, what could correspond to the original painting. Moreover, cadmium red ($CdS(Se)$) was found. This is one of the most recent of the inorganic colors produced on an industrial scale. Introduced by Haen en 1907, it came into use in England soon after [32]. It is unclear whether the different pigments had been applied separately or as a single mixture. If, in fact, their presence corresponds to multiple layers, thus referring to a complex stratigraphy, the use of these compounds obviously resulted from at least two different interventions over time: the first one corresponding to the original coloring scheme, the second one to a later refurbishment, most likely performed in Europe, with materials synthetized from the 19th century onwards. One thing is certain, is that at least a partial intervention took place in the 20th century.

9. Conclusion

The period when the screen under study was created and the attribution or not of the label *Namban* were the main goals of this investigation. We relied on the analytical capabilities of EDXRF and Raman spectroscopy to study the materials present in this folding screen of uncertain provenance. The Raman spectra obtained for some of the collected samples presented significant luminescence background, most probably due to the presence of the different organic-based finish layers applied over the screen. This made the Raman analysis very challenging. However, from the obtained results, one may conclude that there is more than one painting applied to the screen, one of them performed definitely in the 20th century, due to the presence of Cadmium Red. However, it is unclear whether the insinuation of malachite and the presence of vermillion, carbon black and $CaCO_3$ are compelling evidences of an original painting from the 17th century, then improved or modified during the last century, or if these materials, together with the choice of a silver background and the use of chrome yellow, ultramarine blue and lithopone, are rather an indication of an artwork created during a 19th century *Namban* revival.

References

[1] P. Carneiro, The voyage of the Southern barbarians at the Soares dos Reis National Museum: an iconographic analysis, Bulletin of Portuguese/Japanese Studies 12 (2006) 41.
[2] Y. Okamoto, The Art of Japan, Weatherhill, New York, 1972.
[3] S. Pessanha, M.L. Carvalho, M.I. Cabaço, S. Valadas, J.L. Bruneel, M. Besnard, M.I. Ribeiro, Characterization of two pairs of *Namban* folding screens by Raman, EDXRF and FTIR spectroscopies, Journal of Raman Spectroscopy 41 (2010) 1220.
[4] S. Pessanha, A. LeGac, T.I. Madeira, J.-L. Bruneel, S. Longelin, M.L. Carvalho, Journal of Raman Spectroscopy 43 (2012) 1699–1706.

[5] <http://www.polomuseale.firenze.it/it/mostre/mostra.php?t=4f4d04c7f1c3bc7c0c000001> (Online).

[6] Y. Lippit, Encompassing the Globe: Portugal and the World in the 16th and 17th Centuries, MNAA, Lisbon, 2009.

[7] A. Deneckere, W. Schudel, M. van Bos, H. Wouters, A. Bergmans, P. Vandenabeele, L. Moens, In situ investigations of vault paintings in the Antwerp cathedral, Spectrochima Acta Part A 75 (2010) 511.

[8] M. Sawczak, A. Kaminska, G. Rabczuk, M. Ferretti, R. Jendrzejewski, G. Sliwinski, Complementary use of the Raman and XRF techniques for non-destructive analysis of historical paint layers, Applied Surface Science 255 (2009) 5542.

[9] K. Castro, N. Proietti, E. Princi, S. Pessanha, M.L. Carvalho, S. Vicini, D. Capinani, J.M. Madariaga, Analysis of a coloured dutch map from the eighteenth century: the need for a multi-analytical approach using portable instrumentation, Analytica Chimica Acta 623 (2008) 187.

[10] T.D. Chaplin, R.J.H. Clark, M. Martinón-Torres, A combined Raman, XRF and SEM-EDX study of three valuable objects – a large painted leather screen and two illuminated title pages in 17th century books of ordinances of the Worshipful Company of barbers, Journal of Molecular Structure 976 (2010) 350.

[11] K. Castro, S. Pessanha, N. Proietti, E. Princi, D. Capitani, M.L. Carvalho, J.M. Madariaga, Noninvasive and nondestructive NMR, Raman and XRF analysis of a Blaeu coloured map from the seventeeth century, Analytical and Bioanalytical Chemistry 391 (2008) 433.

[12] M. Aceto, A. Agostino, E. Boccaleri, F. Crivello, A. Cerutti Garlanda, Evidence for the degradation of an alloy pigment on an ancient Italian manuscript, Journal Raman Spectroscopy 37 (2006) 1160.

[13] J.J. Rorimer, Ultra-violet Rays and Their use in the Examination of Works of Art, Metropolitan Museum of Art, New York, 1931.

[14] E.R. De La Rie, Fluorescence of paint and varnish layers. Part 1, Studies in Conservation 27 (1982) 1.

[15] E.R. De la Rie, Fluorescence of paint and varnish layers part II, Studies in Conservation 27 (1982) 65.

[16] E.R. De la Rie, Fluorescence of paint and varnish layers part III, Studies in Conservation 27 (1982) 102.

[17] S. Koob, Obsolete fill materials found on ceramics, JAIC 37 (1998) 49–67.

[18] M.L. Carden, Use of ultraviolet light as an aid to pigment identification. 3, APT Bulletin 23 (1991) 26.

[19] J. Winter, East Asian Paintings: Materials, Structures and Deterioration Mechanisms, Archetype publications, Washington, 2008.

[20] R.J. Gettens, G.L. Sout, Painting Materials. A Short Encyclopaedia, Dover publications, New York, 1966.

[21] B. Guineau, Glossaire Des Matériaux De La Couleur, Brepols publishers, Turnhout, 2005.

[22] M.R. Marcelino, V.S.F. Muralha, Synthetic organic pigments in contemporary Balinese painting: a Raman microscopy study, Journal of Raman Spectroscopy 43 (2012) 1281.

[23] M. Bicchieri, M. Nardone, P.A. Russo, A. Sodo, M. Corsi, G. Cristoforetti, V. Palleschi, A. Salvetti, E. Tognoni, Characterization of azurite and lazurite based pigments by laser induced breakdown spectroscopy and micro-Raman spectroscopy, Spectrochima Acta Part B 56 (2001) 915–922.

[24] I. Osticioli, N.F.C. Mendes, A. Nevin, F.P.S.C. Gil, M. Becucci, E. Castellucci, Analysis of natural and artificial ultramarine blue pigments using laser induced breakdown and pulsed raman spectroscopy, statistical analysis and light microscopy, Spectrochima Acta Part A 73 (2009) 521–525.

[25] A.H. Church, The Chemistry of Paints and Painting, Seeley & co Ltd, London, 1901.

[26] N. Eastaugh, V. Walsh, T. Chaplin, R. Siddall, Pigment Compendium, A dictionary of historical pigments, Oxford, 2004.

[27] Art Namban – Catalogue of the Europália89 exposition, Brussels: Musées Royaux d'Art et d'Histoire, 1989.

[28] <http://www.pcv.pt/lot.php?ID=4889>, 2012 (assessed October).

[29] <http://www.cinoa.org/art-and-antiques/detail/97634, 2012 (assesses October).

[30] S. Grantham, Japanese painted paper screens: manufacturing materials and painting techniques, The paper conservator 9 (1985) 83.

[31] J. Winter, Paints and supports in far eastern pictorial art, The paper conservator 9 (1985) 24.

[32] R. Mayer, The Artist's Handbook of Materials and Techniques, Faber & Faber, London, 1990.

Research article

Determination of gold leaf thickness in a Renaissance illumination using a nondestructive approach

Sofia Pessanha,[a] Mauro Guerra,[a] Stephane Longelin,[a] Agnès Le Gac,[a,b] Marta Manso[a] and Maria Luisa Carvalho[a]*

In this work, the thickness of the gold leaf applied in the Manueline foral charter of *Murça* (illuminated in 1512) will be determined using X-ray fluorescence. In the frontispiece of the Manueline foral charter of *Murça*, the capital D was gilded using a gold leaf over a priming made of lead white. The characteristic lines of Pb (namely Lα and Lβ), although attenuated in the Au layer, are still visible in the X-ray fluorescence spectra. By determining the intensity ratio Lα/Lβ and comparing it with the ratio for an infinitely thick sample, the thickness of the attenuating material can be determined. Using this methodology, the thickness of the gold leaf applied in the charter of *Murça* was estimated as 1.6 μm. Copyright © 2013 John Wiley & Sons, Ltd.

Introduction

When dealing with gilded artworks, especially the ones using gold leaf, one of the main objectives is to determine the composition of the gold alloy. Furthermore, the thickness of the applied leaf is of great importance when we want to characterize the gilding technique. Gilding is the attaching of a gold layer on to a surface of another material, and it has been in use since 3000 BC. Several gilding techniques have been discovered in human history; the most important are gilding with gold leaf, gilding with gold foil, gilding with ground gold mixed with a vehicle, and fire gilding.[1] The process of pounding fine gold into leaf is known as goldbeating and has undergone little change since antiquity. It began with a small ingot weighing 72 grains or more (about 3 g) that was hammered until a long ribbon was obtained. The ribbon was then cut into squares corresponding to foils, and these were placed between sheets of heavy paper and hammered in their turn, repacked between parchment, and hand beaten again, with the process repeated successively until the foils of gold have been reduced to dozens of extremely thin leaves. According to several art technological sources, in the early 16th century, more than 150 leaves might be expected from an ingot.[2] The gold leaf could then be applied with a water technique to different kinds of artworks.

There are several strategies to evaluate the gilding of an artwork. Pessanha et al.[1] used SEM-EDS to determine the composition of the gold alloy applied in 17th–18th century folding screens and found a 100 nm order of magnitude for the thickness of the leaf by obtaining a quasi-transversal view in the backscattered electron image of the sample. Le Gac et al. also used SEM imaging to determine the thickness of the gold leaf of the main altarpiece of the Coimbra Old Cathedral.[2] These strategies involve the precise positioning of the sample, and slight deviations can be sufficient to modify the apparent thickness of the layers. X-ray fluorescence (XRF) techniques are nondestructive and often used to determine the thickness of coatings. Fiorini et al.[3] and Trojek et al.[4] studied the substrate under different angles in order to determine the

thickness of the coating layer. By tilting the object around the x-axis, the path length increases the intensities of the Au characteristic lines while the characteristic lines of the elements of the under layer are more attenuated. Instead of rotating the sample, one single measurement with at least two detectors at different angles can be attempted, like what Kataoka et al.[5] performed when studying Zn–Fe alloy coatings. Cesareo et al.[6–8] evaluated the gilding of several artworks by determining the intensity ratio of Lα/Lβ lines of the substrate and compared it with the intensity ratio for an infinitely thick sample. The same procedure was applied in this work to study the gilding in the frontispiece of the Manueline foral charter of *Murça* (Fig. 1). The capital D was gilded using a gold leaf over a priming made of lead white, as Raman measurements on a micro-sample confirmed (Fig. 4). Careful observation through optical microscope of the sample did not show the presence of a bolus layer, usually ochre or vermillion, used to ease the burnishing of the gold, as was also witnessed by Moura et al. in the study of a similar charter.[9] The characteristic lines of Pb are still visible in the XRF spectra although attenuated in the Au layer. This Au layer is assumed to be of a very high grade, even pure gold, because no Ag was detected in the XRF spectra. By determining the Pb intensity ratio Lα/Lβ and comparing it with the corresponding ratio for an infinitely thick sample, we can determine the thickness of the gold leaf.

Methodology

In a multilayered system, the characteristic lines of the elements present in the under layer are attenuated in the upper layer and; most

* *Correspondence to: Maria Luisa Carvalho, Centro de Física Atómica da Universidade de Lisboa, 1649-003 Lisboa, Portugal. E-mail: luisa@cii.fc.ul.pt*

a *Centro de Física Atómica da Universidade de Lisboa, 1649-003 Lisboa, Portugal*

b *Departamento de Conservação e Restauro, Faculdade de Ciências e Tecnologia, Universidade Nova de Lisboa, 2829-516 Caparica, Portugal*

Figure 1. Photograph of the Manueline foral charter of *Murça*.

importantly, the different energies are attenuated in a different way. When photons of the L lines of an element, *a*, cross a layer of another element, *b*, their ratio is further attenuated in the following manner[6]:

$$\left(\frac{L\alpha}{L\beta}\right) = \left(\frac{L\alpha}{L\beta}\right)_{\text{s.a.}} e^{-(\mu_1-\mu_2)\rho_b d_b} \qquad (1)$$

where μ_1 is the mass attenuation coefficient of the material *b* at the energy of Lα, μ_2 is the mass attenuation coefficient of the material *b* at the energy of Lβ, ρ_b is the density of material *b*, and d_b is the thickness of the layer. $(L\alpha/L\beta)_{\text{s.a.}}$ is the intensity ratio of the characteristic lines of the element in the under layer due to self-attenuation effects.

In the case of the lead white covered with a gold leaf, Eqn (1) becomes

$$\text{Pb}\left(\frac{L\alpha}{L\beta}\right) = \text{Pb}\left(\frac{L\alpha}{L\beta}\right)_{\text{s.a.}} e^{-(\mu_1-\mu_2)\rho_{\text{Au}} d_{\text{Au}}} \qquad (2)$$

where μ_1 is the mass attenuation coefficient of Au at 10.55 keV, μ_2 is the mass attenuation coefficient of Au at 12.6 keV, ρ_{Au} is the density of the Au, and d_{Au} is the thickness of the gold layer. $(L\alpha/L\beta)_{\text{s.a.}}$ is the intensity ratio of the characteristic lines of Pb in lead white due to self-attenuation effects.

This last parameter is unknown and has to be determined. The Lα/Lβ intensity ratios are very well documented[10,11]; however, they refer to infinitely thin elemental samples, where the emitted lines are not interacting with matter. The intensity ratio Lα/Lβ of Pb depends therefore on the thickness of the layer[8]:

$$\left(\frac{L\alpha}{L\beta}\right) = \left(\frac{L\alpha}{L\beta}\right)_0 \left(\frac{\varepsilon(L\alpha)}{\varepsilon(L\alpha)}\right)\left[\frac{(\mu_0+\mu_4)}{(\mu_0+\mu_3)}\right]\left[\frac{1-e^{-(\mu_0+\mu_3)d}}{1-e^{-(\mu_0+\mu_3)d}}\right] \qquad (3)$$

where $\left(\frac{L\alpha}{L\beta}\right)_0$ is the ratio for an infinitely thin sample, $\varepsilon(E)$ is the detector efficiency for a given energy, μ_0 is the linear attenuation coefficient of Pb at incident energy E_0, μ_3 is the linear attenuation coefficient of Pb at the energy of Lα (10.55 keV), μ_4 is the linear

attenuation coefficient of Pb at the energy of Lβ (12.6 keV), and *d* is the thickness of the layer.

If considering the detector placed in 45° geometry to the orthogonal to the sample, a correction must be made to Eqn (3):

$$\left(\frac{L\alpha}{L\beta}\right) = \left(\frac{L\alpha}{L\beta}\right)_0 \left(\frac{\varepsilon(L\alpha)}{\varepsilon(L\alpha)}\right)\left[\frac{(\mu_0+\mu_2)}{(\mu_0+\mu_1)}\right]\left[\frac{1-e^{-(\mu_0+\mu_1)\frac{d}{\cos45°}}}{1-e^{-(\mu_0+\mu_2)\frac{d}{\cos45°}}}\right] \qquad (4)$$

In order to determine the self-attenuation parameter for Pb, we plotted the intensity ratio Lα/Lβ (Eqn (4)) for a layer of pure Pb, for lead carbonate (PbCO$_3$), and for lead white (2PbCO$_3$·Pb(OH)$_2$) (Fig. 2). The first conclusion to be drawn is that the behavior is very similar for all the samples, and from a thickness of around 30 μm, the intensity ratio Lα/Lβ becomes constant (~0.867) for all the samples. This means that the samples can be considered bulk or infinitely thick. According to Mantler *et al.*, that thickness should be 24 μm for lead white.[12]

In order to evaluate the influence of the binder in the attenuation of Pb characteristic lines, PbCO$_3$ standards of different thicknesses were prepared by grinding PbCO$_3$ in a mortar and mixing with rabbit-skin glue (5%) to an adequate consistency. They were then applied over a Whatman paper with a pigment applicator to establish thicknesses of 50, 100, 150, and 200 μm and analyzed with our XRF setup. Figure 2 shows the experimental values for the Pb Lα/Lβ intensity ratios. In this figure, we can see that the Lα/Lβ intensity ratio has reached a plateau at these thickness values as the theoretical calculations predicted; however, the value is slightly lower (mean value of 0.847).

Observations made with an optical microscope of a sample collected from the charter of *Murça* indicated a lead white layer greater than 30 μm, and so we can consider our sample as an infinitely thick layer of lead white. According to these results, Eqn (2) can be simplified, considering the self-attenuation Lα/Lβ intensity ratio corresponding to an infinitely thick layer, and the thickness of the gold leaf applied over it can be determined.

Experimental

The EDXRF equipment used in this study for elemental analysis consists of the Amptek XR-100SDD[13] and the X-ray generator Amptek ECLIPSE IV with an Rh anode. For collimating the beam,
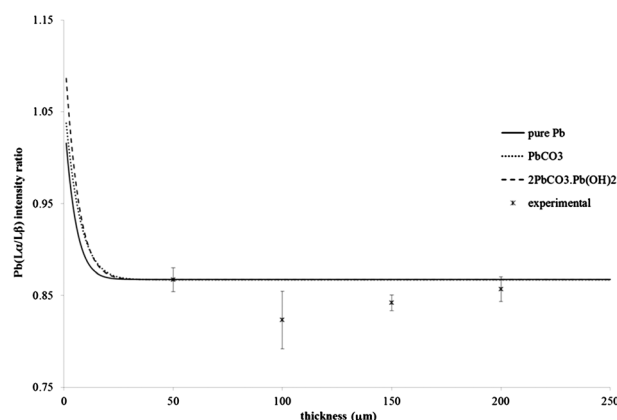

Figure 2. Plot of the intensity ratio Lα/Lβ for a layer of pure Pb (full line), PbCO$_3$ (dotted line), and lead white – 2PbCO$_3$·Pb(OH)$_2$ (dashed line). Experimental values are obtained for PbCO$_3$ standards.

an acrylic support with a 2 mm pinhole in Ta was used. Furthermore, the X-ray tube output was filtered using 2 mm Al and 25 μm Ag filters in order to partially monochromatize the radiation. Acquisitions were performed at 40 kV, 40 μA, and 500 s. Spectrum deconvolution and evaluation was performed using WinAXIL software package by Camberra.

The Raman spectrum of the micro-sample was measured using a Horiba-Jobin Yvon XploRA confocal spectrometer, with 785 nm laser diode. Using an entrance slit of 100 μm, the scattered light collected by the objective was dispersed onto the air cooled CCD array of an Andor iDus detector by a 1200 lines/mm grating. A 100× magnification objective with a pinhole of 500 μm was used to optimize the spatial resolution. Spectrum deconvolution was performed

Figure 3. EDXRF spectra obtained for the gilded capital D charter of *Murça* (black line), for the parchment (gray line).

Figure 4. Raman spectrum obtained for the collected micro-sample. LW, lead white; Gy, gypsum; Ca, calcite. Spectrum obtained with 785 nm laser, 0.1 mW power on the sample, 30 s acquisition time, and 16 accumulations.

using the software LabSpec v 5.78, and an eighth order polynomial baseline correction was carried out on the lmeasured Raman spectrum to remove the fluorescence contribution.

Results

Figure 3 presents the comparison of the EDXRF spectra obtained for a gilded spot and the parchment for the charter of *Murça*. The presences of Ni, Cu, and Zn in the spectra are contributions from the experimental setup. Iron was a constant presence throughout the illuminated area of the charter, probably a contamination from the iron gall ink. Lead is identified in the spectrum and comes from the priming layer, identified as lead white through Raman measurements of a collected micro-sample. Figure 4 shows the characteristic Raman bands of lead white at 671 and 1050 cm^{-1}.[14] The spectrum was acquired transversely and not in a cross section so we also have information from the parchment (between 1100 and 1700 cm^{-1}[15]), like the presence of calcite ($CaCO_3$) and gypsum ($CaSO_4$) and some sort of unidentified organic binder.[9,16] Gypsum is formed by Ca^{2+} ions displaced from $CaCO_3$ (used in parchment making[17] in the presence of metal sulfates coming from the ink.[18]

The Pb Lα/Lβ intensity ratios of the XRF spectra performed on the gilding of the charter of *Murça* were determined, and the corresponding thicknesses were calculated (Eqn (2)) using both the theoretical and experimental values for (Lα/Lβ)$_{s.a.}$. Results are presented in Table 1. Figure 5 shows a plot of the dependence of the Lα/Lβ intensity ratios as a function of the Au thickness, according to Eqn (2), and the thickness values obtained using the (Lα/Lβ)$_{s.a.}$ obtained experimentally. The results obtained using both self-attenuation values are very similar and within the uncertainties of the calculation, 1.6 ± 0.4 and 1.7 ± 0.4 μm;
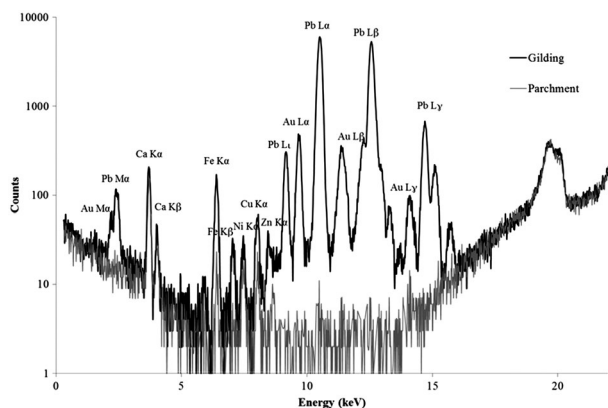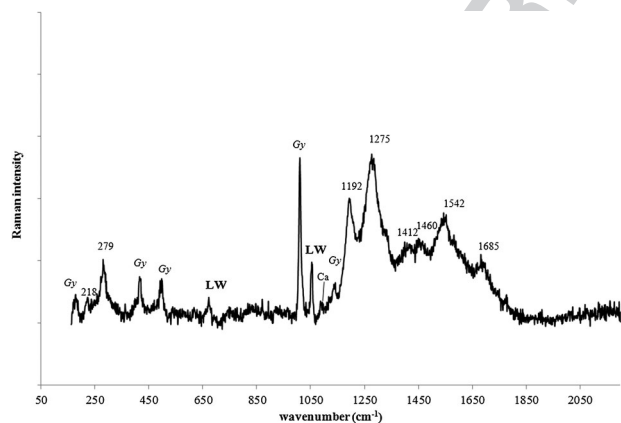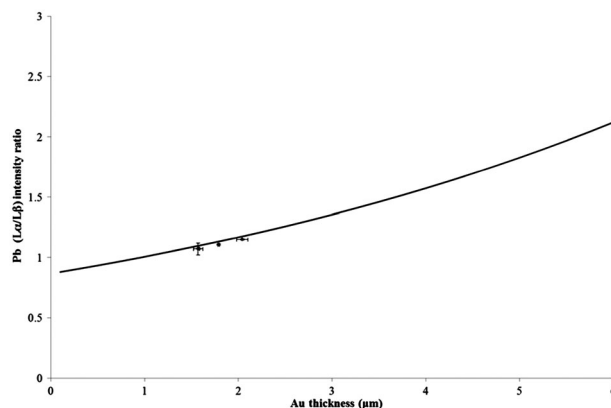

Figure 5. Plot of the intensity ratio of Pb Lα/Lβ as a function of the thickness of the gold layer considering theoretical (Lα/Lβ)$_{s.a.}$. In dots, the calculated Au layer thicknesses considering (Lα/Lβ)$_{s.a.}$ determined experimentally.

Table 1. Results obtained for the thickness of the gold leaf according to Eqn (2), using both the theoretical and experimental values for (Lα/Lβ)$_{s.a.}$–Pb Lα/Lβ due to self-attenuation

	Spot 1		Spot 2		Spot 3		Spot 4		Mean	
Pb (Lα/Lβ)	1.07 ± 0.01		1.11 ± 0.01		1.15 ± 0.06		1.07 ± 0.05		Mean	
(Lα/Lβ)$_{s.a}$	Theor.	Exp.	Theor.	Exp.	Theor.	Exp.	Theor.	Exp.	Theor.	Exp.
Au thickness (μm)	1.42 ± 0.01	1.58 ± 0.01	1.63 ± 0.01	1.79 ± 0.01	1.89 ± 0.06	2.04 ± 0.06	1.42 ± 0.05	1.57 ± 0.05	1.6 ± 0.4	1.7 ± 0.4

therefore, we can assume that they are valid even for a different composition of the lead white layer.

Conclusions

In this work, it is demonstrated how the nondestructive XRF analysis of gilded artworks can reveal precious information regarding the thickness of the gold leaf. The obtained results show that the leaf used in the gilding of the charter of Murça is extremely thin, in the 1 μm order of magnitude, which exemplifies the excellence of the gold beater that provided the gold leaf for the workshop involved in the manufacture of this Renaissance illumination. The methodology described in this paper can be applied in the future to study the gilding in other illuminated manuscripts, and the collection of samples can be avoided.

Acknowledgements

References

[1] S. Pessanha, A. LeGac, T. I. Madeira, A. Guilherme, M. Manso, M. L. Carvalho. *X-Ray Spectrom.* **2013**, *42*, 128.

[2] A. Le Gac, A. I. Seruya, M. Lefftz, A. Alarcão. *Revue d'Archéométrie – ArcheoSciences* **2010**, *33*, 423.

[3] C. Fiorini, A. Gianoncelli, A. Longoni, F. Zaraga. *X-Ray Spectrom.* **2002**, *31*, 92–99.

[4] T. Trojek, M. Hlozek. *Appl. Rad. Isotopes* **2012**, *70*, 1420.

[5] Y. Kataoka, H. Kohno, E. Furusawa, M. Mantler. *X-Ray Spectrom.* **2007**, *36*, 221.

[6] R. Cesareo, A. Brunetti, S. Ridolfi. *X-Ray spectrom.* **2008**, *37*, 309.

[7] R. Cesareo. *Nucl. Inst. Meth. Phys. Res. B* **2003**, *211*, 133.

[8] R. Cesareo, M. A. Rizzutto, A. Brunetti, D. V. Rao. *Nucl. Inst. Meth. Phys. Res. B* **2009**, *267*, 2890.

[9] L. Moura, M. J. Melo, C. Casanova, A. Claro. *J. Cult. Her.* **2007**, *8*, 299.

[10] R. Cesareo, *X-ray Physics: Interaction with Matter, Production, Detection*, in La Rivista del Nuovo Cimento della società Italiana di Fisica, Editrice Compositori, Bologna, **2000**.

[11] R. van Grieken, A. Markowicz, Handbook of X-ray Spectrometry: Methods and Techniques, Marcel Dekker, New York, **1993**.

[12] M. Mantler, M. Schreiner. *X-Ray Spectrom.* **2000**, *29*, 3.

[13] M. Manso, S. Longelin, S. Pessanha, M. L. Carvalho. *J. Inst.* **2012**, *7*, C10004.

[14] L. Burgio, R. J. H. Clark. *Spectrochim. Acta A.* **2001**, *57*, 1491.

[15] H. G. M. Edwards, D. W. Farwell, E. M. Newton, F. Rull Perez, S. Jorge Villar. *Spectrochim. Acta A* **2001**, *57*, 1223.

[16] P. Vandenabeele, B. Wehling, L. Moens, H. Edwards, M. De Reu, G. Van Hooydonk. *Anal. Chim. Acta* **2000**, *407*, 261.

[17] M. Guerra, A. Le Gac, S. Longelin, S. Pessanha, J. C. Frade, M. Guerra, A. J. Candeias, M. L. Carvalho. *Spectrochim. Acta A.* **2013**, *105*, 288.

[18] M. Bicchieri, M. Monti, G. Piantanida, F. Pinzari, A. Sodo. *Vib. Spectrosc.* **2011**, *55*, 267.

Q9

4